THE UNIVERSITY OF MICHIGAN
COLLEGE OF ENGINEERING
Department of Mechanical Engineering
Heat Transfer Laboratory

Technical Report No. 2

BOILING OF LIQUID NITROGEN IN REDUCED GRAVITY FIELDS WITH SUBCOOLING

Eugene W. Lewis
John A. Clark
Herman Merte, Jr.

ORA Project 07461

under contract with:

NATIONAL AERONAUTICS AND SPACE ADMINISTRATION
GEORGE C. MARSHALL SPACE FLIGHT CENTER
CONTRACT NO. NAS 8-20228
HUNTSVILLE, ALABAMA

administered through:

OFFICE OF RESEARCH ADMINISTRATION ANN ARBOR

May 1967

This report was also a dissertation submitted by the first author in partial fulfillment of the requirements for the degree of Doctor of Philosophy in The University of Michigan, 1967.

TABLE OF CONTENTS

TABLE OF CONTENTS (Concluded)

LIST OF TABLES

LIST OF FIGURES

LIST OF FIGURES (Continued)

LIST OF FIGURES (Continued)

LIST OF FIGURES (Concluded)

NOMENCLATURE

(Other nomenclature is defined as necessary)

a	Local acceleration
A	Area
B	Computational parameter—see Eq. (27)
Bi	Biot Number
C_p	Specific heat
C	Constants
D	Diameter
E	Parameter defined in Eq. (38)
f	Friction factor
F	Parameter defined in Eq. (39)
$\vec{F}$	Vector force
,etc.	Force component
g	Acceleration due to standard (terrestrial) gravity
g_o	Mass-force conversion constant
Gr	Grashof Number
h	Enthalpy
$\bar{h}$	Heat transfer coefficient
h_{fg}	Latent heat of vaporization
h'_{fg}	Average enthalpy difference between vapor and liquid
J	Mechanical equivalent of heat
k	Thermal conductivity

ℓ	Average calculated drop thickness
ℓ_1	Length measured along z-coorindate
L	Length measured along x-coordinate
L_e	Equivalent geometrical factor
L_o	Distance from leading edge to onset of turbulence
$\dot{m}$	Mass flow rate
m	Mass
n	Exponent
$\hat{n}$	Outward-drawn normal to dA
Nu	Nusselt Number
Nu"	Doubly modified Nusselt Number—see Eq. (23)
p	Pressure, psia
P	Pressure, atm
Pr	Prandtl Number
q	Heat transfer rate
r	Radial coordinate
Ra	Rayleigh Number
Ra'	Modified Rayleigh Number--see Eq. (14)
Ra"	Doubly modified Rayleigh Number—see Eq. (24)
t	Time
T	Temperature
V	Volume
$\vec{V}$	Vector velocity

V_x,etc.	Velocity component
x,y,z	Cartesian coordinates
y_1,y_2	Local film thickness
Δp	Saturation pressure difference corresponding to heater surface superheat
ΔT_{sat}	Heater surface superheat (T_s-T_{sat})
α	Thermal diffusivity
α_c	Equivalent thermal diffusivity in heat conduction through a substance with change of phase
β	Thermal expansion coefficient
δ	Vapor film thickness
δ_1	Variation in film thickness
δ^*	Vapor film thickness at onset of turbulence—see Eq. (33)
$\eta_{v\delta}$	Dimensionless boundary layer thickness—see Eq. (31)
λ_c	Critical wavelength
λ_d	Most dangerous wavelength
μ	Viscosity
ρ	Density
σ	Surface tension
θ	Cylindrical coordinate

Subscripts

f	Evaluated at film temperature
ℓ	Liquid
min	Minimum
max	Maximum
s	Test object surface
sat	Evaluated at saturation conditions
sc	Subcooled
sd	Solid
v	vapor

ABSTRACT

Pool boiling of liquid nitrogen in a body force field less than standard gravity was studied using a transient calorimeter measurement technique. Experimental variables included: body forces from standard gravity to near-zero; a variety of geometries and orientations of the boiling surface; subcooling from 0°F to 30°F; pressures from 1 to 5 atmospheres; and boiling regimes from film to nucleate, plus free convection. Gravity was varied by using a drop tower and a counterweighted test package. In free fall, the test package achieved a level of less than 0.002 times standard gravity. Heat transfer surfaces included 1/4-, 1/2-, and 1-inch diameter spheres and a 3-inch diameter by 13/16-inch thick disk oriented vertically, horizontally heating up, and horizontally heating down.

Subcooling was achieved by rapid pressurization of the liquid nitrogen; 3 and 5 atmospheres were used, providing maximum subcooling of approximately 20°F and 30°F. Results were obtained in the form of time vs. surface temperature, which were then expressed as heat flux vs. the difference between the test surface temperature and saturated liquid temperature. These results are presented graphically. In addition, high-speed photographs were made showing the film boiling process. These photographs were used to determine vapor film thicknesses for the various geometries. All results were limited to the film-boiling region except for those obtained with the 1-inch diameter sphere, which was used in all boiling regions.

In the film-boiling region, the heat flux on the spheres varied as diameter to the -1/8 power. The heat flux on the disk, within the uncertainty of the measurements, did not exhibit any dependence on the disk orientation, but was approximately 100% higher than the heat flux observed on the spheres with similar liquid conditions. The appearance of the vapor film on the disk as observed in the photographs differed with orientation. The heat flux on the 1/2-inch and 1-inch spheres varied as the 1/3 power of acceleration. The heat flux on the 1/4-inch sphere and the disk varied as the 2/9 power of acceleration. For the 1-inch diameter sphere, the minimum and maximum heat fluxes were proportional to the 1/4 power of acceleration and were increased with subcooling and increased pressure. Nucleate boiling, within the uncertainty of the measurements, was not affected by variations in acceleration, pressure, or subcooling.

CHAPTER I

INTRODUCTION

A. PURPOSE

Of the three modes of heat transfer, radiation, conduction, and convection, only convection is normally affected by a variable force field. In the past, this dependence was not usually significant. Within the last ten years, however, questions which previously had been primarily academic in nature began to have many practical applications in the new field of space technology. The possibility of vehicles being accelerated, in free fall or orbit, or subjected to other gravitational systems, made it desirable to have some reasonably reliable method of predicting how various physical phenomena would be modified under a varying force field.

Because of the compactness possible, it may be anticipated that boiling heat transfer will continue as an important mechanism for power generation and energy dissipation for some time to come. Recently many different models have been proposed which purport to provide a correlation for boiling heat transfer data in the various boiling regimes, but none of them have been able to describe completely the various boiling processes. Most of the correlations include a dependence on the local gravitational field. While variations in the indicated dependence on (a/g) between different boiling regimes is not unexpected, the different predicted dependencies for a single regime appears to indicate shortcomings in at least some of the models. Use of particular correlations in space technology applications should there-

fore be attempted only after comparison with data which have been published on heat transfer with nonstandard force fields.

The purpose of this investigation was to attempt to clarify some of the apparent discrepancies in the predicted dependence of heat flux on the gravitational field in the various boiling regimes. It was recognized that the size, shape, and orientation of the surface from which boiling was taking place could affect the results, so several different surfaces were used to obtain heat transfer data in the film boiling region. The effects of using subcooled and saturated liquid were investigated, and pressure on the boiling system was varied. A transient calorimeter measurement technique was used to study the range of effective gravity from standard earth gravity to near-zero (free fall). Liquid nitrogen was used as the test fluid since it is inert and is convenient with the transient technique.

B. LITERATURE SURVEY*

Boiling heat transfer is characterized by the generation of vapor at a solid-liquid interface due to heat transport from the solid to the liquid. The solid heat transfer surface is at a temperature above the liquid saturation temperature. The liquid bulk temperature is equal to or less than the liquid saturation temperature. The vapor may appear as individual bubbles, as a continuous film, or as a combination of both. Buoyant forces acting on the vapor tend to remove it from the hot surface in the form of bubbles of various shapes and sizes. After departure from the heat transfer surface,

*Superscripts refer to References in the Bibliography.

the bubbles may collapse, coalesce with other bubbles, or move independently. Detailed examinations of the conditions under which these various behaviors are observed and descriptions of the various boiling regimes are presented in standard texts such as those of McAdams[1] and Kreith.[2]

The level of boiling heat flux is affected by the rate at which the vapor is removed from the heat transfer surface. A change in the buoyancy force would be anticipated to affect the vapor removal rate, and therefore the heat flux, for a given heat transfer surface temperature. The effect may vary with the boiling regime. Analyses of the hydrodynamic aspects of nucleate and film boiling (e.g., Refs. 3-5) consider the liquid-vapor interface instability. For film boiling, Taylor instability is observed. The reduction or elimination of the gravity force will reduce or eliminate the liquid-vapor instability, significantly changing the mechanism of heat transfer. The consequences of this effect have been observed in this present work.

Adelberg[6] calculated the forces on a single bubble due to bubble dynamics, surface tension, drag, and gravity induced buoyancy. These calculations indicated that, for water, an effect of (a/g) on heat transfer might be expected only when (a/g) was larger than 50. Clark, et al.,[7] evaluated the bubble Froude number (ratio of inertia to buoyant forces) in nucleate boiling for several liquids at 1 atmosphere pressure, (a/g) = 1, ΔT_{sat} = 16°F, and a bubble radius of 0.005 inch. Their evaluation indicated inertia forces were dominant for all liquids considered; for nitrogen, the bubble Froude number was 452.

Keshock, et al.,[8] evaluated the forces on bubbles in nucleate boiling and found that bubble departure diameter showed a gravity dependence only for slowly growing bubbles; the inertial force controlled departure diameter for a rapidly growing bubble. Cochran, et al.,[9] evaluated the forces acting on a bubble attached to a surface, and found that at (a/g) = 1 and high subcooling (>10°F) the principal removal forces were the pressure and dynamic forces, at low subcooling the principal removal forces were the pressure and buoyant forces, and at zero gravity the pressure and dynamic forces removed the bubbles at all subcoolings.

Beckman and Merte[10] obtained high-speed photographs of nucleate boiling of water at (a/g) from 1-100 and found that variations in acceleration affected the number of nucleating sites, the frequency of bubble departure, and, for values of (a/g) between 1 and 3, the bubble departure size. Later growth period growth rates were also affected by variations in acceleration.

The correlation proposed by Rohsenow[11] for nucleate pool boiling, Eq. (58), predicts that (q/A) is proportional to $(a/g)^{1/2}$ (provided that the empirical constant, given as 2.97×10^{5}, is not a function of (a/g)). The equation developed by Michenko[12] for nucleate boiling, Eq. (59), predicts that (q/A) is proportional to $(a/g)^{-2/3}$. Forster and Zuber[13] and Forster and Greif[14] predicted that (q/A) would be independent of (a/g).

Frederking[15] performed a combined kinematic and fluid dynamic analysis of a bubble column originating at a single site in saturated nucleate boiling. His results indicated that the heat flux at a single site was proportional to $(a/g)^{1/4}$, but did not consider the effect of (a/g) on the number of bubble sites.

Nucleate pool boiling experimental data have been reported for a wide range of (a/g). Merte and Clark[16] using saturated water and (a/g) from 1-20 observed a change in (q/A) with (a/g) for a given ΔT_{sat}. An increase in (q/A) was observed at low ΔT_{sat}, but at higher ΔT_{sat}, (q/A) decreased with increasing (a/g). Costello and Tuthill[17] observed a decreasing (q/A) with (a/g) increasing from 1 to 38 at a given ΔT_{sat}, but did not present data at the low ΔT_{sat} where Merte and Clark[16] had observed a reversal of this trend. Sherley[18] reported a statistical increase of approximately 20% in (q/A) at a given ΔT_{sat} when comparing (q/A) vs. ΔT_{sat} data at (a/g) = 0 with similar data at (a/g) = 1. However, the variation of (q/A) for both levels of (a/g) was approximately ±50%. Merte and Clark[19] obtained (q/A) vs. ΔT_{sat} saturated nucleate boiling data with liquid nitrogen at (a/g) = 1.0, 0.6, 0.33, 0.2, and free fall (0.01-0.03). Their results were consistent with those of Sherley[18] in that no significant effect of (a/g) was observed in the nucleate boiling region.

Numerous correlations have been proposed for predicting the maximum heat flux, $(q/A)_{max}$ (e.g., Refs. 20,21,22,23, and discussion of 3). They all predict $(q/A)_{max}$ is proportional to $(a/g)^{1/4}$. Siegel[24] suggests that this may be because they all use a horizontal infinite flat plate model. Costello and Tuthill[17] observed an $(a/g)^{1/4}$ dependence of $(q/A)_{max}$ for $1 < (a/g) < 38$ on a flat plate. Merte and Clark[19] found an $(a/g)^{1/4}$ dependence for $(q/A)_{max}$ with a 1-inch diameter sphere in the range $0 < (a/g) \leq 1$. Usiskin and Siegel[25] used a platinum wire 0.0453 inch in diameter to obtain $(q/A)_{max}$ data for (a/g) between 1 and free fall and commented that an

$(a/g)^{1/4}$ variation appeared to provide a reasonable lower limit for their data.

In an early work[26] with nucleate boiling of Freon 114 from a horizontal platinum wire, it was observed that upon changing from $(a/g) = 1$ to free fall, that with no change in heat flux, the system changed to film boiling. Evidently the heat flux level was initially above that corrsponding to $(q/A)_{max}$ for the free fall condition, and film boiling was the only possible condition.

A range of ΔT_{sat} over which $(q/A)_{max}$ would be expected to exist was predicted by Chang and Snyder.[21] Merte and Clark[19] observed an empirical constant in this equation had been derived for water. They modified the constant to apply to nitrogen and presented experimental results which fell within the predicted range. This prediction also included a dependence on $(a/g)^{1/4}$.

Results for transition boiling with variations in (a/g) appear to be limited to those of Merte and Clark[19] for $0 < (a/g) \leq 1$. As discussed by Siegel[24] these data suggest that (q/A) as a function of ΔT_{sat} in this region is insensitive to gravity reductions.

Berenson[3] predicted that the minimum heat flux with film boiling, $(q/A)_{min}$, on a horizontal flat plate was proportional to $(a/g)^{1/4}$. He also obtained an expression for ΔT_{sat} at which $(q/A)_{min}$ would occur. This ΔT_{sat} was proportional to $(a/g)^{-1/6}$. The measurements of Merte and Clark[19] for a 1-inch diameter sphere agreed closely with the predicted $(q/A)_{min}$, but the value of ΔT_{sat} at this condition did not.

Analyses of the film-boiling region have been performed using several different models. Bromley[27] analyzed film boiling from a horizontal tube with viscous flow around the tube to the top. The equation he obtained is given as Eq. (20) and predicts (q/A) varies as $(a/g)^{1/4}$. Adelberg[6] performed a similar analysis for a horizontal tube and also predicted that (q/A) would vary as $(a/g)^{1/4}$.

Berenson[3] analyzed film boiling from a horizontal flat plate with a thin film of uniform thickness on which cylindrical bubbles with hemisperical caps were superimposed at regular intervals. The equation he developed is given as Eq. (26), and predicts (q/A) varies as $(a/g)^{3/8}$.

Hamill and Baumeister[28] performed an analysis of film boiling based on a cellular model and obtained an optimum cell diameter (wavelength) which was intermediate between λ_c and λ_d (see Eqs. (21) and (22)). The expression they obtained for film boiling was

$$\bar{h} = 0.410 \left[\frac{k_{vf}^3 h_{fg}^* \rho_{vf} g(\rho_\ell - \rho_{vf})}{\mu_{vf} \Delta T_{sat} \left(\frac{g_o \sigma}{g(\rho_\ell - \rho_{vf})} \right)^{1/2}} \right]^{1/4} \left(\frac{a}{g} \right)^{3/8} \qquad (1)$$

where

$$h_{fg}^* = h_{fg} \left(1 + \frac{19}{20} \frac{C_p \Delta T_{sat}}{h_{fg}} \right) \qquad (2)$$

which they observed agrees with the equation of Berenson (Eq. (26)) within 4%. Equation (1) predicts (q/A) is proportional to $(a/g)^{3/8}$. Baumeister, et al.,[29] considering film boiling to water drops on a flat plate, developed an equation for the heat transfer from the plate as

$$\bar{h} = 0.68 \left[\frac{k_{vf}^3 h_{fg}' g \rho_\ell \rho_{vf}}{\Delta T_{sat} \mu_{vf} L_e} \right]^{1/4} \left(\frac{a}{g} \right)^{1/4} \qquad (3)$$

where

$$L_e = \frac{V_{drop}}{\pi^2 \ell^2} \qquad (4)$$

Equation (3) predicts that (q/A) is proportional to $(a/g)^{1/4}$. The model used to obtain Eq. (3) assumes that the generated vapor moves parallel to the flat plate, rather than normal to it as with the other flat plate models.

An analysis of film boiling on a vertical surface was performed by Hsu and Westwater.[30] They predicted that in the laminar film region (q/A) would be proportional to $(a/g)^{1/4}$, but in the turbulent film region the exponent on (a/g) would be between 1/3 and 1/2. Frederking and Clark[31] analyzed film boiling on a sphere at $(a/g) = 1$ and predicted that (q/A) would be proportional to $(a/g)^{1/3}$. Siegel[24] commented that the relation proposed by Frederking and Clark (Eq. (16)) contained contributions from both the laminar and turbulent regimes.

Results obtained for film boiling on a 1-inch diameter sphere for $0 < (a/g) \leq 1$ by Clark and Merte (Refs. 7, 19, 32, and 33) show (q/A) to be proportional to $(a/g)^{1/3}$. Pomerantz[34] obtained film boiling results on a 0.188-inch diameter horizontal cylinder at $1 \leq (a/g) \leq 10$, and found (q/A) was proportional to $(a/g)^{0.336}$. Heath and Costello[35] obtained results for film boiling of ethanol, pentane, and Freon 113 on horizontal and vertical flat plates, for $1 \leq (a/g) \leq 21$ in a centrifuge. Their plates were 6 inches long and 1 or 1-1/2 inches wide. Their results were adequately predicted by

Berenson's correlation (Eq. (26)—(q/A) proportional to $(a/g)^{1/4}$) when it was modified by a width correction factor. Heath and Costello[35] did not find any significant difference in film boiling heat transfer characteristics between the horizontal and the vertical plate orientation, although Class, et al.,[36] using a plate 22 inches long and 1 inch wide in liquid hydrogen, observed heat fluxes as much as 25% higher on a vertical plate than were observed on a horizontal plate heating up.

CHAPTER II

EXPERIMENTAL APPARATUS

A. INTRODUCTION

The primary object of this investigation was to determine the effects on boiling heat transfer of varying the gravitational field in the range $0 < (a/g) \leq 1$, with additional variables of test surface geometry, bulk liquid subcooling, and pressure.

The most simple way of approaching $(a/g) = 0$ with an experimental package was with the use of a drop tower (alternative techniques include using an aircraft flying a parabolic trajectory or a satellite in earth orbit). This permits continuous direct measurements during free fall. The use of a counterweighted system added the desired capability for obtaining intermediate values of (a/g). (A discussion of the relationship between free fall, counterweighted drop, and various values of the gravitational field, is presented in Appendix E.) The use of a drop tower required a means of bringing the test package to rest, as well as a means of recording data obtained while the package was falling. A test facility with these capabilities was designed and built in the Heat Transfer Laboratory of the Department of Mechanical Engineering.

A drop tower provides relatively short test times, of the order of a few seconds for realistic heights, so that steady-state heat transfer measurements are not practical. A transient technique, using a test surface as a dynamic calorimeter, permitted an accurate determination of heat flux when

the test surface physical characteristics and the variation of temperature with time were known (see Section V.F).

The use of various test surfaces permitted the effects on film boiling of variations in geometry and test surface orientation, in combination with variations in (a/g), to be evaluated. The test fluid used was liquid nitrogen, generally at atmospheric pressure and saturated. In order to investigate the effects of subcooling on boiling, subcooling was achieved by rapid pressurization of the liquid nitrogen with helium just prior to the test (in preference to supplying a cooling system to maintain a subcooled bulk liquid nitrogen temperature level). This also provided the capability for varying the pressure on the boiling liquid. A subsequent need for photographic information on the boiling phenomena with different test surface geometries in the film-boiling regime at (a/g) = 1 necessitated the acquisition of a high-speed motion picture camera.

B. DROP TOWER

The drop tower location in the Heat Transfer Laboratory permitted a total drop distance of 31 feet, which provided approximately 1.4 seconds of test time in free fall. A sketch of the drop tower facility is shown in Fig. 1.

The hydraulic buffer arresting gear shown in Fig. 2 is basically a 6-inch diameter hydraulic piston with programmed orifices designed specifically for this application. The buffer is capable of decelerating a 150-pound mass from 45 feet per second to rest in a distance of 2-1/2 feet with a maximum measured value of (a/g)≈30.

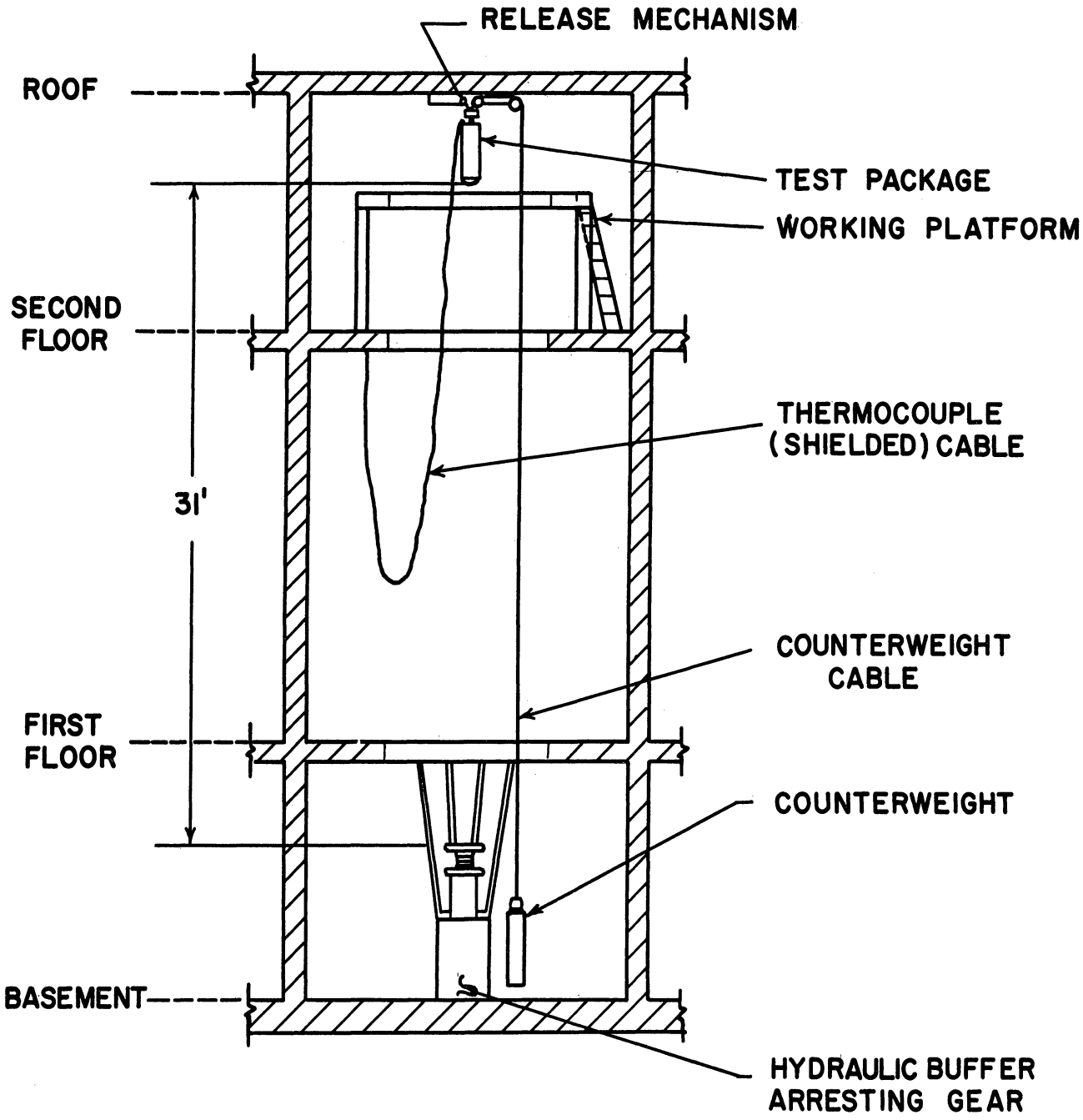

Fig. 1. Drop tower facility.

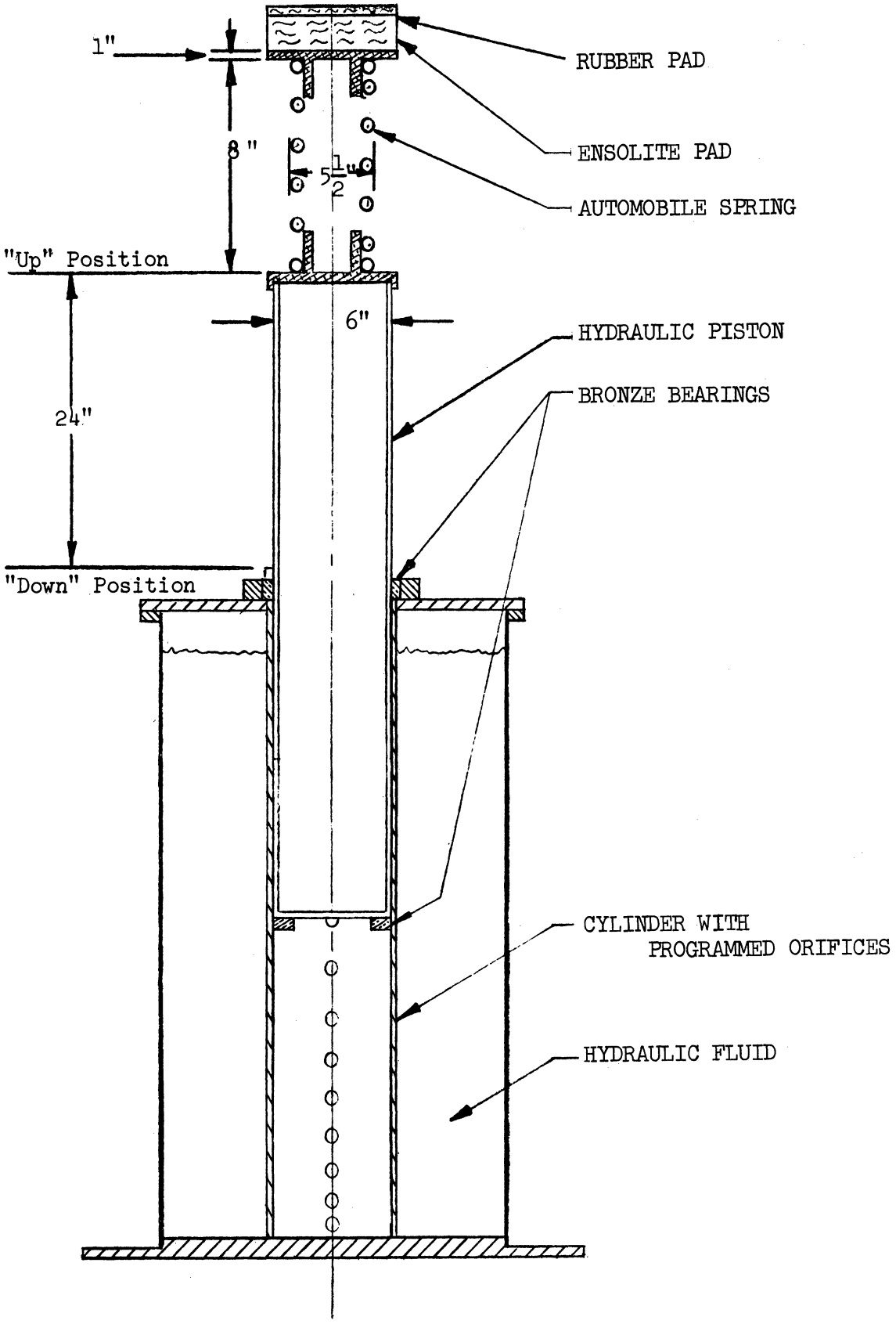

Fig. 2. Buffer assembly.

The use of an automotive-type coil spring, four inches of Ensolite energy-absorbing synthetic rubber compound, and one inch of heavy rubber padding on the top of the piston helped to reduce the initial acceleration of the piston while decreasing the initial deceleration of the test package.

Two different test packages, described in more detail in Section II.C, were utilized. The first package (Fig. 3) was used for obtaining saturated data at one atmosphere pressure, and weighed approximately 120 pounds. The second test package (Fig. 4), which could be pressurized to 100 psia, was used for obtaining both saturated and subcooled data at pressures of from 1 to 5 atmospheres, and weighed approximately 135 pounds.

The counterweight used to provide intermediate values of (a/g) between 0 and 1 (Figs. 3 and 4) was made from a piece of aluminum tubing 6 inches in outside diameter and 5 feet long, and included a provision for varying its weight by adding or removing quantities of lead shot. The empty weight of the counterweight was 11 pounds, 5 ounces, which permitted minimum experimentally measured values of (a/g) of 0.20 to be obtained with the first test package and 0.17 to be obtained with the second test package. The counterweight was decelerated at the end of the drop by two Firestone Rubber Company automotive-type air springs and was guided by two vertical wires which limited its horizontal motion.

Initially the test package was supported by the counterweight cable, and the counterweight was held down by a solenoid-operated latch. It was observed that when the counterweight was released the test package and the

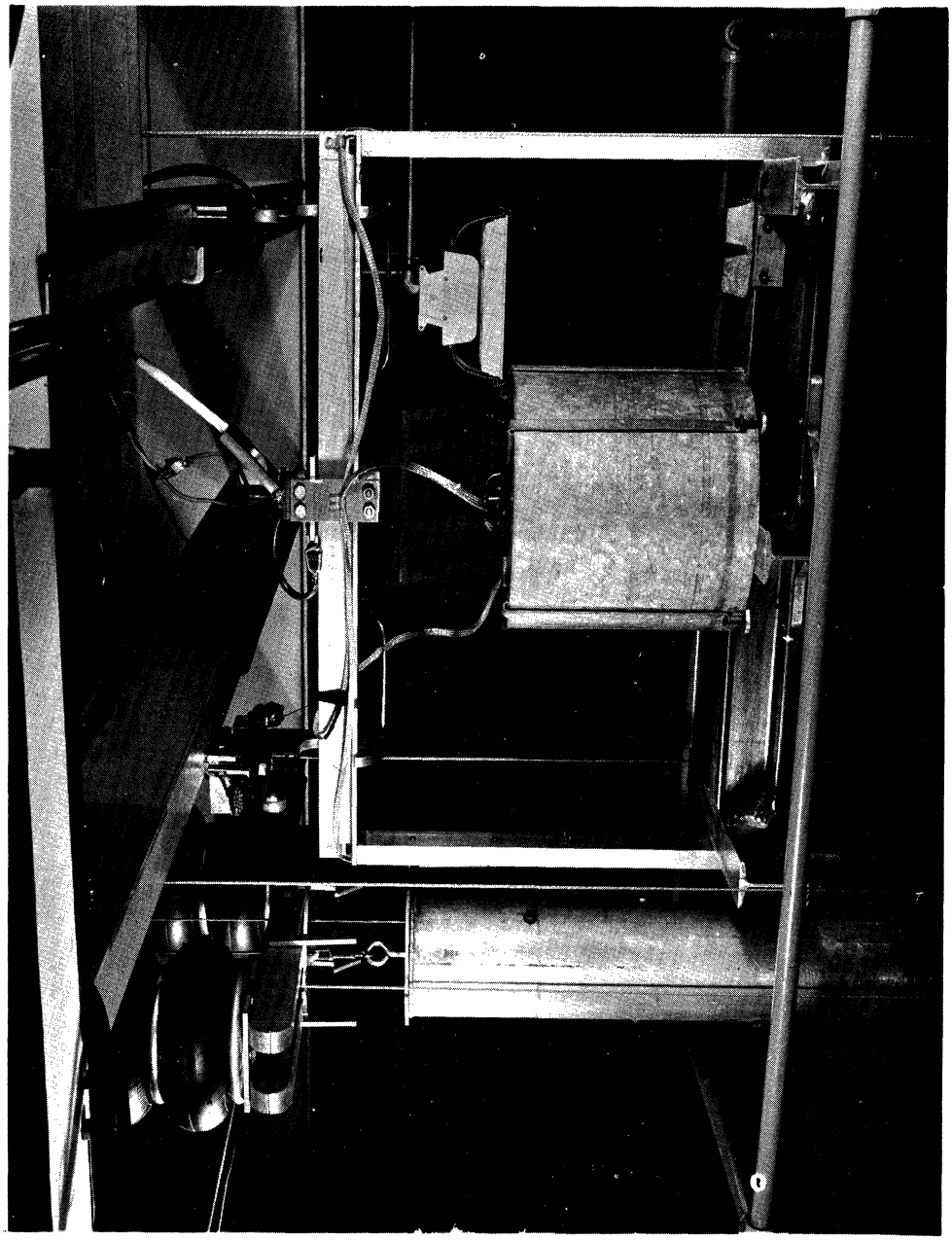

Fig. 3. View of first test package and counterweight.

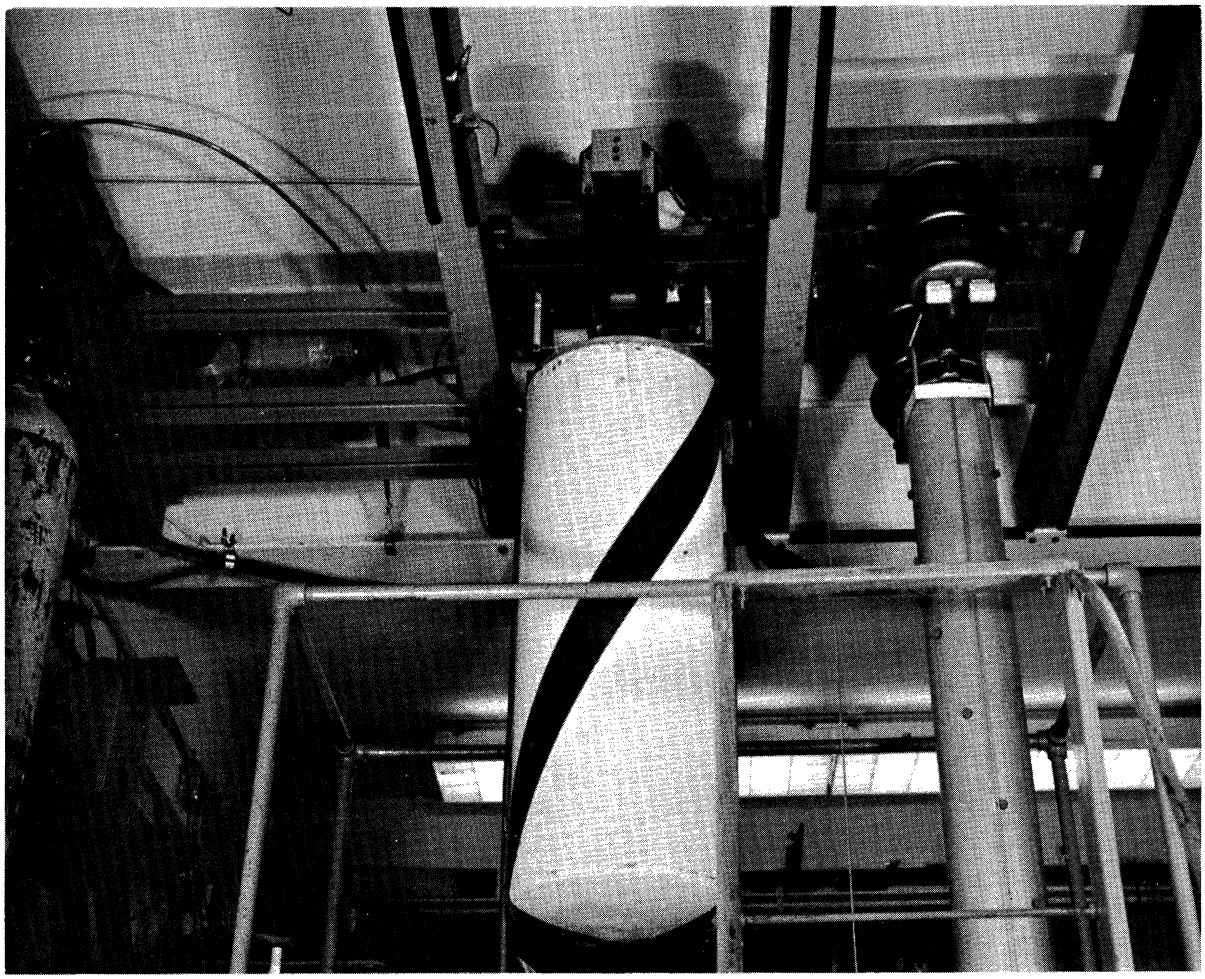

Fig. 4. View of second test package and counterweight.

counterweight in combination with the cable connecting them behaved as a spring-mass system with a resultant sinusoidal variation in the measured value of (a/g). This variation in (a/g), discussed further in Appendix E, was reduced by supporting and releasing the test package directly, so that the cable initially supported the counterweight, rather than the test package.

The test package was raised from the buffer to the release position by means of an electrically driven hoist, which was also used to reposition the buffer piston in the "up" position.

Two flexible shielded cables carried all of the instrumentation leads from the test package to a control panel located on the second floor. From the control panel the wiring led to the appropriate recording equipment, reference junctions, or calibration equipment. These two cables were attached symmetrically to the test package to balance any overturning moments, and had no measurable effect on the values of (a/g).

The first test package was supported by a short length of 17-gauge resistance wire prior to a test. The package was released by passing a large current through the wire, heating it very rapidly. The strength of the wire decreased with increasing temperature until the wire failed, providing a torque-free release. An indication of the current was superimposed on a time record (see Section II.E), and the cessation of current indication identified the release time. The wire normally parted approximately 1.3 seconds after the current was initiated.

The second test package was supported by a stud which engaged a solenoid-

operated latch. The current which activated the solenoid also provided an indication of the time of release on the recorder. This system permitted better control of the time at which the test package was dropped.

C. TEST PACKAGES

The first test package provided for fractional gravity and free-fall testing using liquid nitrogen at saturated 1 atmosphere conditions. It consisted of a simple framework to which a 3-liter stainless steel beaker, insulated on the sides and bottom with 3 inches of Styrofoam, was attached (see Fig. 3). A lid on the beaker reduced convection currents over the nitrogen, and thus the evaporation rate, as well as potential oxygen contamination from the atmosphere. Provision was made for positively positioning any test surface which was used, so that repeatability was ensured. The test surface was manually placed in the test fluid at the start of each test. Four guide wires were provided, one at each corner of the framework. These guide wires kept the package from twisting while it was being raised to or in the release position, aligned with the rectangular openings it passed through while dropping, and supported in an upright position on the buffer piston after completion of a drop.

The first package was found to reach a minimum value of (a/g) which varied from .01 to .03. Part of this departure from zero (a/g) during free fall was attributed to guide-wire drag, which varied from run to run and even during different portions of a run. The remainder was attributed to air drag, which is analyzed in more detail in Appendix C.

The second test package provided a capability for rapidly pressurizing the test fluid up to 100 psia and for shielding the test fluid container from the external air flow. Pressurization permitted both the system pressure and the test fluid subcooling to be varied, while the air flow shielding permitted a more nearly constant value of (a/g), much closer to zero, to be maintained during free fall.

There are two major components of the second test package: an outer package which serves as a pressure vessel, windshield, and mounting structure for fastenings and some instrumentation; and an inner package which contains the test fluid test surface, and additional instrumentation. A sketch of this test package is presented in Fig. 5.

The inner package consists of a 3-liter stainless steel beaker wrapped in fiberglass mat and tinfoil insulation, and a mounting plate. A hinged test surface support is located on the mounting plate, and provides positive positioning of the test surface for all tests. A solenoid operated release permits the test surface to be placed in the test fluid from a remote location with the outer package sealed and pressurized. Support chains which position the inner package prior to a free-fall test are also attached to the mounting plate.

The outer package is a 14-inch diameter cylinder 36 inches long, blunted on the lower end and flat on the upper end. It provided a minimum of 1-inch radial clearance between the inner and outer packages and also between the outer package and the sides of the drop tower, and a 6-inch vertical clearance for the suspended inner package.

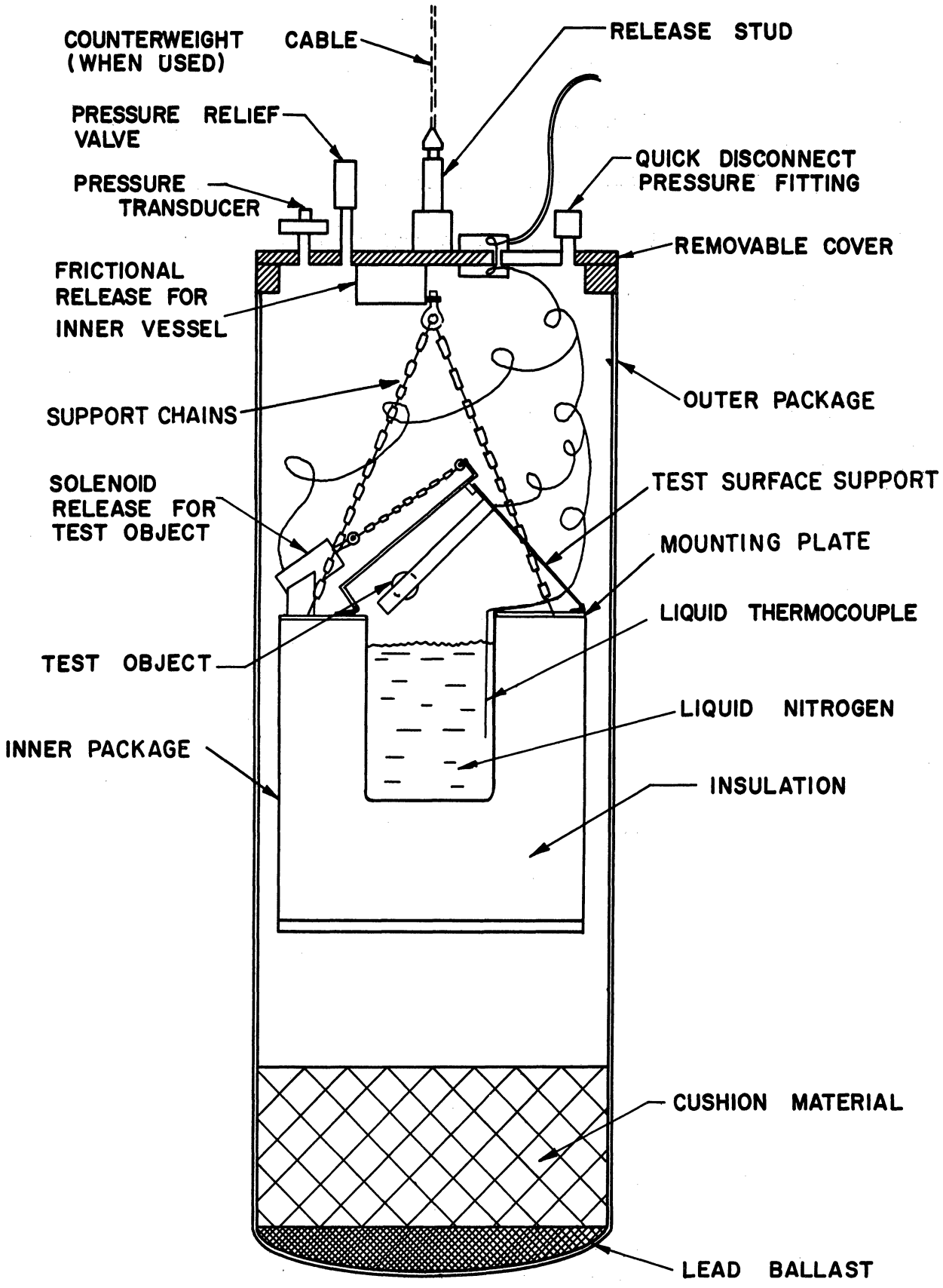

Fig. 5. Second test package.

The initial weight of the combined inner and outer package was approximately 75 pounds, which was too low to provide acceptable initial impact behavior with the buffer system. No further modifications were practical with the existing buffer system, so sufficient ballast was added to the outer package to bring the total weight up to approximately 135 pounds.

The removable cover of the outer package was made in two sections. One section provided access to the interior of the package, and the other section provided a mounting location for fittings, connections, and instrumentation. Pressure was controlled through a quick-disconnect pressure fitting and a pressure relief valve, and monitored with a strain gauge type pressure transducer. A view of the cover showing the pressurizing hose attached to the quick-disconnect fitting is shown in Fig. 6.

For fractional gravity tests, the inner package is placed on the cushion material in the bottom of the outer package. This cushioning serves to reduce the impact felt by the inner package when the outer package first contacts the buffer.

For free-fall tests the inner package is positioned midway between the top and bottom of the outer package by means of the support chains. The upper ends of these chains are fastened to the bottom of a T-shaped bar which in turn rests on a spring-loaded friction catch. When the outer package is dropped, the force between the T-bar and the catch goes to zero, and the spring retracts the catch. This allows the inner package to float freely within the outer package.

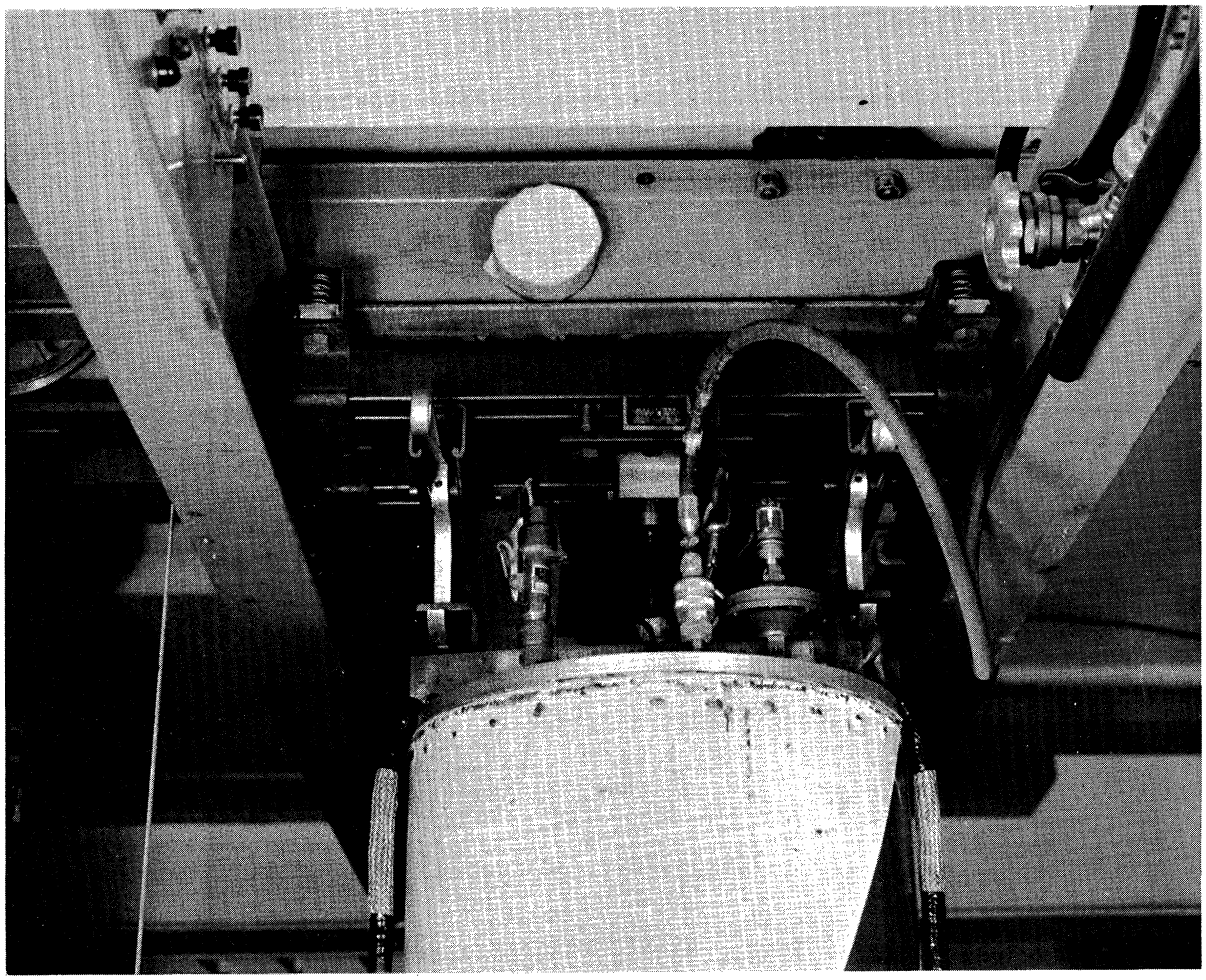

Fig. 6. Pressure cover on second test package.

The position of the inner package relative to the outer package was monitored during several drops, and it was observed that the inner package moved up about one inch during the drop. This was attributed to an initial upward impetus supplied by the elastic energy in the support chains as the load decreased to zero. The relative motion downward which was anticipated due to increasing air drag did not become large enough to overcome this initial upward motion during the 1.4 seconds of free fall which were available. This relative motion had no effect on the measured value of (a/g).

D. TEST SURFACES

Previous work by Merte, et al.,[19] had established the feasibility of using a 1-inch diameter copper sphere as a dynamic calorimeter in boiling liquid nitrogen at one atmosphere. This was chosen as the first test surface here for its inherent symmetry. In order to determine whether there were any size effects with a sphere, 1/2-inch and 1/4-inch diameter copper spheres were also tested. Although a limited amount of testing at one atmosphere was performed with the 1/2-inch diameter sphere, most of the sphere tests were performed with the 1-inch and 1/4-inch diameter spheres.

The 1-inch and 1/2-inch diameter spheres were supported on 1/16-inch diameter stainless steel rods (see Fig. 7), and the 1/4-inch diameter sphere was supported by its thermocouple wires. The 1-inch diameter sphere had three thermocouple holes drilled into it. One was used for a direct measuring junction at the upper surface, one for a differential thermocouple 90° along the surface from the direct measuring junction, and one for a dif-

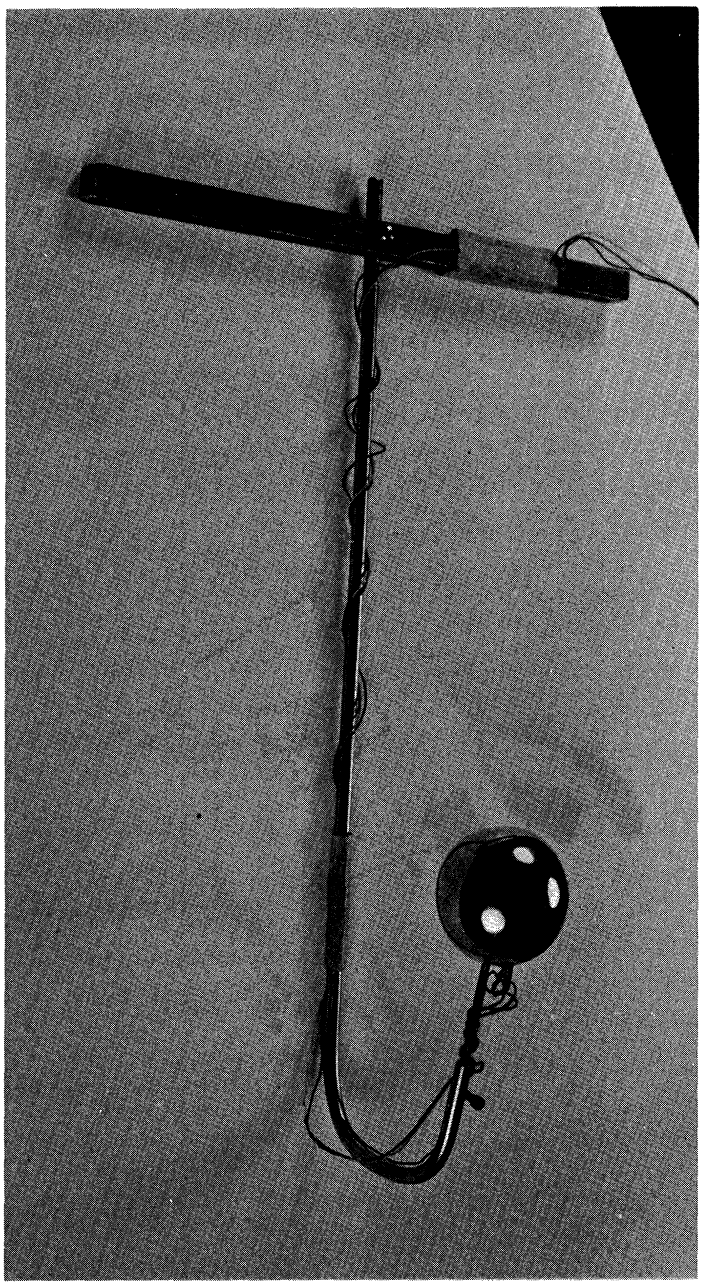

Fig. 7. View of 1-inch diameter sphere with stainless steel support rod.

ferential thermocouple at the center of the sphere. The differential thermocouples used the copper in the test object as the intermediate conductor between the junctions, and so were fabricated of a single 30-gauge constantan wire held in place by a drop of soft solder. They were used only to verify the accuracy of the lumped approximation or to indicate the surface-to-center differential temperature when a distributed analysis was necessary. The wiring schematic for the 1-inch diameter sphere is shown in Fig. 8. The 1/2-inch and 1/4-inch diameter spheres were provided with single direct measuring junctions only, and were otherwise similar to the 1-inch diameter sphere.

The thermocouples used consisted of 30-gauge copper and constantan wires spark welded together and fastened to the bottoms of the drilled thermocouple holes with soft solder. A piece of polyethylene tubing was slid over each pair of thermocouple leads down to the bottom of the drilled holes. The tubing extended a short distance from the sphere surface, where individual pieces of tubing were placed around each wire. The thermocouple holes were sealed with Glyptal, as were the plastic sleeve joints. The tubing served to prevent heat conduction from the thermocouple junctions to the liquid nitrogen through the wire itself, and to provide extra strength in the region where thermocouple wire breakage was most probable.

Much of the experimental data and analyses presented in the literature for boiling heat transfer apply to flat surfaces. To determine what geometrical effects, if any, existed in conjunction with reduced gravity, a disk 3 inches in diameter and 13/16 inch thick was fabricated. The diameter was

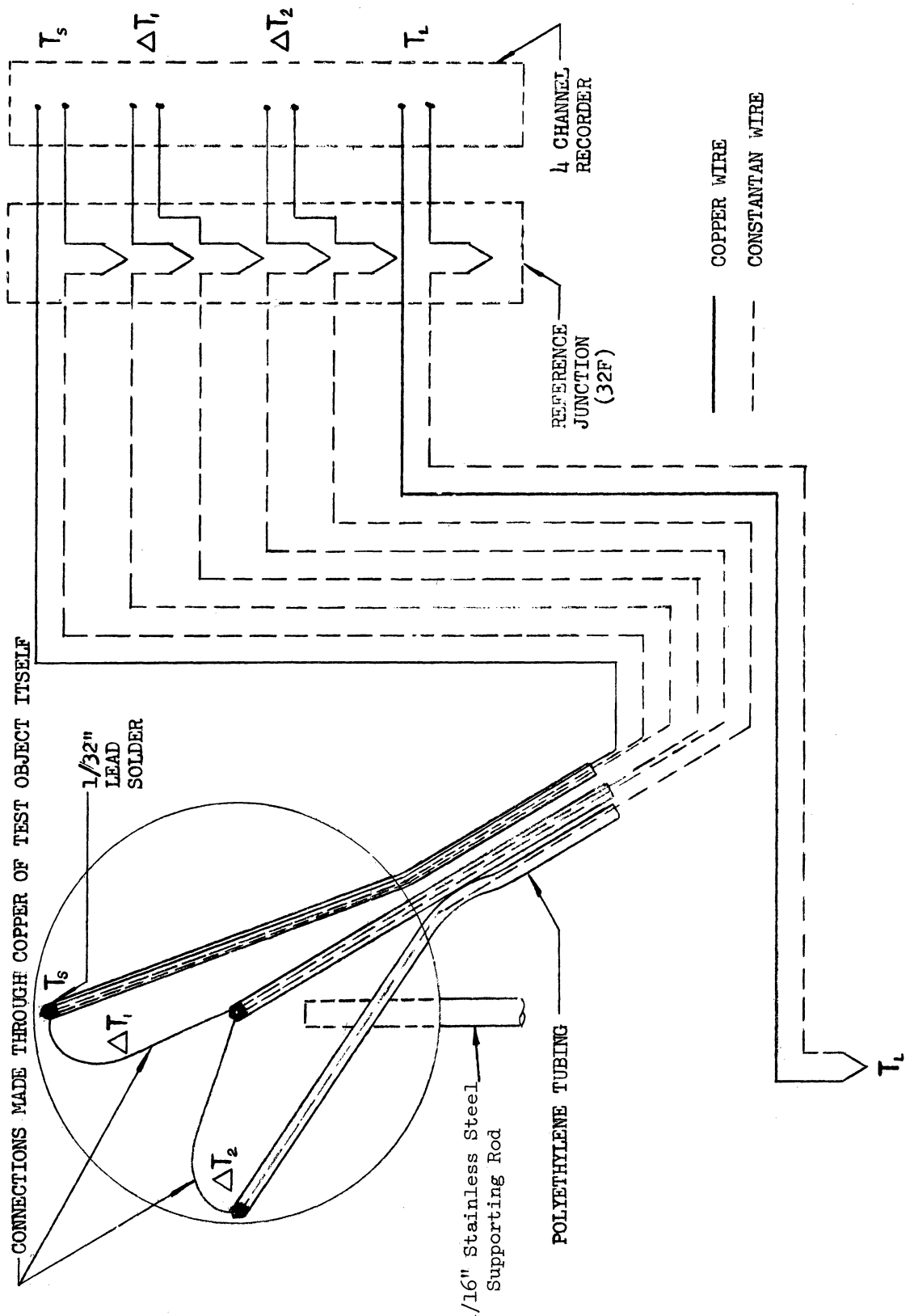

Fig. 8. Wiring schematic of 1-inch diameter sphere.

as large as could be fitted into the 3-liter beaker while preserving sufficient clearance between the test surface and the beaker to prevent the presence of the beaker from affecting the boiling from the disk. The thickness was a compromise between the desired total heat capacity and the undesired temperature differentials within the disk. The disk could be positioned in any orientation, so that possible differences in heat transfer characteristics between horizontally oriented and vertically oriented flat plates could be investigated.

Electrolytic tough pitch copper was chosen as the material for all test surfaces because its properties were well documented down to temperatures below that of saturated liquid nitrogen at one atmosphere. Because of the relatively high thermal conductivity of copper, it was possible to treat the entire test objects as lumped systems in the film-boiling region. In other boiling regimes it was necessary to consider each test object individually to determine whether the lumped approximation was acceptable (see Appendix D).

It was originally intended that radial thermal isolation be provided for the disk test surface by machining several narrow, deep concentric grooves in the underside of the test surface. The machining properties of the electrolytic tough pitch copper made this impossible with the available machine tools, so an alternate gridwork pattern was chosen, as shown in Fig. 9. This figure shows only the test surface portion of the disk; a disk of similar size and construction is attached to the backside to provide a plane of symmetry and to prevent the liquid nitrogen from contacting the

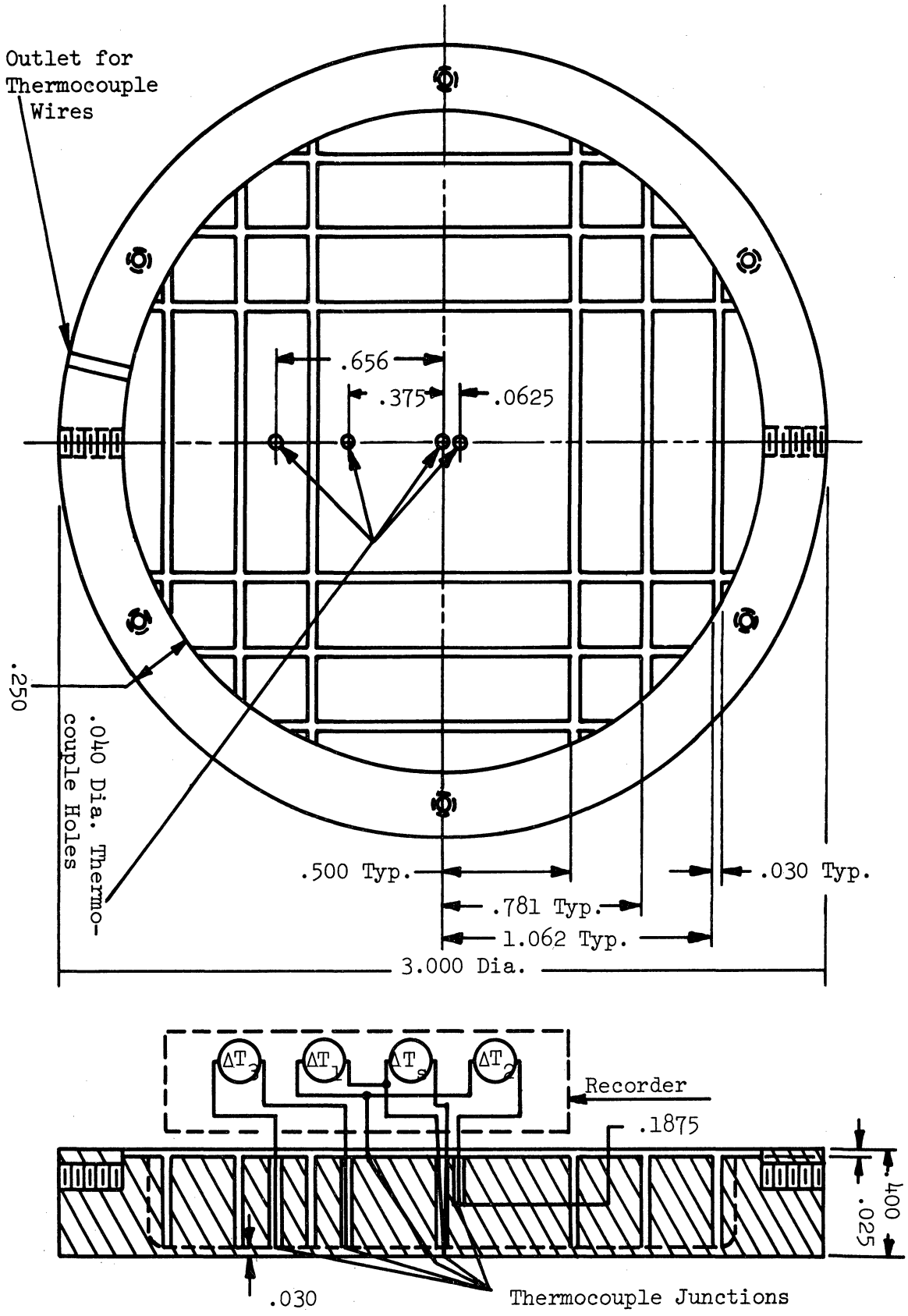

Fig. 9. Disk for transient heat transfer measurements.

thermocouple junctions directly. A small gap at the center plane further isolates the two disks. Five thermocouple locations were provided as indicated. One was a direct-measuring junction located at the center of the test surface. The other four were differential thermocouples located as shown in Fig. 9. The differential thermocouples were used only to verify the validity of the lumped approximation in the film-boiling region. Copper and constantan thermocouples, spark welded together and fastened in place with soft solder, were used.

The disk was supported at two places on the periphery by stainless steel straps. Any desired test surface orientation (e.g., horizontal heating up, horizontal heating down, or vertical) could be achieved by using the appropriate straps.

E. INSTRUMENTATION

1. Recording Equipment

A Sanborn Model 150 four-channel recorder was used for recording thermocouple, accelerometer, and pressure transducer outputs. This recorder has interchangeable preamplifiers so that low-level preamplifiers, AC-DC preamplifiers, or DC coupling preamplifiers could be used depending on the recording requirements. All of these preamplifiers are equipped with zero supression. The maximum sensitivity possible with the low-level preamplifiers used for thermocouple output recording was 10 μv/mm. At liquid nitrogen temperatures one mm corresponds to approximately 1°F when operating with maximum sensitivity.

To minimize the influence of possible drift in the recording system during a test, it was calibrated against a Leeds and Northrup 8662 potentiometer immediately before and after every test.

The four channels were normally used for recording test surface temperature, pressure in the outer test package, and two test fluid temperatures. The test fluid bulk temperatures were measured at two different levels to verify that the fluid was at a uniform temperature throughout, and also that the test fluid free surface was at least 1 inch above the top of the test object. The Sanborn recorder also has provisions for placing a timing mark on the record and this provided the time base for data reduction. Other signals indicating events such as duration of current flow (see Fig. 12) or solenoid operation can be superimposed on this timing record (see bottom trace, Fig. 12).

2. Pressure Transducer

A strain-gauge type force transducer was used to measure pressure within the outer package. A dial face pressure gauge was calibrated to within ±0.2 psi using a dead weight tester, and the pressure transducer was then calibrated against the pressure gauge. The nominal operating range of the transducer is 0-100 psig.

3. Accelerometer

A Kistler Model 303 Servo-Accelerometer was used to monitor the package accelerations under both fractional gravity and free fall. The output from the accelerometer was a voltage which was recorded on the Sanborn re-

corder with the pressure and temperature records. The accelerometer was not used on every test but only on a series of acceleration tests which were used to verify the gravity levels for each of the counterweight masses tested. The maximum resolution achievable in measuring (a/g) with the accelerometer in the range of zero gravity was of the order of ±0.001. This limitation was imposed by the noise level in the recording system including any sixty-cycle pickup.

Calibration of the accelerometer was achieved by means of a special calibration fixture constructed specifically for this purpose. The calibration fixture permitted accurate and repeatable positioning of the accelerometer over all relative positions of the measuring axis of the accelerometer and the normal gravity vector. Thus (a/g) imposed on the accelerometer could be varied from +1 to -1. A zero value of (a/g) was imposed by placing the accelerometer at 90° to the normal gravity vector.

The voltage output from the accelerometer under calibration conditions varied from +5. to -5. volts DC. In order to avoid potential damage to the galvanometer in the Sanborn due to excessive voltage inputs when operating at maximum sensitivity, a set of limiting diodes was installed in the system. These limited the voltage which the Sanborn could see to a level which would not overload the galvanometer. It was possible to change the level at which these limiting diodes acted so they could be used at the various fractional gravity levels (where the galvanometer was operating at reduced sensitivity) as well as at free-fall conditions.

4. High-Speed Camera

Many photographic studies have been made of the boiling phenomenon, but most of these are studies of boiling from horizontal or vertical plates or wires. In order to aid in the understanding of boiling on a horizontal plate heating down and on a sphere, some additional photographic coverage was indicated.

A high-speed framing camera (Dynafax Model 326) manufactured by the Beckman and Whitley Company was utilized to obtain photographs of the boiling process at (a/g) = 1. This camera has a continuously variable framing rate ranging from 200 to 26,000 frames per second; a nominal value of 1000 frames per second was found to provide the best results for this application and was used for all the data presented here. A maximum of 224 frames could be obtained on one film strip.

A sketch of the test setup utilized is shown in Fig. 10. The water and flat glass around the dewar eliminated most of the view distortion caused by diffraction and substantially reduced radiant heating of the liquid nitrogen by the high intensity lights. The black felt provided good photographic contrast for the test objects.

The exposures appeared as two parallel sequences with 16 mm film spacing on a single strip of 35 mm film. After developing, the film was slit and spliced to provide one strip of film suitable for use in a standard 16 mm projector. It was thus possible to examine the film-boiling phenomena both on a frame-by-frame basis and by continuous projection.

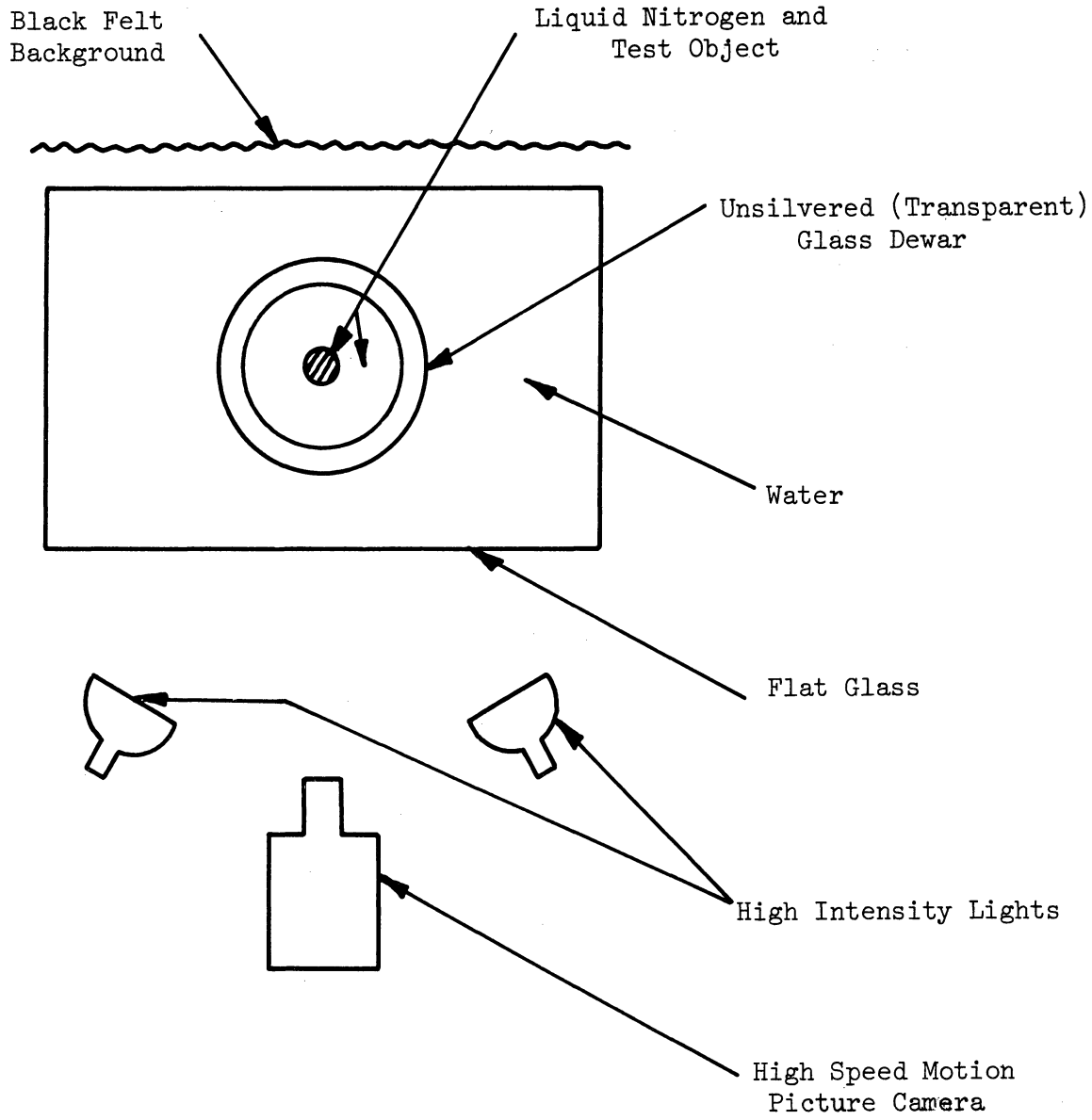

Fig. 10. Sketch of test setup for obtaining high-speed motion pictures.

CHAPTER III

TEST CONDITIONS

Liquid nitrogen was used as the test fluid for this investigation because it is an inexpensive, readily available, easy to handle cryogenic liquid with well known physical properties. It was stored in a dewar at one atmosphere saturation conditions (-321.2°F at 14.7 psia).

The effects on boiling heat transfer of varying (a/g) between 0 and 1 have been reported by Merte, et al.,[19] for the 1-inch diameter sphere with saturated liquid nitrogen at one atmosphere using the first test package. Values of (a/g) of 1.0, 0.6, 0.33, 0.2, and free fall (for these tests, free fall corresponded to $0.01 \leq (a/g) \leq 0.03$) were used. A predictable change in heat transfer rates at a given ΔT_{sat} was observed to occur for (a/g) between 0.2 and 1.0. Therefore, only one value of (a/g) between 0 and 1 was chosen for the present investigation. The value chosen was obtained by using the empty counterweight, and was found to vary with both the test package and the test object. The experimentally measured values were: with the first test package and a spherical test surface, (a/g) = 0.20; with the second test package and a spherical test surface, (a/g) = 0.17; with the second test package and a flat test surface (disk), (a/g) = 0.16. These variations occurred because of the differences in weights of the two test packages and of the different test objects. The free-fall tests performed using the second test package provided measured levels of (a/g) of 0.001 ± 0.001.

In order to perform tests using subcooled liquid, it was necessary to raise the saturation temperature of the nitrogen without raising the bulk temperature. This was accomplished by pressurizing the second test package. After pressure testing the second test package to 100 psig, it was decided to limit test pressures to 60 psig, or 5 atmospheres absolute. This provided a maximum subcooling of approximately 32°F. An intermediate value of 30 psig, or 3 atmospheres absolute, provided a maximum subcooling of approximately 20°F. In practice, considerable deviation from these maximum values was observed. The bulk temperature of the liquid nitrogen was monitored at two different locations during each test, and it was found that the liquid frequently increased in temperature a few degrees between the time that pressurization was completed and the time that the test was actually run. Some of the reasons for this are the convective heat transfer between the relatively warm gas in the test package and the liquid nitrogen, and the fact that when the test object is placed into the liquid nitrogen, the vapor created at the surface of the test object recondenses into the bulk liquid, with a corresponding addition of heat to this liquid. When the test object was the 1-inch or 1/4-inch diameter sphere, the liquid was within a few degrees of the nominal maximum possible subcooling. With the disk, because of its larger thermal mass, some nominally subcooled tests were made with the liquid nitrogen within a few degrees of saturation temperature, and saturated liquid temperature measurements indicated significant amounts of superheat in a few cases. The degree of subcooling was approximately constant during a test run with the exception of the full temperature range

(a/g) = 1 data where, particularly in the case of the disk, as much as 18° variation in indicated subcooling was observed. The exact subcooling, or range of subcooling, for each test is included in Appendix A. Nominal values of 15°F at 3 atmospheres and 25°F at 5 atmospheres were observed for most tests.

To determine which observed changes in boiling characteristics were due solely to subcooling effects and which were due to pressure variation, all subcooled tests were repeated at the same pressures under saturated conditions.

When gaseous nitrogen was used to flush out the test package and pressurize the liquid nitrogen, it reached equilibrium at the new saturation conditions in approximately 5 minutes, aided by condensation of the pressurizing gas. When the vessel was first flushed and then pressurized with gaseous helium, the liquid temperature increased very slowly toward the new equilibrium point, so that saturation conditions were not reached for almost 30 minutes. Consequently, helium gas was used as the pressurizing medium for all subcooled boiling tests, and nitrogen gas was used as the pressurizing medium for all saturated boiling tests at elevated pressures.

Six different test surfaces were employed during the testing: the 1-inch, 1/2-inch, and 1/4-inch diameter spheres, and the 3-inch diameter disk in the vertical, horizontal heating up, and horizontal heating down positions. All of the available combinations of (a/g), subcooling, and pressure were not used with every test object. The conditions under which heat transfer data were obtained for the various test surfaces are summarized in

Table I. For the disk, only film boiling data are reported, although a few runs were made in the nucleate boiling region. The difference between the first test package and the second test package is significant only for free fall, where a large difference in the measured values of (a/g) exists.

The high-speed photographs which were obtained of the boiling phenomena were limited to one atmosphere saturated conditions at (a/g) = 1 using liquid nitrogen. The photographs were taken because of questions which arose after examination of the film-boiling heat transfer results with the disk, so the disk was photographed in the vertical, horizontal heating up, and horizontal heating down positions. The 1-inch diameter sphere was photographed to provide film boiling coverage for another geometry for comparison purposes. Separate sequences were obtained for each test surface at values of ΔT_{sat} of 100°F, 200°F, and 300°F.

TABLE I

SUMMARY OF TEST CONDITIONS

Test Object	P, atm: a/g:	1, Saturated					3, Saturated			3, Subcooled			5, Saturated			5, Subcooled		
		1.0	0.6	0.33	0.2*	0	1.0	0.2*	0	1.0	0.2*	0	1.0	0.2*	0	1.0	0.2*	0
1-inch sphere		x[2]	x[1]	x[1]	x[1]	x[2]	x	x	x	x	x	x	x	x	x	x	x	x
1/2-inch sphere		x[1]				x[1]												
1/4-inch sphere		x			x	x	x	x	x	x	x	x	x	x	x	x	x	x
Disk, heating up		y			y	y							y	y	y	y	y	y
Disk, heating down		y			y	y							y	y	y	y	y	y
Disk vertical		y			y	y	y	y	y	y	y	y	y	y	y	y	y	y

Note: Data obtained using second test package except as indicated:

x - includes some data in the transition, peak and/or nucleate boiling region as well as film boiling data

y - film boiling data only

*a/g value of 0.2 includes data at 0.16 and 0.17 as well.

[1]Data taken with first test package.

[2]Data taken with both first test package and second test package.

CHAPTER IV

TEST PROCEDURES

One test or test run includes all of the operations necessary to obtain one time vs. temperature record for a test surface which has been immersed in liquid nitrogen. A standardized test procedure was prepared with appropriate modifications to satisfy individual test requirements. Operations common to all tests included cleaning and preparation of the test surface, instrumentation calibration, and test surface immersion. Tests under fractional gravity required the use of the counterweight system with the inner test package attached to the outer vessel. In the free-fall tests the inner test package is suspended within the outer vessel prior to being dropped. Pressurized tests required flushing and pressurizing of the outer vessel. At the beginning of each day's testing, the test surface was cleaned using copper polish to remove any tarnish or other corrosion. Additional treatment was limited to careful washing of the test surface with reagent grade acetone prior to each test to remove any contamination deposited by handling. At completion of a test the test object was at liquid nitrogen temperature and had to be heated to room temperature before another test could be made. A jet of high-pressure line air was directed on the surface of the test object to hasten this heating. The 1/4-inch diameter sphere did not require this assistance to return it to room temperature rapidly.

A Leeds and Northrup 8662 potentiometer, which was calibrated against an internal standard cell every hour during testing, was used to supply a

voltage source for calibration of the instrumentation. A resistor in each circuit used for thermocouple calibrations was adjusted to duplicate the resistance of the thermocouple wires, so that the voltage drop from the 8662 potentiometer was matched to that from the thermocouple. This calibration procedure was performed immediately before and immediately after every test for every thermocouple being used. Normally the calibrations were consistent; when they were not, the average of the two calibrations at each increment of voltage was used if the changes were minor, or the test was discarded.

The pressure transducer provided a linear voltage-pressure relationship over its operating range, so standard settings on the Sanborn recorder were used to provide the required calibrations for each run. Pressure was also calibrated immediately before and immediately after each run.

The accelerometer was calibrated using the calibration fixture as described in Chapter II. It was necessary to include a voltage limiting diode circuit in the output from the accelerometer. If the voltage to the Sanborn recorder were not limited, the internal galvanometer would be subjected to excessive current flow at (a/g) = 1 and upon impact with the recorder set at the desired sensitivity level to monitor the fractional gravity or free fall. Potential damage to the pen or the galvanometer windings was prevented by use of the voltage-limiting circuit.

The accelerometer was used only on dummy runs (no other instrumentation functioning, although physical similitude was maintained) to establish the value of (a/g) for each particular combination of test package, test object, and (if used) counterweight. All four channels of the Sanborn recorder were

required for other variables (three temperatures, one pressure) during the test runs.

Time reference was supplied by a pen deflection which occurred every 60 cycles of line current. The recorder strip chart velocity was assumed to be constant between pen deflections as long as the deflections were equally spaced (this was the case except for a starting transient when the chart drive was initially engaged).

Preparation for a test was initiated by filling the stainless steel beaker with liquid nitrogen from a portable 25-liter dewar. The test surface was cleaned with reagent grade acetone, and placed in position for immersion in the nitrogen. For a free-fall test, the inner package was suspended from the spring-loaded pawl attached to the outer test package. For a fractional gravity test, the inner package was placed on the bottom of the outer test package. The thermocouples and the pressure transducer were calibrated. The pressure relief valve was placed in the open position and the cover on the outer package was bolted down. The test package was raised to its release position using the hoist, and the release stud was engaged in the solenoid operated release mechanism. The hoist cable was detached and the package was ready for either pressurization or immersion of the test object.

The liquid nitrogen was initially at one atmosphere saturated conditions. For elevated pressure saturated tests, dry gaseous nitrogen was used as the pressurizing medium. The pressure was monitored and maintained within ±1 psi of the desired pressure until the liquid temperature (also monitored) stabilized at saturation. Saturation conditions were verified

by comparing the actual and tabulated saturation temperatures for the desired pressure, and by observing that a small change in test package pressure was accompanied by a small change in liquid temperature. The system was then ready for immersion of the test object.

For subcooled tests, dry gaseous helium was used as the pressurizing medium. As soon as the desired pressure was reached, the system was ready for immersion of the test object.

The test object was then immersed in the liquid nitrogen. For the pressurized tests, the pressure was continuously monitored and maintained at the desired level ±1 psi. Shortly before the anticipated drop time, the Sanborn chart drive was engaged, and when the test surface reached a predetermined temperature, the test package was released. After the package impacted on the buffer, the chart drive was disengaged and the instrumentation recalibrated.

For the high-speed motion pictures of film boiling at $(a/g) = 1$ the flat walled glass tank (Fig. 10) was filled with water and the unsilvered glass dewar filled with liquid nitrogen. Illumination and camera focus were checked, and the thermocouple recorder was calibrated.

The high-intensity lights were not turned on until the test object had been placed in the liquid nitrogen, to limit radiant heating. When the test surface temperature reached a predetermined level, the camera shutter was opened. The exposure time used provided 60 to 80 frames of film boiling. The remainder of the unexposed frames were used to photograph the nonboiling state, immediately following the run, and served to indicate the precise

location of the heater surface, which was obscured while boiling was taking place.

CHAPTER V

DATA REDUCTION

The following sections describe the techniques used in obtaining from the raw data the numerical values of time, temperature, pressure, acceleration, saturation temperature, heat flux, Nusselt number, and modified Rayleigh number. The procedure used in reducing the photographic results is described. Also included for each measured parameter is an estimate of the errors involved.

A. TIME

Time was obtained on a relative basis only and was used as a reference and correlating parameter. All data (except photographic) are referred to a zero reference time which was taken as occurring 3.8 seconds before test package impact when the data permitted. This allowed up to 2.4 seconds of $(a/g) = 1$ data to be reduced in addition to the free fall or fractional gravity data. The time indication was provided by timing marks on the Sanborn recorder (Figs. 11 and 12).

The location of the timing mark on the strip chart could be read to within ±0.2 mm. At the normal chart speed of 100 mm/second, this corresponds to ±0.002 second. It was necessary to interpolate between the 1-second marks to obtain the times at which the temperatures were read. These intervals varied from 0.2 second in the film-boiling region to less than 0.05 second in the peak heat flux region. The intervals used were chosen so that

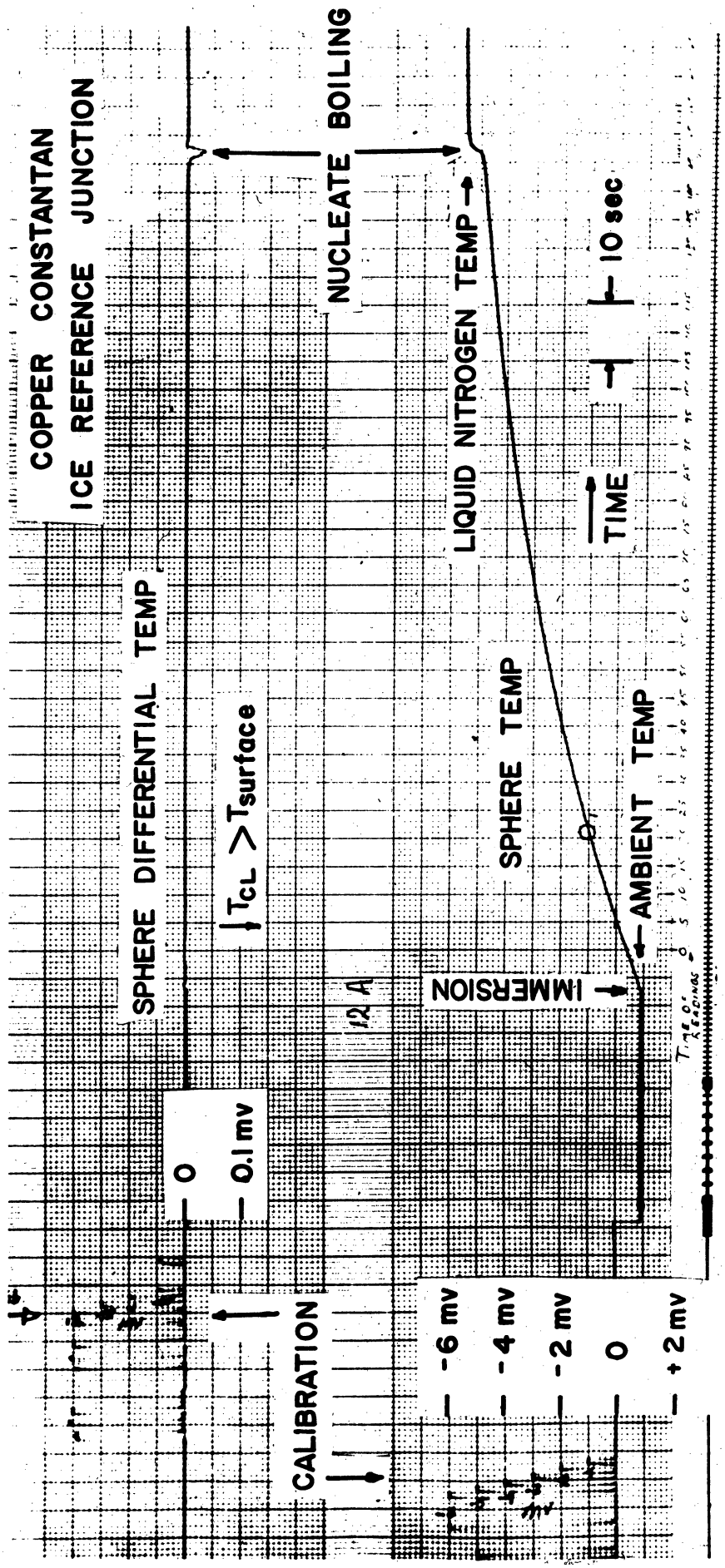

Fig. 11. Typical oscillographic record of temperatures within 1-inch diameter copper sphere with film boiling of liquid nitrogen. (a/g) = 1.

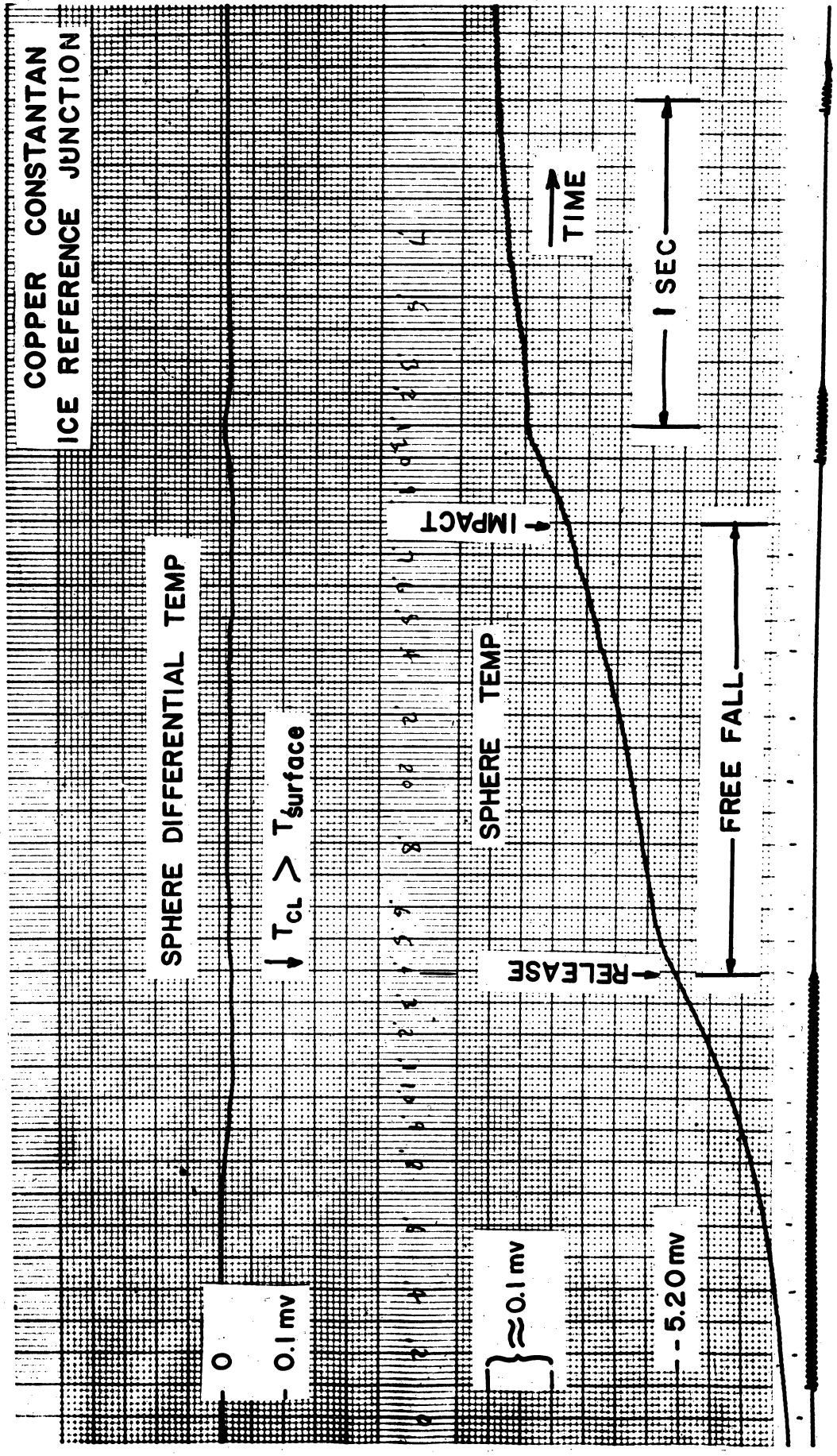

Fig. 12. Typical oscillographic record during free fall with nucleate and transition boiling. (a/g) ≈ 0.

for each interval the value of ΔT_{sat} (see Section V.F) was approximately constant, but with no interval longer than 0.2 second. These interval marks could be read to within ±0.2 mm, or ±0.002 second. The maximum error possible in time determination is ±0.005 second, but probably will not exceed ±0.003 second.

B. TEMPERATURE

The output from the various thermocouples was recorded on Sanborn charts in the form of pen deflection vs. time (see Figs. 11 and 12). The recorder was calibrated for the millivolt range of interest both before and after the test run. These calibration marks are recorded as deflections which correspond to the various calibration voltages, and thus to the thermocouple temperatures which would produce those voltages. The deflections corresponding to the millivolt calibrations and data are measured and recorded as a function of time and converted to temperature values using the thermocouple calibration curve derived for the thermocouple wire which was used.

One roll each of copper and constantan 30-gauge thermocouple wire had been obtained and calibrated with a nitrogen vapor pressure cryostat, at the CO_2, and mercury freezing points, and the steam point. The calibration for these particular wires, rather than the standard copper-constantan conversion tables, was used for all data reduction. All thermocouples were made from these two rolls of wire.

Sanborn recorder pen deflections could be determined to within ±0.2 mm, which corresponds to approximately ±0.2°F at liquid nitrogen temperatures

when the recorder is operating at maximum sensitivity. This is taken to be the error in relative temperature measurements. To determine the error in absolute temperature measurement, liquid nitrogen temperature measurements were made during every test series at one atmosphere, saturated conditions. The local pressure was obtained from a barometer, and the saturation temperature of the liquid nitrogen was determined from tables[37] to the nearest 0.1°F. The measured value of the liquid nitrogen temperature did not deviate from the calculated temperature by more than ±0.5°F, including reading errors as discussed above. This value, ±0.5°F, is taken to be the maximum error in absolute temperature determination.

C. PRESSURE

The pressure transducer was calibrated to within ±0.5 psi at 30 psig and 60 psig, which were the nominal values for the elevated pressure tests. The Sanborn recorder pen deflection was read to within ±0.2 mm, which corresponds to ±0.2 psig at 30 psig, and ±0.4 psi at 60 psig. The pressure at which a run started was regulated manually to within ±1 psi of the nominal pressure, and an attempt was made to keep the pressure on the low side of this range at the start of the test.

The duration of a test during fractional gravity conditions was so short (< 2 seconds) that regulation of pressure during this interval was not considered necessary, since the relatively large volume of the container served to minimize the potential pressure rise due to vapor generation. Pressure increased between the time that the relief valve was closed and the time that

the test package was dropped, and values of this increase were as much as 1 psi at 30 psig and 2 psi at 60 psig. Measured values of pressure therefore varied from 43.3 psia to 46.3 psia at a nominal 3 atmospheres (44.1 psia). The average value of the pressure measured during a run was used for calculations for that particular run.

D. SATURATION TEMPERATURE

The saturation temperature was determined as a function of the pressure at the time of measurement. When saturated liquid tests were being run it was possible to check the tabulated value for that pressure[37] against the value indicated by the liquid thermocouples. These values were found to agree within the ±0.5°F indicated above for thermocouple error in absolute temperature determination. For subcooled tests it was not possible to determine saturation temperature independently by the thermocouple measurements, so it was necessary to use the tabulated value corresponding to the measured pressure in the test vessel. Based on the results obtained under saturated conditions, the determination of saturation temperature under subcooled conditions is estimated to have the same error, i.e., ±0.5°F.

The value of $T_s - T_{sat}$, or ΔT_{sat}, is subject to ±0.5°F errors in the determination of both T_s and T_{sat}, so that the maximum error in ΔT_{sat} is ±1°F.

E. ACCELERATION

The fixture used to calibrate the accelerometer measured the angle between the normal gravity vector and the sensitive axis of the accelerometer.

The angular position was known to within ±0.0005 radian (position locations were accurate to within ±0.002 inch on the periphery of the calibration disk, which is 10 inches in diameter) and the direction of the normal gravity vector was determined to within ±0.0005 radian (checked against spirit levels and the accelerometer itself, which has maximum positive voltage output at (a/g) = +1 and maximum negative voltage output at (a/g) = -1).

The acceleration measured by the accelerometer is equal to the product of the normal acceleration and the cosine of the angle between the normal acceleration vector and the sensitive axis of the accelerometer. The maximum error in the accelerometer measurement thus corresponds to a maximum error in (a/g) of ±0.001.

Two values of (a/g) were of primary interest: those corresponding to free-fall and to counterweighted drop utilizing the empty counterweight. The test package was prepared exactly as it would be for a normal data-taking run except that none of the pressure and temperature instrumentation was used. The accelerometer was installed and calibrated for the region of interest, with the sensitivity setting on the Sanborn recorder being determined by the region being investigated (higher sensitivity was required for free-fall tests).

Operation under free-fall tests revealed a noise level for the accelerometer-recorder system which corresponded to a level of (a/g) of 0.001, owing primarily to AC pickup. Reading errors in this range corresponded to a variation in (a.g) of ±0.0002. The value of (a/g) measured during free fall was less than the AC pickup, so it was read as 0.001±0.001, i.e., less than 0.002.

No AC pickup problem existed with the fractional gravity tests, and the error corresponded to a variation in (a/g) of ±0.001. The actual fractional gravity tests revealed periodic fluctuations about an average value of (a/g). These were attributed to a spring-mass type coupling of the counterweight and the test package with the steel cable acting as a spring. This problem is discussed in more detail in Appendix E. Reading and calibration errors were negligible compared with these oscillations, which limited the accuracy of the determination of (a/g) to approximately ±0.01 in the range of (a/g) of 0.17.

F. HEAT FLUX

Heat flux, or (q/A), was determined from a combination of the properties of the test object and the quantities measured during the tests. A first law analysis assuming a lumped system shows that the heat flux may be expressed as the time rate of enthalpy change of the test object, or

$$\frac{q}{A} = \frac{m}{A}\frac{dh}{dt} = \frac{\rho V}{A} C_p(T) \frac{dT}{dt} \quad . \tag{5}$$

The heat flux can be calculated from the slope of the cooling data (temperature vs. time) and the known body properties.

To determine the value of $C_p(T)$ the experimental data for pure copper were plotted as C_p vs. T. A curve was fitted to these data (Fig. 13) and C_p was read directly as a function of T. The maximum deviation between the two sets of experimental data is estimated to be less than 5% below 200°R, and less than 2% above 200°R.

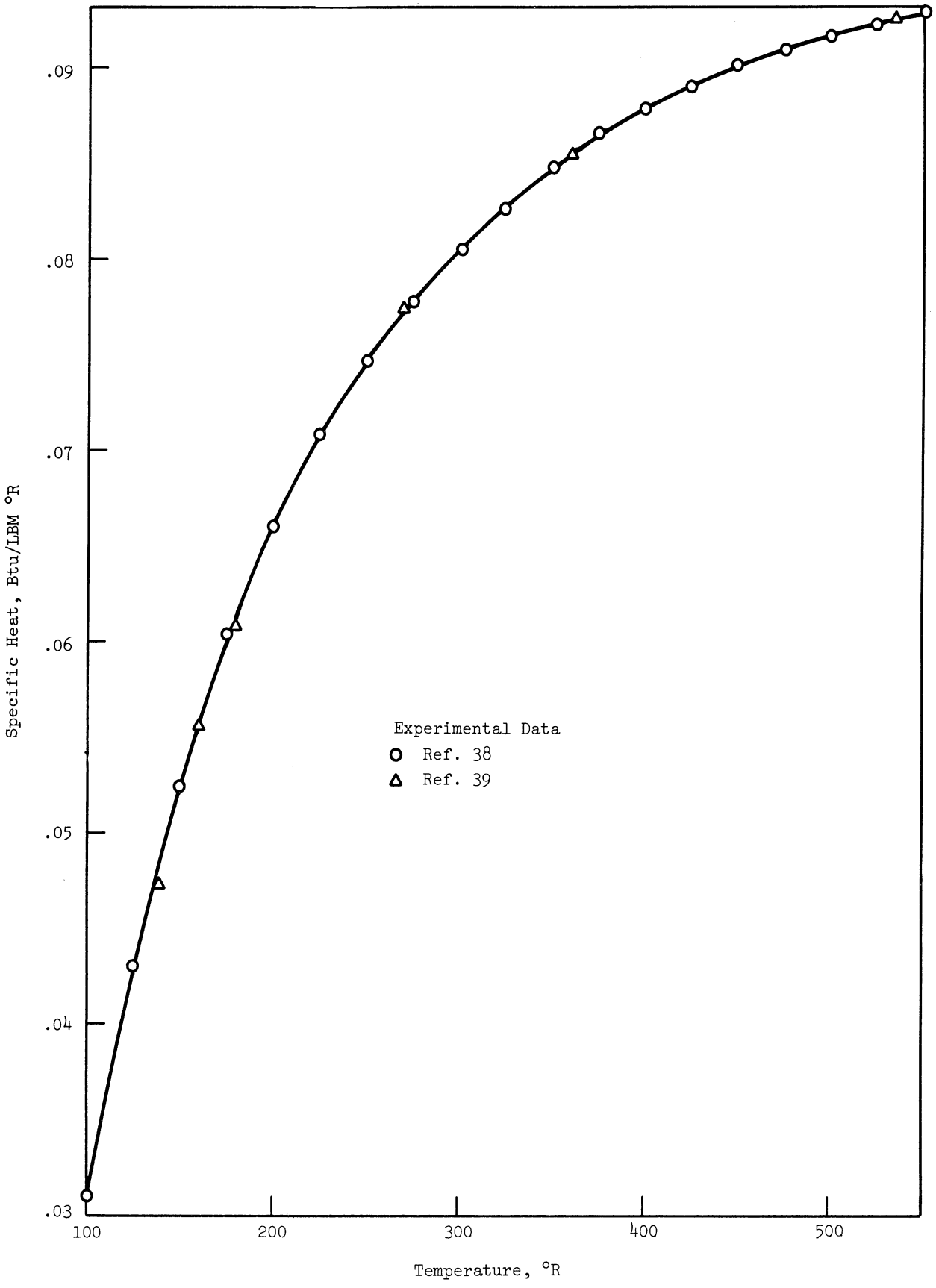

Fig. 13. Specific heat of copper.

A system usually may be treated as a lumped system when the Biot Number is very small (see Appendix D). In the film-boiling region, the Biot Number corresponding to the test objects used here has an order of magnitude of 0.005, so that the assumption of a lumped system in this region is reasonable. In the region near peak heat flux the value of the Biot Number approaches 0.5 and the system may no longer be treated as lumped. For this case it is necessary to use the form of Eq. (5) where (q/A) is expressed in terms of dh/dt, the rate of change of total enthalpy of the test object, since both T and $C_p(T)$ vary over the volume of the test object.

In the film boiling region the value of dT/dt ranges from 1 to 20°F per second, depending on the test surface geometry, size, and temperature. Only a small temperature change is covered in a single test with fractional gravity. The value of d^2T/dt^2 is very small in the film-boiling region in this short time interval, so that the value of dT/dt is considered constant for a particular value of (a/g).

In the transition and nucleate boiling region, the value of dT/dt was normally in the 10 to 50°F per second range (to 200°F per second for the 1/4-inch diameter sphere) and d^2T/dt^2 was also large. A much higher data sampling frequency was utilized in reducing these data, and the reduced data were punched into IBM cards. A computer program was written for the IBM 7090 to calculate the values of (q/A) as a function of ΔT_{sat}. The program treats the sphere as 10 concentric spherical segments and utilizes a finite difference technique to evaluate the rate of total enthalpy change of the entire system, using the measurements as input at the outer shell.

The calculated difference in the temperature of the sphere at the center and at the surface was found to be in good agreement with experimentally measured values in the peak heat flux region (typically of the order of 2 or 3°F). The program included as output a plot of input time vs. temperature data, a logarithmic plot of (q/A) vs. ΔT_{sat} (including a typical plot for the 1-inch diameter sphere at (a/g) = 1 for comparison purposes), and a plot of (q/A) vs. time. Samples of the input to the computer are shown in Fig. 14, and samples of the output from the computer are shown in Fig. 15. TOS-8 is the identification for the 1-inch diameter sphere. "R" indicates when the package was released. A flow diagram and listing of the program are included in Appendix D.

The error in the determination of (q/A) may be approximated by the errors in determining dT/dt. The value dT/dt is obtained by measuring the slope of the curve drawn through the time-temperature data points. In the film-boiling region, the dT/dt for the 1-inch diameter sphere and the disk were approximately equal, while the dT/dt for the 1/4-inch diameter sphere under the same conditions was approximately six times higher than it was for the 1-inch diameter sphere. The temperature could be read to ±0.2°F (see Section V.B), and the time could be read to ±0.003 second (see Section V.A).

The typical increments of temperature and time, regardless of test object or boiling region, produced a maximum error due to reading inaccuracies of ±20%. The (q/A) vs. ΔT_{sat} data were repeated within this range for most of the tests. Repeatability varied with the test object and boiling region.

RUN NO. 60G, 1/10/64, TOS-8, D G, HE PR. 45 PSIA, SUBCOOLING=17F

CALCULATION PARAMETERS

N4 = 45, N = 5, RO = 558.000000, VOA = .013889

DR = 4.167000E-03, TC = 290.000000, DS = 10.000000E-04, SM = 11

RZ = .041670, TSAT = -301.000000

TIME,SEC TIM(1)...TIM(45) RELEASE AT 0.51 SEC

.000000E+00	5.000000E-02	1.000000E-01	1.500000E-01	**2.000000**E-01	2.500000E-01	3.000000E-01	3.250000E-01
3.500000E-01	3.750000E-01	4.000000E-01	4.250000E-01	**4.500000**E-01	4.750000E-01	5.000000E-01	5.250000E-01
5.500000E-01	5.750000E-01	6.000000E-01	6.250000E-01	**6.500000**E-01	7.500000E-01	8.000000E-01	8.500000E-01
9.000000E-01	9.500000E-01	1.000000E+00	1.050000E+00	1.100000E+00	1.150000E+00	1.200000E+00	1.250000E+00
1.300000E+00	1.350000E+00	1.400000E+00	1.450000E+00	1.500000E+00	1.550000E+00	1.600000E+00	1.650000E+00
1.700000E+00	1.750000E+00	1.800000E+00	1.850000E+00	1.900000E+00			

TEMPERATURE, °F TEM(1)...TEM(45)

-2.584400E+02	-2.592500E+02	-2.602000E+02	-2.611800E+02	-2.623000E+02	-2.634800E+02	-2.649000E+02	-2.657600E+02
-2.666000E+02	-2.674600E+02	-2.684000E+02	-2.694000E+02	-2.704000E+02	-2.714000E+02	-2.724800E+02	-2.735500E+02
-2.746500E+02	-2.753000E+02	-2.770000E+02	-2.776800E+02	-2.780800E+02	-2.795800E+02	-2.801800E+02	-2.806500E+02
-2.810800E+02	-2.814800E+02	-2.816800E+02	-2.824000E+02	-2.829400E+02	-2.835600E+02	-2.842200E+02	-2.849800E+02
-2.856500E+02	-2.863000E+02	-2.869400E+02	-2.875600E+02	-2.880500E+02	-2.886000E+02	-2.892000E+02	-2.894200E+02
-2.897800E+02	-2.900800E+02	-2.904000E+02	-2.906200E+02	-2.908800E+02			

(a) Tabular input.

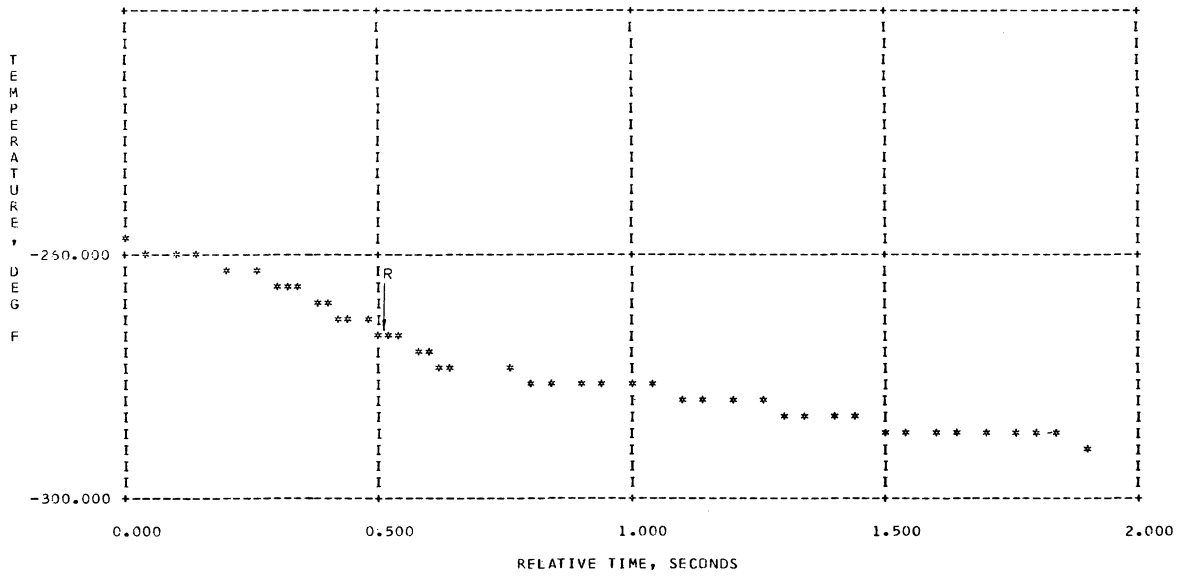

(b) Computer plot of input.

Fig. 14. Typical input to computer.

RUN NO. 60G, 1/10/64, TOS-8, O G, HE PR. 45 PSIA, SUBCOOLING=17F

ΔT_{SAT}, °F	DTT(1)...DTT(39)						
3.980273E+01	3.870377E+01	3.748254E+01	3.606267E+01	3.526641E+01	3.443182E+01	3.352295E+01	3.260134E+01
3.161106E+01	3.060602E+01	2.957911E+01	2.853042E+01	2.744999E+01	2.630710E+01	2.515055E+01	2.377785E+01
2.320514E+01	2.275236E+01	2.150197E+01	2.080997E+01	2.031088E+01	1.992554E+01	1.952208E+01	1.909059E+01
1.860385E+01	1.804663E+01	1.742474E+01	1.674701E+01	1.604855E+01	1.535707E+01	1.468774E+01	1.406399E+01
1.348287E+01	1.290273E+01	1.237276E+01	1.192025E+01	1.152394E+01	1.121276E+01	1.091942E+01	

(q/A), BTU/HR-FT^2	QAB(1)...QAB(39)						
2.545516E+04	2.792063E+04	3.128989E+04	3.703239E+04	3.714034E+04	3.876963E+04	4.088780E+04	4.278188E+04
4.514705E+04	4.588960E+04	4.698259E+04	4.803795E+04	4.904361E+04	5.183785E+04	5.246566E+04	5.095114E+04
3.387158E+04	2.446783E+04	1.723067E+04	1.521606E+04	1.208865E+04	1.005197E+04	9.852527E+03	1.058652E+04
1.201851E+04	1.350115E+04	1.495908E+04	1.625311E+04	1.653247E+04	1.607383E+04	1.561982E+04	1.476045E+04
1.350948E+04	1.329963E+04	1.252756E+04	1.046292E+04	8.420788E+03	7.528122E+03	7.201100E+03	

ΔT_{SAT}, °F	DATAX(1)...DATAX(39)						
3.980273E+01	3.870377E+01	3.748254E+01	3.606267E+01	3.526641E+01	3.443182E+01	3.352295E+01	3.260134E+01
3.161106E+01	3.060602E+01	2.957911E+01	2.853042E+01	2.744999E+01	2.630710E+01	2.515055E+01	2.377785E+01
2.320514E+01	2.275236E+01	2.150197E+01	2.080997E+01	2.031088E+01	1.992554E+01	1.952208E+01	1.909059E+01
1.860385E+01	1.804663E+01	1.742474E+01	1.674701E+01	1.604855E+01	1.535707E+01	1.468774E+01	1.406399E+01
1.348287E+01	1.290273E+01	1.237276E+01	1.192025E+01	1.152394E+01	1.121276E+01	1.091942E+01	

TIME, SEC	TIM(1)...TIM(45)						
.000000E+00	5.000000E-02	1.000000E-01	1.500000E-01	2.000000E-01	2.500000E-01	3.000000E-01	3.250000E-01
3.500000E-01	3.750000E-01	4.000000E-01	4.250000E-01	4.500000E-01	4.750000E-01	5.000000E-01	5.250000E-01
5.500000E-01	5.750000E-01	6.000000E-01	6.250000E-01	6.500000E-01	7.500000E-01	8.000000E-01	8.500000E-01
9.000000E-01	9.500000E-01	1.000000E+00	1.050000E+00	1.100000E+00	1.150000E+00	1.200000E+00	1.250000E+00
1.300000E+00	1.350000E+00	1.400000E+00	1.450000E+00	1.500000E+00	1.550000E+00	1.600000E+00	1.650000E+00
1.700000E+00	1.750000E+00	1.800000E+00	1.850000E+00	1.900000E+00			

(a) Tabular output.

Fig. 15. Typical output from computer.

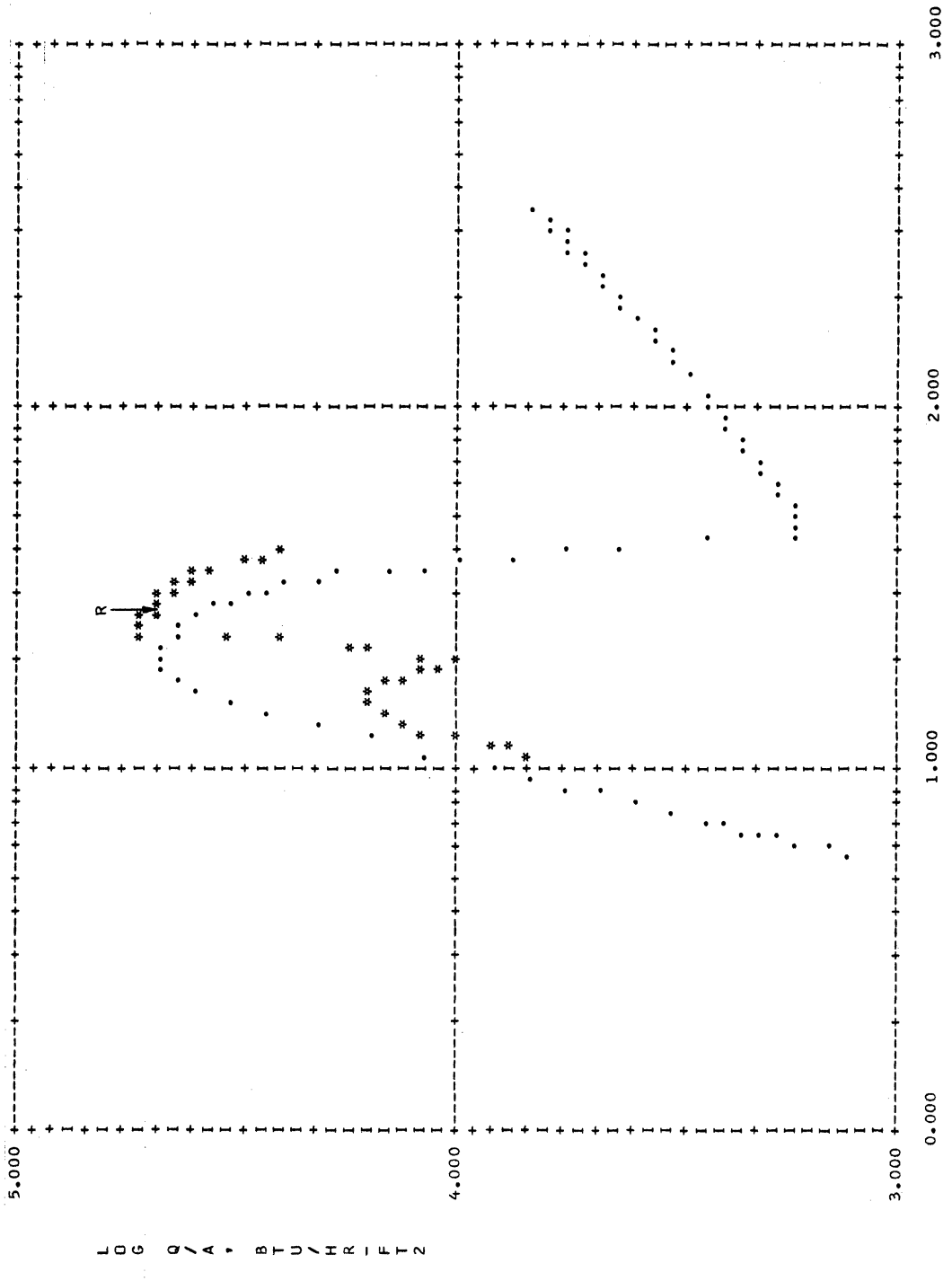

(b) Heat flux vs. ΔT_{sat}

Fig. 15 (Continued)

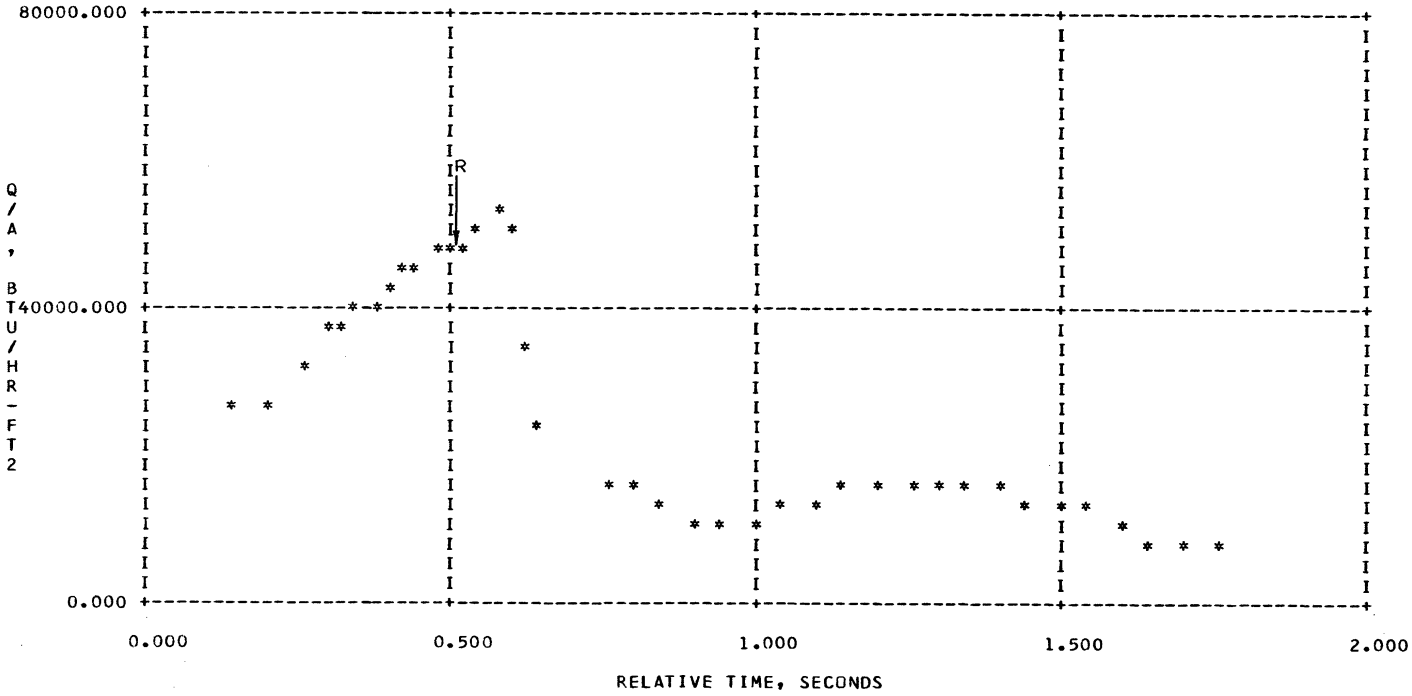

(c) Heat flux vs. time.

Fig. 15 (Concluded)

All 1-inch diameter sphere data and the 1/4-inch diameter sphere data with film boiling repeated within a few percent; the disk data seldom repeated to better than ±10%, and the nucleate boiling data with the 1/4-inch sphere varied by ±20% or more, due primarily to the very large rate of change of temperature.

G. NUSSELT NUMBER, Nu

The Nusselt Number, $(\bar{h}D/k)$, may be expressed in terms of the heat flux and ΔT_{sat} as follows:

$$Nu = \frac{\bar{h}D}{k_{vf}} = \frac{q/A}{\Delta T_{sat}} \frac{D}{k_{vf}} = \frac{q}{A} \frac{D}{k_{vf}\Delta T_{sat}} \tag{6}$$

The value of (q/A) was determined as indicated in Section V.F, D is a constant for each test object and k_{vf} and ΔT_{sat} are functions only of the temperature of the test surface at the point where the heat flux was evaluated. The term $1/k_{vf}\Delta T_{sat}$ was plotted as a function of ΔT_{sat}. For a given ΔT_{sat} and (q/A), the Nusselt Number was calculated using the appropriate value of the body parameter D.

H. MODIFIED RAYLEIGH NUMBER, Ra'

Natural convection heat transfer data may be correlated[1] by an equation of the form

$$Nu = C[Gr \cdot Pr]^n \tag{7}$$

$$= C\left[\frac{D^3\rho\beta(T_s-T_\ell)a}{\mu^2} \cdot \frac{C_p\mu}{k}\right] \tag{8}$$

where the product Gr·Pr is known as the Rayleigh Number, Ra, and β is the

coefficient of volumetric expansion. Frederking[40] has expressed the single phase Rayleigh Number as

$$Ra = \frac{D^3\rho(\rho_\ell-\rho)C_p a}{\mu k} \tag{9}$$

Bromley[27] correlated film boiling heat transfer data with an equation of the form

$$\bar{h} = C\left[\frac{h'_{fg}k^3_{vf}\rho_{vf}(\rho_\ell-\rho_{vf})a}{D\mu_{vf}\Delta T_{sat}}\right]^n \tag{10}$$

which can also be written as

$$Nu = C\left[\frac{D^3\rho_{vf}(\rho_\ell-\rho_{vf})a}{\mu^2_{vf}}\left(\frac{C_p\mu}{k}\right)_{vf}\left(\frac{h'_{fg}}{C_p\Delta T_{sat}}\right)\right]^n \tag{11}$$

or

$$Nu = C\left[Ra\,\frac{h'_{fg}}{C_p\Delta T_{sat}}\right]^n \tag{12}$$

The term in square brackets in Eq. (11) serves the same function in correlating film boiling heat transfer data that the Rayleigh Number serves in correlating natural convection heat transfer data, and therefore is referred to as a modified Rayleigh Number, Ra'. The term h'_{fg} takes into account a portion of the superheat in the vapor film as well as the heat required to vaporize the liquid, and is expressed as

$$h'_{fg} = h_{fg} + C_1C_p\Delta T_{sat} \tag{13}$$

where C_1 was given as 0.4 by Bromley[27] but is now generally taken to be 0.5 (e.g., Refs. 19, 31). Frederking[40] has observed that when the superheat

$C_p\Delta T_{sat} \gg h_{fg}$, the term $\frac{h'_{fg}}{C_p\Delta T_{sat}} \rightarrow$ constant as $\frac{h_{fg}}{C_p\Delta T_{sat}} \rightarrow 0$, and the product $Ra \cdot \frac{h'_{fg}}{C_p\Delta T_{sat}}$ reduces to the ordinary single phase Rayleigh Number. This in turn becomes the product of Gr and Pr when, for small ΔT_{sat}, the density difference is expressed in terms of ΔT_{sat} by means of the isobaric coefficient of thermal expansion.

The modified Rayleigh Number may be written as,

$$Ra' = \frac{D^3\rho_{vf}(\rho_\ell-\rho_{vf})g}{(\mu_{vf})^2}\left(\frac{C_p\mu}{k}\right)_{vf}\left(\frac{h_{fg}}{C_p\Delta T_{sat}} + 0.5\right)\left(\frac{a}{g}\right) \qquad (14)$$

If it is written as the product of three terms,

$$Ra' = \{D^3\}\left\{\frac{\rho_{vf}(\rho_\ell-\rho_{vf})g}{(\mu_{vf})^2}\left(\frac{C_p\mu}{k}\right)_{vf}\left(\frac{h_{fg}}{C_p\Delta T_{sat}} + 0.5\right)\right\}\left(\frac{a}{g}\right) \qquad (15)$$

the first term is a constant for each test object, while the second term is a function of ΔT_{sat} and pressure. A plot of the value of the second term vs. ΔT_{sat} was made for pressures of 1, 3, 5 atmospheres, using properties as given in Ref. 37 and 41.

I. PHOTOGRAPHS

The high-speed photographs provided a means of obtaining the vapor film shape and thickness for the various geometries investigated. This permitted comparisons to be made of the effects of changing disk orientation, geometry and ΔT_{sat} on the vapor film shape and thickness. The test procedure limited coverage to P = 1 atmosphere, saturated liquid conditions.

The photographic data were obtained as sequences of negative frames on a 16 mm format. A wire framework was placed near each test surface to pro-

vide a measurement reference. The dimensions of these frameworks, which appeared on all photographs, were measured to ±0.0005 inch.

The negatives were back projected onto a ground glass screen with a magnification of approximately 50:1. A tracing was made of the test surface for each combination of test surface and ΔT_{sat}.

A sequence of approximately five frames was chosen for each combination of geometry, orientation, and ΔT_{sat}, and the film outlines were superimposed on the test surface tracing. For the sphere, the complete film surface was included; for the disk, approximately five representative points along the surface were included.

The film thicknesses were measured on the tracings and, using the measured reference wire framework, corrected to absolute physical dimensions. The reading error in these measurements corresponds to ±0.010 inch. Another source of uncertainty exists in the assumption that the measured film thickness is representative of film thickness at all points on the test surface. Although short-lived protuberances were deliberately avoided in selecting representative points at which to make the measurements, those made on the disk give the maximum film thickness along a chord. Measurements taken on the sphere probably indicate the local film thickness.

CHAPTER VI

RESULTS

A. GENERAL

The experimental results are presented under three major headings: Film Boiling, Other Boiling Regimes, and Photographic Results for Film Boiling. The results included under the first two headings are presented on graphs showing the relationship between heat flux, (q/A), and the difference between the test object temperature and the saturated liquid temperature, ΔT_{sat}, for the other variables considered. The photographic results of film boiling are presented as composite drawings of vapor film thickness for a sequence of frames. All results were obtained using liquid nitrogen as the test fluid. "Saturated boiling" is used to indicate boiling with a liquid under saturated conditions; "subcooled boiling" indicates boiling with a liquid which has a bulk temperature lower than the saturation temperature.

Comparison of heat fluxes for the different variables is made by plotting them against ΔT_{sat}. The use of log-log coordinates permits the data to be presented conveniently over the approximately two orders of magnitude variation which was obtained for both (q/A) and ΔT_{sat}. A standard (q/A) vs. ΔT_{sat} curve was developed based on the data obtained by Merte, et al.,[19] with the 1-inch diameter sphere in boiling saturated liquid nitrogen at one atmosphere pressure and (a/g) = 1. This curve, or a portion of it, is included on most of the figures for reference purposes.

Various test surface geometries and orientations were used, and the effects of these variations are shown in terms of (q/A) vs. ΔT_{sat} for the film boiling-regime. The pressure and the liquid subcooling were varied, and the effects of these on boiling are shown. The effects of changing (a/g) in addition to the above variables are shown. Only spherical test surfaces were used for tests in boiling regimes other than the film-boiling regime.

The temperature behavior of a test surface at (a/g) = 1 is characterized by a "quasi-steady" change of temperature with time, i.e., there are no discontinuous changes in the slope of the time-temperature curve. When the test package is dropped, a discontinuity in the time-temperature curve is observed, followed by the establishment of a new quasi-steady condition with a different slope of the time-temperature curve. The period of time between the discontinuity and the new quasi-steady condition represents a transitory period between two levels of (a/g), and is shown in the figures by a dotted line connecting two data points.

B. EXPERIMENTAL RESULTS

1. Film Boiling

Film boiling data were obtained for all geometries, orientations, subcoolings, pressures, and accelerations which were investigated. The effects of each variable except acceleration on (q/A) vs. ΔT_{sat} are presented individually, and then the effects of acceleration on each of the other variables are presented.

a. The Effects of Geometry and Orientation

The (q/A) vs. ΔT_{sat} data at (a/g) = 1 for saturated film boiling at P = 1 atmosphere are shown in Fig. 16 for the 1-inch and 1/4-inch diameter spheres and for the disk in the orientations designated as vertical (V), horizontal heating up (HU), and horizontal heating down (HD). The points shown for the 1/4-inch diameter sphere and the disk include all data obtained under these conditions.

For a given ΔT_{sat}, the value of (q/A) for the 1/4-inch diameter sphere is approximately 20% higher than the corresponding value of (q/A) for the 1-inch diameter sphere. The heat flux for the disk in all three orientations is approximately 100% higher than the heat flux for the 1-inch diameter sphere at the same ΔT_{sat}. A larger range in variation of (q/A) at a given ΔT_{sat} was generally observed for the disk than for the spheres. Some of the 1/4-inch diameter sphere data points obtained at ΔT_{sat} less than 80°F may indicate the beginning of the transition boiling region.

b. The Effects of Pressure

The (q/A) vs. ΔT_{sat} data for saturated film boiling at (a/g) = 1 are shown in Fig. 17 for the 1-inch diameter sphere at 1, 3, and 5 atmospheres. For a given ΔT_{sat}, the heat flux is more than 40% higher at 3 atmospheres, and more than 60% higher at 5 atmospheres, than at 1 atmosphere.

Results obtained using the 1/4-inch diameter sphere and the disk in all three orientations also exhibited a similar increase in heat flux with increasing pressure for a given ΔT_{sat} in saturated film boiling.

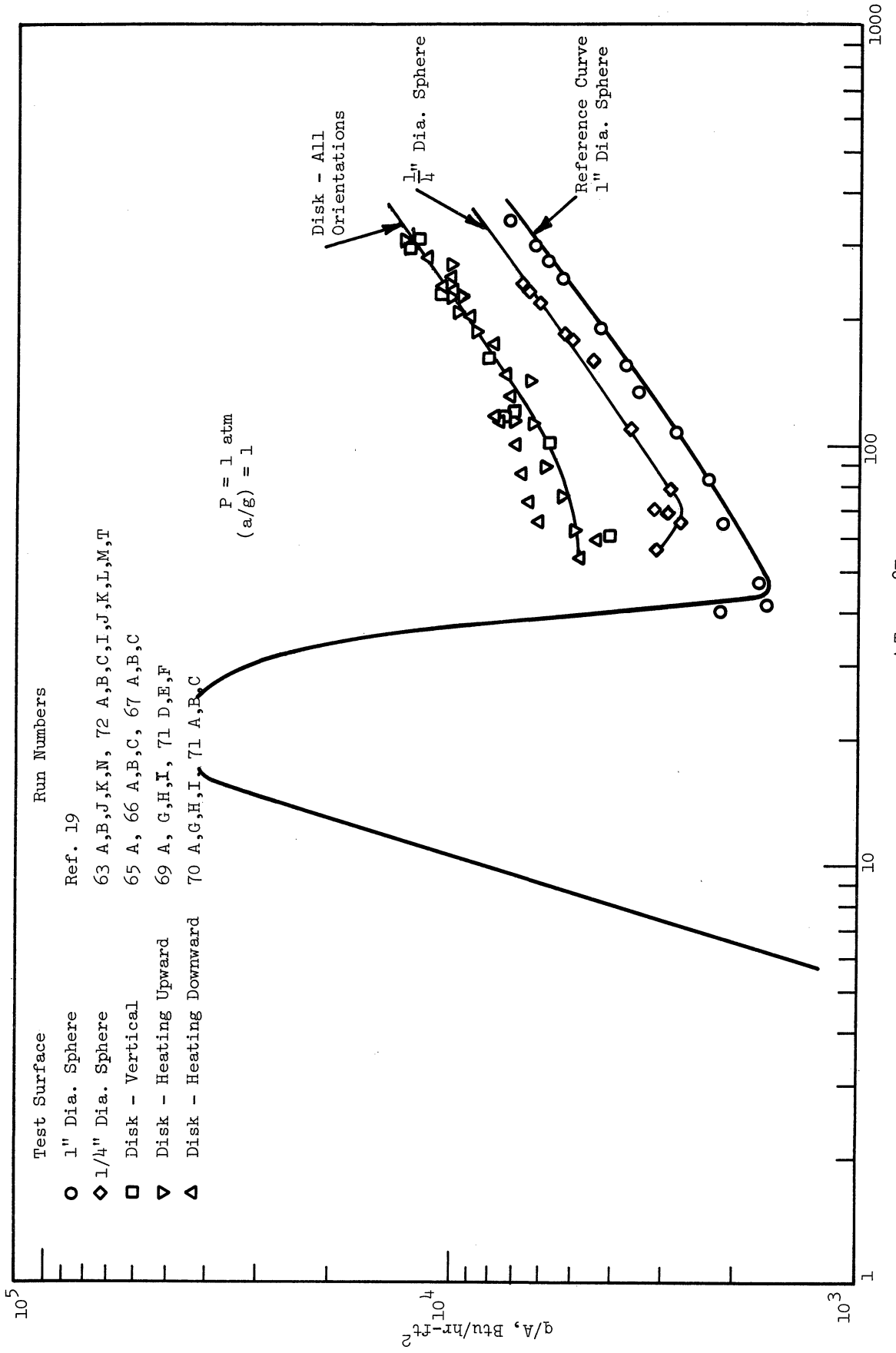

Fig. 16. Effects of geometry and orientation on saturated film boiling.

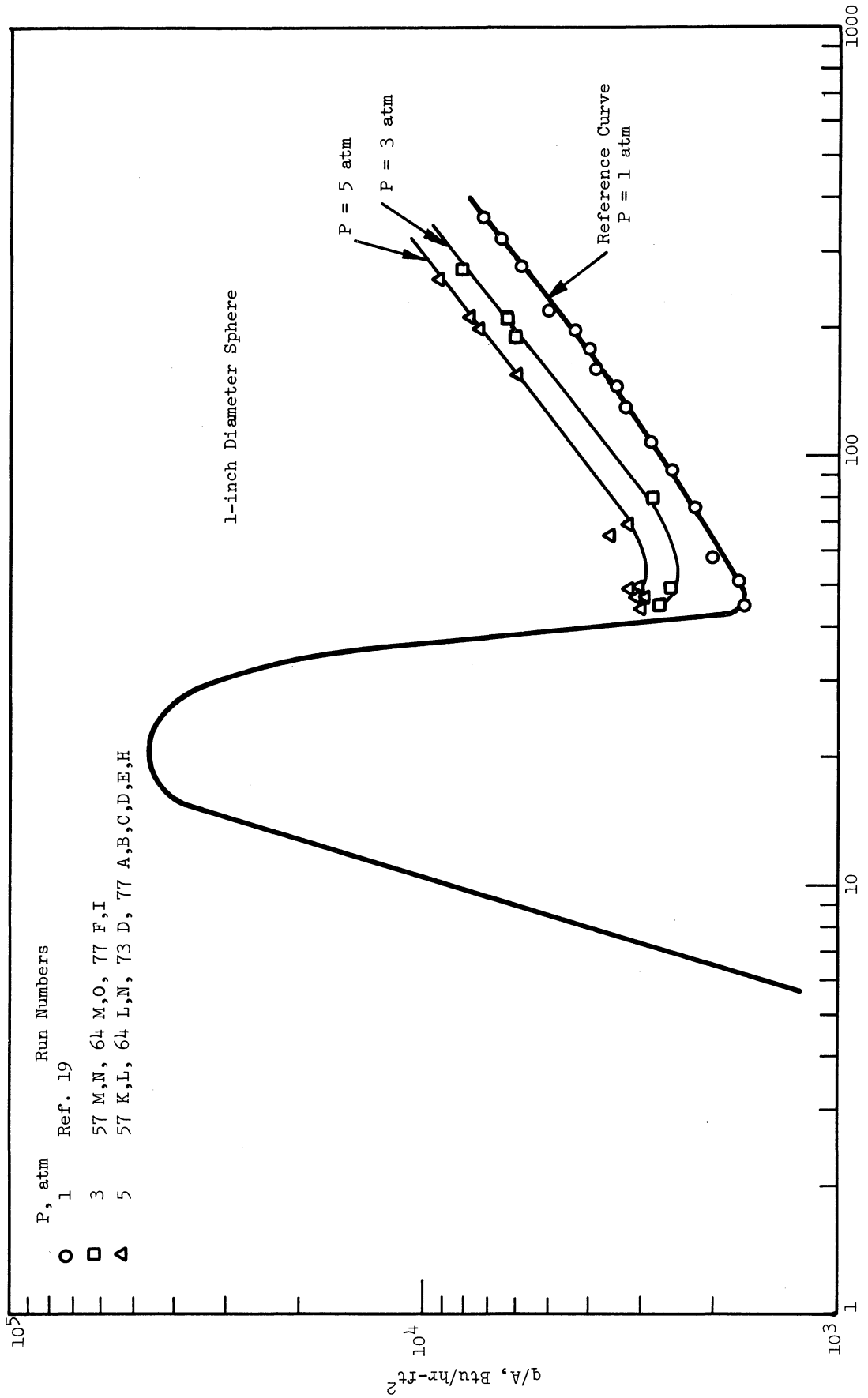

Fig. 17. Effect of pressure on saturated film boiling.

c. The Effects of Subcooling

The (q/A) vs. ΔT_{sat} data at (a/g) = 1 film boiling conditions with 5 atmospheres pressure are shown in Fig. 18 for the 1-inch diameter sphere at both saturated and subcooled conditions. For these test conditions the use of subcooled liquid increased the heat flux from the test surface approximately 50% over that obtained using saturated liquid at a given ΔT_{sat}.

Results obtained at 3 atmospheres pressure with the 1-inch diameter sphere and at both 3 and 5 atmospheres for the other test surfaces were similar. For a given ΔT_{sat}, the heat flux ranged from 10% to 60% higher with subcooled liquid than with saturated liquid.

d. The Effects of (a/g)

The (q/A) vs. ΔT_{sat} data at 1 atmosphere film boiling conditions are shown in Fig. 19a for the 1-inch diameter sphere with (a/g) = 1, (a/g) = 0.17, and (a/g) $\approx$ 0 (free fall). Two different free-fall conditions are shown. A value of (a/g) in the range of 0.01 to 0.03 was measured using the first test package in free fall, and was due primarly to air drag. A value of (a/g) of 0.001$\pm$0.001 was measured using the second test package in free fall, the decrease being due to use of the inner free vessel concept. A continuously decreasing heat flux was measured during free fall with the second package. The heat fluxes obtained after the transitory periods associated with the change from (a/g) = 1 to free fall are shown as two data points connected by a solid line. The point labeled "E" indicates the earliest heat flux data after the transitory period, and the point labeled "L" indicates the last heat flux data obtained prior to impact of

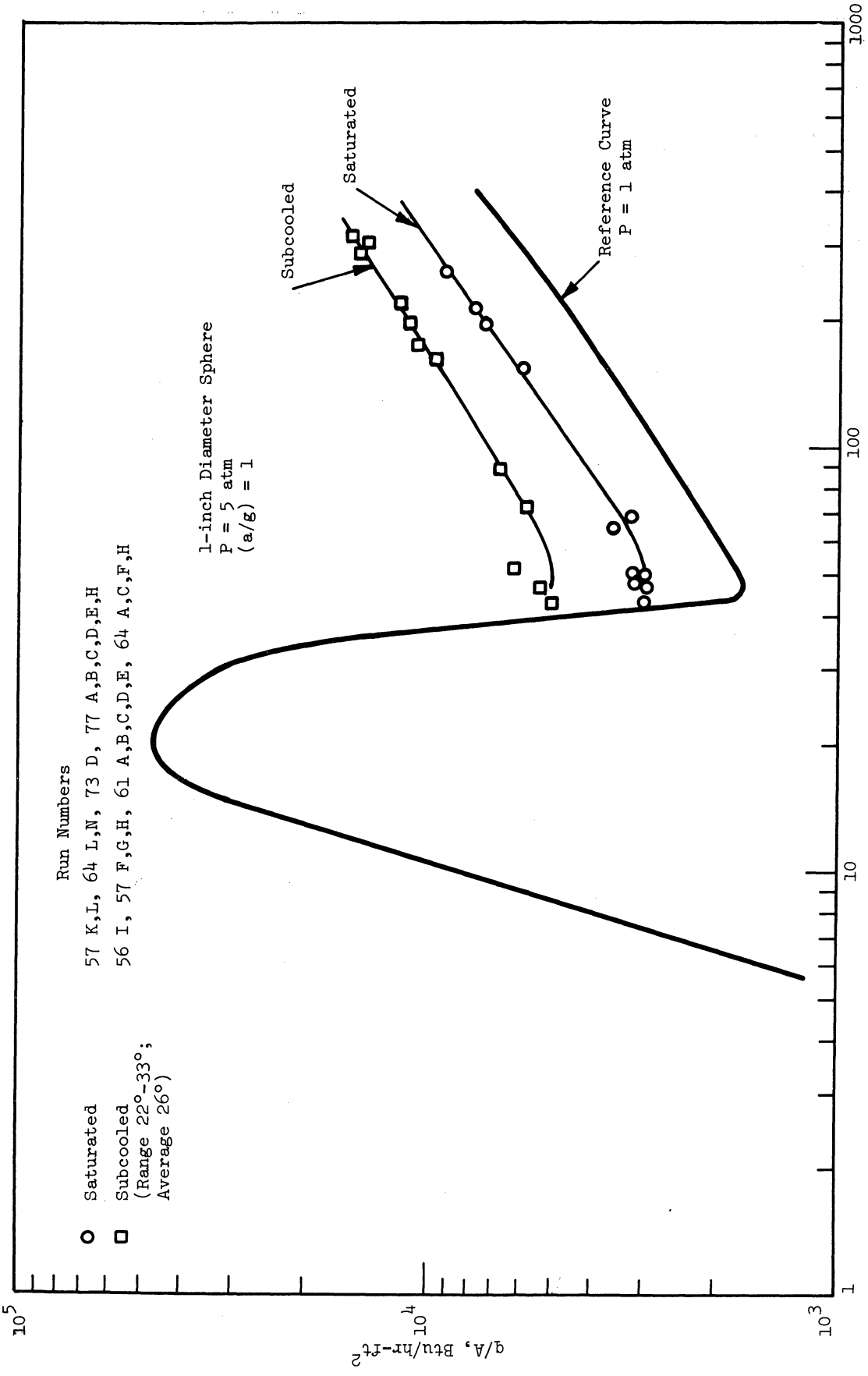

Fig. 18. Effect of subcooling on film boiling.

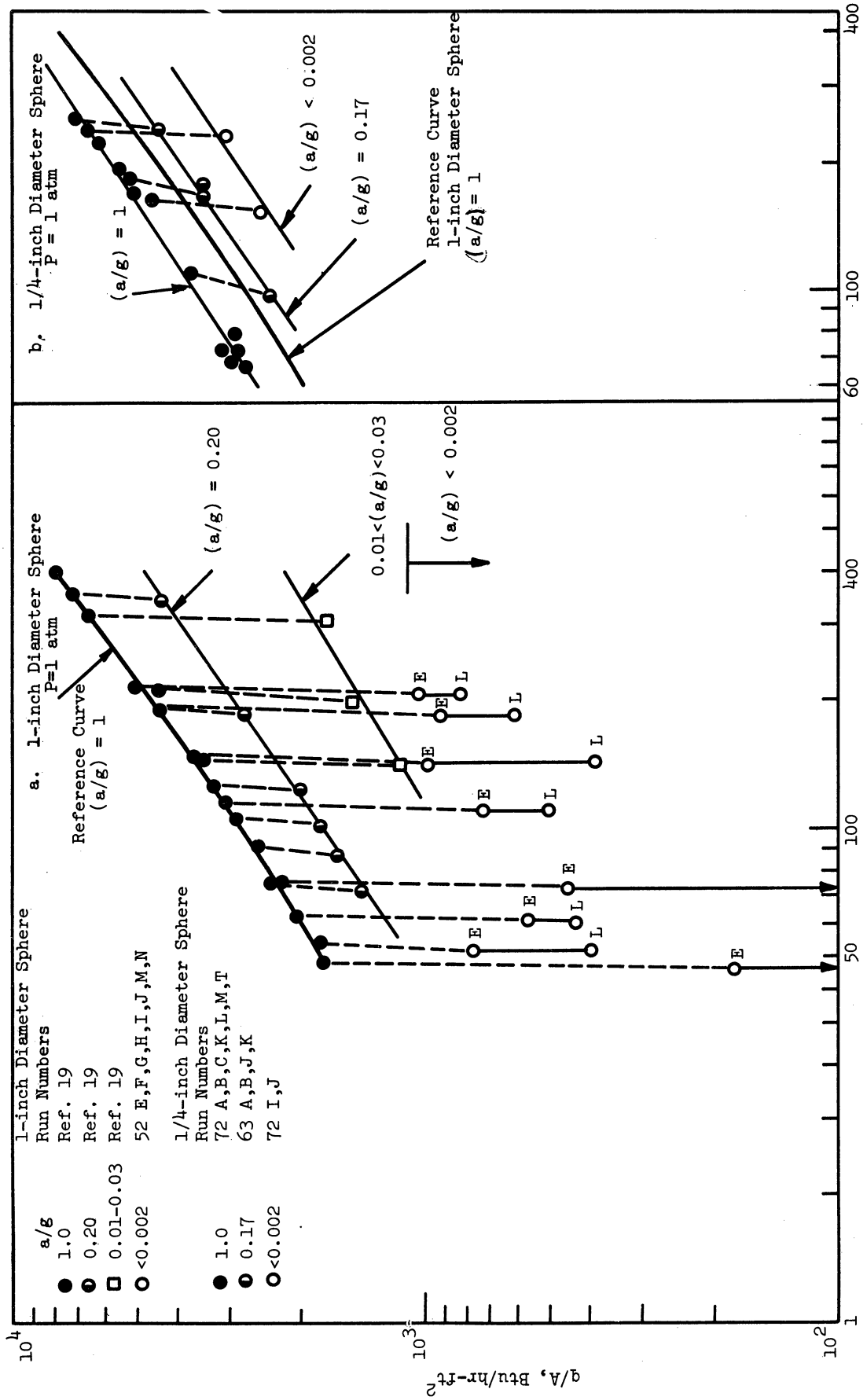

Fig. 19. Effect of (a/g) on saturated film boiling on spheres.

the test package on the buffer. The solid line represents intermediate values.

The heat fluxes measured at (a/g) = 0.17 are approximately 60% of those obtained at (a/g) = 1 for a given ΔT_{sat}. The heat fluxes at (a/g) = 0.01 to 0.03 are approximately 35% of those at (a/g) = 1 for a given ΔT_{sat}. The heat fluxes at (a/g) < 0.002 show a large amount of variation, ranging from 40% to less than 10% of the heat flux at (a/g) = 1 for the points labeled "E," and a similar variation for the points labeled "L."

Film boiling data were obtained with the 1-inch diameter sphere at 3 and 5 atmospheres pressure at (a/g) = 0.17 for both saturated and subcooled liquid. Data were also taken for the subcooled case at elevated pressures and with free fall, but not for saturated liquid at higher pressures. The results obtained with subcooling were similar to those shown in Fig. 19a, i.e., for a given ΔT_{sat}, a decrease in (a/g) was accompanied by a decrease in heat flux. The extremely low values of heat flux associated with free-fall conditions at 1 atmosphere pressure (Fig. 19a) were not observed with the higher pressure tests with subcooled liquid, the average value of heat flux at a given ΔT_{sat} decreasing to approximately 25% of the heat flux at (a/g) = 1, for the 1-inch diameter sphere.

The (q/A) vs. ΔT_{sat} data for the 1/4-inch diameter sphere are shown in Fig. 19b. The conditions were the same as for the 1-inch diameter sphere, i.e., film boiling at P = 1 atmosphere with (a/g) = 1, 0.17, and free fall. The effects of varying (a/g) are not as pronounced with the 1/4-inch diameter sphere as with the 1-inch diameter sphere. At (a/g) = 0.17 the heat flux

is approximately 70% (vs. 60% with the 1-inch diameter sphere) of the heat flux measured at (a/g) = 1 and the same ΔT_{sat}. In free fall, the heat flux is approximately 50% (vs. 35% or less with the 1-inch diameter sphere) of the heat flux measured at (a/g) = 1 and the same ΔT_{sat}.

Single (q/A) vs. ΔT_{sat} data points were obtained with the 1/4-inch diameter sphere at (a/g) = 0.17 at 3 and 5 atmospheres with saturated liquid. Results were obtained with subcooled liquid at 3 and 5 atmospheres at (a/g) = 0.17 and free fall. All of these results showed decreases in heat flux with decreasing (a/g) at a given ΔT_{sat} similar to those shown for 1 atmosphere saturated film boiling.

The (q/A) vs. ΔT_{sat} data obtained with the disk in all three orientations at 1 atmosphere film boiling conditions with (a/g) = 1, 0.16, and free fall are shown in Fig. 20. The variation of heat flux at a given ΔT_{sat} observed at (a/g) = 1 (quite large when compared with the variation of heat flux obtained using the 1-inch diameter sphere) may be indicative of the variation of heat flux to be anticipated at (a/g) = 0.16 and free fall. One point was obtained for each orientation and ΔT_{sat} at (a/g) = 0.16 and free fall, so no variations could be observed.

The heat fluxes measured at (a/g) = 0.16 and free fall were always less than those at (a/g) = 1. This was also observed at pressures of 3 and 5 atmospheres using both saturated and subcooled liquid. However, no consistent orientation dependence is observed at any particular value of (a/g), as was noted also at (a/g) = 1 (Fig. 16) (e.g., although the heat flux from the vertical disk at a given ΔT_{sat} in free fall was lower than that from the

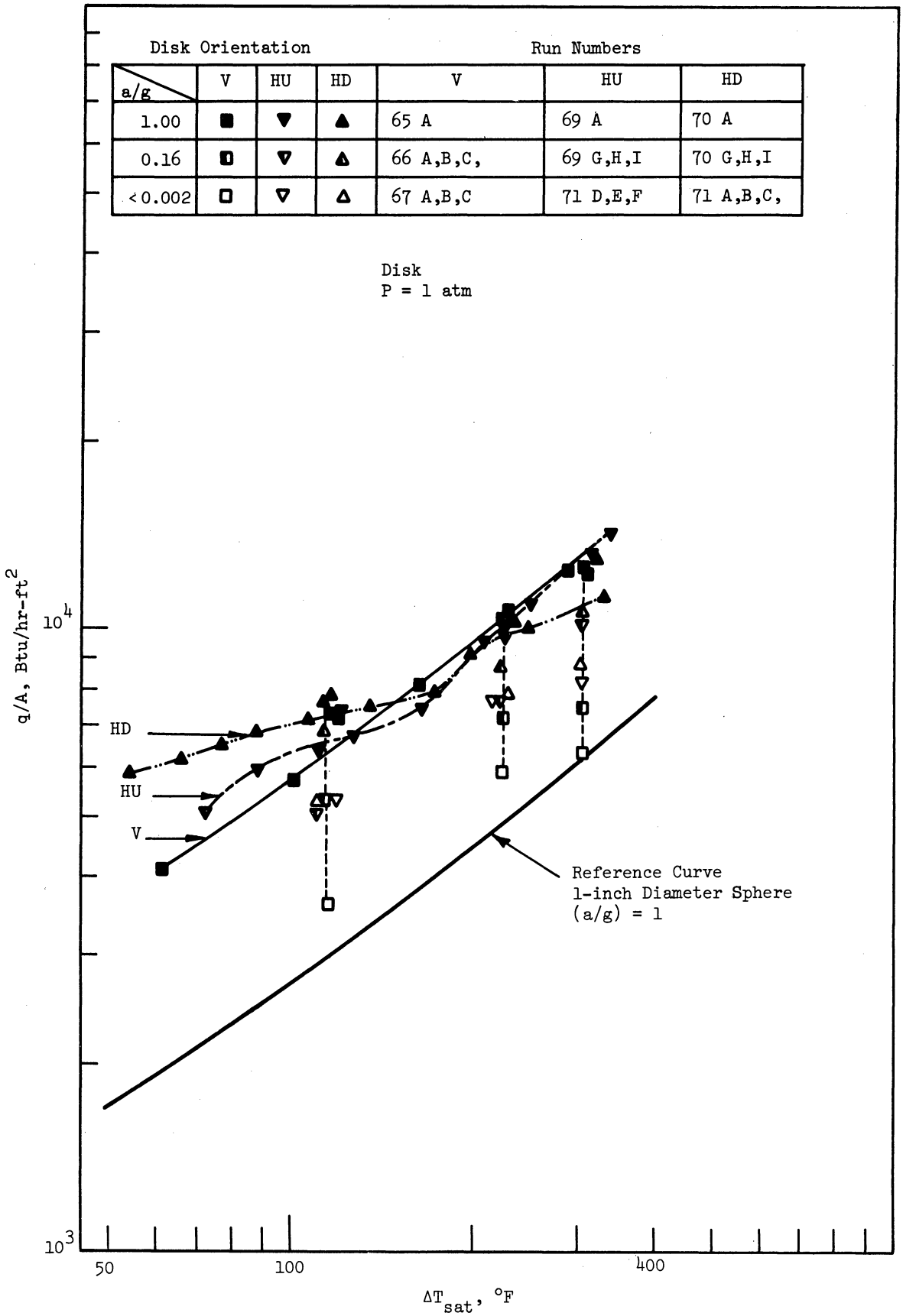

Fig. 20. Effect of (a/g) on saturated film boiling on disks.

disk heating up or heating down at 1 atmosphere saturated conditions, this was not true at 5 atmospheres saturated conditions).

2. Other Boiling Regimes

Time-temperature data were also obtained in the minimum heat flux, transition, peak heat flux, and nucleate boiling and free convection regimes using the spherical test surfaces. All 1/2-inch diameter sphere data were reported by Merte, et al.[19] The 1/4-inch diameter sphere data in the peak heat flux and nucleate boiling regimes are subject to large errors owing to the very rapid temperature transient associated with the small heat capacity. The variations in the computed heat flux associated with these errors obscure the effects of the test variables. The experimental data for the 1/2-inch and 1/4-inch diameter spheres are included in Appendix A.

The heat flux—ΔT_{sat} data obtained with the 1-inch diameter sphere, which are presented in this section, do not represent coverage of the variables investigated as completely as was the case in the film-boiling region. Emphasis is placed on presenting the effects of (a/g), subcooling, and pressure on boiling on the 1-inch diameter sphere in the various regimes.

a. Minimum Heat Flux Boiling

All of the (q/A) vs. ΔT_{sat} data points obtained with the 1-inch diameter sphere which appeared to have the characteristics of the minimum heat flux ($(q/A)_{min}$) are presented in Fig. 21a for saturated boiling at pressures of 1, 3, and 5 atmospheres. A $(q/A)_{min}$ point was obtained when a change in ΔT_{sat} to either a larger or a smaller value was accompanied by an increase

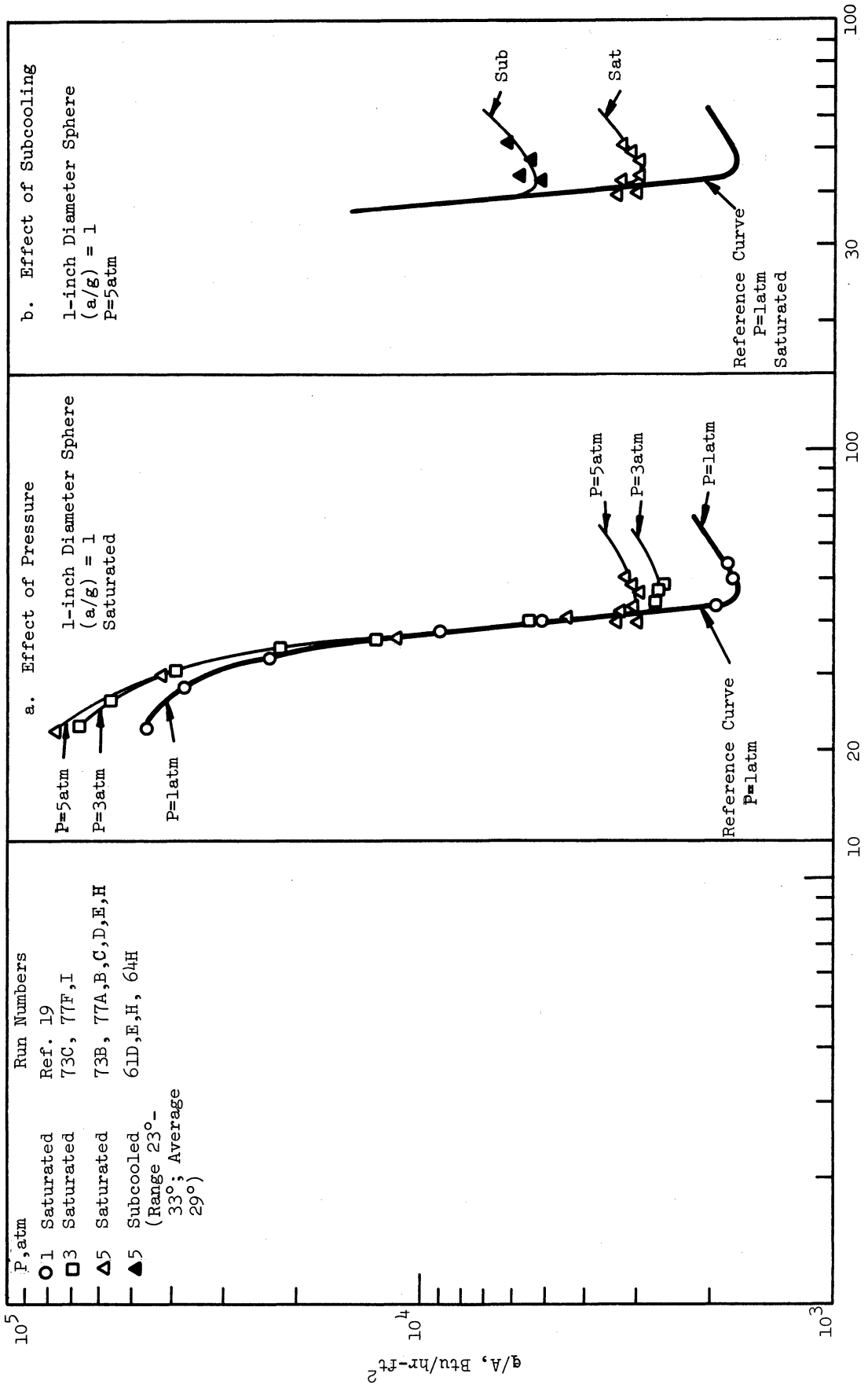

Fig. 21. Effects of pressure and subcooling on $(q/A)_{min}$ and transition boiling.

in (q/A). Each point in Fig. 21a represents the $(q/A)_{min}$ from an individual test run. An increase in $(q/A)_{min}$ with increasing pressure may be seen in Fig. 21a. The value of ΔT_{sat} at which $(q/A)_{min}$ occurs, $(\Delta T_{sat})_{min}$, does not appear to vary with changes in pressure.

The effect of subcooling on $(q/A)_{min}$ is shown in Fig. 21b for 5 atmospheres. The influence of subcooling at 3 atmospheres pressure is similar. The $(q/A)_{min}$ with subcooling is between 50% and 100% higher than the $(q/A)_{min}$ with saturation. Subcooling does not appear to affect $(\Delta T_{sat})_{min}$. There is no apparent effect of the level of subcooling in the range of subcooling covered here.

Merte and Clark,[19] using a 1-inch diameter sphere, obtained (q/A) vs. ΔT_{sat} data in the minimum heat flux region for $0 < (a/g) \leq 1$. No specific effort was made to obtain data in this region at elevated pressures in the course of the present work, but a limited amount of data were obtained. Results obtained with the 1-inch diameter sphere near the minimum heat flux point are shown in Fig. 22 and indicate that $(q/A)_{min}$ is less than 2000 Btu/ft^2-hr for (a/g) = 0.17 and saturated conditions at 3 and 5 atmospheres, less than 4000 Btu/ft^2-hr for (a/g) = 0.17 and subcooled conditions at 3 and 5 atmospheres, and less than 2000 Btu/ft^2-hr for free-fall and subcooled conditions at 3 and 5 atmospheres. No saturated boiling data were obtained at free fall at 3 and 5 atmospheres. The data of Merte and Clark[19] at 1 atmosphere are also indicated on Fig. 22.

b. Transition Boiling

Typical (q/A) vs. ΔT_{sat} data at (a/g) = 1 are presented in Fig. 21a

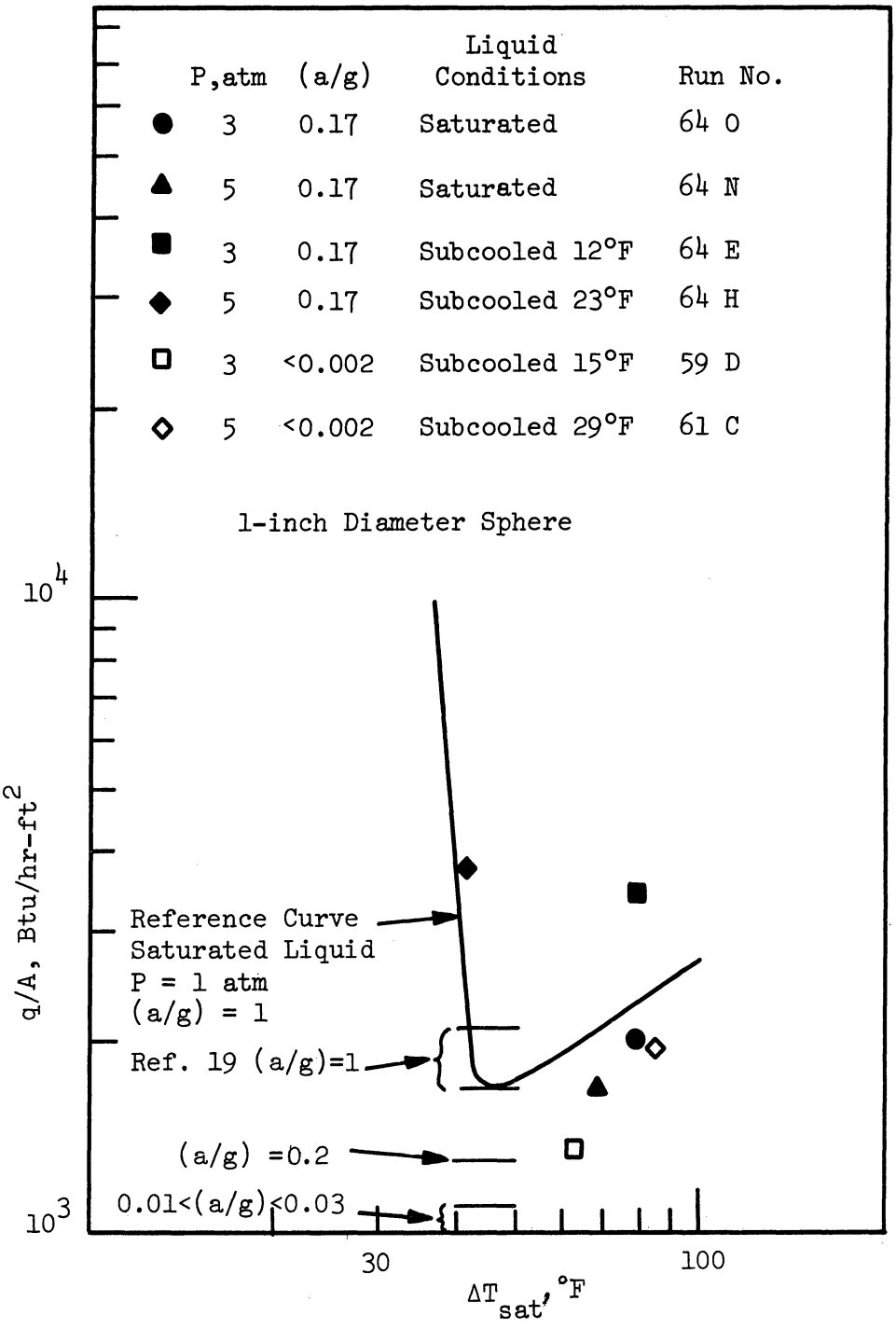

Fig. 22. Effect of (a/g) on $(q/A)_{min}$.

for the transition boiling regime with the 1-inch diameter sphere and saturated conditions at pressures of 1, 3, and 5 atmospheres. Although the minimum and maximum heat flux increase with pressure the effect of pressure in the transition region appears minimal, if any. Data obtained in this region with subcooled liquids also appears to be indistinguishable from that for a saturated liquid.

A limited amount of transition boiling data at (a/g) = 0.17 and free fall was obtained. These data are shown in Figs. 23, 24, and 25. When the test plackage was released at a value of ΔT_{sat} larger than that at which peak heat flux occurred, a decrease in (q/A) to some minimum value was normally observed. This was followed by an increase in (q/A) which was assumed to be transition boiling. If the test package was released after peak heat flux had occurred, there were no indications of transition boiling (e.g., Fig. 23a). When the test package was released at a ΔT_{sat} slightly higher than that at which peak heat flux occurs, any transition boiling which occurred at (a/g) < 1 also occurred during the transitory period (see Section VI.A) represented by the dotted lines in the figures (e.g., Fig. 24c). A few of the (a/g) = 1 data points are shown for each test run in Figs. 23, 24, and 25. The last data point obtained at (a/g) = 1 prior to the release of the test package is designated on the figures by an "R."

Figures 23, 24, and 25 do not show any consistent trends in transition boiling with changes in pressure, subcooling, or (a/g). Transition boiling (defined here as any boiling where a decrease in ΔT_{sat} is accompanied by an increase in (q/A)) is observed over a large range of ΔT_{sat} between $(\Delta T_{sat})_{min}$

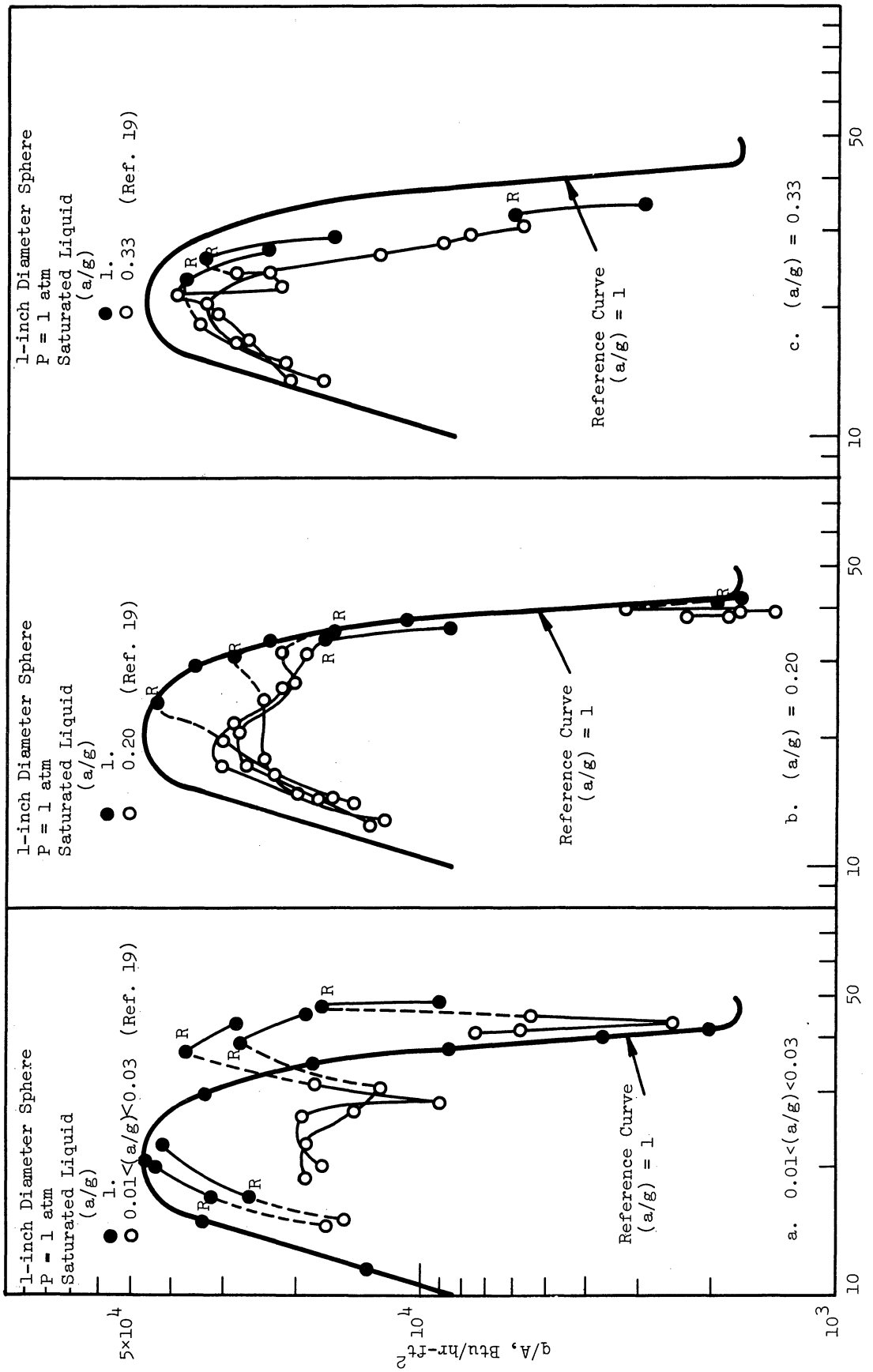

Fig. 23. Effect of (a/g) on transition boiling at one atmosphere.

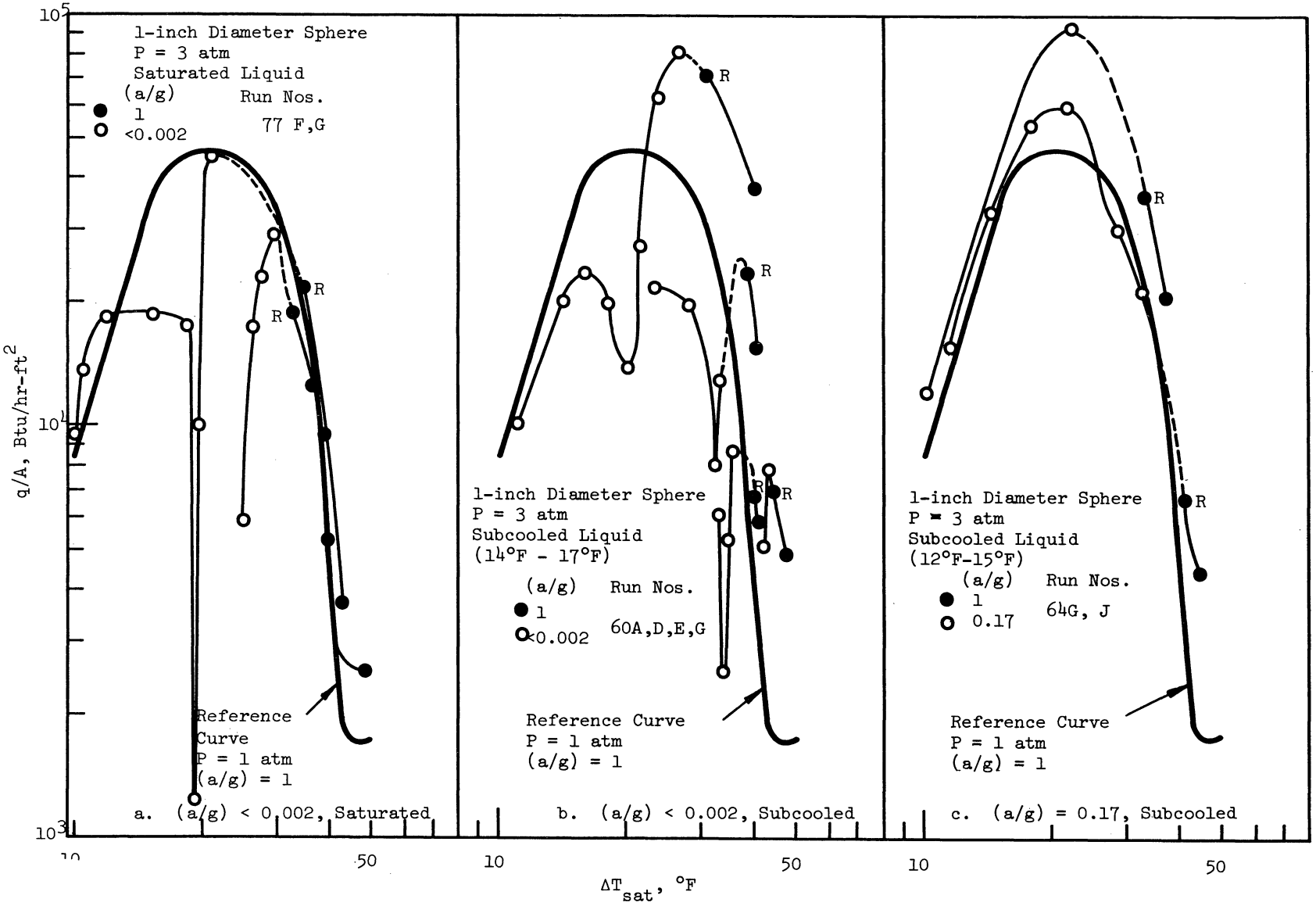

Fig. 24. Effect of (a/g) on transition boiling at three atmospheres.

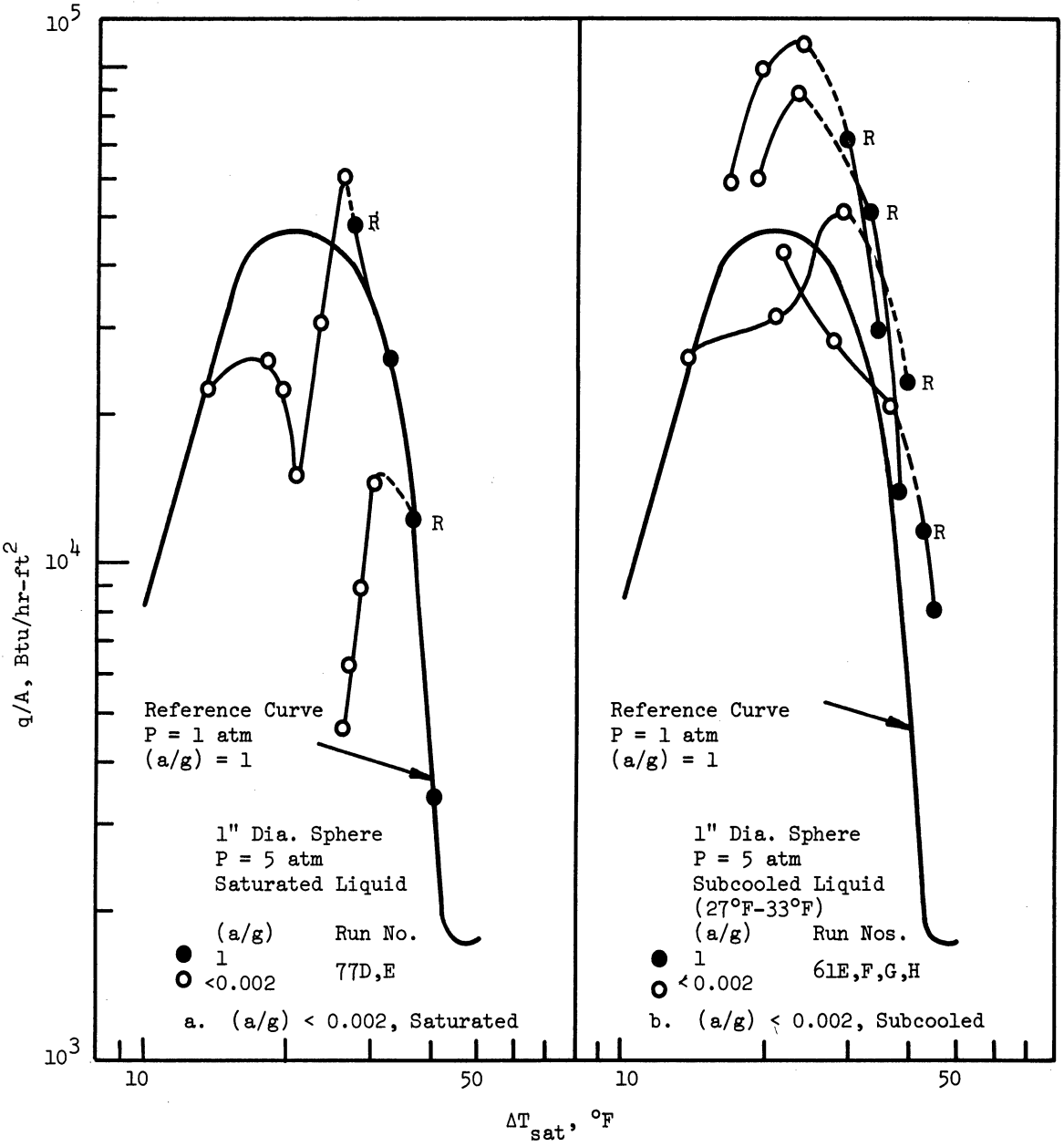

Fig. 25. Effect of (a/g) on transition boiling at five atmospheres.

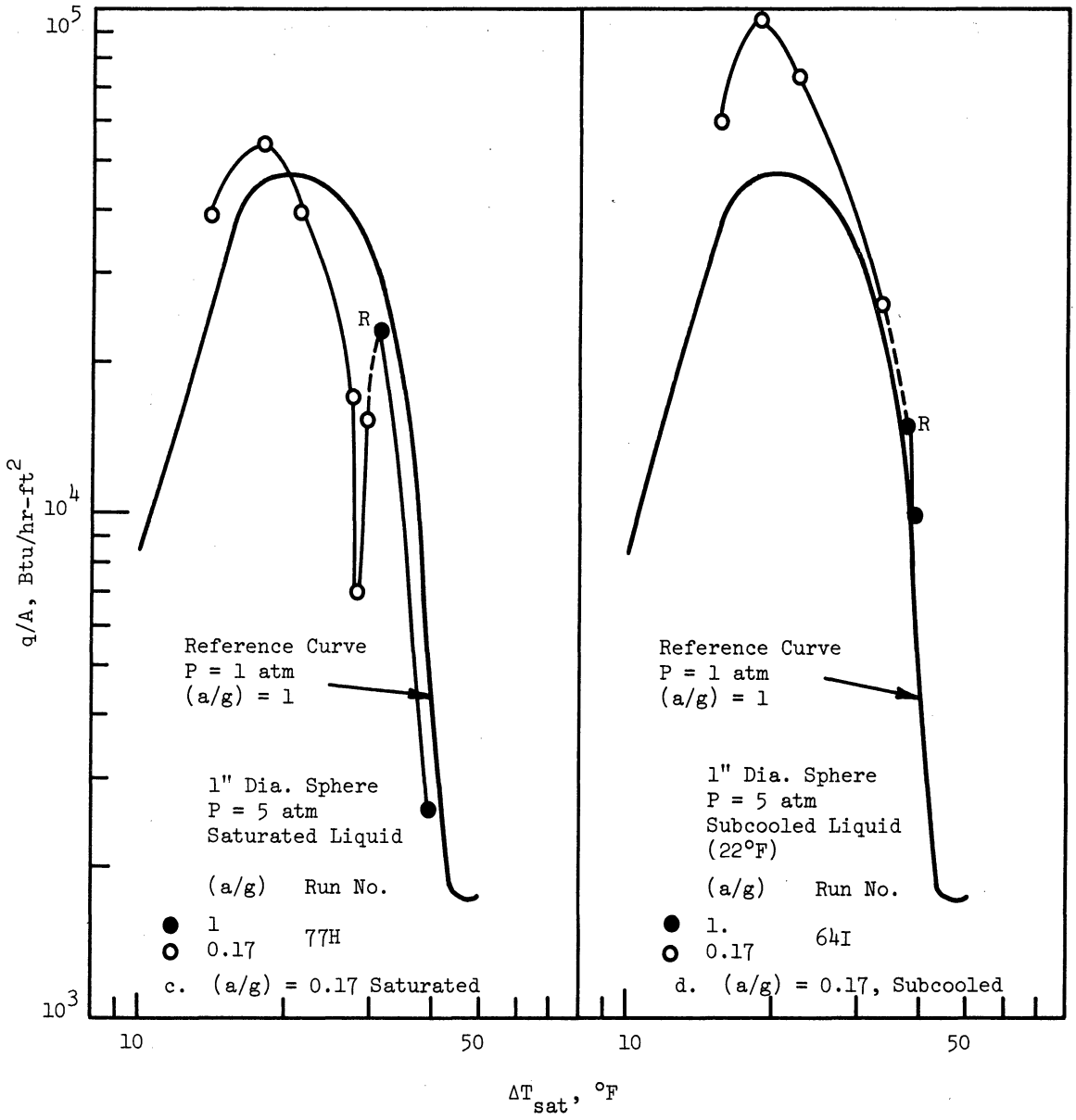

Fig. 25 (Concluded)

and $(\Delta T_{sat})_{max}$ (the ΔT_{sat} at which peak heat flux occurs) at values of $(a/g) < 1$ when initiated by a change from transition boiling at $(a/g) = 1$. The values of heat flux for a given ΔT_{sat} at $(a/g) < 1$ are less than the values of heat flux at $(a/g) = 1$ by as much as an order of magnitude, but specific decreases cannot be predicted. The results of Merte, et al.,[19] for the 1-inch diameter sphere at 1 atmosphere and $(a/g) < 1$ (Fig. 23) led to the same conclusions.

c. Peak Heat Flux Boiling

The effect of pressure on the value of the peak heat flux, $(q/A)_{max}$, is shown in Fig. 26a for saturated liquids at pressure of 1, 3, and 5 atmospheres. For any particular test run, only those data in the vicinity of the peak heat flux are shown. An increase in heat flux with increasing pressure is evident. There does not appear to be any clear influence of pressure on the ΔT_{sat} at which the peak occurs, $(\Delta T_{sat})_{max}$.

The effects of subcooled boiling on $(q/A)_{max}$ are shown in Fig. 26a for pressures of 3 and 5 atmospheres. A definite increase in the value of $(q/A)_{max}$ is observed when subcooling is present, but again there is no trend of ΔT_{sat} at which the peak occurs.

The effects of (a/g) on peak heat flux is shown in Fig. 26b for saturated boiling at 5 atmospheres. A decrease in (a/g) is accompanied by a decrease in the peak heat flux and a slight decrease in the ΔT_{sat} at which it occurs. The results of Merte, et al.,[19] for the 1-inch diameter sphere at 1 atmosphere showed $(q/A)_{max}$ decreasing with decreasing (a/g), as shown in Fig. 26b. A decrease in $(q/A)_{max}$ with decreasing (a/g) was also observed

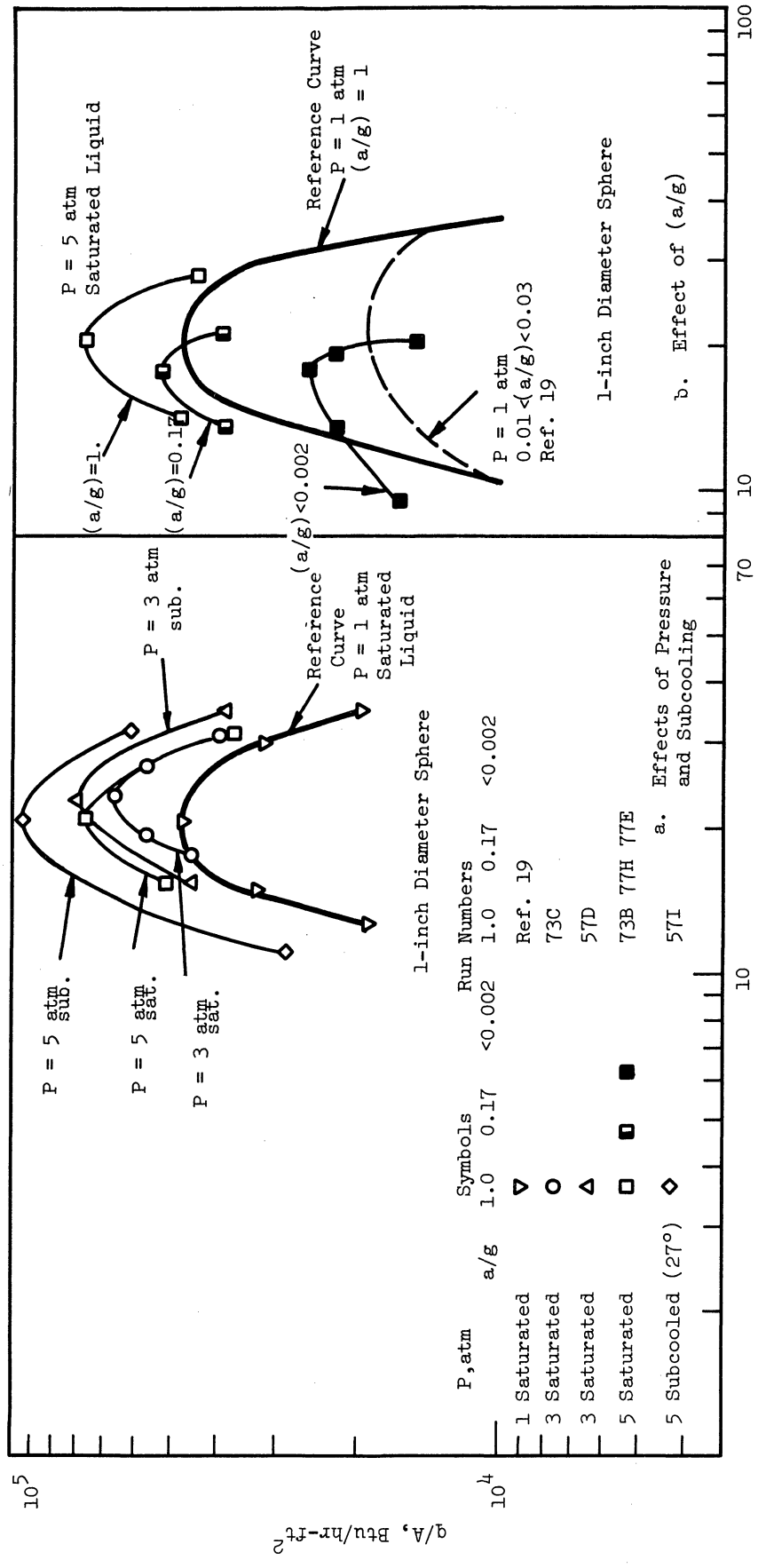

Fig. 26. Effects of pressure, subcooling, and (a/g) on $(q/A)_{max}$.

with subcooled boiling (e.g., Test Runs Nos. 60D, G, 61E, F, 64G, I).

d. Nucleate Boiling

Representative examples of the (q/A) vs. ΔT_{sat} data for nucleate boiling on a 1-inch diameter sphere are presented in Fig. 27. The effects of pressure on saturated nucleate boiling are shown. Except for the pressure-induced differences near the peak heat flux region, the nucleate boiling curves at a given heat flux differ from the reference curve by less than 2°F. Comparable variations were found in the nucleate boiling curves obtained for different test runs at the same pressure of 1 atmosphere, and the results presented here should not necessarily be interpreted as indicating any effect of pressure on saturated nucleate boiling over the range investigated. A larger variation in the experimental ΔT_{sat} for a given (q/A) was found with subcooled liquid, but no consistent trend could be noted.

Typical results of nucleate boiling with reduction in (a/g) are shown in Fig. 28. The last data point obtained at (a/g) = 1 prior to the release of the test package is designated on the figure by an "R." There is no apparent influence of (a/g) on nucleate boiling either with a saturated liquid, as shown, or with subcooled liquids, not shown (e.g., in Test Runs Nos. 60C, F, 61E, G, H, 64G, I, K).

e. Natural Convection

The heat transfer regions of prime interest in this study were those associated with boiling. Operations with subcooled liquids made it possible in some cases to make measurements with nonboiling natural convection taking place. The (q/A) vs. (T_s-T_ℓ) data obtained are presented in Fig. 29.

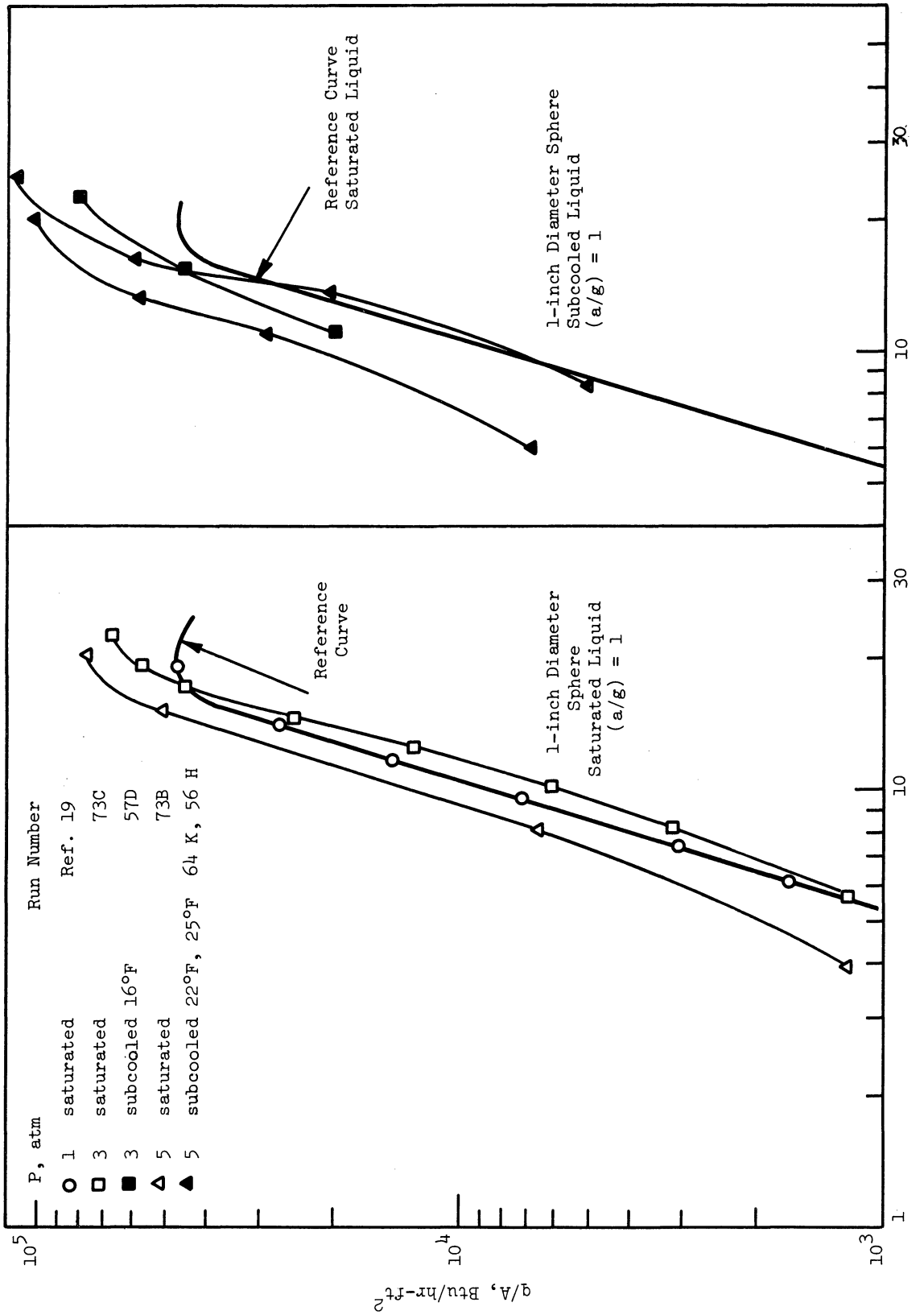

Fig. 27. Effects of pressure and subcooling on nucleate boiling.

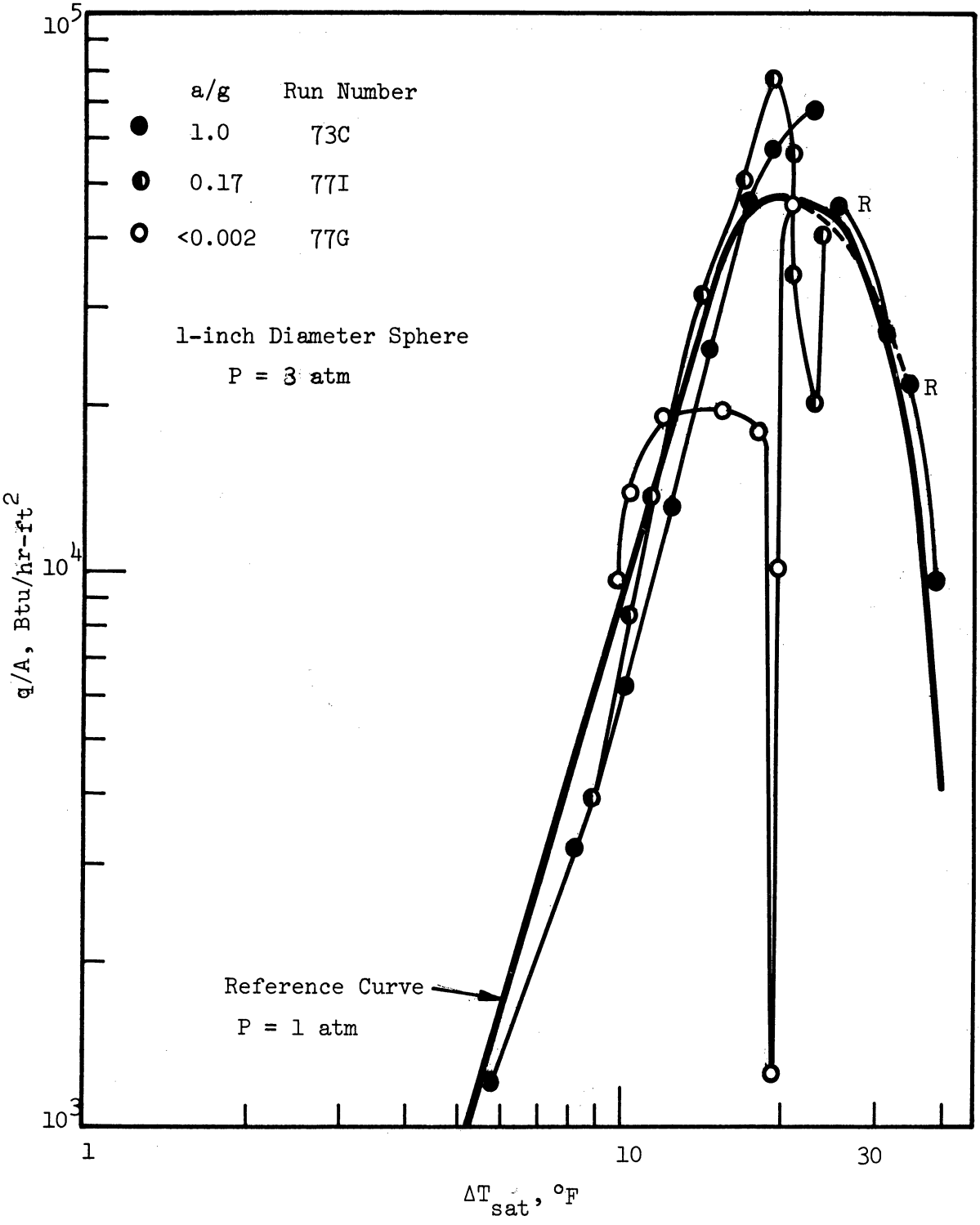

Fig. 28. Effect of (a/g) on saturated nucleate boiling.

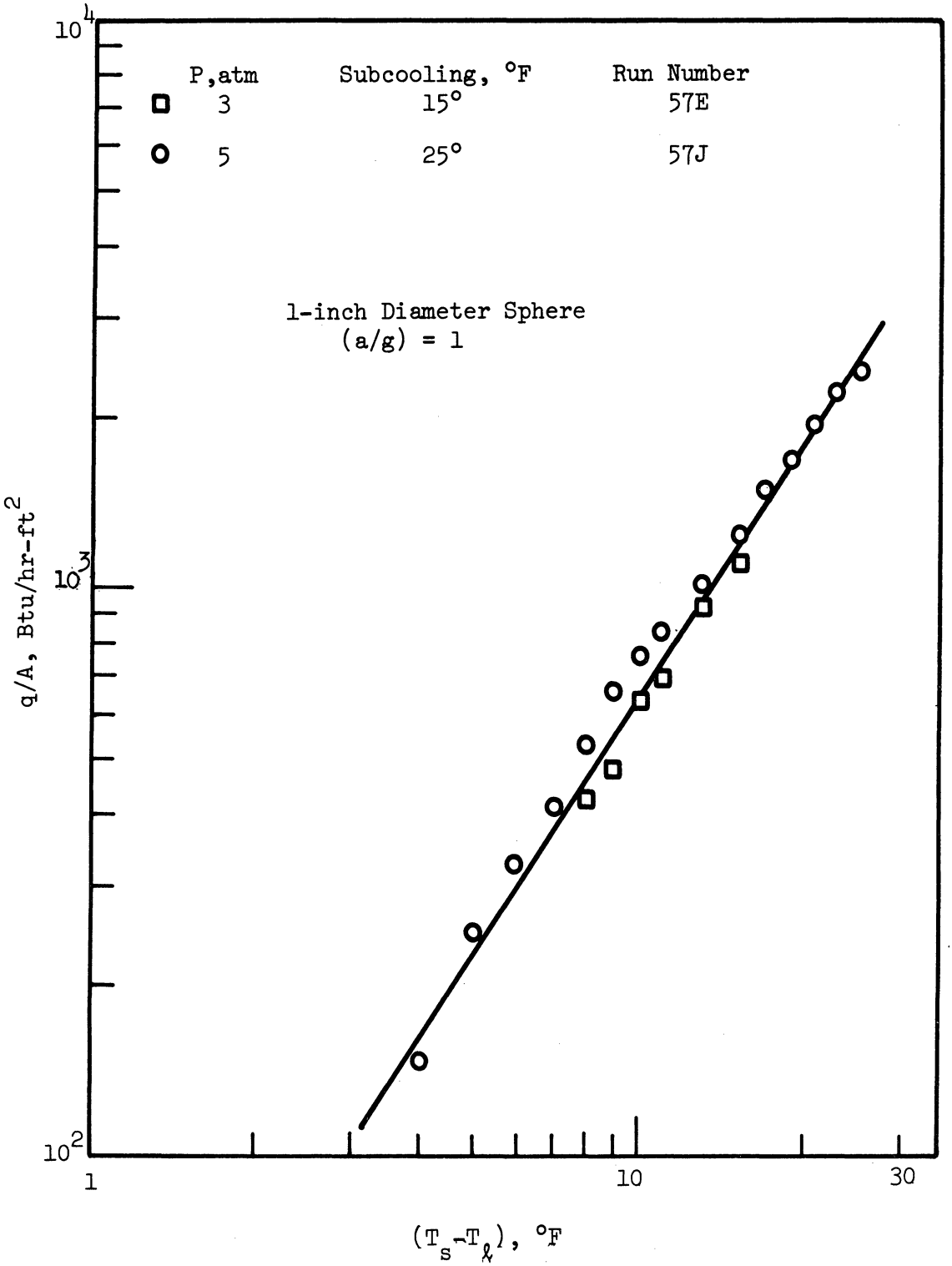

Fig. 29. Effect of pressure on free convection.

There is no effect due to either pressure or degree of subcooling. No data in this region were obtained for (a/g) less than 1.

3. Photographic Results for Film Boiling

The results of film boiling from the disk presented in Fig. 16 did not show any influence of orientation on the process, at standard gravity. Work done by Class, et al.,[36] has shown a definite sensitivity to orientation (orientations used were: vertical, 45° heating up, and horizontal heating up) for film boiling of hydrogen on a 22-inch long strip, although the data of Heath and Costello,[35] with film boiling at high gravity, did not indicate a sensitivity to orientation.

It was intuitively felt that at least the adverse effect of the body force in the horizontal orientation facing downward should give rise to distinct effects, but this was not the case. In an effort to determine if the lack of any significant effect could be related to the thickness of the vapor film, a series of high-speed motion pictures were taken to attempt measurements of the vapor film thickness. The liquid used was saturated liquid nitrogen at 1 atmosphere and all photographs were taken at (a/g) = 1. The disk was positioned in the vertical, horizontal heating up, and horizontal heating down positions. The 1-inch diameter sphere was also photographed to provide information on the effect of geometry on the appearance of film boiling.

Representative composite tracing of several frames for each condition, at various values of ΔT_{sat}, are presented in each of Figs. 30, 31, 32, and 33 for the different orientations and configurations. The measurements of

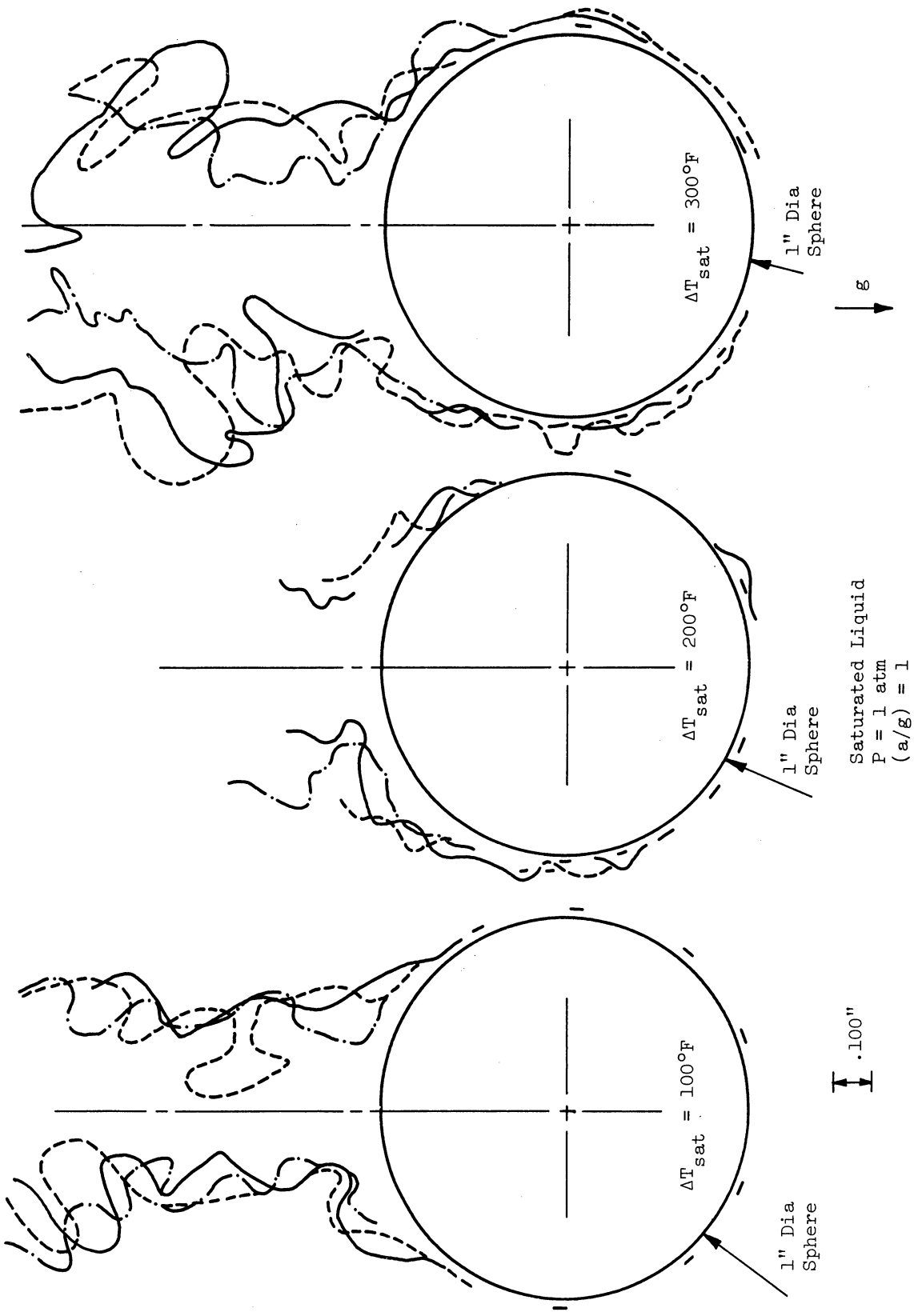

Fig. 30. Composite tracings of photographs of film boiling on a sphere.

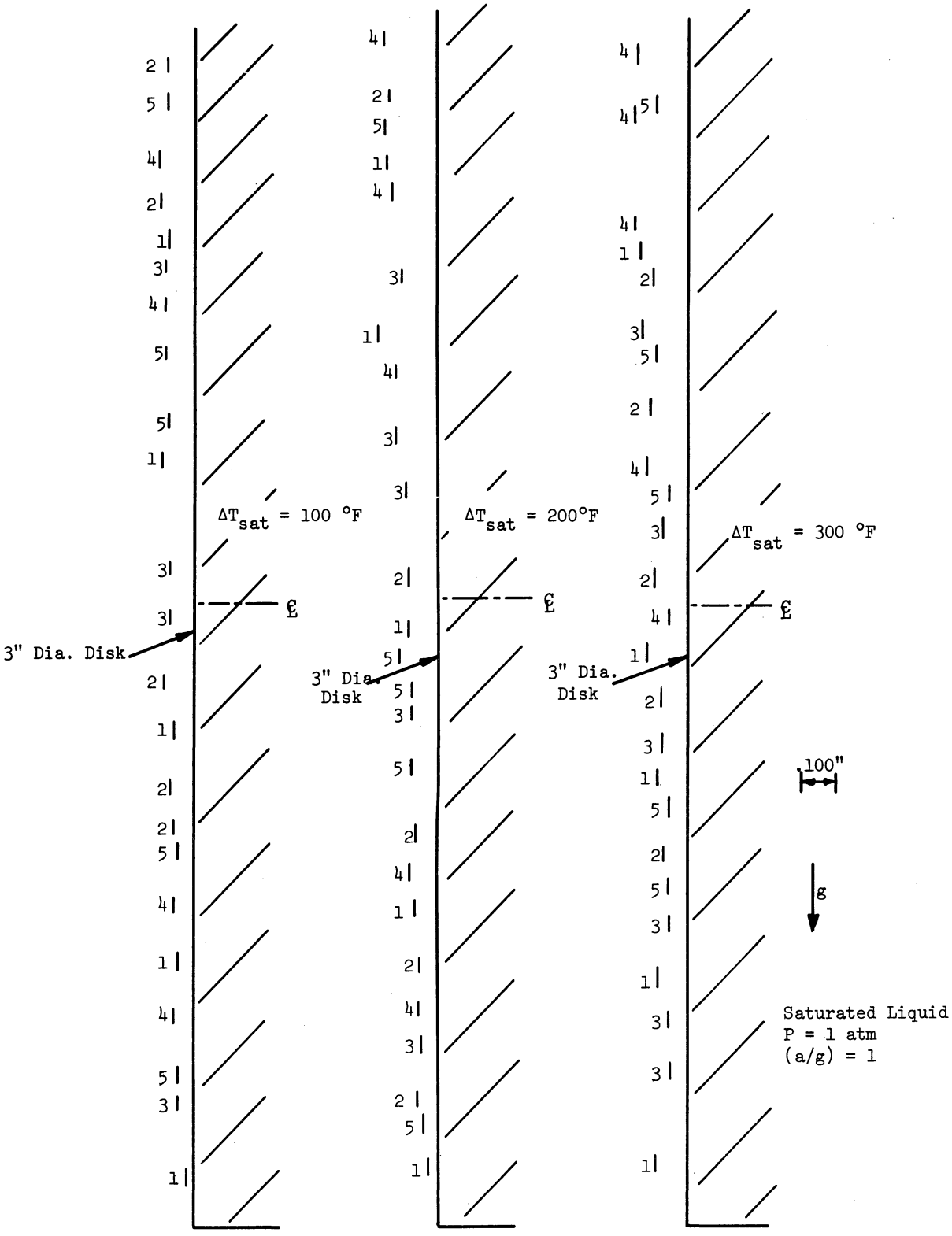

Fig. 31. Composite tracings of photographs of film boiling on a vertical disk.

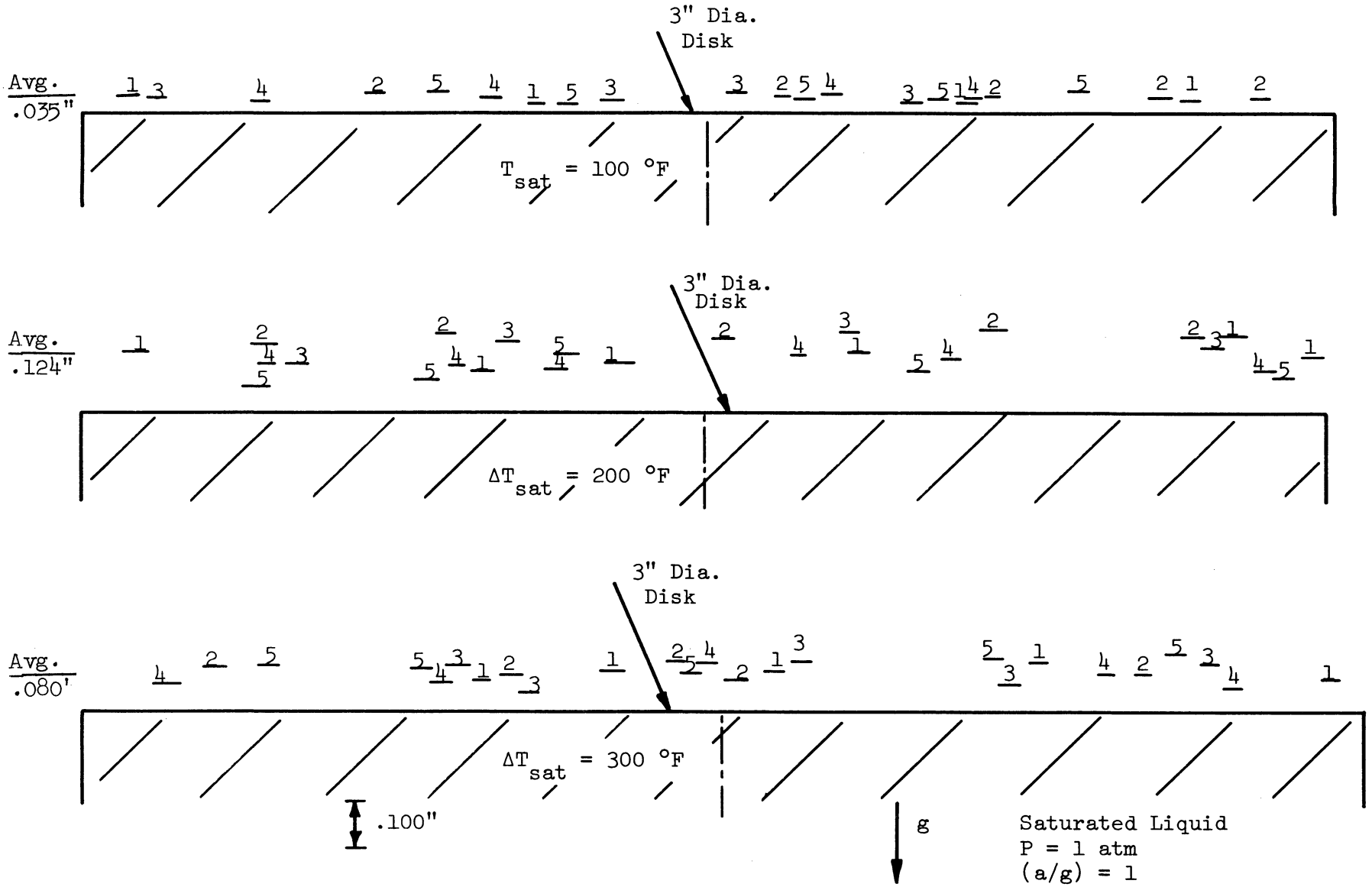

Fig. 32. Composite tracings of photographs of film boiling on a horizontal disk heating up.

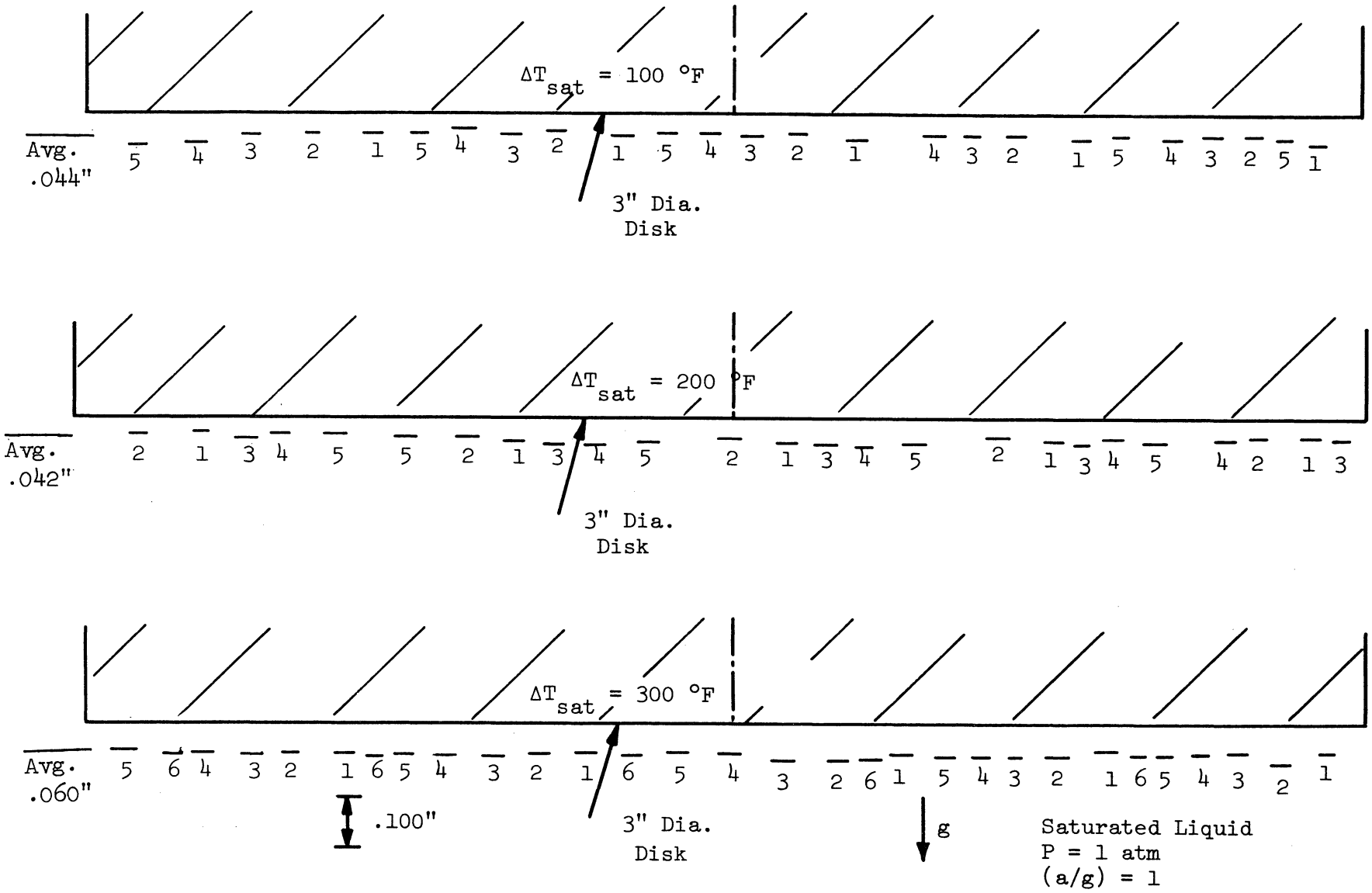

Fig. 33. Composite tracings of photographs of film boiling on a horizontal disk heating down.

vapor film thickness corresponding to those shown on the composite tracings are tabulated in Appendix A.3. Selected film frames corresponding to those presented in the figures are included in Appendix A.2. The frames at each ΔT_{sat} were spliced into continuous strips for viewing with a 16 mm projector. Where appropriate, the results of visual examination of the boiling process (while the movies were being taken) are also indicated.

The viewing angle used for the disk, parallel to the heating surface, gives the maximum film thickness across the entire face of the disk being observed. Any localized disturbance in the flow pattern at any point on the disk surface would result in the thickest film at that position being photographed. Therefore, the measured film thickness establishes only an upper limit for the local dimension, and does not represent the mean film thickness. The use of a composite of observations permits a more accurate assessment of a mean film thickness than a single frame would. This is not a problem for photographs of the sphere for obvious geometrical reasons.

a. One-Inch Sphere

Film boiling on the 1-inch diameter sphere, as shown in Fig. 30, is characterized by a thin film on the bottom and sides of the sphere. The film is attached to the sphere up to about 60° from the top of the sphere, then becomes much thicker and quantities of vapor detach from the surface. At ΔT_{sat} = 200°F, small waves can be identified on the lower hemisphere, and become quite prominent on the upper hemisphere below the point at which the vapor clearly separates from the sphere. At ΔT_{sat} = 300°F waves are visible over almost the entire surface of the sphere. The area on the top

of the sphere from which the vapor leaves, forming a column, does not change significantly over the range of ΔT_{sat} examined. The diameter of the column appears to increase with increasing ΔT_{sat}, as might be expected for the larger mass flow rate of vapor which occurs at larger ΔT_{sat}.

Visual observations made while the film was being taken revealed that the vapor column did not appear as axisymmetrical bubbles released at intervals. A continuous slug of vapor appeared to tear away from the sphere in a helical fashion, with the center of the area of detachment describing a circle about the vertical axis of the sphere. This phenomenon was most pronounced at the highest level of ΔT_{sat} used. It may be seen in Fig. A-1 in Appendix A.2 where it appears as a displacement of the vapor column from the vertical axis of the sphere as a function of height above the sphere (and therefore as a function of the time of release of vapor from the sphere). Photographs taken by Frederking[42] show a similar phenomenon.

b. Vertical Disk

The composite tracings of the film thickness observed on the vertical disk are shown in Fig. 31. Each frame in the sequence used was identified with a number. These numbers are placed beside the lines indicating the vapor-liquid interface on each frame, and show the variation in interface position at approximately 0.001-second intervals.

The vertical disk does not present the same configuration to the boiling liquid as a vertical flat plate with a horizontal leading edge (i.e., a two-dimensional leading edge is present). The vapor film on the disk appears similar to that anticipated for a vertical plate. The film near

the leading edge is initially thin, with a fairly well defined transition to a greater thickness evident at a location below the centerline of the disk.

The lower portion of the vapor film does not appear to show any significant change in thickness with an increase in ΔT_{sat} over the temperature range covered here. The solid-interface spacing in the upper portion of the vapor film is greater at ΔT_{sat} of 200°F and 300°F than at 100°F. An increase in the number and magnitude of localized disturbances with increasing ΔT_{sat} was observed visually while the films were being taken. These disturbances appeared in the form of waves and bubbles. The bubbles separated from the film layer and moved upwards in a path parallel to the vapor film. The waves, which are also represented in Fig. 31 as localized thickenings of the film, moved upwards without actually detaching from the film. The increasing prevalence of these disturbances can be seen quite clearly in Fig. A-2 of Appendix A.2.

c. Horizontal Disk Heating Up

In order to observe the film boiling process taking place at the top of the disk without having the view obscured by the vapor flowing from the bottom and sides of the disk, it was necessary to attach a collar which diverted the flow of vapor from the bottom and sides of the heater to the side of the field of view. While this technique may have had local effects at the edges of the disk, it is felt that the film boiling in the central portions of the disk was substantially unaffected.

Film thickness composites for the horizontal disk heating up are shown in Fig. 32. At ΔT_{sat} = 100°F the measured thickness of the vapor film above the heating surface was nearly constant. No measurements were taken where bubbles were forming or leaving the surface. At higher values of ΔT_{sat} the thickness and irregularity of the film increases drastically. Comparison with the film frames in Fig. A-3 of Appendix A.2 indicates that at ΔT_{sat} = 100°F the number and frequency of bubbles released is relatively low. Large individual bubbles may be clearly distinguished after departure from the vapor film area. At ΔT_{sat} = 200°F, the frequency and number of bubbles has increased with relatively little change in the size of the bubbles and the vapor film has increased in thickness. At ΔT_{sat} = 300°F the spacing between departing vapor bubbles appears to be smaller, indicating that the frequency of bubble departure has increased further. A consequence is that the vapor film thickness appears to be only 2/3 of what it was at ΔT_{sat} = 200°F. At the two higher levels of ΔT_{sat} the increased bubble frequency make it extremely difficult to obtain a measurement of either an average or minimum film thickness. This is indicated by the extreme variation in film thickness as shown in the composites of Fig. 32. The average film thickness obtained from the composites is indicated, but is probably a maximum value rather than a true average.

Visual observations made while the photographs were being taken revealed that, after detachment, the individual bubbles moved upwards very slowly. There was little mixing or coalescence of these bubbles. The physical size of bubbles ranges up to 1/2 inch major dimension, with the bubbles

showing a slight increase in size with increasing ΔT_{sat}.

d. Horizontal Disk Heating Down

Observation of the vapor film on the disk surface in the heating down orientation is not obscured by release of the vapor generated, as it flows up and around the sides of the disk, and therefore away from the interface being examined. Inspection of Fig. 33 shows that the composite interface at each ΔT_{sat} is much smoother in appearance than those for the other orientations.

It might be anticipated that the film thickness would increase with increasing ΔT_{sat}, because of the higher heat flux. This generates more vapor, which should result in a thicker vapor film owing to the increased buoyant forces necessary for removal of the vapor. This is examined in detail in Appendix B. No difference could be discerned in film thickness between ΔT_{sat} = 100°F and ΔT_{sat} = 200°F, while at ΔT_{sat} = 300°F it increased by approximately 50%. Visual observations made while the film was being taken revealed a number of waves and protrusions appearing sporadically on the vapor-liquid interface. The protrusions, which can be seen in Fig. A-4 of Appendix A.2, generally appeared briefly, then subsided back into the interface. The waves could be observed moving across the surface of the disk for a considerable distance before either disappearing or going past the edge of the disk and being absorbed in the upward flow of vapor. The overall effect was one of continuous motion, in both horizontal and vertical planes, of the vapor-liquid interface.

The mean values of the vapor film thickness for the horizontal disks, along with an estimate of the maximum deviation, are listed in Table II.

TABLE II

MEAN VAPOR FILM THICKNESS

(inch)

3-inch diameter disk, P = 1 atm, (a/g) = 1, saturated liquid

Disk Orientation	ΔT_{sat} 100°F	200°F	300°F
Horizontal heating up	0.035 ± 0.020	0.124 ± 0.020	0.080 ± 0.020
Horizontal heating down	0.044 ± 0.010	0.042 ± 0.010	0.060 ± 0.010

4. Anomalous Results

The measured heat flux in film boiling at a given ΔT_{sat} for a particular set of conditions (geometry, pressure, etc.) could normally be repeated to within ±35%, and in many cases it could be repeated to within ±10%. In a few cases involving film boiling on a disk, deviations from the average values of (q/A) at a given ΔT_{sat} of from 50% to 500% were observed. In one case such a deviant run was duplicated within a few percent at (a/g) = 1 and 0.16. These anomalous data are shown in Fig. 34.

Anomalous results were obtained for both saturated and subcooled liquid, and for the disk in both vertical and horizontal heating up orientations. These results could indicate an incipient instability in the liquid-vapor interface on a flat plate which occasionally is manifested as a substantial reduction in the thickness of the vapor film. Normally such an effect may

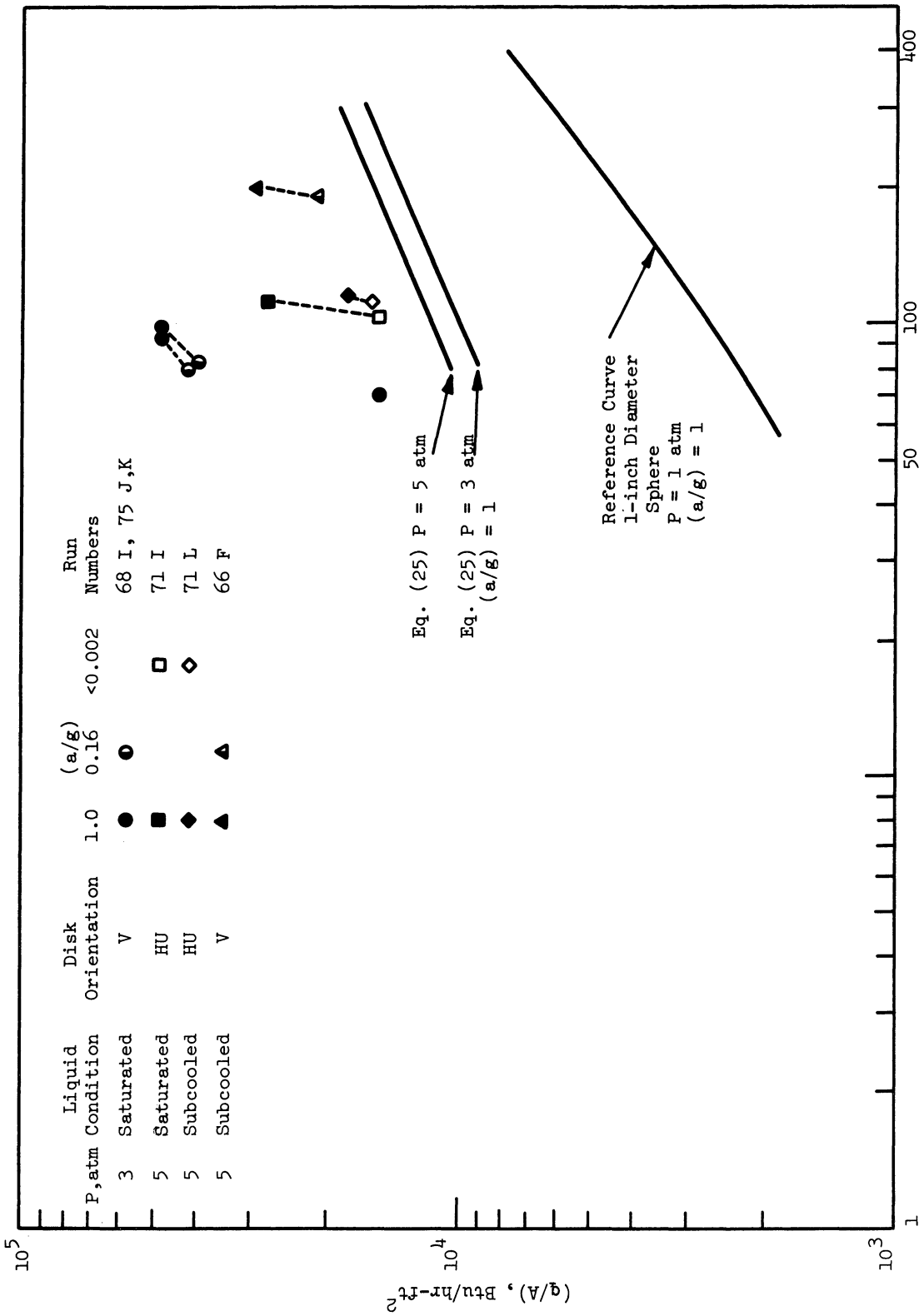

Fig. 34. Anomalous film boiling.

tend to be damped out or localized, being evidenced only by a relatively large variation in values when attempts are made to repeat particular results. Hosler and Westwater[43] obtained variations of almost 100% from their average curve on a few runs with film boiling of water at atmospheric pressure on an 8-inch x 8-inch horizontal flat plate.

Further speculation on possible causes for the results observed is not warranted at this time. The possibility of investigating the phenomenon in detail is intriguing.

CHAPTER VII

DISCUSSION AND ANALYSIS

Many correlations have been proposed for the various boiling regimes in attempts to fit or describe the various published data. The data for liquid nitrogen are largely summarized by Fig. 35, which has been reproduced from Ref. 44. The correlations are discussed by Seader, et al.,[44] who show that no correlation has been advanced which fits all of the experimental data in any single boiling regime. This is anticipated in light of Fig. 35, where the nonreproducibility of results is most likely due to the nonuniformity of the significant parameters, some known and others as yet unknown. A variety of materials, test surfaces, and orientations were used in obtaining the data presented.

The objectives of this study were to determine the effects of varying test surface configuration and orientation on boiling heat transfer, along with variations of gravity field, system pressure, and subcooling. Discussion and analysis of the experimental results of the previous section are presented below in the order of film boiling, minimum heat flux, peak heat flux, nucleate boiling, and free convection, i.e., following the course of the cooling curve used to obtain the data.

A. FILM BOILING

Saturated Liquid Boiling Correlations

Frederking and Clark[31] correlated the film boiling data obtained by

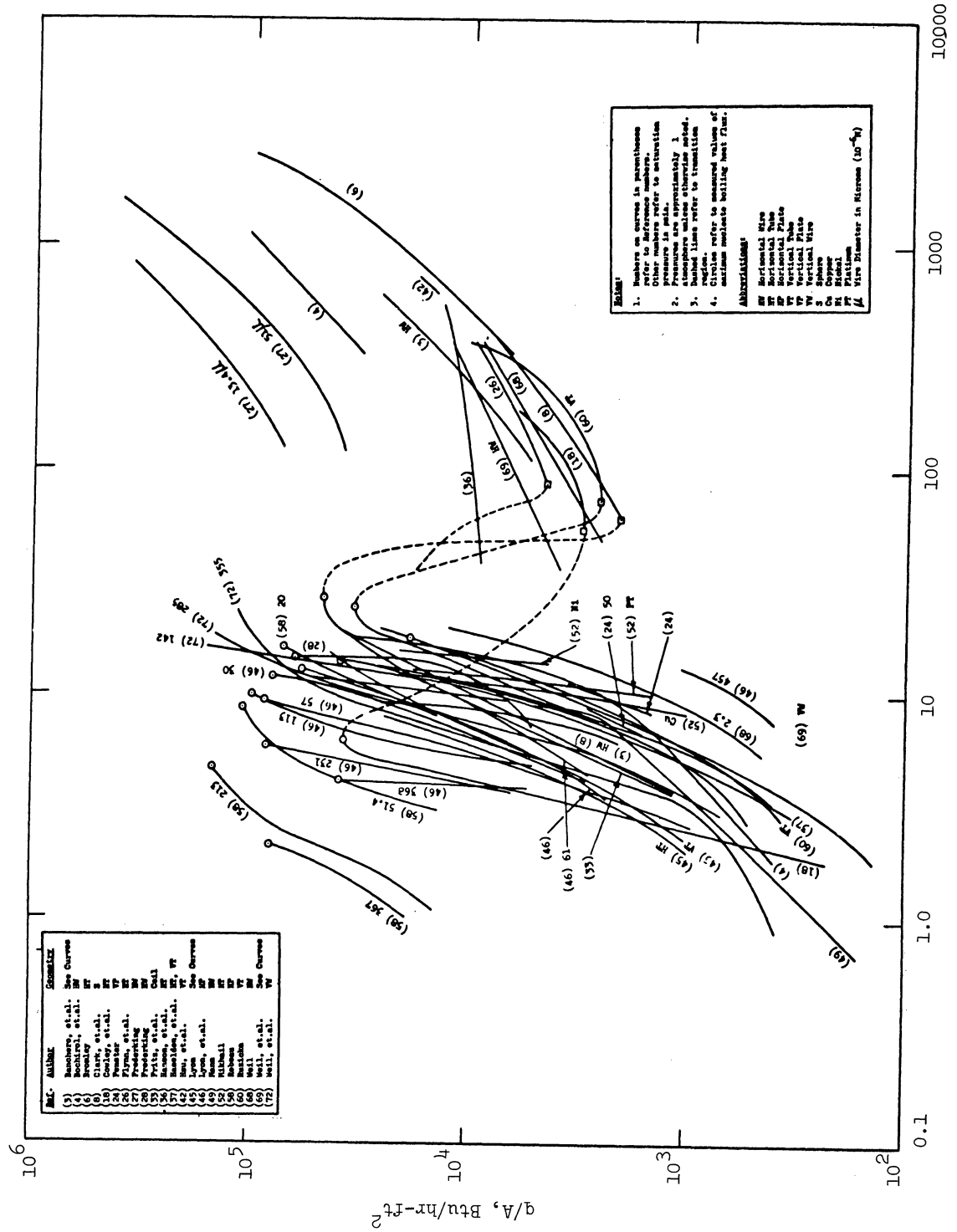

Fig. 35. Experimental pool boiling data for nitrogen.

Merte, et al.,[19] for a sphere by using the Nusselt (Nu) and modified Rayleigh (Ra') numbers. The relationship obtained was:

$$Nu = C_1(Ra')^{1/3} \tag{16}$$

where

$$Nu = \frac{\bar{h}D}{k_{vf}} \tag{17}$$

and

$$Ra' = \{D\}^3 \left\{ \frac{\rho_{vf}(\rho_\ell - \rho_{vf})g}{(\mu_{vf})^2} \left(\frac{C_p\mu}{k}\right)_{vf} \left(\frac{h_{fg}}{C_p\Delta T_{sat}} + 0.5\right) \right\} \left(\frac{a}{g}\right) \tag{18}$$

with $C_1 = 0.14$. The correlation was developed on the basis of data from film boiling of saturated liquid nitrogen at atmospheric pressure and standard gravity only.

The film boiling results obtained with saturated liquids at pressure of 1, 3, and 5 atmospheres for the 1-inch, 1/2-inch, and 1/4-inch diameter spheres and for the various levels of (a/g) are plotted on Fig. 36 in terms of Nu and Ra'. The Frederking-Clark correlation is also shown and except for the results with the 1/4-inch diameter sphere correlates the data quite well, including the variations in pressure and (a/g). For a given Ra', the Nu for the 1/2-inch diameter sphere is approximately 7% higher, and for the 1/4-inch diameter sphere approximately 20% higher than that corresponding for the 1-inch diameter sphere. If the constant C_1 is evaluated independently for each diameter, values of 0.14, 0.15, and 0.17 are obtained for the 1-inch, 1/2-inch, and 1/4-inch diameter spheres, respectively. C_1 may

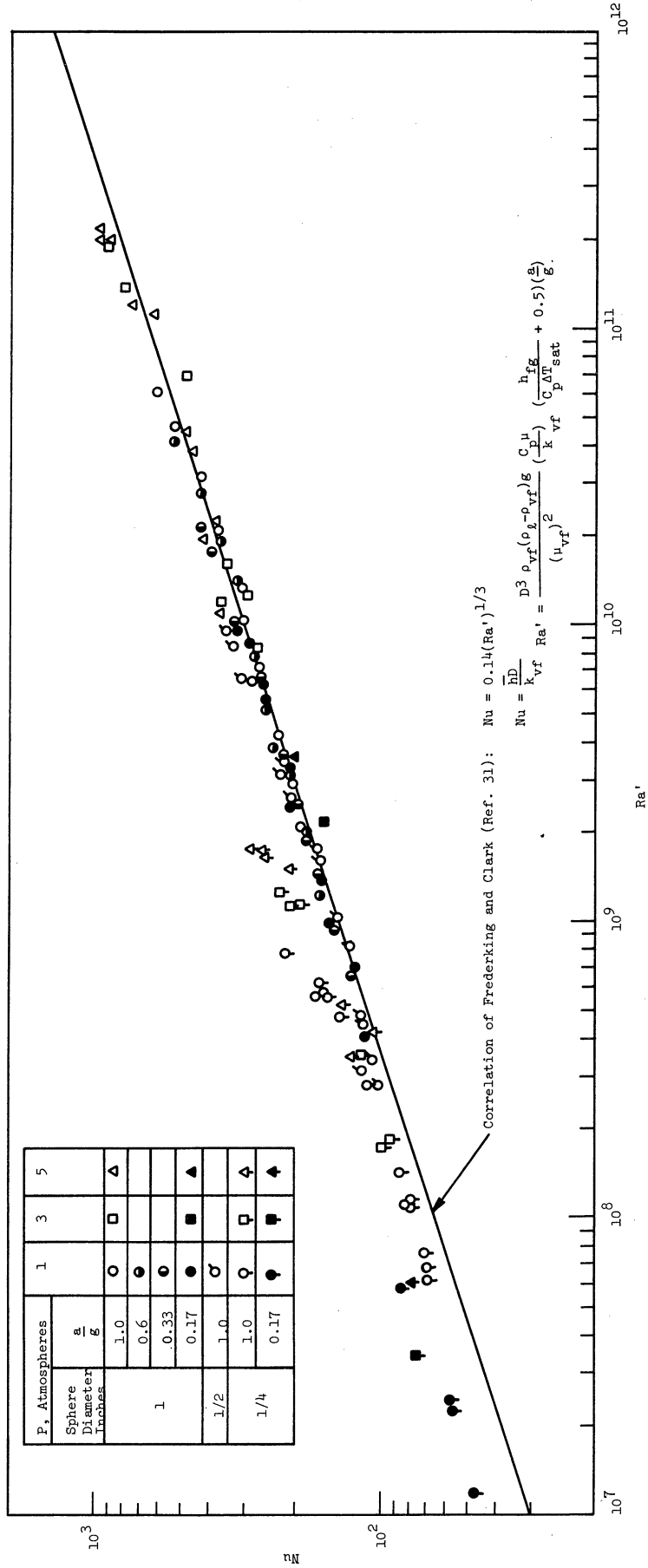

Fig. 36. Correlation of saturated film boiling on spheres.

be related to the diameter by:

$$C_1 = 0.14 \left(\frac{D}{D_{ref}}\right)^{-1/8} \tag{19}$$

where D_{ref}, the reference diameter, is chosen to be that of the 1-inch diameter sphere for which the correlation was originally developed.

Manson and Seader[45] obtained (q/A) vs. ΔT_{sat} film boiling data for a 4-inch diameter sphere in saturated liquid nitrogen at 1 atmosphere and (a/g) = 1. They reported that, for a given ΔT_{sat}, their (q/A) results were approximately 10% lower than those of Merte, et al.[19] The decrease in heat flux between a 1-inch and 4-inch diameter sphere predicted by Eqs. (16) and (19) is 16%. Equations (16) and (19) are thus shown to be applicable with sphere diameters varying by a factor of 16 and Ra' covering a range of 4 orders of magnitude.

The saturated film boiling data obtained with the spheres are replotted as Nu vs. $[Ra' \times (D/D_{ref})^{-3/8}]$ in Fig. 37. Also included are the data for film boiling of Freon-113 from a cylinder over the range $1 \leq (a/g) \leq 10$, and Bromley's correlation[27] for laminar flow film boiling from a horizontal cylinder. Bromley's correlation for the heat transfer coefficient, $\bar{h}$, in film boiling from cylinders[27] is

$$\bar{h} = 0.62 \left[\frac{k_{vf}^3 \rho_{vf} g(\rho_\ell - \rho_{vf}) h'_{fg}}{\mu_{vf} \Delta T_{sat} D}\right]^{1/4} \tag{20}$$

With the exception of some of the 1/4-inch diameter sphere results at (a/g) = 0.17, Eqs. (16) and (19) fit the experimental data within ±25%. The diameter of the test cylinders used by Pomerantz,[34] 0.188 inch, was

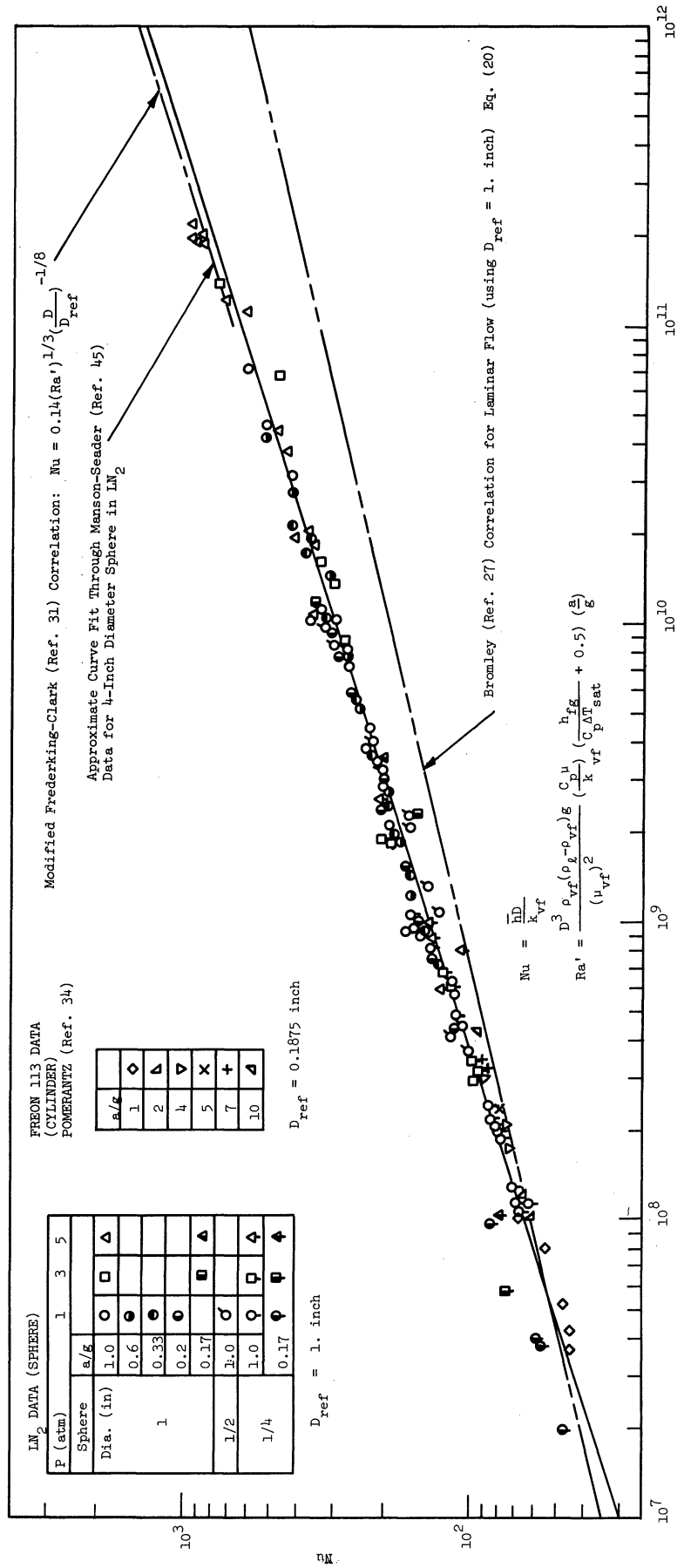

Fig. 37. Correlation of saturated film boiling on spheres and cylinders.

used as the reference diameter for the cylinder data.

The saturated film boiling results obtained using the disk were also plotted as Nu vs. Ra' in an attempt to determine if this data would be correlated by the same parameters as were the data from the sphere. The plot for the vertical disk is shown in Fig. 38. The value of D used in Fig. 38 was the disk diameter, 3 inches. A straight line fit through the (a/g) = 1 data on Fig. 38 can be used to predict most of the experimental points within ±25%. The data points for (a/g) = 0.16 deviate considerably from such a fit, indicating that a correlation of the form $Nu = C_1(Ra')^n$ does not properly describe the film boiling process for the disk in this case. This was also true for other orientations of the disk.

Other investigators (Refs. 34, 43, 46, 47) indicate the appropriate dimensions for correlating film boiling data from a flat surface may be what are referred to as the critical wavelength, λ_c, and the most dangerous wavelength, λ_d. The heat flux of a flat plate heating upward should not be influenced by its physical dimensions at a given ΔT_{sat} provided the plate is large enough to neglect edge effects.

It is possible that changes in properties or other relevant parameters which influence the vapor film thickness and vapor flow patterns, and thereby influence the heat flux, may be reflected in changes of λ_c and λ_d.

Bellman and Pennington[48] showed that the smallest wave which will be unstable along a vapor-liquid interface, in an adverse gravity direction, has a length, called the critical wavelength, given by

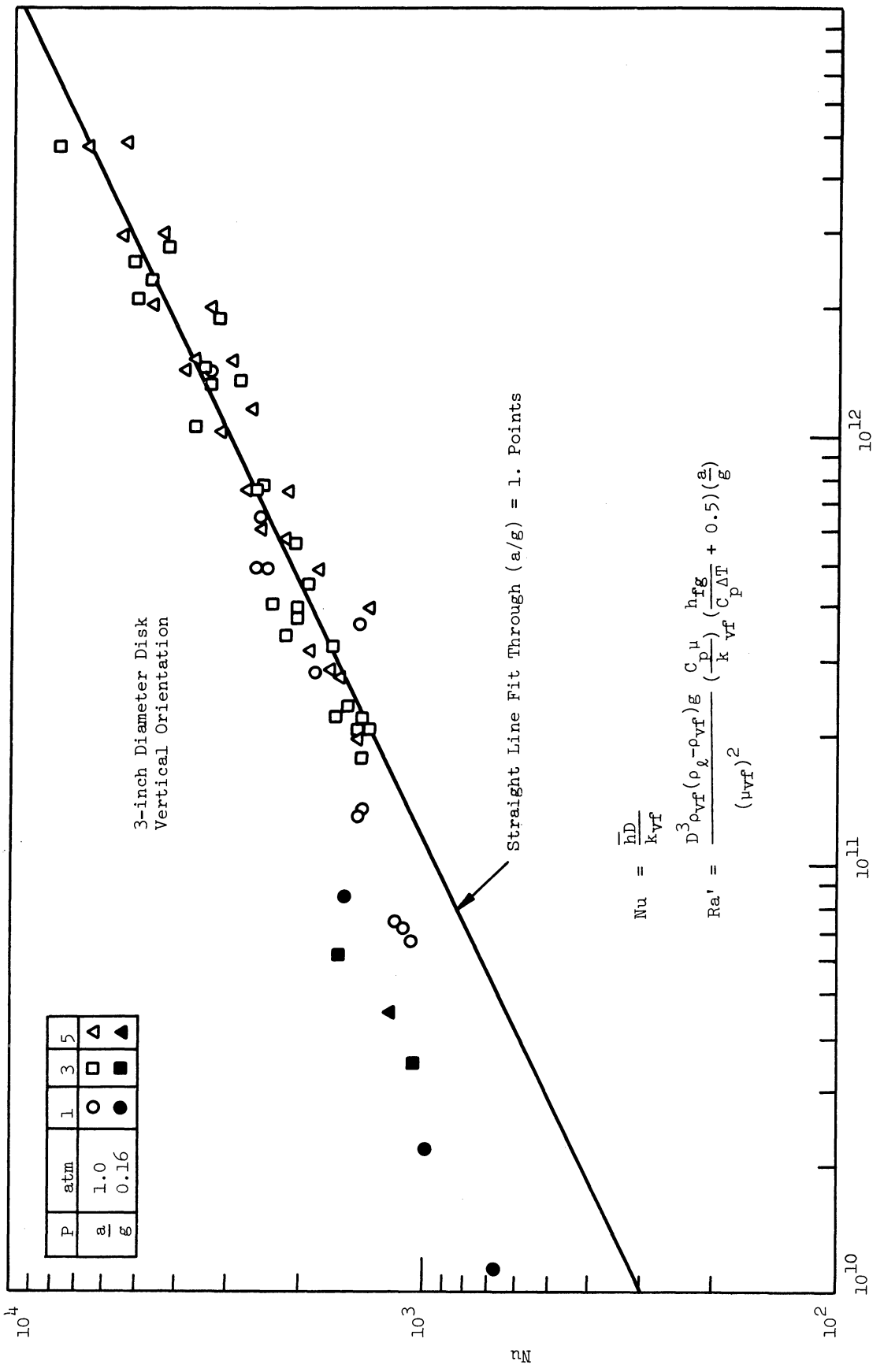

Fig. 38. Correlation of saturated film boiling on a disk.

$$\lambda_c = 2\pi\left[\frac{g_o\sigma}{g(\rho_\ell-\rho_v)}\right]^{1/2}\left(\frac{a}{g}\right)^{-1/2} \qquad (21)$$

When the wavelength is shorter than λ_c, the interface is stable, and disturbances will be damped out. When the wavelength is longer than λ_c, the interface is unstable, and disturbances will grow. In the case of film boiling, this implies that if the wavelength is longer than λ_c, bubbles will form and detach from the vapor film, while if the wavelength is shorter than λ_c, interface motion may be observed but no bubbles will form.

Bellman and Pennington[48] also showed that the rate at which a disturbance grew was a function of the wavelength. The wavelength for which the amplitude of a disturbance grows most rapidly is called the most dangerous wavelength, given by

$$\lambda_d = 2\pi\left[\frac{3g_o\sigma}{g(\rho_\ell-\rho_v)}\right]^{1/2}\left(\frac{a}{g}\right)^{-1/2} \qquad (22)$$

The critical wavelength increases with decreasing (a/g), indicating that for film boiling at very low values of (a/g) there is no hydrodynamic justification for the formation of bubbles as such. The analysis is based on the existence of a vapor-liquid interface with an adverse gravity direction (Taylor instability) so extension of the analysis to true zero gravity conditions is meaningless.

The critical wavelength, λ_c, was substituted for the characteristic dimension D in Eqs. (17) and (18) to determine whether it might be a more appropriate characteristic dimension for the horizontal flat surfaces. The exponent on (a/g) in Ra' was changed from 1 to 2/3 to reflect the ex-

perimentally observed decreased sensitivity of (q/A) to changes in (a/g) at a given ΔT_{sat}. The disk data were thus expressed in terms of parameters designated by Nu" and Ra", where

$$Nu'' = \frac{\bar{h}\lambda_c}{k_{vf}} \tag{23}$$

$$Ra'' = \frac{\lambda_c^3 \rho_{vf}(\rho_\ell - \rho_{vf})g}{(\mu_{vf})^2}\left(\frac{C_p\mu}{k}\right)_{vf}\left(\frac{h_{fg}}{C_p\Delta T_{sat}} + 0.5\right)\left(\frac{a}{g}\right)^{2/3} \tag{24}$$

The results are shown in Figs. 39, 40, and 41 for the disk in the vertical, horizontal heating up, and horizontal heating down orientations, respectively. The disk data for all orientations, pressures, and values of (a/g) = 1 and 0.16 may be represented with an accuracy of ±35% by the relation ship

$$Nu'' = 0.012\ (Ra'')^{1/2} \tag{25}$$

Hosler and Westwater[43] measured heat flux as a function of ΔT_{sat} for saturated film boiling on an 8-inch square horizontal, heating up, flat plate at atmospheric pressure using water and Freon-11 (CCl_3F) as test fluids. Representative points from these results are also included in Figs. 40 and 42. They fall about 40 to 60% below the disk data at the same value of Ra". If the boiling phenomena were identical (i.e., solely a function of λ_c) regardless of plate size, the data might be expected to agree.

Berenson[3] analyzed film boiling from a horizontal flat surface heating up and developed a correlation for the heat transfer coefficient,

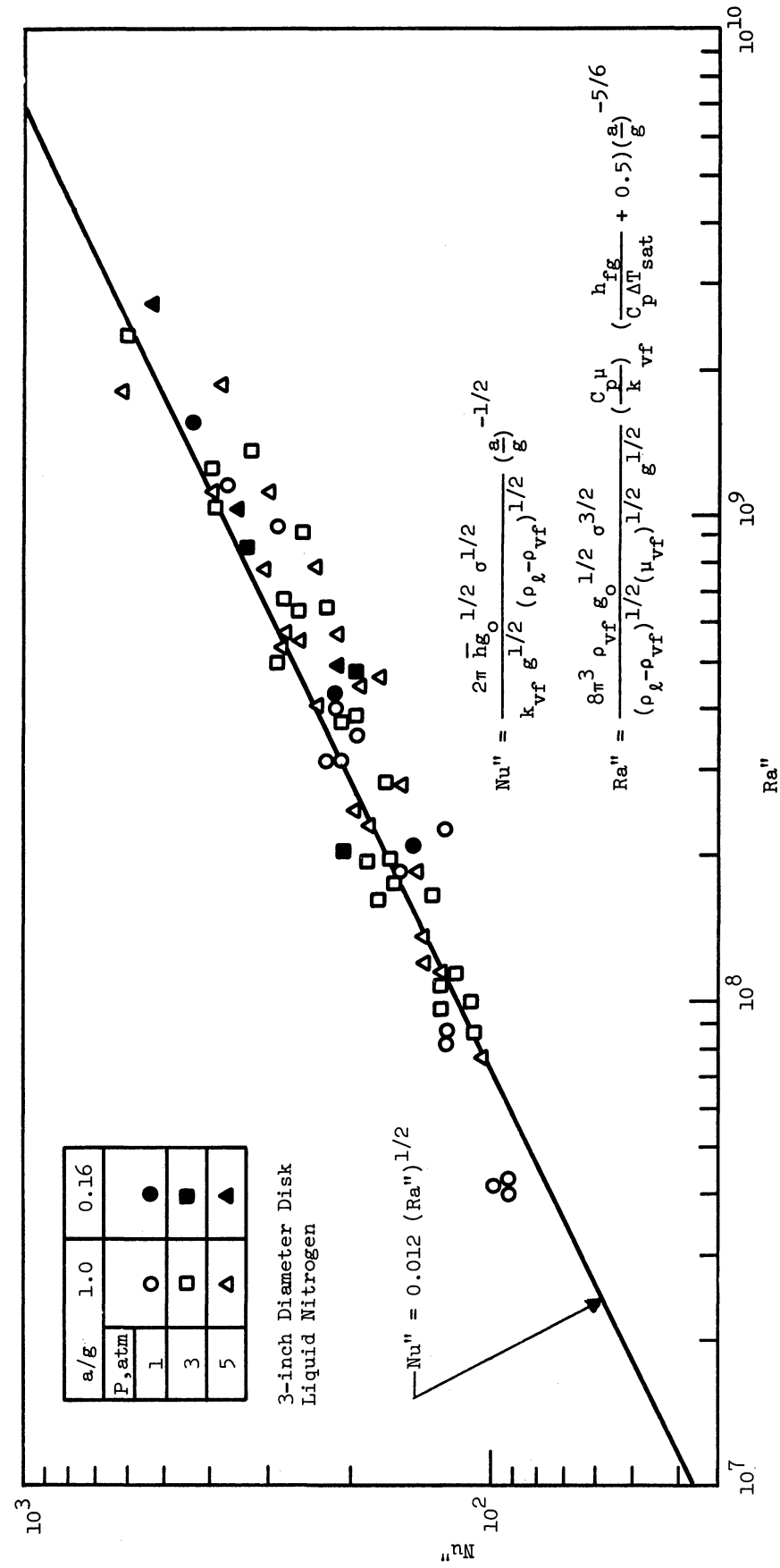

Fig. 39. Saturated film boiling correlation for a vertical disk.

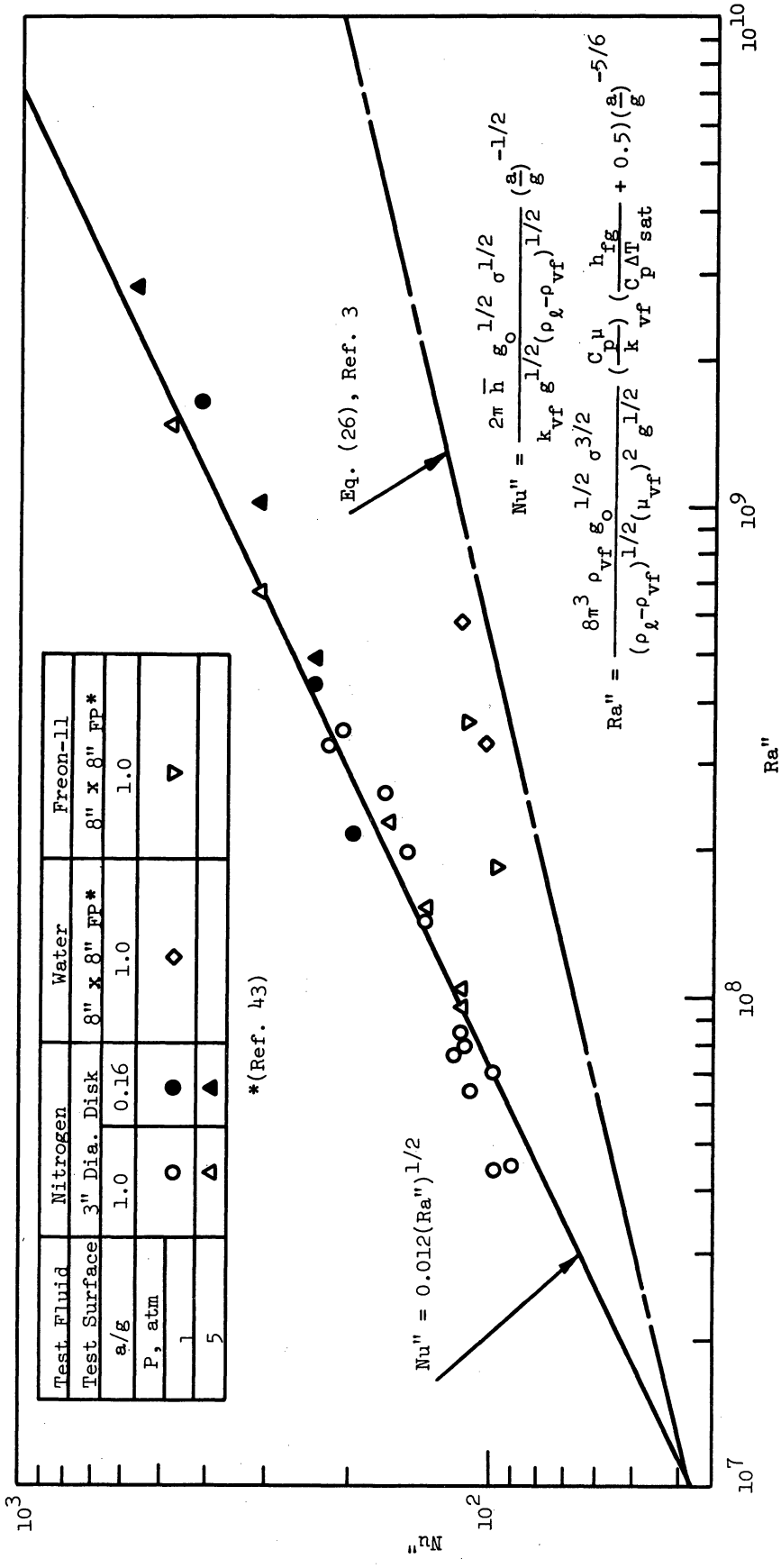

Fig. 40. Saturated film boiling correlation for a horizontal disk heating up.

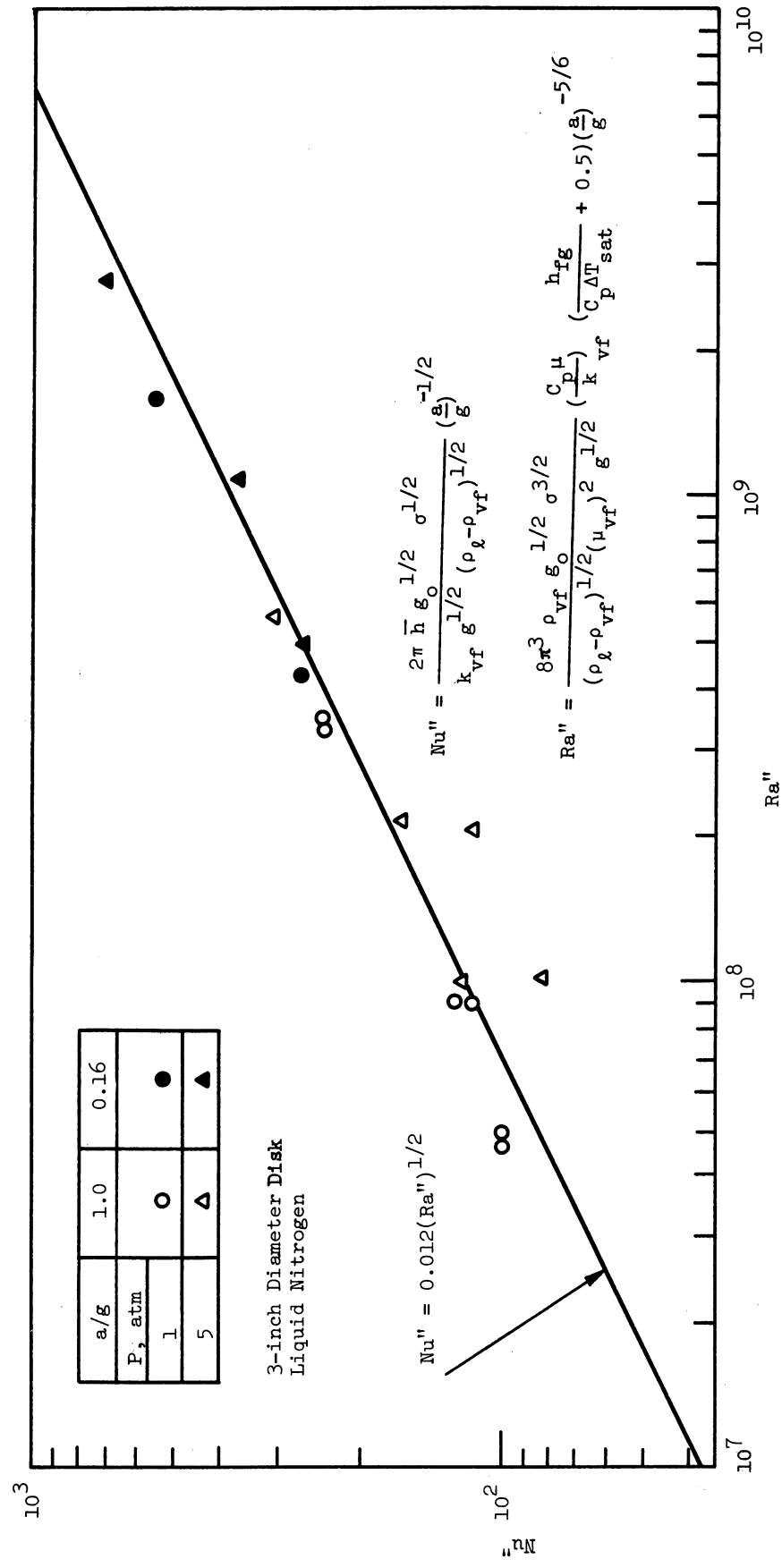

Fig. 41. Saturated film boiling correlation for a horizontal disk heating down.

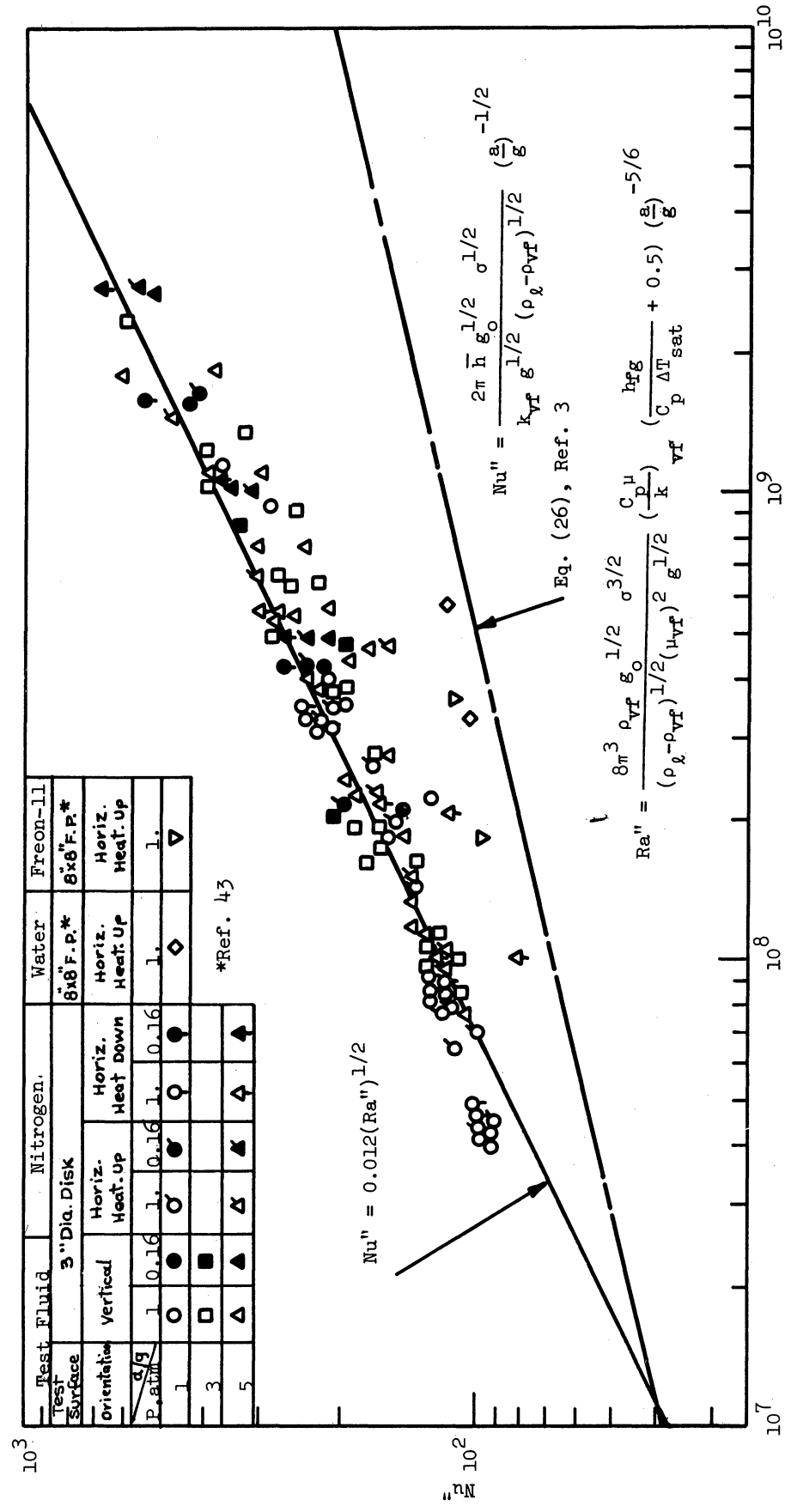

Fig. 42. Saturated film boiling correlation for flat plates.

$$\bar{h} = 0.425 \left[\frac{k_{vf}^3 \rho_{vf} g(\rho_\ell - \rho_v) h'_{fg}}{\mu_{vf} \Delta T_{sat} \left(\frac{g_o \sigma}{g(\rho_\ell - \rho_v)} \right)^{1/2}} \right]^{1/4} \left(\frac{a}{g} \right)^{3/8} \qquad (26)$$

This correlation, developed for a plate of infinite extent, is included in Figs. 40 and 42, and predicts a behavior considerably different from that of this study. This may indicate that a size effect, such as the one given for the spheres in Eq. (19), is also present with flat plates. The difference in slope between the correlation of Berenson[3] (1/4) and the experimental data (1/2) may indicate that laminar conditions do not exist in the present experimental conditions. This is discussed further in Section VII. A.3.e.

The calculated value of λ_c at $(a/g) = 0.17$ is more than twice the diameter of the 1/4-inch diameter sphere at all pressures, but is less than the diameter of the 1-inch diameter sphere. Breen and Westwater[49] observed a change in hydrodynamic behavior, from a two-dimensional wave pattern to a one-dimensional wave pattern (Pomerantz[34] considered these as three-dimensional and two-dimensional wave patterns, respectively) when cylinder dimensions were decreased from greater than λ_d to less than λ_c. Adopting Pomerantz' terms, a two-dimensional wave pattern is characterized by flow of the vapor around a cylinder or sphere to the very top, where it is released from a narrow slit along the top of the cylinder or a narrow tube at the top of the sphere. A three-dimensional wave pattern is characterized by bubbles leaving the entire top half of the cylinder or sphere at many different circumferential positions. If the three-dimensional wave pattern

on the 1/4-inch diameter sphere at (a/g) = 1 changed to a two-dimensional wave pattern at (a/g) = 0.17, the characteristic dimension for use in the correlations might well be λ_c rather than the sphere diameter. The test facility did not permit examination of the wave patterns on a test object during package drop. If the change from a three-dimensional to a two-dimensional wave pattern with the 1/4-inch diameter sphere results in an increased heat flux for a given ΔT_{sat}, similar to that observed on the disk, then a reduced effect of (a/g) should also be observed and the exponent, n, on $(a/g)^n$ in (Ra') should be reduced from 1 to 2/3. The results obtained with the 1/4-inch diameter sphere at (a/g) = 0.17 are plotted in terms of Nu vs.$[Ra' \times (D/D_{ref})^{-3/8}]$ on Fig. 43 using n = 1 and 2/3. The points plotted using n = 1 correspond to those shown in Fig. 37. The points plotted using n = 2/3 very closely approximate the correlation used for all of the other sphere results.

Saturated film boiling appears to be governed by a number of factors in addition to the physical properties of the liquid and the temperature difference. Among these are geometry and orientation of the heater surface, which influence the hydrodynamic behavior of the liquid-vapor interface. Changes in the applied gravitational field also affect film boiling and these factors must all be taken into account if a single correlation for saturated film boiling is the desired result.

A composite of correlations for boiling under saturated conditions in the various regimes is presented in Fig. 44. The reference curve, introduced in Chapter VI as applying to the 1-inch diameter sphere at atmos-

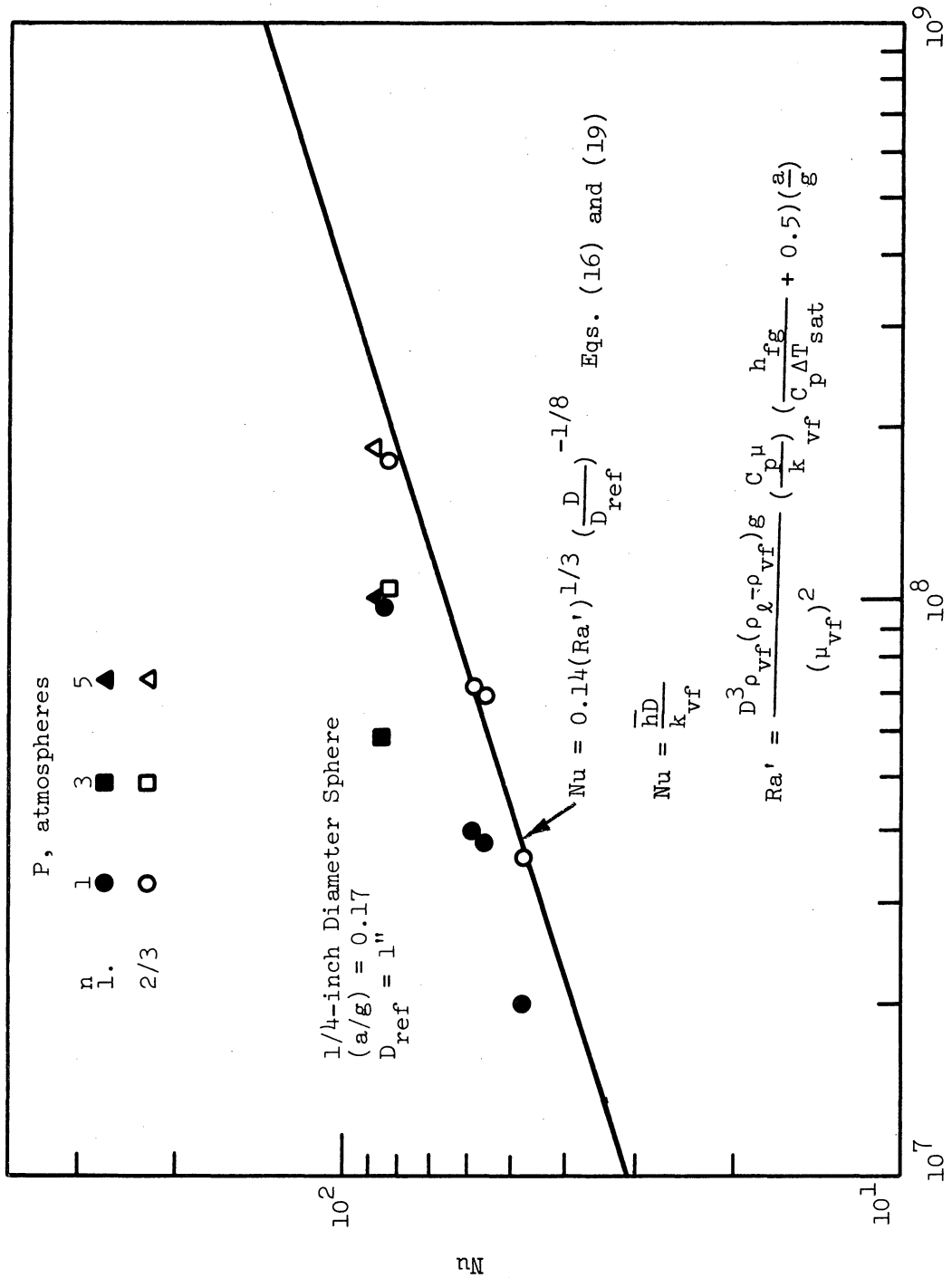

Fig. 43. Effect of exponent on (a/g) on a saturated film boiling correlation.

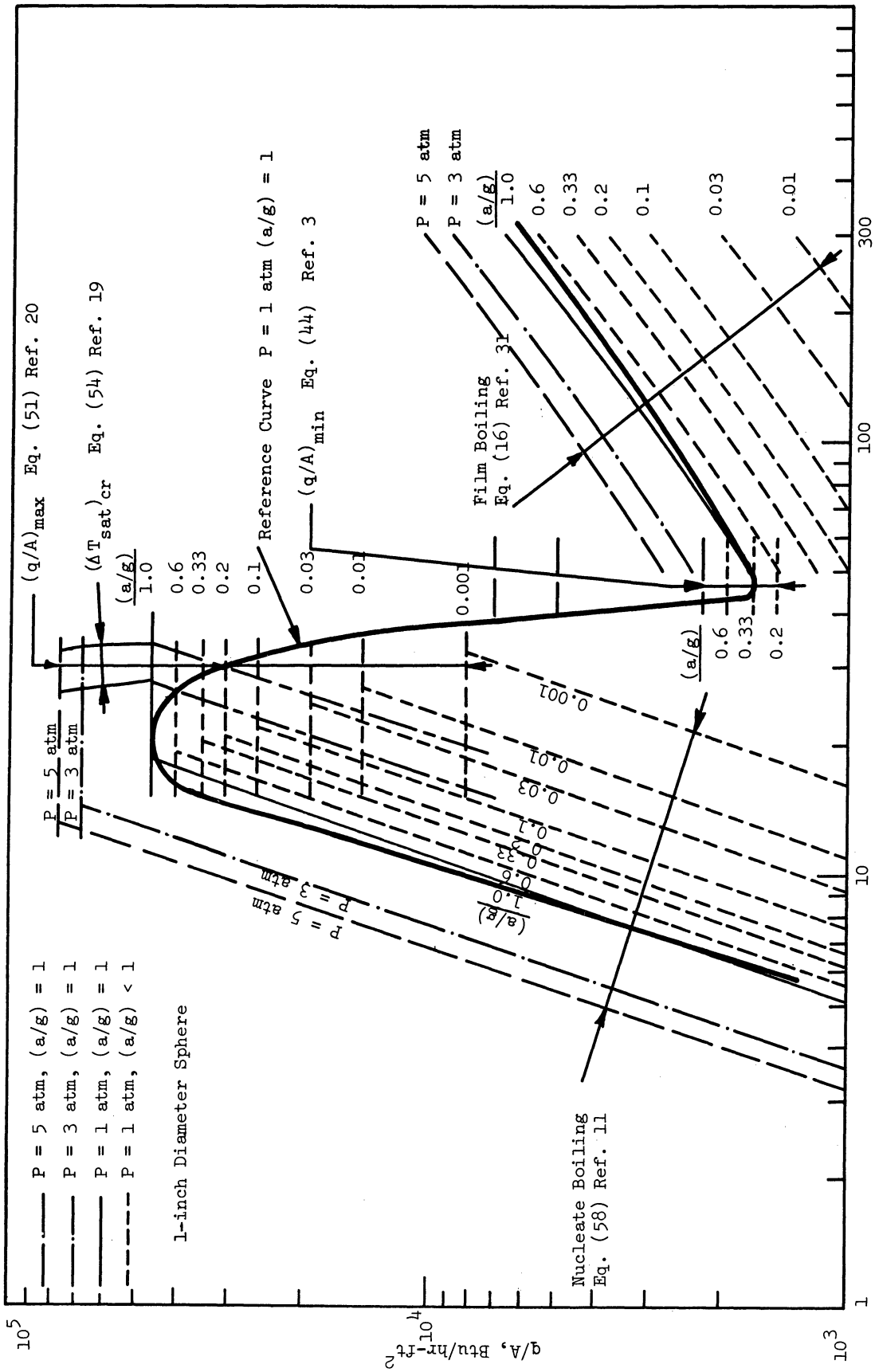

Fig. 44. Saturated boiling correlations.

pheric pressure and (a/g) = 1, is shown to provide a basis for comparison. For saturated film boiling, Eq. (16) is shown, and the correlations for the other regions will be discussed in the following sections.

2. Subcooled Liquid Boiling Correlations

Subcooled film boiling occurs when the bulk liquid temperature is maintained below the liquid saturation temperature. This is normally accomplished by circulating the liquid, replacing the heated liquid by cooler liquid. The resultant liquid motion along the heated surface generally classifies subcooled film boiling as a forced convection problem (see, e.g., Ref. 50). Where film boiling is to take place for relatively short periods of time only, as is present with the transient technique used here, it is possible to provide subcooling on a batch basis, without the necessity for a circulating system, by pressurizing the system just prior to conducting the test.

Ellion[50] found experimentally that, for a given ΔT_{sat}, heat flux in the film boiling region was larger with subcooled liquid than with saturated liquid. This had also been predicted analytically (e.g., Ref. 51).

Sparrow and Cess[52] studied the problem of subcooled laminar film boiling for the case of the isothermal vertical plate. The two-phase flow and heat transfer problem was formulated within the framework of boundary layer theory, and a solution developed an expression for the local heat flux as

$$q/A = \frac{k_{vf}\left[0.84 + \frac{1}{B}\right]^{1/4}\left[g\rho_{vf}(\rho_{\ell}-\rho_{vf})\right]^{1/4}}{2(\mu_{vf})^{1/2}(x)^{1/4}} \Delta T_{sat} \left(\frac{a}{g}\right)^{1/4} \qquad (27)$$

The distance x is measured from the leading edge of the plate, and B is a computational parameter defined in Ref. 52 as a function of the thermodynamic and physical properties of the boiling liquid and the degree of subcooling.

Equation (27) is plotted in Fig. 45 for liquid nitrogen at several different pressures and levels of subcooling in terms of (q/A) vs. ΔT_{sat}. The height above the bottom edge of the plate, x, was taken as 0.125 foot which corresponds to the distance from the bottom of the vertical disk to the thermocouple position. The data obtained with the vertical disk at pressures of 3 and 5 atmospheres with subcooled liquid and at (a/g) = 1 are also shown in Fig. 45. For a given ΔT_{sat}, the experimental levels of heat fluxes are approximately four times larger than that predicted by Eq. (27).

The correlation for saturated boiling on the disk given in Eq. (25) is included in Fig. 45. To determine if the trend of the effect of subcooling as predicted by Eq. (27) is correct even if the absolute level is not, the ratio of the subcooled (q/A) (experimental data) to the saturated (q/A) (correlation) for various values of ΔT_{sat} was calculated and is given in Table III. This ratio as predicted by Eq. (27) is also given. The experimental results show an increase in the ratio $(q/A)_{sc}/(q/A)_{sat}$ with increasing ΔT_{sat}, while Eq. (27) predicts that this ratio will decrease with increasing ΔT_{sat}.

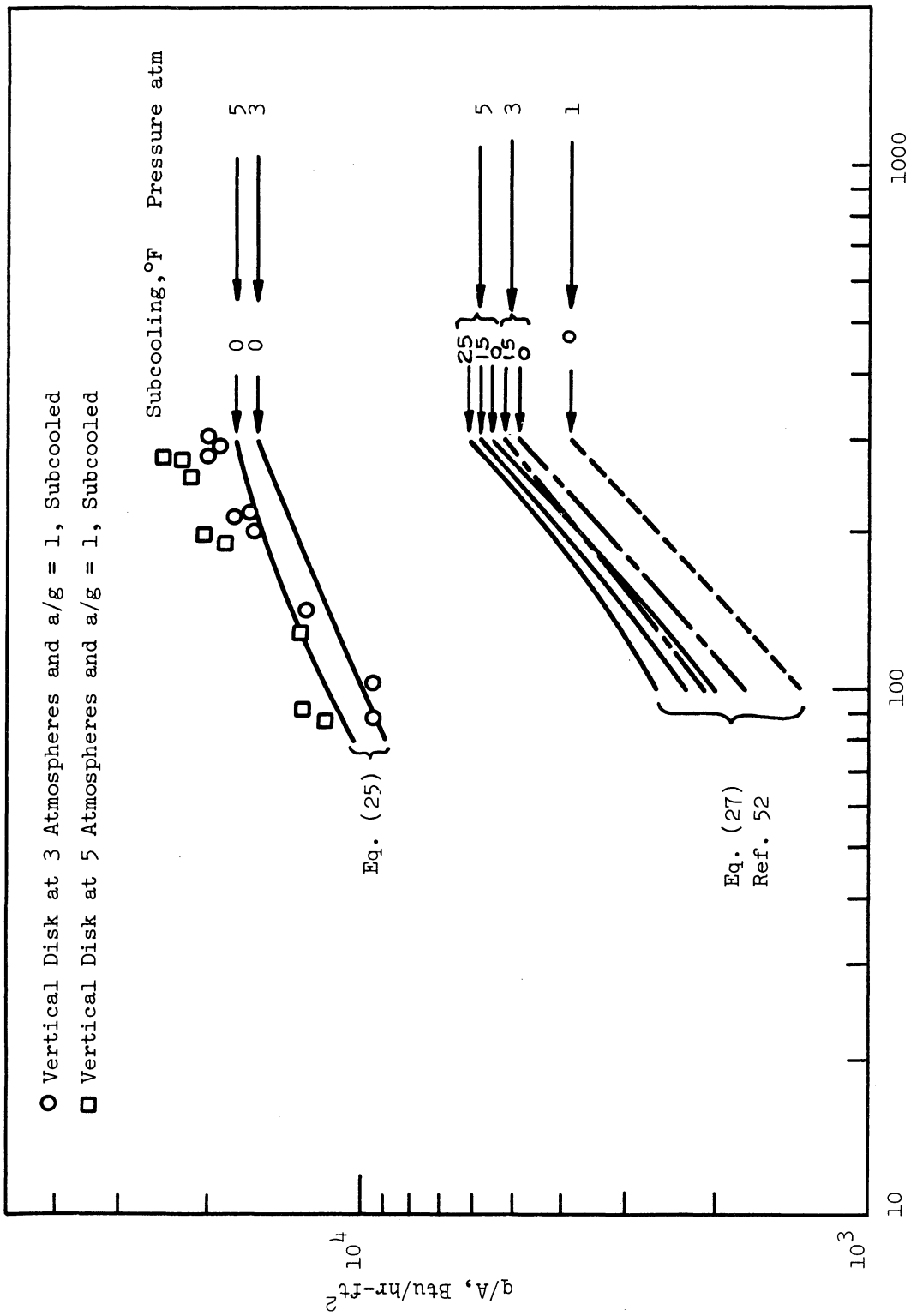

Fig. 45. Subcooled film boiling correlation.

TABLE III

COMPARISON OF ANALYTICAL PREDICTIONS AND EXPERIMENTAL RESULTS FOR THE RATIO $(q/A)_{sc}/(q/A)_{sat}$ FOR A VERTICAL DISK AT 3 AND 5 ATMOSPHERES

	P, atm					
	3			5		
ΔT_{sat}, °F	100	200	300	100	200	300
Experimental Results (subcooling, °F)	0.974 (2)	1.213 (8)	1.233 (12)	1.130 (10)	1.260 (18)	1.343 (20)
Eq. (27) (Ref. 54) (subcooling, °F)	1.192 (15)	1.110 (15)	1.067 (15)	1.302 (25)	1.140 (25)	1.098 (25)

There are several possible reasons why the correlation of Sparrow and Cess,[52] as given in Eq. (27), does not follows the experimental data obtained. First, the boiling film may have been turbulent, so a laminar film analysis does not apply. Second, the flow pattern over the disk may be sufficiently different from the flow over a vertical flat plate so the analysis does not apply. Examination of the photographic composites of the vertical disk (Fig. 31) indicates a thickening of the film near the thermocouple location, which may be an indication of the onset of turbulent flow.

3. Boiling Film Thickness Analyses

The physical picture of film boiling is a superheated solid surface separated from a liquid by a vapor film. This may be compared with a picture of nucleate boiling where bubbles form on a superheated solid surface, grow, and leave the surface. An exact mathematical model of the film boiling process probably cannot be formulated to include temporal variations in

the shape of the vapor liquid interface along with the departure of vapor bubbles from the film. It should be possible, however, to develop a model which approaches the actual phenomenon more closely than is possible in the nucleate boiling region.

The physical appearance of the film was carefully examined in the composites presented in Figs. 30, 31, 32, and 33. The film around the 1-inch diameter sphere at (a/g) = 1 was not easily approximated by a simple model. The film thickness on the disk in all three positions did not vary appreciably with time, and models were feasible. Models from the literature were used where available. Mathematical models were developed where required. Evaluation of the film thickness was the desired result.

a. Film Formation at Zero Gravity

A simple model of the vapor film is one in which there is no mass flux, which would exist in a true zero-gravity environment. If the liquid was in contact with the solid surface at time t = 0, the vapor film would form and continue to increase in thickness with increasing time. There would be no convection in the absence of gravity, and if radiation is negligible the problem is one of pure conduction.

This problem has been formulated by Chang[46] and more recently by Yang[53]. The solution presented by Yang takes into account finite values of thermal capacity and thermal conductivity of the solid surface and is presented here. This solution was developed for the transient condensation of a pressurizing gas in a suddenly pressurized cryogenic tank. The physical system analyzed consisted of a semi-infinite wall in the region

$x < 0$ and a semi-infinite body of phase 1 in the region $x > 0$. Initially the temperature of the system was uniform. At time $t = 0$ the temperature of the wall was changed and immediately phase 2 began to form on the wall. The temperature of the interface adjusts to the saturation temperature corresponding to the system pressure, and subsequently remains at that temperature. As applied to the problem of vapor film formation in a zero-gravity environment, the solution for the film thickness may be expressed as

$$\delta = 2(\alpha_c t)^{1/2} \tag{28}$$

where α_c must satisfy the transcendental algebraic equation:

$$\frac{\rho_\ell C_{p\ell}(T_{sat}-T_s)}{\left[\frac{(\rho C_p k)_\ell}{(\rho C_p k)_{sd}}\right]^{1/2} + \operatorname{erf}\left[\left(\frac{\alpha_c}{\alpha_\ell}\right)^{1/2}\right]} \left(\frac{\alpha_\ell}{\pi}\right)^{1/2} e^{-(\alpha_c/\alpha_\ell)}$$

$$- \frac{\rho_\ell C_{p\ell}(T_\ell - T_{sat})}{\operatorname{erfc}\left[\frac{\rho_\ell}{\rho_v}\left(\frac{\alpha_c}{\alpha_v}\right)^{1/2}\right]} \left(\frac{\alpha_\ell}{\pi}\right)^{1/2} \left[\frac{(\rho C_p k)_v}{(\rho C_p k)_\ell}\right]^{1/2} e^{-\left(\frac{\rho_\ell}{\rho_v}\right)^2 \frac{\alpha_c}{\alpha_v}}$$

$$= \rho_\ell h_{fg} (\alpha_c)^{1/2} \tag{29}$$

α_c may be termed[46] the equivalent thermal diffusivity in heat conduction through a substance with change of phase.

Once α_c has been obtained, (q/A) may be expressed as

$$q/A = \frac{2k_v \Delta T_{sat}}{(\pi \alpha_v t)^{1/2} \operatorname{erf}\left[\left(\frac{\alpha_c}{\alpha_v}\right)^{1/2}\right]} \tag{30}$$

as in Ref. 46.

The solution as applied to the problem presented here is a function of ΔT_{sat}, pressure, and subcooling. For a given ΔT_{sat}, pressure, and subcooling, film thickness is proportional to $(t)^{1/2}$ and heat flux is proportional to $(t)^{-1/2}$.

b. Film Thickness on a Vertical Plate

Film boiling heat transfer measurements were made using the disk in three orientations: vertical, horizontal heating up, and horizontal heating down. Film formation in a gravity field must be treated separately for each orientation because the action of the buoyant forces in removal of the vapor generated is different in each case.

The analysis of laminar subcooled film boiling on a vertical plate performed by Sparrow and Cess[52] and discussed in Section VII.A.2 included development of an expression for film thickness. This was

$$\delta = \eta_{v\delta} \left[\frac{4\mu_{vf}^2}{g\rho_{vf}(\rho_\ell - \rho_{vf})} \right]^{1/4} x^{1/4} \left(\frac{a}{g}\right)^{-1/4} \qquad (31)$$

where x is measured from the leading edge of the plate. The parameter $\eta_{v\delta}$, which is a dimensionless boundary layer thickness, was evaluated by Sparrow and Cess[52] as a function of the parameter B for $Pr_v = 1$.

Hsu and Westwater[30] performed an approximate analysis of the flow in a vapor film on a vertical plate. An expression was obtained for the height above the leading edge of a vertical plate at which the onset of turbulence could be anticipated. This distance was

$$L_o = \frac{\mu_{vf}(100)h'_{fg}\delta^*}{2k_{vf}\Delta T_{sat}} \tag{32}$$

where δ^*, the film thickness at the onset of turbulence, is

$$\delta^* = \left[\frac{2\mu_{vf}^2(100)}{g\rho_{vf}(\rho_\ell-\rho_{vf})}\right]^{1/3}\left(\frac{a}{g}\right)^{-1/3} \tag{33}$$

The value (100) appearing in Eqs. (32) and (33) represents the critical value of the flow Reynolds Number as given in Ref. 30, at which it is stated transition between viscous and turbulent flow may be expected to occur.

c. Film Thickness on a Horizontal Flat Plate, Heating Up

Berenson[3] obtained an equation for the heat transfer coefficient in film boiling from a horizontal flat plate heating upward (see Eq. (26)). An expression was developed for the average vapor film thickness for the entire surface, given as

$$\delta = 2.35\left[\frac{\mu_{vf}k_{vf}\Delta T_{sat}}{h'_{fg}\rho_{vf}g(\rho_\ell-\rho_{vf})}\sqrt{\frac{g_o\sigma}{g(\rho_\ell-\rho_{vf})}}\right]^{1/4}\left(\frac{a}{g}\right)^{-3/8} \tag{34}$$

The film boiling model used consisted of a thin film of uniform thickness on which cylindrical bubbles with hemispherical caps were superimposed at regular intervals.

Chang[46] considered the film thickness to be dependent on the establishment of a stable wave motion wherein the buoyant and viscous forces are in an equilibrium condition. He obtained the value of this equilibrium film thickness to be

$$\delta = \left[\frac{8\pi^2\mu_{vf}\alpha_c}{g(\rho_\ell-\rho_{vf})}\right]^{1/3}\left(\frac{a}{g}\right)^{-1/3} \tag{35}$$

where α_c must be evaluated from Eq. (29).

Comparisons between Eqs. (34) and (35) and experimental measurements are made in Section VII.A.3.e.

d. Film Thickness on a Horizontal Flat Plate, Heating Down

An analysis of the steady-state vapor film thickness below a horizontal flat plate heating down was made and is included as Appendix B. For the case of a disk with a parabolic velocity profile in the film, the solution giving the vapor film thickness is

$$\delta_1 y_1^2 - \frac{2}{3}\delta_1^2 y_1 = \frac{3}{10}\left[\frac{(q/A)\cdot R}{h'_{fg}}\right]^2 \frac{1}{\rho_\ell \rho_{vf} g} \qquad (36)$$

where y_1 is the film thickness at the center of the disk, δ_1 is the difference in film thickness between the center and the edge of the disk, and R is the radius of the disk, as shown in Fig. B-1. It is noted that both y_1 and δ_1 are unknowns, and an estimate of one is required from other sources.

e. Comparison of Vapor Film Thickness Analyses with Experimental Results

The analysis presented for vapor film formation at zero gravity predicts that (q/A) will change with time. The experimental results obtained using the 1-inch diameter sphere and the second test package to obtain $(a/g) < 0.002$ at 1 atmosphere saturated conditions exhibited such a temporal variation in heat flux. The drastic reduction in body forces reduced or removed the Taylor instability, changing the character of the film boiling process from a steady convective one to a transient conduction one.

These results were presented in Fig. 19 and are also shown in Fig. 46. Equations (28) and (30), developed for the flat plate under zero gravity, were evaluated for saturated film boiling of liquid nitrogen at a pressure of 1 atmosphere.

The results obtained for heat flux and vapor film thickness at (a/g) = 0 are shown in Fig. 47 for ΔT_{sat} = 200°F. Also shown are the heat flux measurements from Run 52H at (a/g) = 1 and at (a/g) < 0.002, 0.7 second and 1.3 seconds after the package was released. Although Eq. (30) does not accurately predict the heat flux as a function of time, the predicted dependence of (q/A) on $t^{-1/2}$ is shown to be fairly good for this run.

The (q/A) calculated using Eq. (30) at t = 1.4 seconds is shown on Fig. 46 for a range of ΔT_{sat}. Most of the experimental heat fluxes at 1.4 seconds are higher than those predicted by Eq. (30). The flat plate model should apply to the sphere in this case since the vapor film thickness predicted by Eq. (28) is less than 10% of the 1-inch diameter sphere radius even after 1.4 seconds.

Equation (30) predicts that $(q/A) \propto (t)^{-1/2}$. The "early" data points shown in Fig. 46 were all obtained 0.7 second after the package was released. The "late" points were obtained 1.2 to 1.4 seconds after the package was released. Using these times for t in Eq. (30), predicted values of "late" (q/A) were calculated and are shown on Fig. 46. Reasonable comparisons are noted.

In this region ((q/A) < 1000 Btu/hr-ft^2) the value of dT/dt is less than 0.5°F per second. The individual temperatures are read to ±0.2°F,

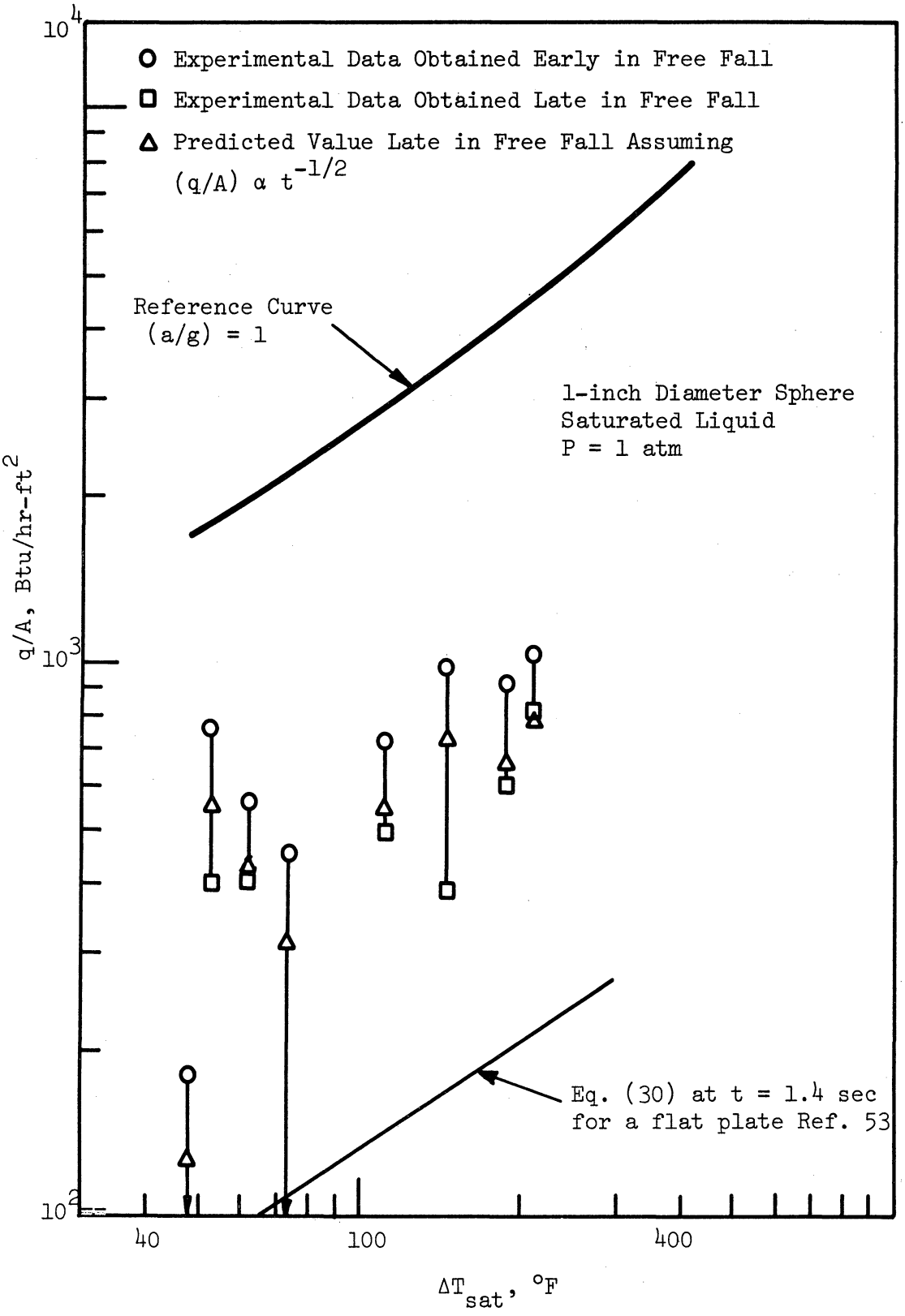

Fig. 46. Dependence of film boiling heat flux on time.

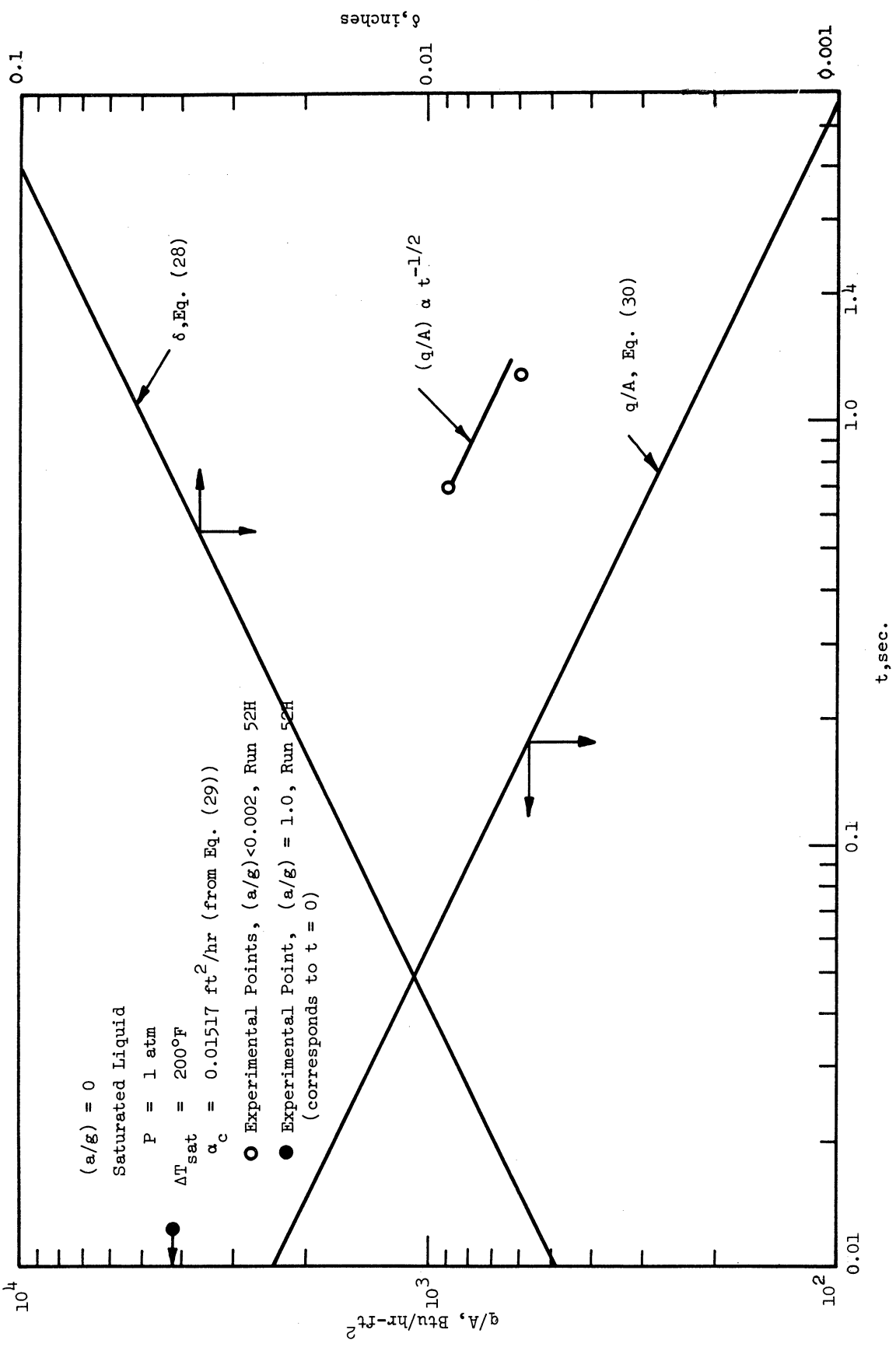

Fig. 47. Variation of heat flux and vapor film thickness with time.

and for these runs readings were made every 0.1 second. Tangents were fit to the data points over a 0.4 second range (i.e., a change in temperature of 0.2°F, which is equal to the reading error). An error of 0.1°F in dT (estimated to be the maximum error for these runs) over this range is 0.25°F per second, which is an error of 50% or more in (q/A). The $(t)^{-1/2}$ power dependence of (q/A) predicted for zero gravity appears supported by the experimental results.

The photographic results obtained permit the film thickness to be measured. The variables covered included test surface geometry, disk orientation, and ΔT_{sat}. All photographs were taken using saturated liquid nitrogen at 1 atmosphere and at (a/g) = 1, so comparison of the predicted and observed film thickness is possible only under these conditions. The effects of (a/g), subcooling, and pressure on film thickness are predicted, but are not compared with experimental results.

The equation for laminar vapor film thickness on a vertical plate obtained by Sparrow and Cess[52] (Eq. (31)) was evaluated for a value of x = 1.5 inches (the distance from the leading edge of the vertical disk to the point at which the thermocouple used for the temperature measurements was located). The results are shown in Fig. 48 as a function of ΔT_{sat}. Experimental measurements obtained from Fig. 31 are also shown, and are approximately one order of magnitude larger than the predicted values. It should be recalled, however, that owing to the optical configuration used, the observed values of film thickness are most likely the maximum values across the surface.

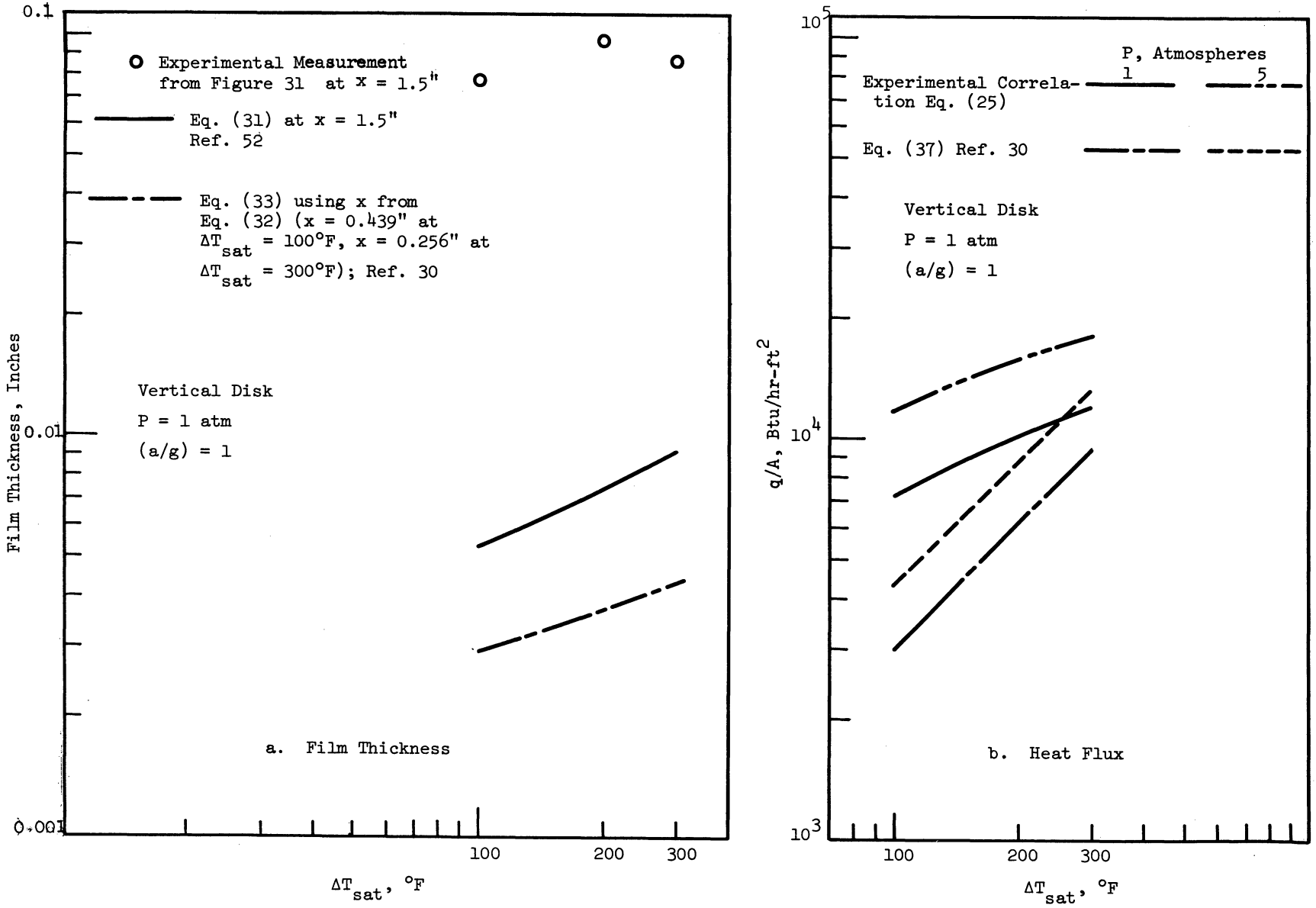

Fig. 48. Film thickness and heat flux in saturated film boiling on a vertical disk.

The film thickness at which Hsu and Westwater[30] (Eq. (33)) predict transition from laminar to turbulent flow is also shown in Fig. 48. It is seen to be thinner than the thickness predicted by Eq. (31), and the x at which transition is predicted to occur is less than 1.5 inches. This implies that turbulent flow is present near the thermocouple location, and the analysis of Sparrow and Cess[52] for laminar flow does not apply.

Hsu and Westwater[30] also predicted the turbulent heat flux on a vertical plate as a function of pressure and ΔT_{sat}, obtaining

$$q/A = k_{vf}\left[\frac{2}{3}\left(\frac{3E}{3F+1}\right)(x-L_o) + \left(\frac{1}{\delta^*}\right)^2\right]^{1/2} \Delta T_{sat} \qquad (37)$$

where

$$E = \left[\frac{g(\rho_\ell-\rho_v)}{\rho_v}\right]\left[\frac{\rho_{vf}}{\mu_{vf}(100)}\right]^2 \qquad (38)$$

and

$$F = \frac{\mu_{vf} + \dfrac{f\rho_v\mu_{vf}(100)}{2\rho_{vf}} + \dfrac{k_{vf}\Delta T_{sat}}{h_{fg}}}{\dfrac{k_{vf}\Delta T_{sat}}{h_{fg}}} \qquad (39)$$

Equation (37) is included in Fig. 48 for saturated boiling at 1 and 5 atmospheres. Also shown is the experimental correlation obtained in Section VII.A.1. (Eq. (25)). The prediction is lower than the experimental curve by 25% to 60%, and shows a different slope for (q/A) vs. ΔT_{sat} than was obtained experimentally. Although Eq. (37) does not accurately predict the experimental results, it could be useful in obtaining an order of magnitude approximation to anticipated experimental heat flux.

The agreement of Eq. (37) to within 60% or less of experimental data,

coupled with the predicted location of the transition point being small, and the observed vapor film being an order of magnitude greater than a laminar flow analysis, all appear to indicate that turbulent flow may exist over a relatively large portion of the heater surface.

An accurate determination of the location of the laminar to turbulent transition point along the vertical disk could be made by experimentally measuring the velocity profile in the film, but this would be a formidable task and was outside the scope of the project at this time. Examination of Fig. 31 does show more variation from frame to frame in the observed film thickness on the upper portion of the disk than on the lower portion. This could be indicative of turbulent flow, but no obvious transition point is apparent from examining Fig. 31. The variation in the observed film thickness from frame to frame is most pronounced at the highest ΔT_{sat} = 300°F.

The prediction of Berenson[3] for the vapor film thickness on a horizontal flat plate heating up (Eq. (34)) has been evaluated for saturated liquid nitrogen at 1 atmosphere and (a/g) = 1. The results are plotted on Fig. 49. The prediction of Chang[46] for film thickness under the same conditions (Eq. (35)) is also shown. Experimental measurements obtained from Fig. 32 are presented. Berenson's prediction of film thickness is five times larger than Chang's prediction of film thickness at a given ΔT_{sat}, but is an order of magnitude less than the experimental data. The models proposed by Berenson and Chang thus do not appear to follow the observed results.

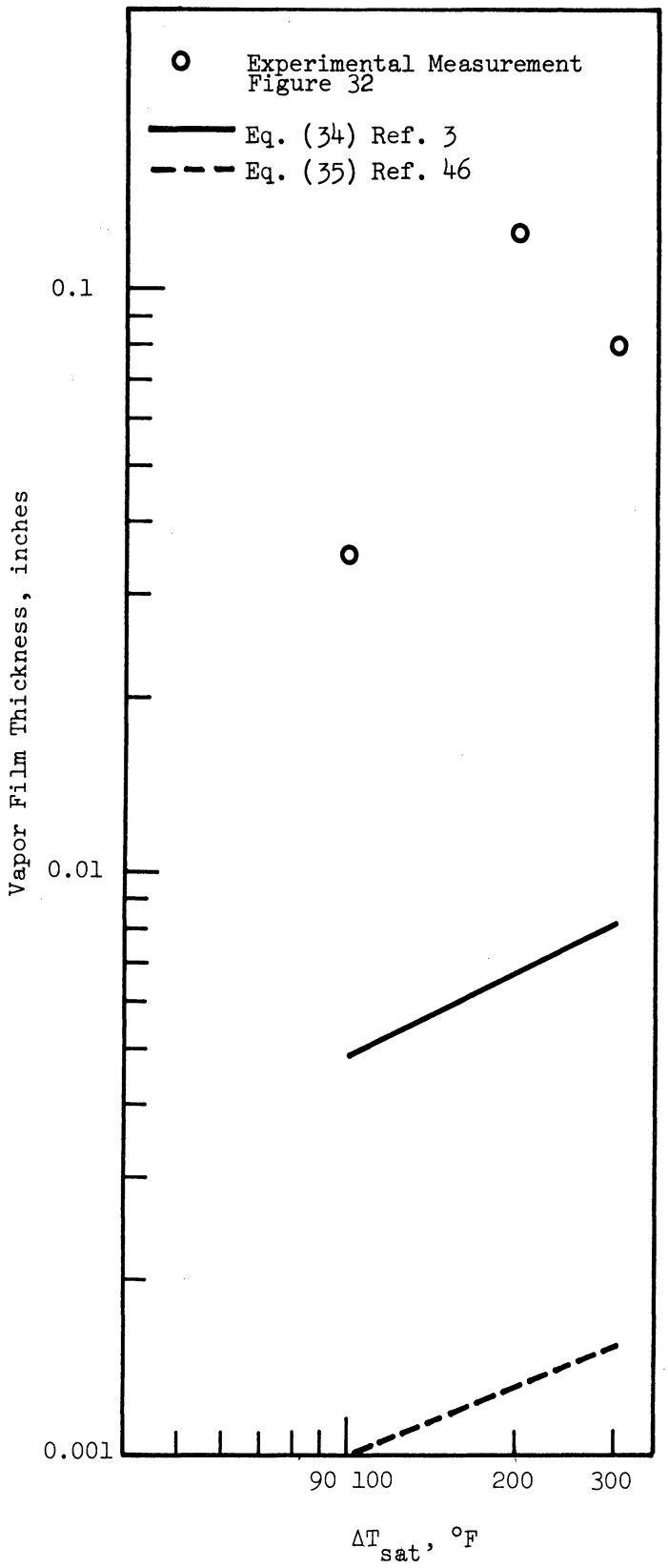

Fig. 49. Vapor film thickness in saturated film boiling on a horizontal disk heating up.

A comparison of Figs. 48 and 49 shows that the experimental vapor film thickness measurements are similar for the two disk orientations. The predicted thicknesses, although different from the observed thicknesses, are also similar. It has been shown on Fig. 16 that the (q/A) vs. ΔT_{sat} results from the disk are similar for the two orientations. One might conclude then that the heat flux with film boiling can be directly related to the vapor film thickness.

Chang[54] has indicated that there should not be any significant difference between horizontal heaters and vertical heaters after the onset of turbulence. The film thickness on a vertical plate, as a consequence of turbulent motion, would thus be similar to that on a horizontal surface. Chang[46] also stated that, for a small plate, the heat transfer coefficient for a horizontal plate heating down should be the same as that for a vertical plate. Flow along the vertical disk has been tentatively identified as turbulent over a portion of the disk. If the flow over the horizontal disk, heating up, is also turbulent, the proposed laminar models for the vapor film behavior would probably not apply. Chang's conclusion about similarity in heat transfer behavior between horizontal and vertical plates with turbulent flow would apply, and appears to be supported by the experimental results observed here with regard both to film thickness and heat flux. The correlations for laminar flow predict film thicknesses in the vertical and horizontal heating up positions which are quite similar, and may indicate that the insensitivity of a flat plate to orientation holds in laminar flow as well. There is no experimental data available to examine this contention.

It has been pointed out (e.g., Ref. 1) that a similar lack of sensitivity to orientation exists for free convection heat transfer. In the turbulent regime, McAdams[1] gives, for a horizontal plate heating up,

$$Nu = 0.14\ (Ra)^{1/3} \tag{40}$$

and for a vertical plate

$$Nu = 0.13\ (Ra)^{1/3} \tag{41}$$

a difference of approximately 8%. These equations are very similar in form to Eq. (16) for a sphere with saturated film boiling.

McAdams also found a lack of sensitivity in the laminar regime. He gives, for a horizontal plate heating up,

$$Nu = 0.54\ (Ra)^{1/4} \tag{42}$$

and for a vertical plate

$$Nu = 0.59\ (Ra)^{1/4} \tag{43}$$

a difference of approximately 9%.

The predicted film appearance for a horizontal plate heating down may be obtained by using Eq. (36). The variation of δ_1 with y_1 is shown in Fig. 50 as a function of ΔT_{sat}. δ_1 and y_1 are defined in Fig. B-1. For each ΔT_{sat} the measured value of y_1 obtained from Fig. 33 is indicated. Predicted values of δ_1 range from 0.0041 to 0.011 inch. The value of y_1 was measured to ±0.010 inch. Variations in δ_1 of the range predicted

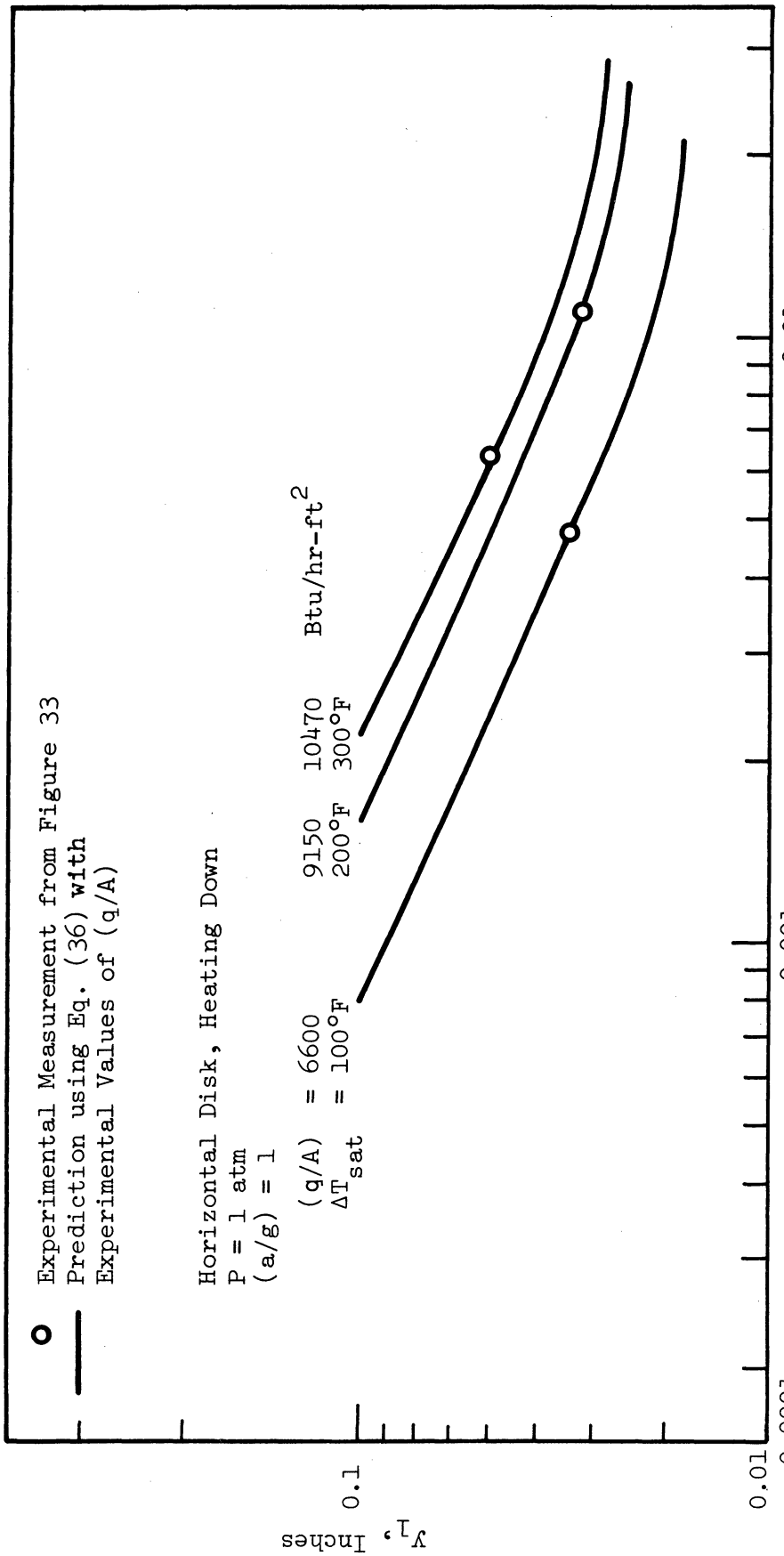

Fig. 50. Vapor film thickness variation in saturated film boiling on a horizontal disk heating down.

could not be observed in the photographs taken.

Equation (36) predicts that δ_1 must have a positive value for any (q/A) different from zero. It also predicts a minimum possible value of y_1 which increases with increasing ΔT_{sat}. From a physical standpoint, this implies that the flow of vapor radially from the center of the disk is accompanied by a reduced thickness of the film as the distance from the center is increased. It also implies that there is a minimum film thickness which can exist on the disk for a given (q/A). This minimum thickness is necessary to remove the generated vapor. The minimum possible thickness increases with increasing ΔT_{sat}, since the increasing rate of vapor generation results in a larger flow volume. The numerical values predicted for the minimum possible y_1, and the corresponding δ_1 are probably in error in this region because the assumption that $\delta_1 \ll y_1$ is no longer valid.

B. OTHER BOILING REGIMES

1. Minimum Heat Flux Boiling

Most of the results presented in the minimum heat flux boiling region were obtained with the 1-inch diameter sphere. Insufficient data were obtained with the 1/4-inch diameter sphere and the disk to permit any conclusions to be reached from comparisons with existing correlations for $(q/A)_{min}$. The results obtained with the 1-inch diameter sphere were compared with the behavior predicted by correlations.

Berenson[3] developed an equation for $(q/A)_{min}$ as

$$(q/A)_{min} = 0.09\ \rho_{vf} h'_{fg} \left[\frac{g(\rho_\ell - \rho_v)}{\rho_\ell + \rho_v}\right]^{1/2} \left[\frac{g_o \sigma}{g(\rho_\ell - \rho_v)}\right]^{1/4} \left(\frac{a}{g}\right)^{1/4} \quad (44)$$

Equation (44) is plotted on Figs. 44 and 51 for pressures of 1, 3, and 5 atmospheres. The experimental results for the 1-inch diameter sphere are also shown on Fig. 51. A range of $(q/A)_{min}$ at a particular (a/g) is shown by the two extreme points connected by a vertical line. A range of $(q/A)_{min}$ combined with an uncertainty in (a/g) is shown by two points connected by a diagonal line. Some (q/A)'s were obtained at ΔT_{sat} differing from that at which $(q/A)_{min}$ was anticipated by -10°F to +35°F. Since no data were obtained which were identified as $(q/A)_{min}$ for these conditions, the measured values, shown in Fig. 22, were taken as upper limits on $(q/A)_{min}$. They are indicated by a vertical line originating at the data points and terminating in an arrowhead.

Equation (44) was developed for flat plates, but previous work done with the 1-inch sphere at 1 atmosphere pressure had shown reasonable agreement with the predicted values for $(q/A)_{min}$ at both standard and fractional gravity.[19] Equation (44) does not predict the experimental results at higher pressures. An increase in $(q/A)_{min}$ of approximately 120% at 3 atmospheres and 200% at 5 atmospheres is predicted, but the experimental values increase by approximately 30% and 50%, respectively. The values of $(q/A)_{min}$ are predicted to follow a 1/4 power dependence on (a/g). The data shown in Fig. 51 appear to follow this predicted dependence. The power dependence n in $(a/g)^n$ is larger than 0.15 at a pressure of 3 atmospheres,

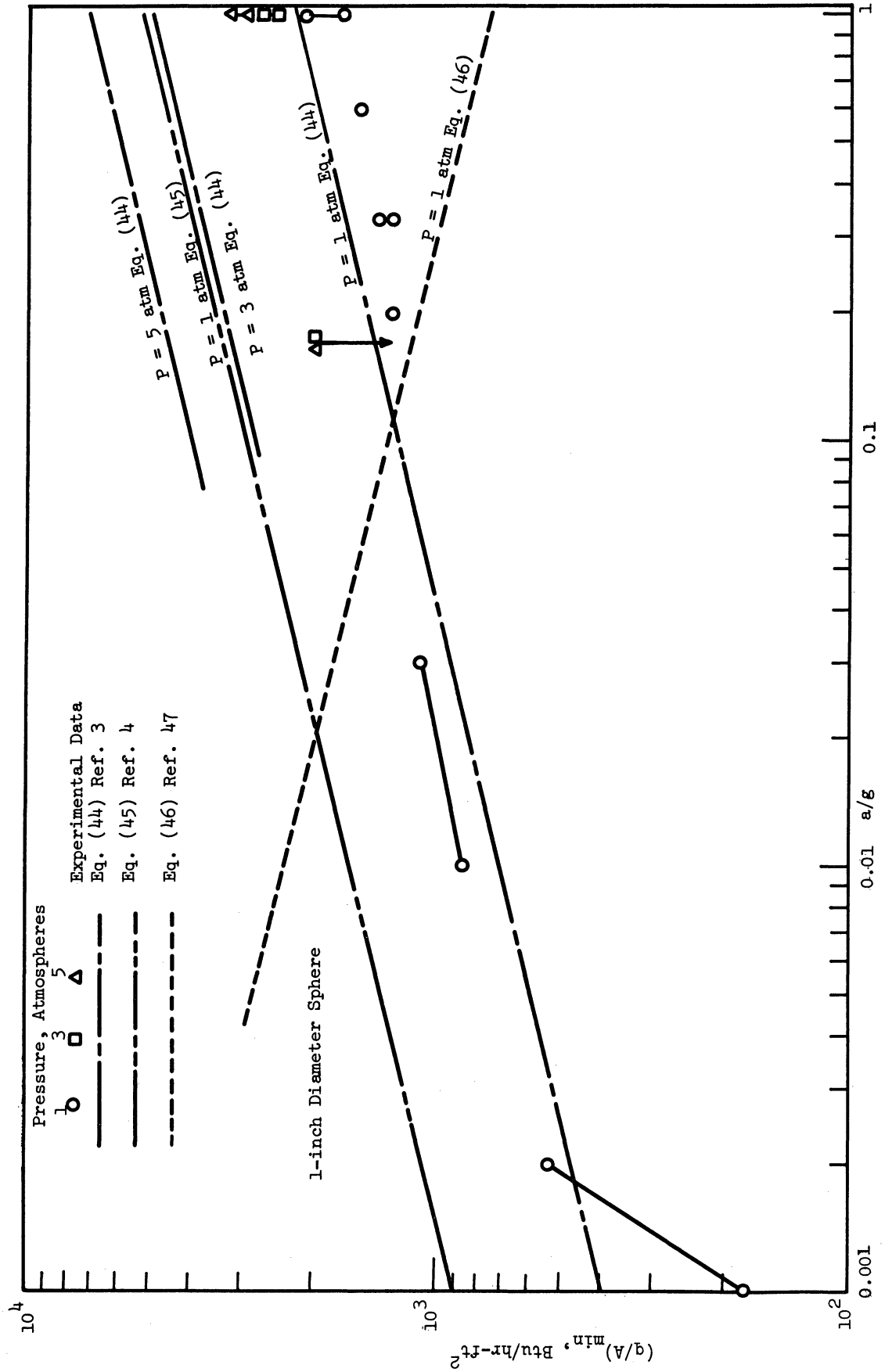

Fig. 51. $(q/A)_{min}$ in saturated boiling.

and larger than 0.22 at a pressure of 5 atmospheres.

Other correlations for $(q/A)_{min}$ were developed by Zuber[4] and by Lienhard and Wong[47]. Zuber's equation,

$$(q/A)_{min} = \frac{\pi^2}{60}\sqrt[4]{\frac{4}{3}}\,\rho_v h_{fg}\left[\sigma g g_o\,\frac{\rho_\ell-\rho_v}{(\rho_\ell+\rho_v)^2}\right]^{1/4}\left(\frac{a}{g}\right)^{1/4} \qquad (45)$$

is very similar to Berenson's except for the coefficient $\left(\frac{\pi^2}{60}\sqrt[4]{\frac{4}{3}} = 0.177\right)$. It also differs in that it evaluates properties at saturation conditions rather than at an average film temperature. Equation (45) is plotted on Fig. 51 for P = 1 atmosphere. It predicts values of $(q/A)_{min}$ which are approximately 200% higher than the experimental values.

Lienhard and Wong[47] predicted $(q/A)_{min}$ for a horizontal cylinder. Their expression accounts for the effect of surface tension in the transverse direction upon the Taylor instability of the interface. They obtained.

$$(q/A)_{min} = \frac{\pi^2}{60}\sqrt[4]{3}\,\frac{\rho_v h_{fg}}{R}\left[2g\,\frac{\rho_\ell-\rho_v}{\rho_\ell+\rho_v}+\frac{\sigma g_o}{(\rho_\ell+\rho_v)R^2}\right]^{1/2}\left[\frac{g(\rho_\ell-\rho_v)}{\sigma g_o}+\frac{1}{2R^2}\right]^{-3/4} \qquad (46)$$

For cylinders larger than 1/4-inch diameter, this equation indicates that $(q/A)_{min}$ is inversely proportional to the test object radius within a few percent. It also indicates that $(q/A)_{min}$ is proportional to $(a/g)^{-1/4}$ rather than $(a/g)^{+1/4}$ as indicated by Berenson and Zuber and experimentally verified.[19] Equation (46) is shown on Fig. 51 for P = 1 atmosphere.

A few $(q/A)_{min}$ values were obtained for the 1-inch diameter sphere with subcooled boiling at 3 and 5 atmospheres (see Fig. 21). They were approximately 65% higher than the $(q/A)_{min}$ values obtained with saturated

boiling at 3 and 5 atmospheres.

Berenson[3] also developed an equation for $(\Delta T_{sat})_{min}$ as

$$(\Delta T_{sat})_{min} = 0.127 \frac{\rho_{vf} h'_{fg}}{k_{vf}} \left[\frac{g(\rho_\ell - \rho_v)}{\rho_\ell + \rho_v}\right]^{2/3} \left[\frac{g_o \sigma}{g(\rho_\ell - \rho_v)}\right]^{1/2} \left[\frac{\mu_f}{g(\rho_\ell - \rho_v)}\right]^{1/3} \left(\frac{a}{g}\right)^{-1/8} \quad (47)$$

Equation (47) is plotted on Fig. 52 for P = 1 atmosphere. The experimental results for the 1-inch diameter sphere are also shown. A range of $(\Delta T_{sat})_{min}$ at a particular value of (a/g) is shown by the two extreme points connected by a vertical line. An uncertainty in (a/g) is shown by two extreme points connected by a horizontal line. When an upper limit was obtained for $(\Delta T_{sat})_{min}$, it is indicated by a vertical line originating at the data point and terminating in an arrowhead.

The values predicted for $(\Delta T_{sat})_{min}$ were higher than the experimental values by a factor of approximately two[19] at (a/g) = 1, and the difference increases with decreasing (a/g). Berenson[3] had determined $(\Delta T_{sat})_{min}$ from the relationship

$$(\Delta T_{sat})_{min} = \frac{(q/A)_{min}}{\bar{h}_{min}} \quad (48)$$

where $(q/A)_{min}$ is given in Eq. (44) and $\bar{h}$ was given in Eq. (26). The relationship for $\bar{h}$ determined by Frederking and Clark[31] for the 1-inch diameter sphere is

$$\bar{h} = 0.14\, k_{vf} \left[\frac{\rho_{vf}(\rho_\ell - \rho_{vf})g}{\mu_{vf}^2} \left(\frac{C_p \mu}{k}\right)_{vf} \left(\frac{h_{fg}}{C_p \Delta T_{sat}} + 0.5\right) \left(\frac{a}{g}\right)\right]^{1/3} \quad (49)$$

This was substituted for Eq. (26) in Eq. (48) to obtain

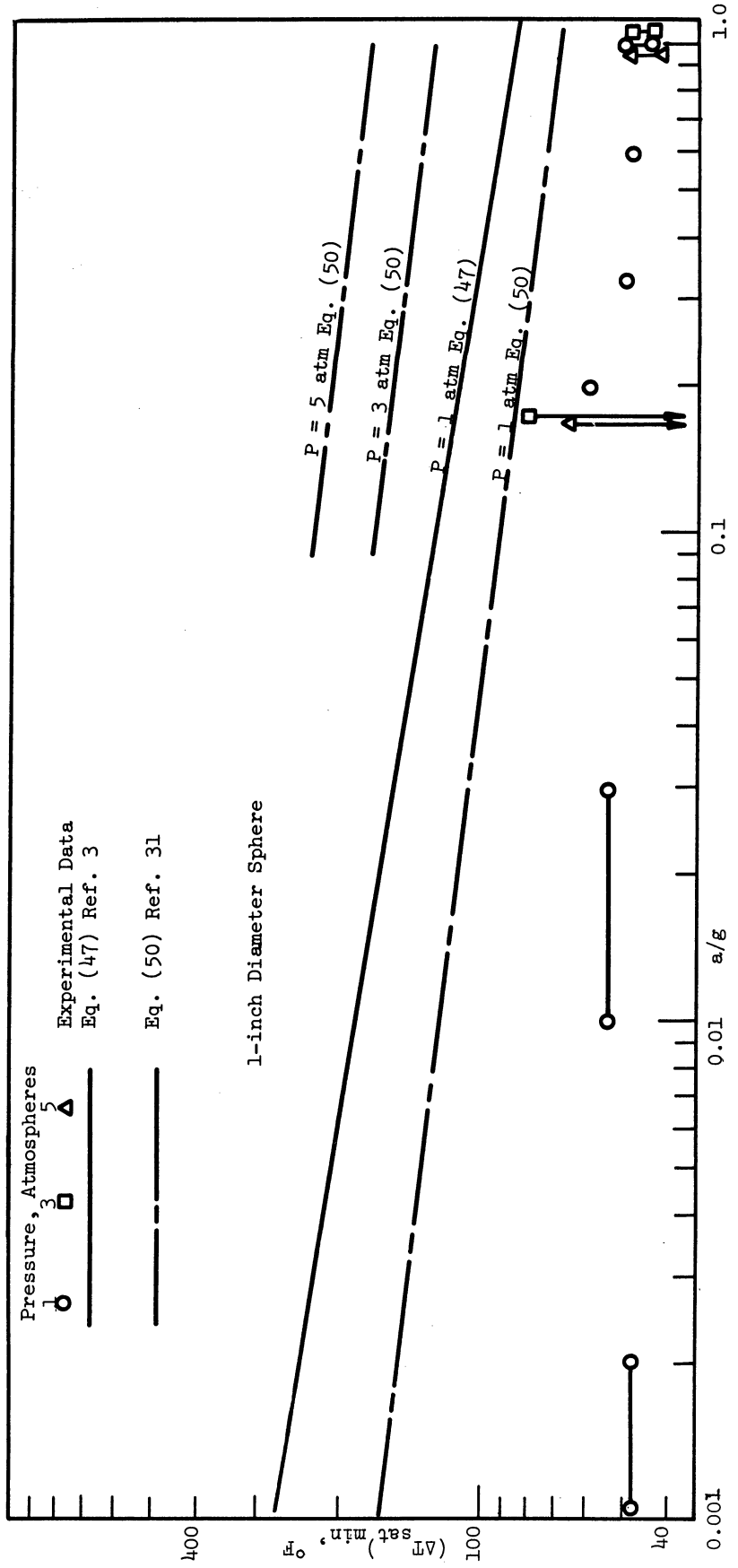

Fig. 52. $(\Delta T_{sat})_{min}$ in saturated boiling.

$$(\Delta T_{sat})_{min} = 0.465 \frac{\rho_{vf} h'_{fg}}{k_{vf}} \mu_{vf}^{1/2} \left[\frac{g_o \sigma}{(\rho_\ell + \rho_v)^2}\right]^{3/8} \left[\frac{1}{g(\rho_\ell - \rho_v)}\right]^{1/8} \left(\frac{a}{g}\right)^{-1/8} \quad (50)$$

This reduced the predicted value of $(\Delta T_{sat})_{min}$ to 50% higher than the experimental values at P = 1 atmosphere and (a/g) = 1. Equation (50) is shown on Fig. 52 for P = 1, 3, and 5 atmospheres. A large increase is predicted in the value of $(\Delta T_{sat})_{min}$ with increasing pressure. The experimental range of $(\Delta T_{sat})_{min}$ at (a/g) = 1 shown in Fig. 52 for 1, 3, and 5 atmospheres does not appear to be affected by a change in pressure. The accuracy of the determination of $(\Delta T_{sat})_{min}$ is ±5°F, so a small effect of pressure would not be apparent.

Berenson's equation for $(\Delta T_{sat})_{min}$, Eq. (47), indicates a dependence on $(a/g)^{-1/6}$. Equation (50), which utilizes Frederking and Clark's correlation for spheres in evaluating $\bar{h}$, indicates a dependence on $(a/g)^{-1/8}$. As may be seen in Fig. 52, this difference is small. The experimental data do not show any effect of (a/g): All of the $(\Delta T_{sat})_{min}$, regardless of pressure or (a/g), fell in the range $(\Delta T_{sat})_{min}$ = 50°±10°F.

A few $(\Delta T_{sat})_{min}$ values were obtained for the 1-inch diameter sphere with subcooled boiling at 3 and 5 atmospheres (see Fig. 21). They fell in the 50°±10°F range found with saturated boiling.

2. Peak Heat Flux Boiling

Figure 26 shows the peak heat flux is affected by both pressure and (a/g). The correlations of Noyes[20] and Zuber (discussion in Ref. 3) for saturated boiling most nearly predict the observed results. Noyes' cor-

relation is

$$(q/A)_{max} = 0.144\, h_{fg}\rho_v^{1/2}\left[\frac{(\rho_\ell-\rho_v)^2}{\rho_\ell}\, gg_o\sigma\right]^{1/4} Pr^{-0.245}\left(\frac{a}{g}\right)^{1/4} \qquad (51)$$

and Zuber's correlation is

$$(q/A)_{max} = C_2 h_{fg}\rho_v^{1/2}\,[gg_o\sigma(\rho_\ell-\rho_v)]^{1/4}\left(\frac{a}{g}\right)^{1/4} \qquad (52)$$

where

$$0.120 \leq C_2 \leq 0.157 \qquad (53)$$

For $Pr_\ell \cong 1$ and $\rho_\ell \gg \rho_v$, these correlations are identical. They are shown in Fig. 53 for $(a/g) = 1$ and pressures from 1 to 5 atmospheres. Equation (51) is also shown for $(a/g) < 1$, and is included on Fig. 44.

Values of $(q/A)_{max}$ obtained with the 1-inch diameter sphere at 1, 3, and 5 atmospheres and with the 1/2-inch diameter sphere at 1 atmosphere are shown in Fig. 53. The agreement between the experimental and the predicted results over a range of pressures and (a/g) indicates that the correlation has wide applicability.

Chang and Snyder[21] also developed a correlation for $(q/A)_{max}$ identical to Eq. (52) with $C_2 = 0.145$. They also developed an expression for the "critical temperature difference," which has been modified by Merte and Clark[19] to apply to liquid nitrogen. In this form it appears as

$$(\Delta T_{sat})_{cr} = C_3 x 10^3\, \frac{(h_{fg}\rho_v)^{9/5}\sigma[gg_o\sigma(\rho_\ell-\rho_v)]^{1/4}J^{2/5}}{\rho_v^{1/2}k_\ell[C_pT_s(\rho_\ell-\rho_v)]^{2/5}\Delta p^{7/5}}\left(\frac{a}{g}\right)^{1/4} \qquad (54)$$

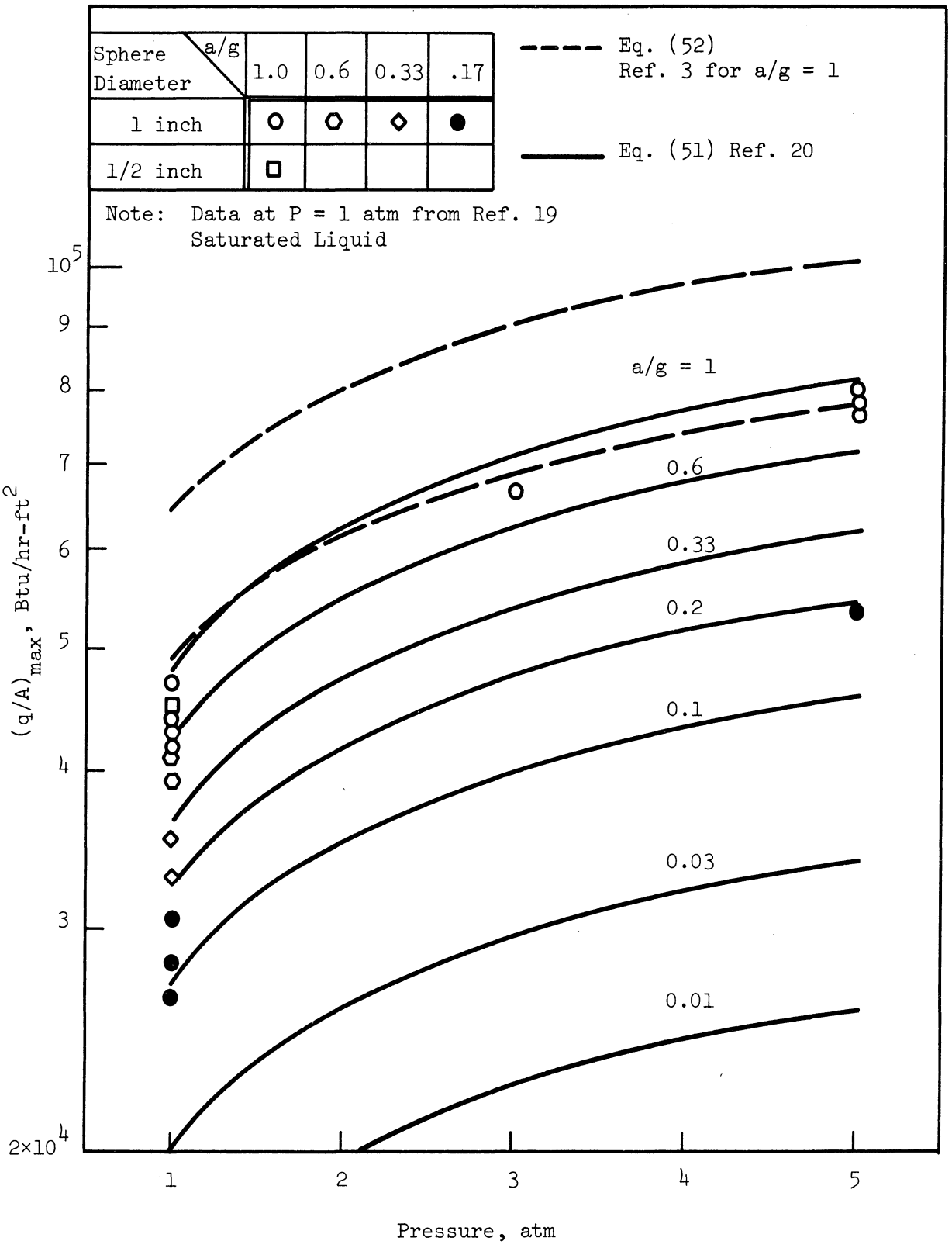

Fig. 53. Comparison of experimental and predicted $(q/A)_{max}$.

where

$$0.26 \leq C_3 \leq 0.52 \tag{55}$$

and $(\Delta T_{sat})_{cr}$ is the temperature difference at which $(q/A)_{max}$ is obtained. Equation (55) is shown in Fig. 44 for P = 1 atmosphere and a range of values of (a/g), and also for P = 3 and 5 atmospheres at (a/g) = 1. It may be noted that Eq. (55) predicts that $(\Delta T_{sat})_{cr}$ will decrease as (a/g) decreases and also as the pressure is increased. A decrease of $(\Delta T_{sat})_{cr}$ with decreasing (a/g) was observed on Fig. 26, but the predicted decrease of $(\Delta T_{sat})_{cr}$ with increasing pressure is not seen on this figure.

The effect of subcooling on peak heat flux is pronounced, as may be seen on Fig. 26. One correlation for predicting this effect is that proposed by Zuber,Tribus, and Westwater[55] as quoted by Kreith[2], which is given as

$$(q/A)_{max_{sc}} = (q/A)_{max_{sat}} \left\{ 1 + \left[\frac{2k_\ell (T_{sat}-T_\ell)}{(\pi \alpha_\ell \tau g_o)^{1/2}} \right] \frac{24}{\pi h_{fg} \rho_v} \left[\frac{g_o \rho_v^2}{\sigma g(\rho_\ell - \rho_v)} \right]^{1/4} \left(\frac{a}{g} \right)^{-5/8} \right\} \tag{56}$$

where

$$\tau = \frac{\pi}{3} \sqrt{2\pi} \left[\frac{\sigma}{g(\rho_\ell - \rho_v)} \right]^{1/2} \left[\frac{g_o \rho_v^2}{\sigma g(\rho_\ell - \rho_v)} \right]^{1/4} \tag{57}$$

The correlation of Noyes,[20] Eq. (51), which predicted the experimental data quite accurately, was used for evaluating $\left((q/A)_{max}\right)_{sat}$. The $\left((q/A)_{max}\right)_{sc}$ was evaluated for 3 atmospheres at 15°F subcooling and for 5 atmospheres at 25°F subcooling at (a/g) = 1 and 0.17. The ratios of $\left((q/A)_{max}\right)_{sc}$ to $\left((q/A)_{max}\right)_{sat}$ were formed and are shown in Fig. 54. Also shown are the same

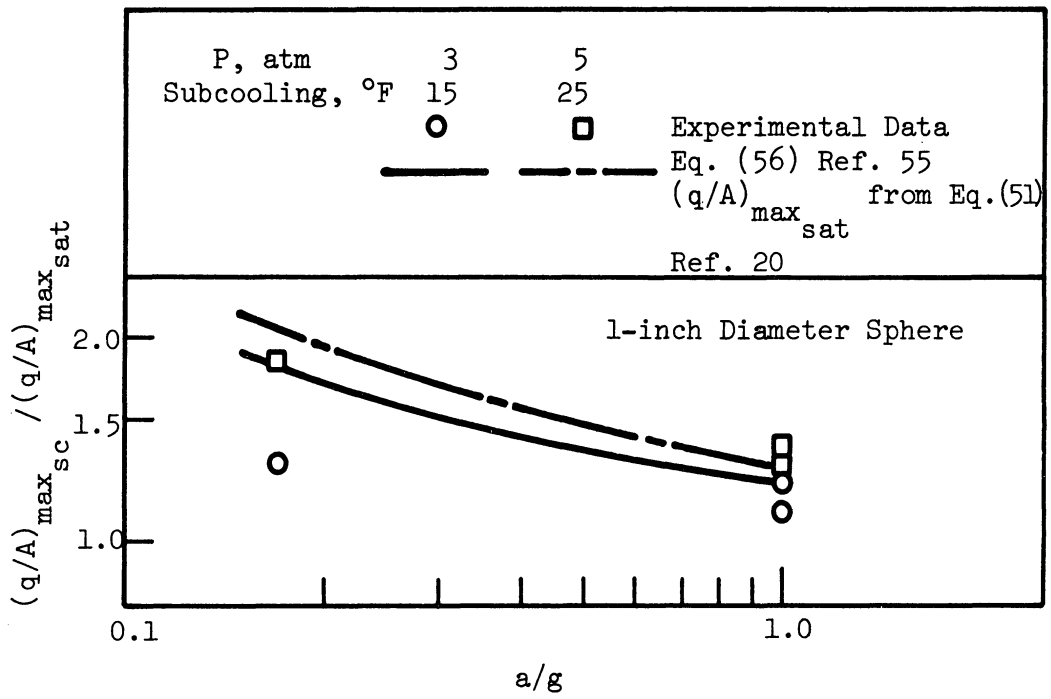

Fig. 54. Effect of subcooling on $(q/A)_{max}$.

ratios obtained from the experimental results with the 1-inch diameter sphere.

The limited number of data points, particularly at (a/g) = 0.17, restricts the validity of the comparison of predicted and experimental values. With this restriction in mind, the prediction seems good at (a/g) = 1, but predicts too high a value at (a/g) = 0.17. The predicted value of $\left((q/A)_{max}\right)_{sc} / \left((q/A)_{max}\right)_{sat}$ at (a/g) = 0.01 and 5 atmospheres with 25°F subcooling (not shown on Fig. 54) is 7.72. Although no data were obtained at this (a/g), the results shown on Fig. 25 for (a/g) < 0.002 do not indicate that a difference of this magnitude is probable. Until more experimental results at (a/g) < 1 are available, it appears Eq. (56) should be used with caution at (a/g) < 1.

3. Nucleate Boiling

Saturated nucleate pool boiling has been investigated extensively, and many correlations have been developed which predict (q/A) as a function of ΔT_{sat} (see, e.g., Fig. 5 of Ref. 44). The experimental results have exhibited wide variations of (q/A) with ΔT_{sat} (see Fig. 35), so it is not surprising that the correlations exhibit similar variations. A survey was made to determine which correlations most accurately predicted the results obtained with the 1-inch diameter sphere with saturated nucleate boiling at 1 atmosphere and (a/g) = 1. The equation of Rohsenow[11], given as

$$(q/A) = 2.97 \times 10^{5} \frac{\mu_{\ell}[g(\rho_{\ell}-\rho_{v})]^{1/2}(C_{p\ell})^{3}}{(\sigma)^{1/2}(h_{fg})^{2}(g_{o})^{1/2}(Pr_{\ell})^{5.1}} (\Delta T)^{3} \left(\frac{a}{g}\right)^{1/2} \qquad (58)$$

and of Michenko[12], given as

$$(q/A) = 6.3\times10^{-11} \frac{\mu_\ell[g(\rho_\ell-\rho_v)]}{(\sigma)^{1/2}(h_{fg}\rho_v)^{7/3}(g_o)^{1/2}(Pr_\ell)^{1.0}} \left\{\frac{(g_o)^{1/2}P}{[\sigma g(\rho_\ell-\rho_v)]^{1/2}}\right\}^{7/3}$$
$$(x)\ (C_{p\ell})^{10/3}(\rho_\ell)^{7/3}(\Delta T)^{10/3}(a/g)^{-2/3} \qquad (59)$$

most nearly predicted the experimental results. Rohsenow predicts (q/A) is proportional to $(\Delta T_{sat})^3$, which is virtually the same as that of Michenko, $(\Delta T_{sat})^{10/3}$. The measured slope of the reference curve (as introduced in Chapter VI) in the nucleate boiling region is 3.4. The prediction of Rohsenow incorporates an empirical constant which must be reevaluated for each system.

Variations in saturated nucleate boiling heat flux with variations in pressure have been predicted (see, e.g., Ref. 44). The variations predicted by Eq. (58) and (59) are shown on Fig. 55, evaluated for liquid nitrogen with ΔT_{sat} = 10°F. Experimental results are shown in Fig. 55. The point at 1 atmosphere is taken from the reference curve, and the error limits represent a combination of ±20% maximum error in (q/A) and ±1°F maximum error in ΔT_{sat}; the maximum total error is estimated to be +65%, -45%. Equation (58) predicts a decreasing effect of pressure on (q/A) as pressure increases; Eq. (59) predicts an increasing effect of pressure on (q/A) as pressure increases. The data appear to demonstrate an increasing effect of pressure on (q/A) as pressure increases.

There is no apparent effect of variations in (a/g) on nucleate boiling. This has been observed by several authors (see, e.g., Refs. 16, 17, 18, 19,

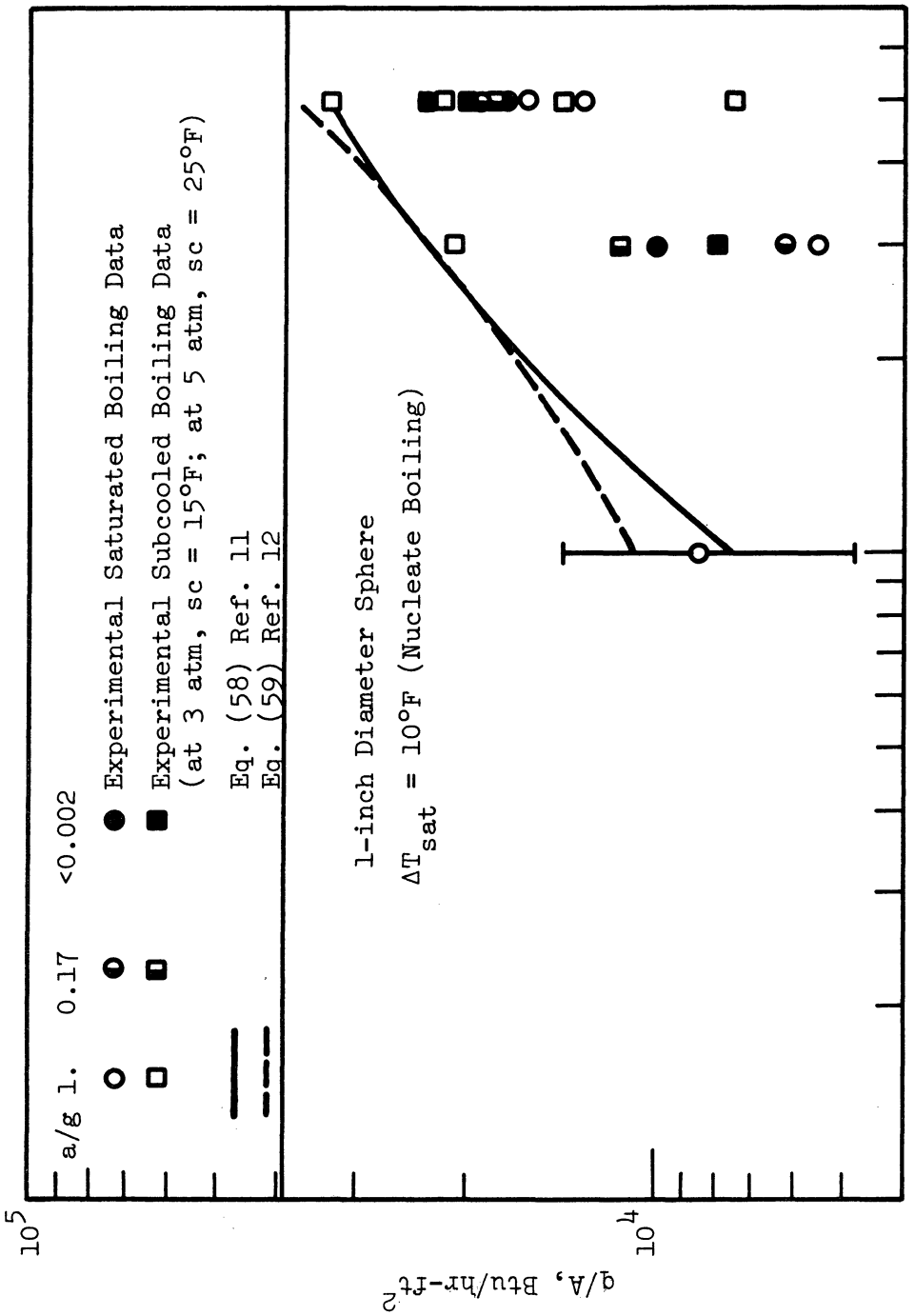

Fig. 55. Effect of pressure and subcooling on nucleate boiling heat flux.

and 56). It may be noted that Eq. (58) predicts a 1/2 power dependence on (a/g) and Eq. (59) predicts a -2/3 power, which indicates inadequacies in the models used in developing these correlations. Equation (58) is plotted on Fig. 44 to show the predicted effects of (a/g) and pressure.

There are no apparent effects of subcooling on nucleate boiling as may be seen from Figs. 27 and 55. McAdams[1] and Krieth[2] have shown data plotted as (q/A) vs. ΔT_{sat} over a wide range of variables and demonstrated that, for a given value of (q/A), nucleate boiling data fall within a range of ±35% of the nominal value of ΔT_{sat} regardless of the degree of subcooling. Forster and Greif[14] examined several proposed nucleate boiling mechanisms and concluded that the process of liquid-vapor exchange taking place every time a bubble grows and then collapses on, or detaches from, the heating surface can account for the heat flux in nucleate boiling. The effect of subcooling on the maximum bubble radius and the bubble lifetime largely cancel each other, accounting for the apparent insensitivity of heat flux to subcooling. When both of these factors were taken into account, Forster and Greif[14] showed that the data of Ellion[50] for water which was subcooled from 35°F to 150°F would not be expected to show more than 15% variation in heat flux.

The correlations suggested for use with saturated nucleate boiling should be equally applicable to subcooled nucleate boiling. Figure 55 shows that subcooled nucleate boiling is not sensitive to variations in (a/g) within the range examined, again in contrast to the dependence predicted by the correlations.

4. Free Convection

McAdams[1] presents an equation for the correlation of data for single horizontal cylinders with heat transfer by natural convection. Kreith[2] notes that this equation may also be applied to spheres. McAdams recommends application to cylinders only for $10^3 < Gr \cdot Pr < 10^9$. Kreith suggests use for $10^3 < Gr < 10^9$ and $Pr > 0.5$ for cylinders, and suggests that for spheres, using the sphere radius as the characteristic length, Gr should be greater than 10^3. The equation is given by Kreith as

$$Nu = 0.53\ (Gr \cdot Pr)^{1/4} \tag{60}$$

which may be rewritten as

$$q/A = 0.53 \left(\frac{k_\ell^3 \rho_\ell^3 g \beta_\ell C_{p\ell}}{R \mu_\ell} \right)^{1/4} (T_s - T_\ell)^{5/4} \left(\frac{a}{g} \right)^{1/4} \tag{61}$$

Equation (61) is shown on Fig. 56 with the subcooled free convection data presented in Fig. 29. Agreement is good. Equation (60) was derived for laminar flow. The calculated values of Gr for these tests were between 10^6 and 10^7. This normally indicates laminar flow, justifying application of Eq. (60). The correlation is relatively insensitive to variations in pressure in the region investigated because of the incompressibility of the liquid. The calculated value of (q/A) decreased by less than 4% when the pressure was increased from 3 to 5 atmospheres.

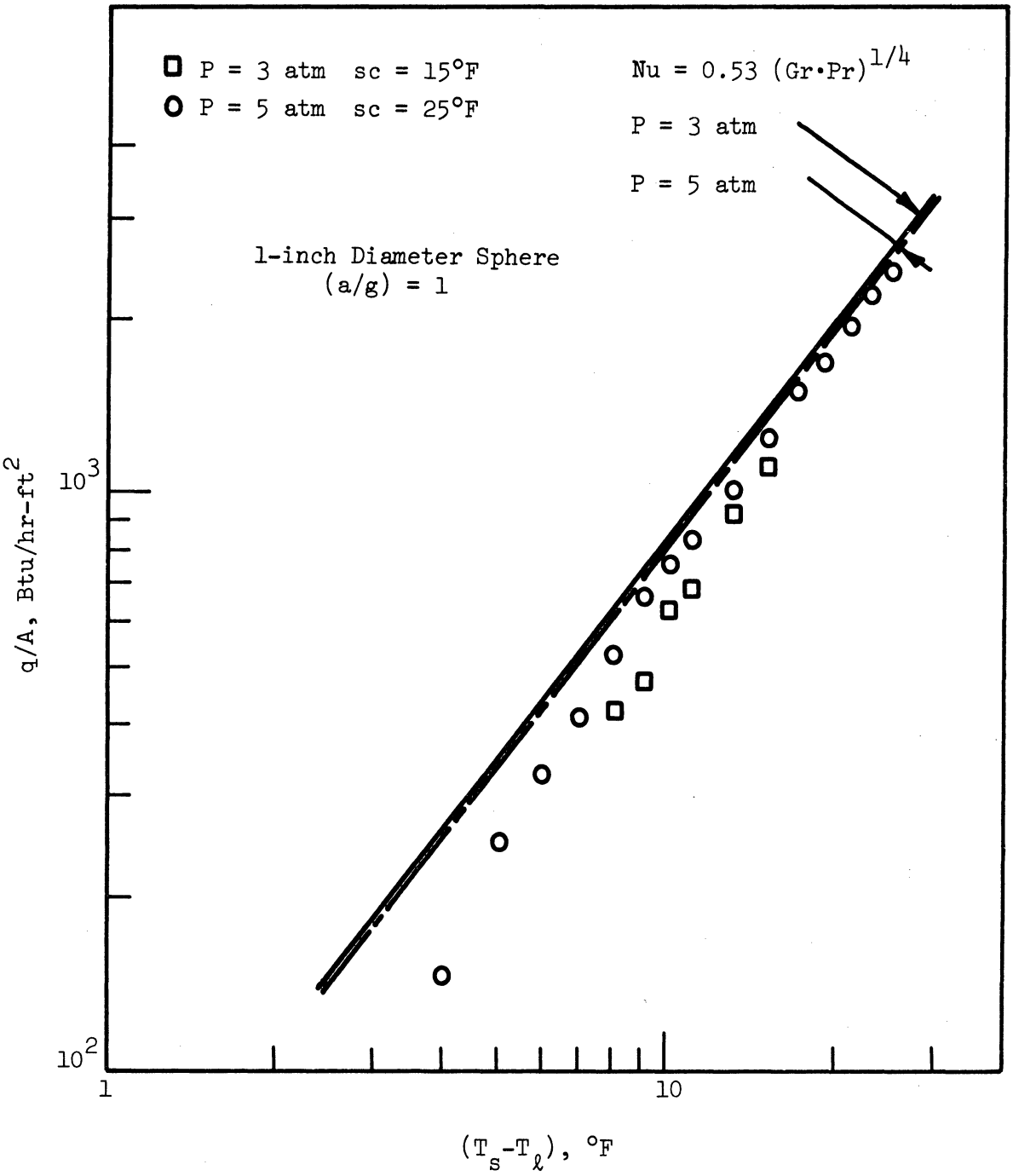

Fig. 56. Heat flux with free convection.

CHAPTER VIII

SUMMARY AND CONCLUSIONS

The purpose of this study was to investigate the effect of variations in the gravitational field on the boiling phenomena. In order to make the results as general as possible, several different physical configurations were investigated at various pressures and degrees of subcooling.

The results obtained, in addition to providing quantitative data, also permitted more complete comparisons between these data and various correlations which have been suggested for various boiling regimes. These comparisons in turn aid in determining the significance of various parameters in the effect they have on the boiling phenomena.

The configurations investigated were a 1-inch diameter sphere, a 1/4-inch diameter sphere, and a 3-inch diameter disk with the heating surface in a vertical, a horizontal heating up, and a horizontal heating down orientation. All of these configurations were investigated in the film-boiling region, but only the 1-inch diameter sphere results are presented in the other boiling regimes (minimum heat flux, transition, maximum heat flux, nucleate, and free-convection regions). Pressures used were 1, 3, and 5 atmospheres. Nominal subcooling levels of 15°F at 3 atmospheres and 25°F at 5 atmospheres were used as well as saturated conditions at all three pressures. The nonfilm boiling regions were not covered as comprehensively as the film boiling region, and in general only one or at most a few points were taken at any particular set of conditions. The reason

for this was the desire to examine a very wide range of new situations, rather than to cover a single combination in great depth.

Over the range of accelerations, pressures, subcoolings, and configurations covered in this study, the following conclusions can be drawn: For a sphere for which the diameter is larger than the calculated value of λ_d,

1. In the film-boiling region, (q/A) is proportional to $(a/g)^{1/3}$ and decreases with increasing sphere diameter.
2. In the minimum heat flux region, $(q/A)_{min}$ is proportional to $(a/g)^{1/4}$, but $(\Delta T_{sat})_{min}$ is not affected by variations in (a/g), pressure, or subcooling.
3. For values of ΔT_{sat} between $(\Delta T_{sat})_{min}$ and $(\Delta T_{sat})_{max}$, a sudden decrease in (a/g) causes a sudden decrease in (q/A) followed by an increasing (q/A) with decreasing ΔT_{sat} which has the appearance of transition boiling. The transient technique used here thus makes the relationship between (q/A) and ΔT_{sat} a many-valued, rather than a single-valued, function in the transition boiling region with (a/g) less than 1. At $(a/g) = 1$, the (q/A) vs. ΔT_{sat} relationship in the transition boiling regime was not affected by pressure or subcooling.
4. The values of the peak heat flux and of $(\Delta T_{sat})_{max}$ are proportional to $(a/g)^{1/4}$.
5. Nucleate boiling is not affected by variations in (a/g), pressure, or subcooling; (q/A) is proportional to $(\Delta T_{sat})^{3.4}$.

For a disk or for a sphere for which the diameter is smaller than the calculated value of λ_c, in the film-boiling region,

6. The heat flux is proportional to $(a/g)^{2/9}$.
7. The appearance of the vapor film on the disk changes significantly with a change in orientation.
8. For a flat plate or disk of sufficiently small dimensions (i.e., largest dimension 3 to 6 inches) there does not appear to be any effect of orientation on heat flux.
9. A change in the shape of the test surface (as from a sphere to a disk) may be accompanied by a change in (q/A) at a given ΔT_{sat}.

APPENDIX A

REDUCED DATA AND SAMPLE PHOTOGRAPHS

1. REDUCED HEAT TRANSFER DATA

Column Headings:

Run Number:	for identification purposes
Boiling Region:	F, film; Min, $(q/A)_{min}$; T, transition; Max, $(q/A)_{max}$; N, nucleate; FC, free convection
Pressure:	in psia
Subcooling:	in °F
a/g:	measured
q/A:	in Btu/hr-ft^2
$T-T_{sat}$:	ΔT_{sat} in °F
Configuration:	test object shape, size, or orientation
Pressurizing Medium:	for pressures of approximately 14 psia, medium is understood to be atmospheric air; at higher pressures, compressed gas of indicated constitution was used

Run Number	Boiling Region	Pressure	Subcooling	a/g	q/A	$T-T_{sat}$	Configuration	Pressurizing Medium
				Run 27				
27-B	F	14.7	0	1	7,400	325	1/2-inch sphere	
27-B	F	14.7	0	1	6,900	298	1/2-inch sphere	
27-B	F	14.7	0	1	6,300	268	1/2-inch sphere	
27-B	F	14.7	0	1	4,480	180	1/2-inch sphere	
27-B	F	14.7	0	1	3,640	142	1/2-inch sphere	
27-B	F	14.7	0	1	3,250	111	1/2-inch sphere	
27-B	F	14.7	0	1	2,980	98	1/2-inch sphere	
27-D	F	14.7	0	1	2,210	60	1/2-inch sphere	
27-D	F	14.7	0	1	2,150	155	1/2-inch sphere	
27-D	Min	14.7	0	1	2,110	51	1/2-inch sphere	
27-D	T	14.7	0	1	2,350	45	1/2-inch sphere	
27-D	T	14.7	0	1	6,200	42	1/2-inch sphere	
27-D	T	14.7	0	1	10,300	41	1/2-inch sphere	
27-D	T	14.7	0	1	10,650	35	1/2-inch sphere	
27-D	T	14.7	0	1	35,000	30.5	1/2-inch sphere	
27-D	T	14.7	0	1	41,500	25	1/2-inch sphere	
27-D	Max	14.7	0	1	42,000	20.5	1/2-inch sphere	
27-D	N	14.7	0	1	32,000	15.5	1/2-inch sphere	
27-D	N	14.7	0	1	15,200	12.4	1/2-inch sphere	
27-D	N	14.7	0	1	7,580	10.4	1/2-inch sphere	
27-D	N	14.7	0	1	2,200	7.4	1/2-inch sphere	
27-E	F	14.7	0	1	7,980	310	1/2-inch sphere	
27-E	F	14.7	0	0	3,120	308	1/2-inch sphere	
27-F	F	14.7	0	1	6,100	258	1/2-inch sphere	
27-F	F	14.7	0	0	2,310	254	1/2-inch sphere	
27-G	F	14.7	0	1	4,740	200	1/2-inch sphere	
27-G	F	14.7	0	0	1,850	194	1/2-inch sphere	
27-H	F	14.7	0	1	3,520	135	1/2-inch sphere	
27-H	F	14.7	0	0	1,400	130	1/2-inch sphere	
				Run 28				
28-A	F	14.7	0	1	2,040	61	1/2-inch sphere	
28-A	F	14.7	0	0	880	51.2	1/2-inch sphere	
28-B	F	14.7	0	1	2,050	60	1/2-inch sphere	
28-B	Min	14.7	0	1	2,000	50	1/2-inch sphere	
28-B	T	14.7	0	1	2,420	44	1/2-inch sphere	
28-B	T	14.7	0	0	1,450	43	1/2-inch sphere	
28-B	T	14.7	0	0	1,850	41	1/2-inch sphere	
28-C	F	14.7	0	1	1,800	49	1/2-inch sphere	
28-C	Min	14.7	0	1	1,770	42	1/2-inch sphere	
28-C	T	14.7	0	1	2,550	40	1/2-inch sphere	
28-C	T	14.7	0	0	920	39	1/2-inch sphere	
28-C	T	14.7	0	0	1,700	39	1/2-inch sphere	
28-D	T	14.7	0	1	2,100	43.5	1/2-inch sphere	
28-D	T	14.7	0	1	2,250	43	1/2-inch sphere	
28-D	T	14.7	0	1	2,650	42.5	1/2-inch sphere	
28-D	T	14.7	0	1	3,050	41.5	1/2-inch sphere	
28-D	T	14.7	0	1	4,700	40	1/2-inch sphere	
28-D	T	14.7	0	1	7,300	38	1/2-inch sphere	
28-D	T	14.7	0	1	14,600	32	1/2-inch sphere	
28-D	T	14.7	0	1	19,500	31	1/2-inch sphere	
28-D	T	14.7	0	1	25,500	27.5	1/2-inch sphere	
28-D	T	14.7	0	1	39,500	23.5	1/2-inch sphere	
28-D	Max	14.7	0	1	45,000	20.5	1/2-inch sphere	
28-D	N	14.7	0	1	43,800	18	1/2-inch sphere	

Run Number	Boiling Region	Pressure	Subcooling	a/g	q/A	$T-T_{sat}$	Configuration	Pressurizing Medium
28-D	N	14.7	0	1	43,000	15	1/2-inch sphere	
28-D	N	14.7	0	1	27,500	12.3	1/2-inch sphere	
28-D	N	14.7	0	1	17,700	10.7	1/2-inch sphere	
28-D	N	14.7	0	0	7,700	8.4	1/2-inch sphere	
28-D	N	14.7	0	0	3,300	7	1/2-inch sphere	
28-D	N	14.7	0	0	1,950	6.2	1/2-inch sphere	
28-D	N	14.7	0	0	1,580	4.8	1/2-inch sphere	
28-E	T	14.7	0	1	2,000	48	1/2-inch sphere	
28-E	T	14.7	0	1	2,600	47	1/2-inch sphere	
28-E	T	14.7	0	1	4,100	44	1/2-inch sphere	
28-E	T	14.7	0	1	5,100	42	1/2-inch sphere	
28-E	T	14.7	0	1	7,380	40.2	1/2-inch sphere	
28-E	T	14.7	0	1	12,000	37	1/2-inch sphere	
28-E	T	14.7	0	1	15,100	34.5	1/2-inch sphere	
28-E	T	14.7	0	0	14,800	32	1/2-inch sphere	
28-E	T	14.7	0	0	6,800	30.5	1/2-inch sphere	
28-E	T	14.7	0	0	10,600	27.5	1/2-inch sphere	
28-E	T	14.7	0	0	20,400	24.5	1/2-inch sphere	
28-E	T	14.7	0	0	15,200	22.5	1/2-inch sphere	
28-E	T	14.7	0	0	13,300	21	1/2-inch sphere	
28-E	T	14.7	0	0	25,400	18	1/2-inch sphere	
28-F	Min	14.7	0	1	1,850	49	1/2-inch sphere	
28-F	T	14.7	0	1	2,150	46	1/2-inch sphere	
28-F	T	14.7	0	1	3,850	42	1/2-inch sphere	
28-F	T	14.7	0	1	6,700	39	1/2-inch sphere	
28-F	T	14.7	0	1	10,300	36	1/2-inch sphere	
28-F	T	14.7	0	1	16,700	33	1/2-inch sphere	
28-F	T	14.7	0	0	6,900	29	1/2-inch sphere	
28-F	T	14.7	0	0	13,400	26	1/2-inch sphere	
28-F	T	14.7	0	0	15,000	22.5	1/2-inch sphere	
28-F	T	14.7	0	C	18,800	20.2	1/2-inch sphere	
28-F	Max	14.7	0	0	21,000	17.2	1/2-inch sphere	
28-F	N	14.7	0	0	17,300	11.4	1/2-inch sphere	
28-F	N	14.7	0	0	11,500	9.8	1/2-inch sphere	
28-F	N	14.7	0	0	9,400	8.5	1/2-inch sphere	
					Run 52			
52-A	Min	14.3	0	1	1,900	46	1-inch sphere	
52-A	T	14.3	0	1	2,140	45	1-inch sphere	
52-A	T	14.3	0	1	2,300	44	1-inch sphere	
52-A	T	14.3	0	0	1,005	43	1-inch sphere	
52-B	T	14.3	0	1	3,610	37	1-inch sphere	
52-B	T	14.3	0	1	3,800	36	1-inch sphere	
52-B	T	14.3	0	0	1,900	34	1-inch sphere	
52-B	T	14.3	0	0	1,550	34	1-inch sphere	
52-C	T	14.3	0	1	9,150	33	1-inch sphere	
52-C	T	14.3	0	1	18,560	30	1-inch sphere	
52-C	T	14.3	0	1	34,400	27	1-inch sphere	
52-C	T	14.3	0	1	58,900	24	1-inch sphere	
52-C	T	14.3	0	0	10,500	22	1-inch sphere	
52-C	T	14.3	0	0	7,200	21	1-inch sphere	
52-C	T	14.3	0	0	8,750	20	1-inch sphere	
52-C	T	14.3	0	0	10,780	19	1-inch sphere	
52-C	T	14.3	0	0	12,620	18	1-inch sphere	
52-C	T	14.3	0	0	12,730	17	1-inch sphere	
52-C	Max	14.3	0	0	14,470	16	1-inch sphere	
52-C	N	14.3	0	0	14,030	15	1-inch sphere	

Run Number	Boiling Region	Pressure	Subcooling	a/g	q/A	$T-T_{sat}$	Configuration	Pressurizing Medium
52-C	N	14.3	0	0	14,180	14	1-inch sphere	
52-C	N	14.3	0	0	13,820	13	1-inch sphere	
52-D	T	14.3	0	0	18,800	32	1-inch sphere	
52-D	T	14.3	0	0	34,500	29	1-inch sphere	
52-D	T	14.3	0	0	37,100	23	1-inch sphere	
52-D	Max	14.3	0	0	41,900	20.5	1-inch sphere	
52-D	N	14.3	0	0	8,820	13.5	1-inch sphere	
52-D	N	14.3	0	0	6,810	10.5	1-inch sphere	
52-E	F	14.3	0	1	2,338	76	1-inch sphere	
52-E	F	14.3	0	0	442	74	1-inch sphere	
52-E	F	14.3	0	0	0	74	1-inch sphere	
52-F	F	14.3	0	1	3,035	115	1-inch sphere	
52-F	F	14.3	0	0	714	113	1-inch sphere	
52-F	F	14.3	0	0	494	113	1-inch sphere	
52-G	F	14.3	0	1	3,625	150	1-inch sphere	
52-G	F	14.3	0	0	986	148	1-inch sphere	
52-G	F	14.3	0	0	380	148	1-inch sphere	
52-H	F	14.3	0	1	4,180	192	1-inch sphere	
52-H	F	14.3	0	0	900	190	1-inch sphere	
52-H	F	14.3	0	0	600	190	1-inch sphere	
52-I	F	14.3	0	1	4,405	213	1-inch sphere	
52-I	F	14.3	0	0	1,056	210	1-inch sphere	
52-I	F	14.3	0	0	808	210	1-inch sphere	
52-J	F	14.3	0	1	2,220	51	1-inch sphere	
52-J	F	14.3	0	1	1,800	50	1-inch sphere	
52-J	F	14.3	0	1	1,760	49	1-inch sphere	
52-J	F	14.3	0	0	178	48	1-inch sphere	
52-J	F	14.3	0	0	0	48	1-inch sphere	
52-K	T	14.3	0	1	2,014	43	1-inch sphere	
52-K	T	14.3	0	1	2,566	42	1-inch sphere	
52-K	T	14.3	0	1	3,034	41	1-inch sphere	
52-K	T	14.3	0	1	3,908	40	1-inch sphere	
52-K	T	14.3	0	0	588	40	1-inch sphere	
52-K	T	14.3	0	0	859	39	1-inch sphere	
52-L	T	14.3	0	1	30,800	31	1-inch sphere	
52-L	T	14.3	0	1	34,260	28	1-inch sphere	
52-L	Max	14.3	0	1	41,300	24	1-inch sphere	
52-L	N	14.3	0	1	34,600	21	1-inch sphere	
52-L	N	14.3	0	1	29,000	18	1-inch sphere	
52-L	N	14.3	0	0	24,700	16	1-inch sphere	
52-L	N	14.3	0	0	20,360	15	1-inch sphere	
52-L	N	14.3	0	0	14,970	14	1-inch sphere	
52-L	N	14.3	0	0	10,970	13	1-inch sphere	
52-L	N	14.3	0	0	8,080	12	1-inch sphere	
52-L	N	14.3	0	0	5,910	11	1-inch sphere	
52-L	N	14.3	0	0	4,600	10	1-inch sphere	
52-L	N	14.3	0	0	3,870	9	1-inch sphere	
52-M	F	14.3	0	1	2,064	65	1-inch sphere	
52-M	F	14.3	0	1	2,058	64	1-inch sphere	
52-M	F	14.3	0	1	2,052	63	1-inch sphere	
52-M	F	14.3	0	0	545	62	1-inch sphere	
52-M	F	14.3	0	0	425	62	1-inch sphere	
52-N	F	14.3	0	1	2,226	56	1-inch sphere	
52-N	F	14.3	0	1	1,774	55	1-inch sphere	
52-N	F	14.3	0	1	1,770	54	1-inch sphere	
52-N	F	14.3	0	0	755	53	1-inch sphere	
52-N	F	14.3	0	0	389	53	1-inch sphere	

Run Number	Boiling Region	Pressure	Subcooling	a/g	q/A	$T-T_{sat}$	Configuration	Pressurizing Medium
				Run 55				
55-A	F	36.2	3-7	1	8,360	292	1-inch sphere	Air
55-A	F	36.2	3-7	1	7,310	246	1-inch sphere	Air
55-A	F	36.2	3-7	1	5,970	205	1-inch sphere	Air
55-A	F	36.2	3-7	1	4,850	152	1-inch sphere	Air
55-A	F	36.2	3-7	1	3,840	118	1-inch sphere	Air
55-A	F	36.2	3-7	1	3,170	84	1-inch sphere	Air
55-A	F	36.2	3-7	1	2,660	63	1-inch sphere	Air
55-B	F	37.3	8	1	6,600	192	1-inch sphere	Air
55-C	F	37.2	8	1	6,770	192	1-inch sphere	Air
55-D	F	37.2	6	1	3,860	104	1-inch sphere	Air
55-D	F	37.2	6	1	3,590	94	1-inch sphere	Air
55-D	F	37.2	6	1	3,340	84	1-inch sphere	Air
55-E	F	39.8	7	1	3,280	57	1-inch sphere	Air
55-E	Min	39.8	7	1	4,200	51	1-inch sphere	Air
55-E	T	39.8	1	1	12,340	40	1-inch sphere	Air
55-E	T	39.8	1	1	23,570	31	1-inch sphere	Air
55-E	T	39.8	1	1	53,130	25	1-inch sphere	Air
55-E	Max	39.8	1	1	76,020	21	1-inch sphere	Air
55-E	N	39.8	1	1	38,090	16	1-inch sphere	Air
55-E	N	39.8	1	1	10,560	12	1-inch sphere	Air
55-E	N	39.8	1	1	7,940	11.3	1-inch sphere	Air
55-F	F	37.5	10	1	9,060	285	1-inch sphere	Air
55-F	F	37.5	10	1	8,450	270	1-inch sphere	Air
				Run 56				
56-A	F	65.3	6-11	1	12,070	315	1-inch sphere	Air
56-A	F	65.3	6-11	1	9,630	252	1-inch sphere	Air
56-A	F	65.3	6-11	1	8,340	206	1-inch sphere	Air
56-A	F	65.3	6-11	1	7,410	156	1-inch sphere	Air
56-A	F	65.3	6-11	1	5,140	108	1-inch sphere	Air
56-A	Min	65.3	6-11	1	3,980	65	1-inch sphere	Air
56-A	T	65.3	6-11	1	4,530	45	1-inch sphere	Air
56-B	F	66.4	11	1	14,650	312.5	1-inch sphere	Air
56-C	F	66.0	13	1	10,630	268	1-inch sphere	Air
56-C	F	66.0	13	1	9,830	256	1-inch sphere	Air
56-D	F	67.0	17	1	9,600	182	1-inch sphere	Air
56-E	F	66.6	13	1	6,040	96	1-inch sphere	Air
56-E	F	66.6	13	1	5,740	85	1-inch sphere	Air
56-E	F	66.6	13	1	5,340	74	1-inch sphere	Air
56-F	F	69.0	14	1	5,620	66	1-inch sphere	Air
56-F	F	69.0	14	1	4,890	56	1-inch sphere	Air
56-F	Min	69.0	14	1	4,690	48	1-inch sphere	Air
56-F	T	69.0	14	1	5,860	39	1-inch sphere	Air
56-F	T	69.0	14	1	10,960	38	1-inch sphere	Air
56-F	T	69.0	14	1	35,600	32	1-inch sphere	Air
56-G	Min	66.2	10	1	4,500	47	1-inch sphere	Air
56-G	T	66.2	10	1	8,350	42	1-inch sphere	Air
56-G	T	66.2	10	1	25,260	39	1-inch sphere	Air
56-G	T	66.2	10	1	53,110	28	1-inch sphere	Air
56-G	Max	66.2	10	1	90,930	22	1-inch sphere	Air
56-G	N	66.2	10	1	47,960	18	1-inch sphere	Air
56-G	N	66.2	10	1	16,460	14	1-inch sphere	Air
56-G	N	66.2	10	1	7,700	11	1-inch sphere	Air
56-G	N	66.2	10	1	1,320	7.2	1-inch sphere	Air

Run Number	Boiling Region	Pressure	Subcooling	a/g	q/A	$T-T_{sat}$	Configuration	Pressurizing Medium
56-H	T	69.6	25	1	7,580	44	1-inch sphere	Helium
56-H	T	69.6	25	1	19,010	37	1-inch sphere	Helium
56-H	T	69.6	25	1	61,340	32	1-inch sphere	Helium
56-H	Max	69.6	25	1	117,850	25	1-inch sphere	Helium
56-H	N	69.6	25	1	59,270	17	1-inch sphere	Helium
56-H	N	69.6	25	1	20,710	14	1-inch sphere	Helium
56-H	N	69.6	25	1	5,030	8.4	1-inch sphere	Helium
56-I	F	69.2	24	1	15,400	310	1-inch sphere	Helium
				Run 57				
57-A	F	44.5	18	1	11,200	305	1-inch sphere	Helium
57-A	F	44.5	18	1	10,750	292	1-inch sphere	Helium
57-B-1	F	45.1	11	1	9,000	186	1-inch sphere	Helium
57-B-1	F	45.1	11	1	8,600	179	1-inch sphere	Helium
57-B-2	F	44.5	17	1	8,900	200	1-inch sphere	Helium
57-B-2	F	44.5	17	1	8,600	190	1-inch sphere	Helium
57-B-2	F	44.5	17	1	8,150	179	1-inch sphere	Helium
57-C	F	44.4	16	1	6,300	101	1-inch sphere	Helium
57-C	F	44.4	16	1	6,200	96	1-inch sphere	Helium
57-C	F	44.4	16	1	5,900	86	1-inch sphere	Helium
57-D	Min	44.9	16	1	4,270	53	1-inch sphere	Helium
57-D	T	44.9	16	1	13,200	41	1-inch sphere	Helium
57-D	T	44.9	16	1	38,100	34.5	1-inch sphere	Helium
57-D	Max	44.9	16	1	80,240	22.6	1-inch sphere	Helium
57-D	N	44.9	16	1	45,660	15.5	1-inch sphere	Helium
57-D	N	44.9	16	1	19,920	11	1-inch sphere	Helium
57-E	Max	45.3	15	1	88,900	20.8	1-inch sphere	Helium
57-E	N	45.3	15	1	29,580	11.1	1-inch sphere	Helium
57-E	N	45.3	15	1	8,300	7.2	1-inch sphere	Helium
57-F	F	73.3	28	1	14,800	290	1-inch sphere	Helium
57-G	F	73.3	27	1	10,800	175	1-inch sphere	Helium
57-H	F	73.3	26	1	7,010	94	1-inch sphere	Helium
57-H	F	73.3	26	1	6,250	82	1-inch sphere	Helium
57-H	F	73.3	26	1	5,960	71	1-inch sphere	Helium
57-I	T	74.9	27	1	7,400	39	1-inch sphere	Helium
57-I	T	74.9	27	1	18,130	37	1-inch sphere	Helium
57-I	T	74.9	27	1	64,450	34	1-inch sphere	Helium
57-I	Max	74.9	27	1	104,710	20.3	1-inch sphere	Helium
57-I	N	74.9	27	1	56,840	13.2	1-inch sphere	Helium
57-I	N	74.9	27	1	22,130	8.1	1-inch sphere	Helium
57-J	FC	74.4	25	1	2,530	1.1	1-inch sphere	Helium
57-K	F	73.3	- 1.3	1	7,680	212	1-inch sphere	Helium
57-L	F	74.3	- 1.0	1	9,150	260	1-inch sphere	Helium
57-M	F	45.9	0	1	8,110	271	1-inch sphere	Helium
57-N	F	46.8	0	1	6,120	190	1-inch sphere	Helium
				Run 58				
58-A	F	43.3	16	1	14,120	272	1/4-inch sphere	Helium
58-B	F	43.8	14	1	14,370	269	1/4-inch sphere	Helium
58-C	Min	42.5	13	1	9,960	69	1/4-inch sphere	Helium
58-C	T	42.5	13	1	25,420	45	1/4-inch sphere	Helium
58-C	T	42.5	13	1	47,120	35	1/4-inch sphere	Helium
58-C	Max	42.5	13	1	67,730	24	1/4-inch sphere	Helium
58-C	N	42.5	13	1	37,070	12	1/4-inch sphere	Helium
58-C	N	42.5	13	1	8,470	5	1/4-inch sphere	Helium
58-D	T	73.1	25	1	11,060	60	1/4-inch sphere	Helium

Run Number	Boiling Region	Pressure	Subcooling	a/g	q/A	$T-T_{sat}$	Configuration	Pressurizing Medium
58-D	T	73.1	25	1	19,420	51	1/4-inch sphere	Helium
58-D	T	73.1	25	1	41,480	36	1/4-inch sphere	Helium
58-D	T	73.1	25	1	63,100	32	1/4-inch sphere	Helium
58-D	T	73.1	25	1	87,210	25	1/4-inch sphere	Helium
58-D	Max	73.1	25	1	134,990	20	1/4-inch sphere	Helium
58-D	N	73.1	25	1	83,620	18.4	1/4-inch sphere	Helium
58-D	N	73.1	25	1	55,750	11.7	1/4-inch sphere	Helium
58-D	N	73.1	25	1	34,270	9.5	1/4-inch sphere	Helium
58-D	N	73.1	25	1	19,890	7.6	1/4-inch sphere	Helium
58-D	N	73.1	25	1	15,180	6.4	1/4-inch sphere	Helium
58-E	F	74.6	23	1	18,930	311	1/4-inch sphere	Helium
58-E	F	74.6	23	1	17,870	282	1/4-inch sphere	Helium
58-E	F	74.6	23	1	17,320	253	1/4-inch sphere	Helium
58-E	F	74.6	23	1	16,150	210	1/4-inch sphere	Helium
58-E	F	74.6	23	1	14,000	171	1/4-inch sphere	Helium
58-E	F	74.6	23	1	13,050	135	1/4-inch sphere	Helium
58-E	F	74.6	23	1	11,570	100	1/4-inch sphere	Helium
58-E	Min	74.6	23	1	11,400	72	1/4-inch sphere	Helium
58-E	T	74.6	23	1	13,570	44	1/4-inch sphere	Helium
				Run 59				
59-A	F	44.0	14	1	9,400	231	1-inch sphere	Helium
59-A	F	44.0	14	0	3,600	229	1-inch sphere	Helium
59-A	F	44.0	14	0	1,885	228	1-inch sphere	Helium
59-B	F	44.0	15	1	7,210	166	1-inch sphere	Helium
59-B	F	44.0	15	0	3,800	162	1-inch sphere	Helium
59-B	F	44.0	15	0	1,747	161	1-inch sphere	Helium
59-C	F	45.0	14	1	6,190	105	1-inch sphere	Helium
59-C	F	45.0	14	0	3,060	101	1-inch sphere	Helium
59-C	F	45.0	14	0	1,905	100	1-inch sphere	Helium
59-D	F	44.0	15	1	4,960	66	1-inch sphere	Helium
59-D	F	44.0	15	0	3,260	62.6	1-inch sphere	Helium
59-D	F	44.0	15	0	1,352	61.5	1-inch sphere	Helium
				Run 60				
60-A	T	44.1	14	1	5,030	44	1-inch sphere	Helium
60-A	T	44.1	14	1	6,800	40	1-inch sphere	Helium
60-A	T	44.1	14	0	8,790	35	1-inch sphere	Helium
60-A	T	44.1	14	0	5,310	34.2	1-inch sphere	Helium
60-A	T	44.1	14	0	2,590	33.8	1-inch sphere	Helium
60-A	T	44.1	14	0	6,130	33	1-inch sphere	Helium
60-B	No Data							
60-C	T	44.2	16	1	42,230	30.5	1-inch sphere	Helium
60-C	T	44.2	16	1	95,750	25.4	1-inch sphere	Helium
60-C	Max	44.2	16	0	104,270	22.4	1-inch sphere	Helium
60-C	N	44.2	16	0	78,670	19.7	1-inch sphere	Helium
60-C	N	44.2	16	0	38,750	16.2	1-inch sphere	Helium
60-C	N	44.2	16	0	16,470	12.5	1-inch sphere	Helium
60-C	N	44.2	16	0	5,010	8.8	1-inch sphere	Helium
60-D	T	44.2	15	1	16,060	41	1-inch sphere	Helium
60-D	T	44.2	15	0	13,140	33	1-inch sphere	Helium
60-D	T	44.2	15	0	8,100	32.2	1-inch sphere	Helium
60-D	T	44.2	15	0	20,580	28	1-inch sphere	Helium
60-D	T	44.2	15	0	22,290	23.4	1-inch sphere	Helium
60-E	T	44.0	15	1	4,920	47	1-inch sphere	Helium
60-E	T	44.0	15	1	7,080	43	1-inch sphere	Helium

Run Number	Boiling Region	Pressure	Subcooling	a/g	q/A	$T-T_{sat}$	Configuration	Pressurizing Medium
60-E	T	44.0	15	0	7,810	42.7	1-inch sphere	Helium
60-E	T	44.0	15	0	6,080	39.3	1-inch sphere	Helium
60-F	N	44.5	17	1	2,750	7	1-inch sphere	Helium
60-F	N	44.5	17	1	2,520	6.1	1-inch sphere	Helium
60-F	N	44.5	17	0	2,420	5.7	1-inch sphere	Helium
60-F	N	44.5	17	0	1,830	5	1-inch sphere	Helium
60-F	N	44.5	17	0	1,270	4.7	1-inch sphere	Helium
60-G	T	44.5	17	1	38,580	40	1-inch sphere	Helium
60-G	T	44.5	17	1	72,240	30.6	1-inch sphere	Helium
60-G	T	44.5	17	0	80,890	26.3	1-inch sphere	Helium
60-G	T	44.5	17	0	63,720	23.8	1-inch sphere	Helium
60-G	T	44.5	17	0	27,470	22.8	1-inch sphere	Helium
60-G	T	44.5	17	0	13,990	19.9	1-inch sphere	Helium
60-G	T	44.5	17	0	20,000	18	1-inch sphere	Helium
60-G	Max	44.5	17	0	23,710	16	1-inch sphere	Helium
60-G	N	44.5	17	0	20,550	14.1	1-inch sphere	Helium
60-G	N	44.5	17	0	10,210	10.9	1-inch sphere	Helium
					Run 61			
61-A	F	73.7	27	1	11,800	215	1-inch sphere	Helium
61-A	F	73.7	27	0	2,990	209	1-inch sphere	Helium
61-B	F	73.0	25	1	9,790	158	1-inch sphere	Helium
61-B	F	73.0	25	0	2,930	153	1-inch sphere	Helium
61-C	F	72.4	29	1	6,770	89	1-inch sphere	Helium
61-C	F	72.4	29	0	1,986	84	1-inch sphere	Helium
61-D	F	74.0	30	1	6,080	52	1-inch sphere	Helium
61-D	F	74.0	30	0	3,440	46	1-inch sphere	Helium
61-E	T	74.0	33	1	5,111	42.6	1-inch sphere	Helium
61-E	T	74.0	33	1	23,633	38.6	1-inch sphere	Helium
61-E	T	74.0	33	1	49,488	37.3	1-inch sphere	Helium
61-E	T	74.0	33	1	62,739	35.3	1-inch sphere	Helium
61-E	T	74.0	33	1	58,344	29.6	1-inch sphere	Helium
61-E	N	74.0	33	0	51,575	29	1-inch sphere	Helium
61-E	N	74.0	33	0	31,139	20.8	1-inch sphere	Helium
61-E	N	74.0	33	0	26,211	13.7	1-inch sphere	Helium
61-E	N	74.0	33	0	16,187	10.6	1-inch sphere	Helium
61-F	T	74.4	27	1	8,059	44.8	1-inch sphere	Helium
61-F	T	74.4	27	1	11,733	41.9	1-inch sphere	Helium
61-F	T	74.4	27	0	21,573	36.3	1-inch sphere	Helium
61-F	T	74.4	27	0	28,540	27.9	1-inch sphere	Helium
61-F	T	74.4	27	0	42,570	21.4	1-inch sphere	Helium
61-G	T	74.0	28	1	8,450	40.2	1-inch sphere	Helium
61-G	T	74.0	28	1	14,245	37.2	1-inch sphere	Helium
61-G	T	74.0	28	1	51,580	32.5	1-inch sphere	Helium
61-G	N	74.0	28	0	90,473	23.2	1-inch sphere	Helium
61-G	N	74.0	28	0	59,886	18.9	1-inch sphere	Helium
61-G	N	74.0	28	0	16,558	9.2	1-inch sphere	Helium
61-G	N	74.0	28	0	7,054	7.0	1-inch sphere	Helium
61-H	T	75.0	30	1	5,771	43.3	1-inch sphere	Helium
61-H	T	75.0	30	1	30,231	33.5	1-inch sphere	Helium
61-H	T	75.0	30	1	71,408	28.9	1-inch sphere	Helium
61-H	N	75.0	30	0	98,431	19.7	1-inch sphere	Helium
61-H	N	75.0	30	0	60,958	17.1	1-inch sphere	Helium
61-H	N	75.0	30	0	17,935	9.0	1-inch sphere	Helium
61-H	N	75.0	30	0	3,064	5.9	1-inch sphere	Helium

Run Number	Boiling Region	Pressure	Subcooling	a/g	q/A	$T-T_{sat}$	Configuration	Pressurizing Medium
				Run 62				
62-A	F	74.2	28	0	5,810	185	1/4-inch sphere	Helium
62-B	F	75.6	28	1	9,010	62	1/4-inch sphere	Helium
62-B	F	75.6	28	1	8,070	45	1/4-inch sphere	Helium
62-B	Min	75.6	28	0	7,940	33	1/4-inch sphere	Helium
62-B	T	75.6	28	1	9,510	30	1/4-inch sphere	Helium
62-B	T	75.6	28	0	16,360	26	1/4-inch sphere	Helium
62-B	T	75.6	28	1	34,870	23	1/4-inch sphere	Helium
62-B	T	75.6	28	1	42,150	21	1/4-inch sphere	Helium
62-B	T	75.6	28	1	44,300	16.8	1/4-inch sphere	Helium
62-B	T	75.6	28	0	54,380	13.8	1/4-inch sphere	Helium
62-B	Max	75.6	28	0	63,050	10.8	1/4-inch sphere	Helium
62-B	N	75.6	28	0	61,540	7.6	1/4-inch sphere	Helium
62-C	Min	74.8	28	1	7,160	61	1/4-inch sphere	Helium
62-C	T	74.8	28	1	7,700	45	1/4-inch sphere	Helium
62-C	T	74.8	28	0	8,380	34	1/4-inch sphere	Helium
62-C	T	74.8	28	0	14,370	26	1/4-inch sphere	Helium
62-C	T	74.8	28	0	27,890	19	1/4-inch sphere	Helium
62-C	T	74.8	28	0	31,360	14	1/4-inch sphere	Helium
62-C	T	74.8	28	0	35,860	8.3	1/4-inch sphere	Helium
62-C	T	74.8	28	0	36,080	5.6	1/4-inch sphere	Helium
62-D	F	75.2	29	1	9,440	157	1/4-inch sphere	Helium
62-D	F	75.2	29	1	8,390	147	1/4-inch sphere	Helium
62-D	F	75.2	29	0	7,630	136	1/4-inch sphere	Helium
62-D	F	75.2	29	0	6,470	126	1/4-inch sphere	Helium
62-E	F	73.2	28	1	7,550	84	1/4-inch sphere	Helium
62-E	F	73.2	28	0	7,130	57	1/4-inch sphere	Helium
				Run 63				
63-A	F	14.6	- 2	1	6,720	242	1/4-inch sphere	
63-A	F	14.6	- 2	0.17	4,360	229	1/4-inch sphere	
63-B	F	14.6	0	1	4,360	184	1/4-inch sphere	
63-B	F	14.6	0	0.17	3,370	168	1/4-inch sphere	
63-C	F	44.0	16	1	7,400	221	1/4-inch sphere	Helium
63-C	F	44.0	16	0.17	3,550	202	1/4-inch sphere	Helium
63-D	F	73.9	26	1	12,000	203	1/4-inch sphere	Helium
63-D	F	73.9	26	0.17	7,050	178	1/4-inch sphere	Helium
63-E	F	76.9	0	1	8,800	177	1/4-inch sphere	Helium
63-F	F	77.1	- 1	1	9,400	204	1/4-inch sphere	Helium
63-F	F	77.1	- 1	0.17	5,400	175	1/4-inch sphere	Helium
63-G	F	46.0	0	1	8,850	218	1/4-inch sphere	Helium
63-G	F	46.0	0	0.17	6,000	200	1/4-inch sphere	Helium
63-H	F	44.7	14	1	9,560	166	1/4-inch sphere	Helium
63-H	F	44.7	14	1	8,370	156	1/4-inch sphere	Helium
63-H	F	44.7	14	0.17	5,770	136	1/4-inch sphere	Helium
63-I	F	74.7	26	1	10,550	150	1/4-inch sphere	Helium
63-I	F	74.7	26	0.17	6,060	120	1/4-inch sphere	Helium
63-J	F	14.0	0	1	5,140	180	1/4-inch sphere	
63-J	F	14.0	0	0.17	3,400	165	1/4-inch sphere	
63-K	F	14.0	0	1	3,670	110	1/4-inch sphere	
63-K	F	14.0	0	0.17	2,360	98	1/4-inch sphere	
63-L	F	45.5	18	1	7,300	100	1/4-inch sphere	Helium
63-L	F	45.5	18	0.17	5,770	70	1/4-inch sphere	Helium
63-M	F	73.8	27	1	9,070	85	1/4-inch sphere	Helium
63-M	F	73.8	27	0.17	7,800	50	1/4-inch sphere	Helium
63-N	F	14.0	0	1	3,120	57	1/4-inch sphere	Helium

Run Number	Boiling Region	Pressure	Subcooling	a/g	q/A	$T-T_{sat}$	Configuration	Pressurizing Medium
63-N	F	14.0	0	0.17	2,050	49	1/4-inch sphere	Helium
63-O	F	44.3	17	1	7,470	72	1/4-inch sphere	Helium
63-O	Min	44.3	17	1	6,570	56	1/4-inch sphere	Helium
63-O	T	44.3	17	1	6,940	42	1/4-inch sphere	Helium
63-O	T	44.3	17	1	9,700	40	1/4-inch sphere	Helium
63-O	T	44.3	17	0.17	19,770	37	1/4-inch sphere	Helium
63-O	T	44.3	17	0.17	35,020	32	1/4-inch sphere	Helium
63-O	Max	44.3	17	0.17	57,060	21	1/4-inch sphere	Helium
63-O	N	44.3	17	0.17	48,560	14.2	1/4-inch sphere	Helium
63-O	N	44.3	17	0.17	35,530	10.9	1/4-inch sphere	Helium
63-O	N	44.3	17	0.17	21,010	8.2	1/4-inch sphere	Helium
63-O	N	44.3	17	0.17	9,570	5.4	1/4-inch sphere	Helium
63-P	T	76.0	29	1	9,330	57	1/4-inch sphere	Helium
63-P	T	76.0	29	1	10,190	50	1/4-inch sphere	Helium
63-P	T	76.0	29	0.17	13,700	42	1/4-inch sphere	Helium
63-P	T	76.0	29	0.17	41,640	33	1/4-inch sphere	Helium
63-P	Max	76.0	29	0.17	79,230	18.4	1/4-inch sphere	Helium
63-P	N	76.0	29	0.17	55,370	10.2	1/4-inch sphere	Helium
63-P	N	76.0	29	0.17	26,240	5.3	1/4-inch sphere	Helium
63-Q	F	74.8	28	0.17	9,590	60	1/4-inch sphere	Helium
63-Q	Min	74.8	28	0.17	9,580	42	1/4-inch sphere	Helium
63-Q	T	74.8	28	0.17	30.560	34	1/4-inch sphere	Helium
63-Q	T	74.8	28	0.17	49,480	31	1/4-inch sphere	Helium
63-Q	Max	74.8	28	0.17	73,550	24	1/4-inch sphere	Helium
63-Q	N	74.8	28	0.17	72,270	16	1/4-inch sphere	Helium
63-Q	N	74.8	28	0.17	58,680	12	1/4-inch sphere	Helium
63-Q	N	74.8	28	0.17	22,050	7	1/4-inch sphere	Helium
63-R	N	14.0	- 1	1	19,600	10.9	1/4-inch sphere	
63-R	N	14.0	- 1	1	14,050	9.9	1/4-inch sphere	
63-R	N	14.0	- 1	1	10,120	9.2	1/4-inch sphere	
63-R	N	14.0	- 1	1	6,940	8.8	1/4-inch sphere	
63-R	N	14.0	- 1	1	4,050	7.8	1/4-inch sphere	
63-R	N	14.0	- 1	0.17	3,450	7.2	1/4-inch sphere	
63-R	N	14.0	- 1	0.17	2,380	6.0	1/4-inch sphere	
63-R	N	14.0	- 1	0.17	1,620	4.6	1/4-inch sphere	
63-R	N	14.0	- 1	0.17	1,080	4.0	1/4-inch sphere	
63-S	N	44.5	16	1	49,240	10.6	1/4-inch sphere	Helium
63-S	N	44.5	16	1	23,920	8.0	1/4-inch sphere	Helium
63-S	N	44.5	16	1	13,830	6.1	1/4-inch sphere	Helium
63-S	N	44.5	16	1	8,200	5.0	1/4-inch sphere	Helium
63-T	FC	75.8	28	1	2,610	- 9	1/4-inch sphere	Helium
63-T	FC	75.8	28	0.17	957	-15	1/4-inch sphere	Helium
63-U	FC	44.4	16	1	659	- 9	1/4-inch sphere	Helium
63-U	FC	44.4	16	0.17	404	-12	1/4-inch sphere	Helium
63-V	N	75.8	27	1	107,260	13.3	1/4-inch sphere	Helium
63-V	N	75.8	27	1	59,100	9.3	1/4-inch sphere	Helium
63-V	N	75.8	27	1	27,980	6.3	1/4-inch sphere	Helium
				Run 64				
64-A	F	74.4	23	1	11,600	202	1-inch sphere	Helium
64-A	F	74.4	23	1	10,350	198	1-inch sphere	Helium
64-A	F	74.4	23	0.17	6,000	193	1-inch sphere	Helium
64-B	F	45.1	10	1	8,550	213	1-inch sphere	Helium
64-C	F	74.8	26	1	14,680	299	1-inch sphere	Helium
64-C	F	74.8	26	0.17	8,530	295	1-inch sphere	Helium
64-D	F	45.1	15	1	12,450	316	1-inch sphere	Helium
64-D	F	45.1	15	1	10,940	312	1-inch sphere	Helium

Run Number	Boiling Region	Pressure	Subcooling	a/g	q/A	$T-T_{sat}$	Configuration	Pressurizing Medium
64-D	F	45.1	15	0.17	5,750	306	1-inch sphere	Helium
64-E	F	45.1	12	0.17	5,100	83	1-inch sphere	Helium
64-E	F	45.1	12	0.17	3,450	78	1-inch sphere	Helium
64-F	F	74.2	22	1	5,850	72	1-inch sphere	Helium
64-F	F	74.2	22	0.17	4,340	67	1-inch sphere	Helium
64-G	Min	44.2	15	1	4,420	44	1-inch sphere	Helium
64-G	T	44.2	15	1	6,690	41	1-inch sphere	Helium
64-G	T	44.2	15	0.17	21,120	34	1-inch sphere	Helium
64-G	T	44.2	15	0.17	30,400	29	1-inch sphere	Helium
64-G	Max	44.2	15	0.17	60,880	22	1-inch sphere	Helium
64-G	N	44.2	15	0.17	33,460	14.7	1-inch sphere	Helium
64-G	N	44.2	15	0.17	15,450	11.6	1-inch sphere	Helium
64-H	Min	75.2	23	1	5,350	46	1-inch sphere	Helium
64-H	T	75.2	23	0.17	3,800	41	1-inch sphere	Helium
64-H	T	73.8	22	1	9,910	38.7	1-inch sphere	Helium
64-H	T	73.8	22	1	14,560	38	1-inch sphere	Helium
64-I	T	73.8	22	0.17	25,990	33.8	1-inch sphere	Helium
64-I	T	73.8	22	0.17	73,200	22.3	1-inch sphere	Helium
64-I	T	73.8	22	0.17	87,890	19.9	1-inch sphere	Helium
64-I	Max	73.8	22	0.17	97,250	18.9	1-inch sphere	Helium
64-I	N	73.8	22	0.17	60,220	15.5	1-inch sphere	Helium
64-I	N	73.8	22	0.17	14,850	9.5	1-inch sphere	Helium
64-J	T	44.2	12	1	36,900	33	1-inch sphere	Helium
64-J	Max	44.2	12	0.17	94,130	22.4	1-inch sphere	Helium
64-J	N	44.2	12	0.17	53,220	18	1-inch sphere	Helium
64-J	N	44.2	12	0.17	12,050	10.2	1-inch sphere	Helium
64-K	Max	73.7	22	1	114,290	19	1-inch sphere	Helium
64-K	N	73.7	22	1	28,560	10.8	1-inch sphere	Helium
64-K	N	73.7	22	1	6,890	6	1-inch sphere	Helium
64-K	N	73.7	22	0.17	4,430	4	1-inch sphere	Helium
64-K	N	73.7	22	0.17	1,710	2.3	1-inch sphere	Helium
64-L	F	79.2	1	1	7,370	199	1-inch sphere	Helium
64-L	F	79.2	1	0.17	3,940	194	1-inch sphere	Helium
64-M	F	45.0	1	1	6,350	211	1-inch sphere	Helium
64-M	F	45.0	1	0.17	3,130	205	1-inch sphere	Helium
64-N	F	72.8	1	1	3,200	69	1-inch sphere	Helium
64-N	F	72.8	1	0.17	1,700	67	1-inch sphere	Helium
64-N	F	72.8	1	0.17	2,040	66	1-inch sphere	Helium
64-O	F	44.7	0	1	2,820	80	1-inch sphere	Helium
64-O	F	44.7	0	0.17	2,050	78	1-inch sphere	Helium
				Run 65				
65-A	F	14.3	0	1	12,800	301	Vertical disk	
65-A	F	14.3	0	1	10,710	231	Vertical disk	
65-A	F	14.3	0	1	8,150	161	Vertical disk	
65-A	F	14.3	0	1	5,780	101	Vertical disk	
65-A	F	14.3	0	1	4,110	61	Vertical disk	
65-B	F	44.3	0-12	1	19,930	281	Vertical disk	Helium
65-B	F	44.3	0-12	1	16,300	201	Vertical disk	Helium
65-B	F	44.3	0-12	1	12,920	141	Vertical disk	Helium
65-B	F	44.3	0-12	1	9,440	101	Vertical disk	Helium
65-B	F	44.3	0-12	1	6,860	61	Vertical disk	Helium
65-C	F	74.3	2-18	1	21,990	260	Vertical disk	Helium
65-C	F	74.3	2-18	1	18,560	190	Vertical disk	Helium
65-C	F	74.3	2-18	1	13,050	130	Vertical disk	Helium
65-C	F	74.3	2-18	1	9,080	90	Vertical disk	Helium
65-C	F	74.3	2-18	1	8,080	70	Vertical disk	Helium

Run Number	Boiling Region	Pressure	Subcooling	a/g	q/A	$T-T_{sat}$	Configuration	Pressurizing Medium
65-C	F	74.3	2-18	1	7,540	60	Vertical disk	Helium
65-D	Min	14.3	0	1	5,190	49	Vertical disk	
65-D	T	14.3	0	1	15,300	46	Vertical disk	
65-D	T	14.3	0	1	54,020	40	Vertical disk	
65-D	Max	14.3	0	1	71,560	31	Vertical disk	
65-D	N	14.3	0	1	60,620	22	Vertical disk	
65-D	N	14.3	0	1	20,650	13	Vertical disk	
65-D	N	14.3	0	1	10,070	10	Vertical disk	
65-D	N	14.3	0	1	2,530	3.7	Vertical disk	
				Run 66				
66-A	F	14.0	1.5	1	12,250	309	Vertical disk	
66-A	F	14.0	1.5	0.16	7,500	305	Vertical disk	
66-B	F	14.0	- 1.5	1	10,420	229	Vertical disk	
66-B	F	14.0	- 1.5	0.16	7,200	225	Vertical disk	
66-C	F	14.0	1	1	7,330	117	Vertical disk	
66-C	F	14.0	1	0.16	5,570	114	Vertical disk	
66-D	F	42.9	11	1	19,270	292	Vertical disk	Helium
66-D	F	42.9	11	0.16	13,300	286	Vertical disk	Helium
66-E	F	44.3	6	1	16,760	211	Vertical disk	Helium
66-E	F	44.3	6	0.16	11,040	205	Vertical disk	Helium
66-F	F	70.9	19	1	29,000	201	Vertical disk	Helium
66-F	F	70.9	19	0.16	20,960	193	Vertical disk	Helium
66-G	F	73.4	20	1	22,800	279	Vertical disk	Helium
66-G	F	73.4	20	0.16	16,000	274	Vertical disk	Helium
66-H	F	74.4	11	1	13,040	91	Vertical disk	Helium
66-H	F	74.4	11	0.16	8,610	88	Vertical disk	Helium
66-H	F	74.4	11	0.16	6,210	86	Vertical disk	Helium
66-I	F	45.7	3	1	9,480	88	Vertical disk	Helium
66-I	F	45.7	3	0.16	7,150	84	Vertical disk	Helium
				Run 67				
67-A	F	14.3	- 1	1	7,130	119	Vertical disk	
67-A	F	14.3	- 1	0	3,600	117	Vertical disk	
67-B	F	14.3	0	1	12,500	307	Vertical disk	
67-B	F	14.3	0	0	6,360	303	Vertical disk	
67-C	F	14.3	0	1	10,630	228	Vertical disk	
67-C	F	14.3	0	0	5,900	224	Vertical disk	
67-D	F	75.3	20	1	24,200	279	Vertical disk	Helium
67-D	F	75.3	20	0	12,150	273	Vertical disk	Helium
67-E	F	75.3	9	1	11,930	89	Vertical disk	Helium
67-E	F	75.3	9	0	5,520	85	Vertical disk	Helium
67-F	F	79.3	17	1	20,550	200	Vertical disk	Helium
67-F	F	79.3	17	0	8,800	194	Vertical disk	Helium
67-G	F	42.8	9	1	17,100	211	Vertical disk	Helium
67-G	F	42.8	9	0	8,820	206	Vertical disk	Helium
67-H	F	44.3	1	1	8,710	99	Vertical disk	Helium
67-H	F	44.3	1	0	5,460	96	Vertical disk	Helium
67-I	F	46.3	12	1	19,500	290	Vertical disk	Helium
67-I	F	46.3	12	0	8,900	285	Vertical disk	Helium
				Run 68				
68-A	F	50.8	2	1	15,160	287	Vertical disk	Nitrogen
68-A	F	50.8	2	0	8,325	283	Vertical disk	Nitrogen
68-B	F	47.8	0	1	14,420	199	Vertical disk	Nitrogen
68-B	F	47.8	0	0	6,340	196	Vertical disk	Nitrogen

Run Number	Boiling Region	Pressure	Subcooling	a/g	q/A	$T-T_{sat}$	Configuration	Pressurizing Medium
68-C	F	45.5	1	1	8,670	99	Vertical disk	Nitrogen
68-C	F	45.5	1	0	5,990	96	Vertical disk	Nitrogen
68-D	F	77.3	2	1	11,350	234	Vertical disk	Nitrogen
68-D	F	77.3	2	0	5,580	231	Vertical disk	Nitrogen
68-E	F	76.3	1	1	16,000	183	Vertical disk	Nitrogeh
68-E	F	76.3	1	0	11,160	179	Vertical disk	Nitrogen
68-E	F	76.3	1	0	10,180	177	Vertical disk	Nitrogen
68-F	F	74.5	0	1	12,610	114	Vertical disk	Nitrogen
68-F	F	74.5	0	0	9,150	110	Vertical disk	Nitrogen
68-G	F	44.6	- 5	1	13,710	207	Vertical disk	Nitrogen
68-G	F	44.6	- 5	0.16	11,080	203	Vertical disk	Nitrogen
68-H	F	46.1	- 3	1	14,960	288	Vertical disk	Nitrogen
68-H	F	46.1	- 3	0.16	10,590	284	Vertical disk	Nitrogen
68-I	F	45.4	0	1	47,800	94	Vertical disk	Nitrogen
68-I	F	45.4	0	0.16	41,200	80	Vertical disk	Nitrogen
68-J	F	77.1	0	1	16,800	275	Vertical disk	Nitrogen
68-J	F	77.1	0	0.16	12,230	270	Vertical disk	Nitrogen
68-K	F	73.1	- 6	1	14,150	196	Vertical disk	Nitrogen
68-K	F	73.1	- 6	0.16	12,170	191	Vertical disk	Nitrogen
68-L	F	78.3	- 4	1	11,080	110	Vertical disk	Nitrogen
68-L	F	78.3	- 4	0.16	8,590	107	Vertical disk	Nitrogen
68-M	F	74.3	0	1	18,420	260	Vertical disk	Nitrogen
68-M	F	74.3	- 2	1	15,650	190	Vertical disk	Nitrogen
68-M	F	74.3	- 1.9	1	12,880	140	Vertical disk	Nitrogen
68-M	F	74.3	- 1.7	1	10,080	90	Vertical disk	Nitrogen
68-M	F	74.3	- 1.3	1	9,400	70	Vertical disk	Nitrogen
68-M	F	74.3	- 1.3	1	7,810	50	Vertical disk	Nitrogen
68-N	F	43.7	1.6	1	16,320	281	Vertical disk	Nitrogen
68-N	F	43.7	- 1.9	1	13,200	201	Vertical disk	Nitrogen
68-N	F	43.7	- 0.7	1	10,410	141	Vertical disk	Nitrogen
68-N	F	43.7	0.1	1	8,500	101	Vertical disk	Nitrogen
68-N	F	43.7	0.5	1	7,567	65	Vertical disk	Nitrogen
68-N	F	43.7	0.8	1	6,865	41	Vertical disk	Nitrogen
				Run 69				
69-A	F	14.4	- 6— -13	1	9,570	308	Disk heating up	
69-A	F	14.4	- 6— -13	1	10,990	244	Disk heating up	
69-A	F	14.4	- 6— -13	1	8,900	202	Disk heating up	
69-A	F	14.4	- 6— -13	1	7,010	155	Disk heating up	
69-A	F	14.4	- 6— -13	1	6,540	117	Disk heating up	
69-A	F	14.4	- 6— -13	1	6,250	95	Disk heating up	
69-A	Min	14.4	- 6— -13	1	5,340	75	Disk heating up	
69-A	T	14.4	- 6— -13	1	5,920	60	Disk heating up	
69-A	T	14.4	- 6— -13	1	8,650	56	Disk heating up	
69-A	T	14.4	- 6— -13	1	18,610	49	Disk heating up	
69-B	F	69.6-80.8	1-4	1	16,510	271	Disk heating up	Nitrogen
69-B	F	69.6-80.8	1-4	1	13,980	202	Disk heating up	Nitrogen
69-B	F	69.6-80.8	1-4	1	12,250	160	Disk heating up	Nitrogen
69-B	F	69.6-80.8	1-4	1	11,550	119	Disk heating up	Nitrogen
69-B	F	69.6-80.8	1-4	1	10,500	90	Disk heating up	Nitrogen
69-B	F	69.6-80.8	1-4	1	9,840	69	Disk heating up	Nitrogen
69-B	Min	69.6-80.8	1-4	1	8,810	58	Disk heating up	Nitrogen
69-B	T	69.6-80.8	1-4	1	15,000	48	Disk heating up	Nitrogen
69-C	F	76.6	- 5	1	16,770	275	Disk heating up	Nitrogen
69-C	F	76.6	- 5	0.16	13,500	270	Disk heating up	Nitrogen
69-D	F	72.9	- 4	1	13,920	196	Disk heating up	Nitrogen
69-D	F	72.9	- 4	0.16	11,100	192	Disk heating up	Nitrogen

Run Number	Boiling Region	Pressure	Subcooling	a/g	q/A	$T-T_{sat}$	Configuration	Pressurizing Medium
69-E	F	80.3	- 2	1	11,410	110	Disk heating up	Nitrogen
69-E	F	80.3	- 2	0.16	8,970	106	Disk heating up	Nitrogen
69-F	F	73.1-78.3	0-18	1	31,170	265	Disk heating up	Helium
69-F	F	73.1-78.3	0-18	1	17,300	207	Disk heating up	Helium
69-F	F	73.1-78.3	0-18	1	13,330	163	Disk heating up	Helium
69-F	F	73.1-78.3	0-18	1	11,160	122	Disk heating up	Helium
69-F	F	73.1-78.3	0-18	1	9,880	87	Disk heating up	Helium
69-F	F	73.1-78.3	0-18	1	8,120	68	Disk heating up	Helium
69-F	Min	73.1-78.3	0-18	1	7,300	51	Disk heating up	Helium
69-F	T	73.1-78.3	0-18	1	10,140	46	Disk heating up	Helium
69-F	T	73.1-78.3	0-18	1	13,120	39	Disk heating up	Helium
69-G	F	14.3	0	1	13,160	306	Disk heating up	
69-G	F	14.3	0	0.16	10,200	303	Disk heating up	
69-H	F	14.3	-15	1	9,750	225	Disk heating up	
69-H	F	14.3	-15	0.16	7,680	222	Disk heating up	
69-I	F	14.3	-13	1	6,400	112	Disk heating up	
69-I	F	14.3	-13	0.16	5,070	110	Disk heating up	
69-J	F	74.2	10	1	21,750	277	Disk heating up	Helium
69-J	F	74.2	10	0.16	17,500	271	Disk heating up	Helium
69-K	F	74.2	2	1	16,340	196	Disk heating up	Helium
69-K	F	74.2	2	0.16	13,250	191	Disk heating up	Helium
69-L	F	77.7	2	1	12,370	110	Disk heating up	Helium
69-L	F	77.7	2	0.16	9,380	106	Disk heating up	Helium
				Run 70				
70-A	F	14.1	- 9	11,270		320	Disk heating dn	
70-A	F	14.1	- 9	1	10,200	254	Disk heating dn	
70-A	F	14.1	- 9	1	9,410	209	Disk heating dn	
70-A	F	14.1	- 9	1	7,700	164	Disk heating dn	
70-A	F	14.1	- 9	1	7,200	130	Disk heating dn	
70-A	F	14.1	- 9	1	6,990	100	Disk heating dn	
70-A	F	14.1	- 9	1	6,510	77	Disk heating dn	
70-A	Min	14.1	- 9	1	4,400	60	Disk heating dn	
70-A	T	14.1	- 9	1	9,820	60	Disk heating dn	
70-A	T	14.1	- 9	1	15,890	43	Disk heating dn	
70-B	F	72.7-81.4	- 1— -4	1	16,580	288	Disk heating dn	Nitrogen
70-B	F	72.7-81.4	- 1— -4	1	14,470	231	Disk heating dn	Nitrogen
70-B	F	72.7-81.4	- 1— -4	1	14,000	185	Disk heating dn	Nitrogen
70-B	F	72.7-81.4	- 1— -4	1	13,600	153	Disk heating dn	Nitrogen
70-B	F	72.7-81.4	- 1— -4	1	12,980	120	Disk heating dn	Nitrogen
70-B	F	72.7-81.4	- 1— -4	1	10,900	95	Disk heating dn	Nitrogen
70-B	F	72.7-81.4	- 1— -4	1	8,840	74	Disk heating dn	Nitrogen
70-B	Min	72.7-81.4	- 1— -4	1	8,280	56	Disk heating dn	Nitrogen
70-B	T	72.7-81.4	- 1— -4	1	15,390	44	Disk heating dn	Nitrogen
70-C	F	76.3	- 4	1	17,620	275	Disk heating dn	Nitrogen
70-C	F	76.3	- 4	0.16	14,710	269	Disk heating dn	Nitrogen
70-D	F	78.6	- 2	1	14,270	194	Disk heating dn	Nitrogen
70-D	F	78.6	- 2	0.16	12,600	189	Disk heating dn	Nitrogen
70-E	F	77.7	- 3	1	12,810	112	Disk heating dn	Nitrogen
70-E	F	77.7	- 3	0.16	11,290	107	Disk heating dn	Nitrogen
70-F	F	74.1	0-19	1	23,570	272	Disk heating dn	Helium
70-F	F	74.1	0-19	1	19,890	225	Disk heating dn	Helium
70-F	F	74.1	0-19	1	16,680	174	Disk heating dn	Helium
70-F	F	74.1	0-19	1	14,630	136	Disk heating dn	Helium
70-F	F	74.1	0-19	1	12,190	102	Disk heating dn	Helium
70-F	F	74.1	0-19	1	9,780	80	Disk heating dn	Helium
70-F	F	74.1	0-19	1	8,860	63	Disk heating dn	Helium

Run Number	Boiling Region	Pressure	Subcooling	a/g	q/A	$T-T_{sat}$	Configuration	Pressurizing Medium
70-G	F	14.1	-10	1	12,730	305	Disk heating dn	
70-G	F	14.1	-10	0.16	10,700	301	Disk heating dn	
70-H	F	14.1	- 9	1	10,210	226	Disk heating dn	
70-H	F	14.1	- 9	0.16	8,720	222	Disk heating dn	
70-I	F	14.1	- 6	1	7,800	116	Disk heating dn	
70-I	F	14.1	- 6	0.16	6,850	113	Disk heating dn	
70-J	F	78.6	15	1	24,040	275	Disk heating dn	Helium
70-J	F	78.6	15	0.16	18,380	268	Disk heating dn	Helium
70-K	F	72.2	3	1	16,040	195	Disk heating dn	Helium
70-K	F	72.2	3	0.16	14,200	190	Disk heating dn	Helium
70-L	F	75.2	2	1	13,780	113	Disk heating dn	Helium
70-L	F	75.2	2	0.16	11,430	108	Disk heating dn	Helium
				Run 71				
71-A	F	14.3	- 8	1	12,960	305	Disk heating dn	
71-A	F	14.3	- 8	0	8,780	301	Disk heating dn	
71-B	F	14.3	- 9	1	9,860	226	Disk heating dn	
71-B	F	14.3	- 9	0	7,750	223	Disk heating dn	
71-C	F	14.3	- 8	1	7,630	114	Disk heating dn	
71-C	F	14.3	- 8	0	5,550	112	Disk heating dn	
71-D	F	14.3	- 7	1	12,960	308	Disk heating dn	
71-D	F	14.3	- 7	0	8,200	304	Disk heating dn	
71-E	F	14.3	0	1	10,050	226	Disk heating dn	
71-E	F	14.3	0	0	7,710	223	Disk heating dn	
71-F	F	14.3	1	1	7,240	116	Disk heating dn	
71-F	F	14.3	1	0	5,480	114	Disk heating dn	
71-G	F	74.3	0	1	16,900	276	Disk heating dn	Nitrogen
71-G	F	74.3	0	0	9,920	272	Dish heating dn	Nitrogen
71-H	F	74.3	2	1	14,580	197	Disk heating dn	Nitrogen
71-H	F	74.3	2	0	9,700	194	Disk heating dn	Nitrogen
71-I	F	76.3	4	1	27,900	112	Disk heating dn	Nitrogen
71-I	F	76.3	4	0	15,410	103	Disk heating dn	Nitrogen
71-J	F	73.9	19	1	20,850	275	Disk heating dn	Helium
71-J	F	73.9	19	0	10,590	269	Disk heating dn	Helium
71-K	F	73.3	7	1	16,750	195	Disk heating dn	Helium
71-K	F	73.3	7	0	11,590	190	Disk heating dn	Helium
71-L	F	76.3	8	1	17,900	111	Disk heating dn	Helium
71-L	F	76.3	8	0	15,380	105	Disk heating dn	Helium
71-M	F	73.8	17	1	21,900	277	Disk heating dn	Helium
71-M	F	73.8	17	0	15,420	270	Disk heating dn	Helium
71-N	F	73.6	13	1	19,440	199	Disk heating dn	Helium
71-N	F	73.6	13	0	13,300	193	Disk heating dn	Helium
71-O	F	81.3	5	1	13,560	110	Disk heating dn	Helium
71-O	F	81.3	5	0	10,220	106	Disk heating dn	Helium
				Run 72				
72-A	F	14.3	- 1	1	6,820	240	1/4-inch sphere	
72-A	F	14.3	- 1	1	6,100	220	1/4-inch sphere	
72-A	F	14.3	- 1	1	5,650	205	1/4-inch sphere	
72-B	F	14.3	0 (EST)	1	5,000	180	1/4-inch sphere	
72-B	F	14.3	0 (EST)	1	4,560	160	1/4-inch sphere	
72-B	F	14.3	0 (EST)	1	4,280	150	1/4-inch sphere	
72-B	F	14.3	0 (EST)	1	3,820	140	1/4-inch sphere	
72-C	F	14.3	- 1	1	3,110	86	1/4-inch sphere	
72-C	F	14.3	- 1	1	2,960	76	1/4-inch sphere	
72-C	F	14.3	- 1	1	2,760	66	1/4-inch sphere	

Run Number	Boiling Region	Pressure	Subcooling	a/g	q/A	$T-T_{sat}$	Configuration	Pressurizing Medium
72-C	F	14.3	- 1	1	2,596	56	1/4-inch sphere	
72-C	Min	14.3	- 1	1	2,560	46	1/4-inch sphere	
72-C	T	14.3	- 1	1	2,800	36	1-4-inch sphere	
72-C	T	14.3	- 1	1	6,990	31	1/4-inch sphere	
72-C	T	14.3	- 1	1	18,010	27	1/4-inch sphere	
72-C	Max	14.3	- 1	1	39,150	17	1/4-inch sphere	
72-C	N	14.3	- 1	1	24,820	12	1/4-inch sphere	
72-C	N	14.3	- 1	1	10,750	9	1/4-inch sphere	
72-D	F	46.8	0	1	4,030	70	1/4-inch sphere	Nitrogen
72-D	Min	46.8	0	1	3,720	55	1/4-inch sphere	Nitrogen
72-D	T	46.8	0	1	8,310	36.5	1/4-inch sphere	Nitrogen
72-D	T	46.8	0	1	10,610	34.4	1/4-inch sphere	Nitrogen
72-D	T	46.8	0	1	16,230	30.6	1/4-inch sphere	Nitrogen
72-D	T	46.8	0	1	25,310	27.0	1/4-inch sphere	Nitrogen
72-D	T	46.8	0	1	36.480	23.5	1/4-inch sphere	Nitrogen
72-D	T	46.8	0	1	48,880	18.4	1/4-inch sphere	Nitrogen
72-D	T	46.8	0	1	55,960	15.8	1/4-inch sphere	Nitrogen
72-D	Max	46.8	0	1	59,460	12.8	1/4-inch sphere	Nitrogen
72-D	N	46.8	0	1	54,710	11.2	1/4-inch sphere	Nitrogen
72-D	N	46.8	0	1	46,060	9.8	1/4-inch sphere	Nitrogen
72-D	N	46.8	0	1	37,270	8.7	1/4-inch sphere	Nitrogen
72-D	N	46.8	0	1	26,960	7.8	1/4-inch sphere	Nitrogen
72-D	N	46.8	0	1	18,860	7.5	1/4-inch sphere	Nitrogen
72-D	N	46.8	0	1	14,320	7.2	1/4-inch sphere	Nitrogen
72-D	N	46.8	0	1	10,140	6.5	1/4-inch sphere	Nitrogen
72-E	F	46.1	0	1	8,480	225	1/4-inch sphere	Nitrogen
72-E	F	46.1	0	1	7,980	210	1/4-inch sphere	Nitrogen
72-E	F	46.1	0	1	7,140	185	1/4-inch sphere	Nitrogen
72-F	F	45.1	0	1	6,900	165	1/4-inch sphere	Nitrogen
72-F	F	45.1	0	1	6,060	145	1/4-inch sphere	Nitrogen
72-F	F	45.1	0	1	5,390	120	1/4-inch sphere	Nitrogen
72-G	F	75.5	0	1	8,150	160	1/4-inch sphere	Nitrogen
72-G	F	75.5	0	1	7,120	140	1/4-inch sphere	Nitrogen
72-G	F	75.5	0	1	6,350	125	1/4-inch sphere	Nitrogen
72-G	F	75.5	0	1	5,980	110	1/4-inch sphere	Nitrogen
72-H	F	74.7	0	1	4,560	70	1/4-inch sphere	Nitrogen
72-H	F	74.7	0	1	4,140	55	1/4-inch sphere	Nitrogen
72-H	Min	74.7	0	1	3,950	40	1/4-inch sphere	Nitrogen
72-I	F	14.3	0	1	6,990	250	1/4-inch sphere	
72-I	F	14.3	0	1	6,550	243	1/4-inch sphere	
72-I	F	14.3	0	1	6,510	233	1/4-inch sphere	
72-I	F	14.3	0	0	3,000	227	1/4-inch sphere	
72-I	F	14.3	0	0	3,130	223	1/4-inch sphere	
72-J	F	14.3	0	1	5,230	179	1/4-inch sphere	
72-J	F	14.3	0	1	4,720	167	1/4-inch sphere	
72-J	F	14.3	0	0	2,480	158	1/4-inch sphere	
72-K	F	14.3	0	1	2,850	71	1/4-inch sphere	
72-K	Min	14.3	0	1	2,400	51	1/4-inch sphere	
72-K	T	14.3	0	1	4,420	43	1/4-inch sphere	
72-K	T	14.3	0	0	5,000	41	1/4-inch sphere	
72-K	T	14.3	0	0	1,390	38.5	1/4-inch sphere	
72-K	T	14.3	0	0	3,390	36.8	1/4-inch sphere	
72-K	T	14.3	0	0	9,750	32.1	1/4-inch sphere	
72-K	T	14.3	0	0	21,220	27.5	1/4-inch sphere	
72-L	F	14.3	1	1	3,140	72	1/4-inch sphere	
72-L	Min	14.3	1	1	2,720	55	1/4-inch sphere	
72-L	T	14.3	1	1	3,030	38	1/4-inch sphere	

Run Number	Boiling Region	Pressure	Subcooling	a/g	q/A	$T-T_{sat}$	Configuration	Pressurizing Medium
72-L	T	14.3	1	0	1,800	35	1/4-inch sphere	
72-L	T	14.3	1	0	1,290	31	1/4-inch sphere	
72-M	F	14.3	- 1	1	2,900	78	1/4-inch sphere	
72-M	F	14.3	- 1	1	2,500	61	1/4-inch sphere	
72-M	Min	14.3	- 1	1	2,360	43	1/4-inch sphere	
72-M	T	14.3	- 1	0	735	35	1/4-inch sphere	
72-M	T	14.3	- 1	0	1,650	33	1/4-inch sphere	
72-N	F	44.3	12	1	10,780	223	1/4-inch sphere	Helium
72-N	F	44.3	12	1	10,270	209	1/4-inch sphere	Helium
72-N	F	44.3	12	1	9,760	203	1/4-inch sphere	Helium
72-N	F	44.3	12	0	3,410	191	1/4-inch sphere	Helium
72-O	F	44.3	14 (EST)	1	8,340	161	1/4-inch sphere	Helium
72-O	F	44.3	14 (EST)	1	7,770	151	1/4-inch sphere	Helium
72-O	F	44.3	14 (EST)	0	4,290	136	1/4-inch sphere	Helium
72-O	F	44.3	14 (EST)	0	3,350	133	1/4-inch sphere	Helium
72-P	Min	44.3	14	1	5,990	66	1/4-inch sphere	Helium
72-P	T	44.3	14	1	7,010	37	1/4-inch sphere	Helium
72-P	T	44.3	14	1	20,890	31	1/4-inch sphere	Helium
72-P	T	44.3	14	1	48,300	19.9	1/4-inch sphere	Helium
72-P	Max	44.3	14	0	61,330	14.1	1/4-inch sphere	Helium
72-P	N	44.3	14	0	39,300	8.9	1/4-inch sphere	Helium
72-P	N	44.3	14	0	17,560	4.7	1/4-inch sphere	Helium
72-Q	Min	44.6	12	1	7,080	70	1/4-inch sphere	Helium
72-Q	T	44.6	12	1	10,760	46	1/4-inch sphere	Helium
72-Q	T	44.6	12	1	36,890	31	1/4-inch sphere	Helium
72-Q	Max	44.6	12	0	61,730	21	1/4-inch sphere	Helium
72-Q	N	44.6	12	0	40,630	12.3	1/4-inch sphere	Helium
72-Q	N	44.6	12	0	13,470	7.0	1/4-inch sphere	Helium
72-R	Min	43.7	12 (EST)	1	7,120	71	1/4-inch sphere	Helium
72-R	T	43.7	12 (EST)	1	14,760	41	1/4-inch sphere	Helium
72-R	T	43.7	12 (EST)	0	32,360	29	1/4-inch sphere	Helium
72-R	T	43.7	12 (EST)	0	33,810	22	1/4-inch sphere	Helium
72-R	Max	43.7	12 (EST)	0	37,430	12.8	1/4-inch sphere	Helium
72-R	N	43.7	12 (EST)	0	24,350	8.9	1/4-inch sphere	Helium
72-R	N	43.7	12 (EST)	0	17,370	7.5	1/4-inch sphere	Helium
72-S	F	43.8	11	1	6,200	76	1/4-inch sphere	Helium
72-S	Min	43.8	11	1	5,540	58	1/4-inch sphere	Helium
72-S	T	43.8	11	0	5,520	51	1/4-inch sphere	Helium
72-S	T	43.8	11	0	8,920	41	1/4-inch sphere	Helium
72-S	T	43.8	11	0	14,190	39	1/4-inch sphere	Helium
72-S	T	43.8	11	0	22,470	36	1/4-inch sphere	Helium
72-T	Min	14.3	- 1	1	2,910	70	1/4-inch sphere	
72-T	T	14.3	- 1	1	2,920	50	1/4-inch sphere	
72-T	T	14.3	- 1	1	3,240	40	1/4-inch sphere	
72-T	T	14.3	- 1	1	4,020	37	1/4-inch sphere	
72-T	T	14.3	- 1	1	11,060	31	1/4-inch sphere	
72-T	T	14.3	- 1	0	19,510	21	1/4-inch sphere	
72-T	Max	14.3	- 1	0	22,660	12.3	1/4-inch sphere	
72-T	N	14.3	- 1	0	8,920	8.5	1/4-inch sphere	
				Run 73				
73-A	T	76.0	- 2	1	12,500	35	1-inch sphere	Nitrogen
73-A	T	76.0	- 2	1	44,430	28	1-inch sphere	Nitrogen
73-A	Max	76.0	- 2	1	76,590	19.5	1-inch sphere	Nitrogen
73-A	N	76.0	- 2	1	46,740	14.2	1-inch sphere	Nitrogen
73-A	N	76.0	- 2	1	6,480	7.5	1-inch sphere	Nitrogen
73-A	N	76.0	- 2	1	1,130	3.7	1-inch sphere	Nitrogen

Run Number	Boiling Region	Pressure	Subcooling	a/g	q/A	$T-T_{sat}$	Configuration	Pressurizing Medium
73-B	T	75.0	- 3	1	3,000	40	1-inch sphere	Nitrogen
73-B	T	75.0	- 3	1	13,240	37.5	1-inch sphere	Nitrogen
73-B	T	75.0	- 3	1	39,110	30.4	1-inch sphere	Nitrogen
73-B	Max	75.0	- 3	1	77,530	20.8	1-inch sphere	Nitrogen
73-B	N	75.0	- 3	1	51,430	15.1	1-inch sphere	Nitrogen
73-B	N	75.0	- 3	1	6,570	7.1	1-inch sphere	Nitrogen
73-B	N	75.0	- 3	1	1,200	3.9	1-inch sphere	Nitrogen
73-C	T	45.0	- 4	1	6,880	42	1-inch sphere	Nitrogen
73-C	T	45.0	- 4	1	13,920	39	1-inch sphere	Nitrogen
73-C	T	45.0	- 4	1	23,380	36	1-inch sphere	Nitrogen
73-C	T	45.0	- 4	1	39,660	30	1-inch sphere	Nitrogen
73-C	T	45.0	- 4	1	56,630	26	1-inch sphere	Nitrogen
73-C	Max	45.0	- 4	1	66,500	23	1-inch sphere	Nitrogen
73-C	N	45.0	- 4	1	56,090	19	1-inch sphere	Nitrogen
73-C	N	45.0	- 4	1	44,750	17.7	1-inch sphere	Nitrogen
73-C	N	45.0	- 4	1	24,930	14.7	1-inch sphere	Nitrogen
73-C	N	45.0	- 4	1	12,830	12.5	1-inch sphere	Nitrogen
73-C	N	45.0	- 4	1	6,030	10.2	1-inch sphere	Nitrogen
73-C	N	45.0	- 4	1	3,190	8.1	1-inch sphere	Nitrogen
73-C	N	45.0	- 4	1	1,180	5.7	1-inch sphere	Nitrogen
73-D	F	79.0	- 2	1	5,900	153	1-inch sphere	Nitrogen
73-D	F	79.0	- 2	1	5,630	140	1-inch sphere	Nitrogen
73-D	F	79.0	- 2	1	5,350	127	1-inch sphere	Nitrogen
73-D	F	79.0	- 2	1	4,730	115	1-inch sphere	Nitrogen
				Run 75				
75-A	F	44.3	0	1	18,600	331	Vertical disk	Helium
75-A	F	44.3	0	1	16,400	291	Vertical disk	Helium
75-A	F	44.3	0	1	13,820	251	Vertical disk	Helium
75-A	F	44.3	0	1	12,060	211	Vertical disk	Helium
75-A	F	44.3	0	1	10,680	171	Vertical disk	Helium
75-A	F	44.3	0	1	8,630	131	Vertical disk	Helium
75-A	F	44.3	0	1	7,480	91	Vertical disk	Helium
75-A	F	44.3	0	1	6,530	71	Vertical disk	Helium
75-A	F	44.3	0	1	5,080	51	Vertical disk	Helium
75-B	F	44.3	0	1	16,220	301	Vertical disk	Nitrogen
75-B	F	44.3	0	1	14,420	261	Vertical disk	Nitrogen
75-B	F	44.3	0	1	12,420	221	Vertical disk	Nitrogen
75-B	F	44.3	0	1	10,810	181	Vertical disk	Nitrogen
75-B	F	44.3	0	1	10,000	141	Vertical disk	Nitrogen
75-B	F	44.3	0	1	7,280	101	Vertical disk	Nitrogen
75-B	F	44.3	0	1	6,295	81	Vertical disk	Nitrogen
75-B	F	44.3	0	1	5,850	61	Vertical disk	Nitrogen
75-C	F	74.3	0	1	17,950	310	Vertical disk	Nitrogen
75-C	F	74.3	0	1	17,200	270	Vertical disk	Nitrogen
75-C	F	74.3	0	1	13,020	210	Vertical disk	Nitrogen
75-C	F	74.3	0	1	11,620	170	Vertical disk	Nitrogen
75-C	F	74.3	0	1	9,880	130	Vertical disk	Nitrogen
75-C	F	74.3	0	1	8,930	110	Vertical disk	Nitrogen
75-C	F	74.3	0	1	7,750	90	Vertical disk	Nitrogen
75-C	F	74.3	0	1	7,235	70	Vertical disk	Nitrogen
75-C	F	74.3	0	1	6,200	50	Vertical disk	Nitrogen
75-D	F	73.9	0	1	17,570	310	Vertical disk	Helium
75-D	F	73.9	0	1	16,570	270	Vertical disk	Helium
75-D	F	73.9	0	1	14,800	230	Vertical disk	Helium
75-D	F	73.9	0	1	12,800	190	Vertical disk	Helium

Run Number	Boiling Region	Pressure	Subcooling	a/g	q/A	$T-T_{sat}$	Configuration	Pressurizing Medium
75-D	F	73.9	0	1	10,720	150	Vertical disk	Helium
75-D	F	73.9	0	1	9,100	110	Vertical disk	Helium
75-D	F	73.9	0	1	7,610	70	Vertical disk	Helium
75-D	F	73.9	0	1	6,630	50	Vertical disk	Helium
75-E	F	77.0	- 1	1	7,790	125	Disk heating up	Nitrogen
75-E	F	77.0	- 1	1	6,750	112	Disk heating up	Nitrogen
75-E	F	77.0	- 1	0	6,180	109	Disk heating up	Nitrogen
75-E	F	77.0	- 1	0	2,285	108.5	Disk heating up	Nitrogen
75-F	F	78.3	0	1	11,710	274	Disk heating dn	Nitrogen
75-F	F	78.3	0	0	10,680	269	Disk heating dn	Nitrogen
75-G	F	73.7	0	1	10,500	198	Disk heating dn	Nitrogen
75-G	F	73.7	0	0	9,680	193	Disk heating dn	Nitrogen
75-H	F	74.3	- 1	1	8,100	124	Disk heating dn	Nitrogen
75-H	F	74.3	- 1	1	7,400	119	Disk heating dn	Nitrogen
75-H	F	74.3	- 1	1	7,420	115	Disk heating dn	Nitrogen
75-H	F	74.3	- 1	0	7,500	111.5	Disk heating dn	Nitrogen
75-H	F	74.3	- 1	0	6,635	110.5	Disk heating dn	Nitrogen
75-I	F	73.9	- 2	1	16,400	238	Vertical disk	Nitrogen
75-I	F	73.9	- 2	0	10,800	234	Vertical disk	Nitrogen
75-J	F	52	2	1	48,220	98	Vertical disk	Nitrogen
75-J	F	52	2	0.16	39,900	82	Vertical disk	Nitrogen
75-K	Min	44.3	1	1	15,200	70	Vertical disk	Nitrogen
75-K	T	44.3	1	1	15,900	60	Vertical disk	Nitrogen
75-K	T	44.3	1	1	16,600	50	Vertical disk	Nitrogen
75-K	T	44.3	1	1	16,940	41	Vertical disk	Nitrogen
75-K	T	44.3	1	1	33,710	31	Vertical disk	Nitrogen
75-K	T	44.3	1	1	62,520	21	Vertical disk	Nitrogen
75-K	Max	44.3	1	1	84,390	16.2	Vertical disk	Nitrogen
75-K	N	44.3	1	1	54,520	13	Vertical disk	Nitrogen
75-K	N	44.3	1	1	28,890	10	Vertical disk	Nitrogen
75-K	N	44.3	1	1	10,750	7	Vertical disk	Nitrogen
75-K	N	44.3	1	1	3,170	3.7	Vertical disk	Nitrogen
75-K	N	44.3	1	1	889	1.4	Vertical disk	Nitrogen
75-L	F	44.3	- 1	1	15,650	270	Vertical disk	Nitrogen
75-L	F	44.3	- 1	1	14,000	200	Vertical disk	Nitrogen
75-L	F	44.3	- 1	1	11,560	150	Vertical disk	Nitrogen
75-L	F	44.3	- 1	1	9,190	100	Vertical disk	Nitrogen
75-L	F	44.3	- 1	1	6,840	60	Vertical disk	Nitrogen
				Run 76				
76-A	F	76.6	- 1	1	5,470	63	1/4-inch sphere	Nitrogen
76-A	Min	76.6	- 1	1	4,950	47	1/4-inch sphere	Nitrogen
76-A	T	76.6	- 1	1	5,070	34	1/4-inch sphere	Nitrogen
76-A	T	76.6	- 1	0.17	9,330	30	1/4-inch sphere	Nitrogen
76-A	T	76.6	- 1	0.17	21,140	24	1/4-inch sphere	Nitrogen
76-A	T	76.6	- 1	0.17	44,690	16.4	1/4-inch sphere	Nitrogen
76-A	Max	76.6	- 1	0.17	74,460	13.6	1/4-inch sphere	Nitrogen
76-A	N	76.6	- 1	0.17	34,470	10.6	1/4-inch sphere	Nitrogen
76-A	N	76.6	- 1	0.17	9,010	6.3	1/4-inch sphere	Nitrogen
76-B	F	44.6	- 2	1	5,030	76	1/4-inch sphere	Nitrogen
76-B	F	44.6	- 2	1	4,380	66	1/4-inch sphere	Nitrogen
76-B	F	44.6	- 2	1	3,640	56	1/4-inch sphere	Nitrogen
76-B	F	44.6	- 2	1	3,890	46	1/4-inch sphere	Nitrogen
76-B	Min	44.6	- 2	1	3,020	40	1/4-inch sphere	Nitrogen
76-B	T	44.6	- 2	0.17	4,830	37	1/4-inch sphere	Nitrogen
76-B	T	44.6	- 2	0.17	9,100	30	1/4-inch sphere	Nitrogen

Run Number	Boiling Region	Pressure	Subcooling	a/g	q/A	$T-T_{sat}$	Configuration	Pressurizing Medium
76-B	T	44.6	- 2	0.17	33,190	22	1/4-inch sphere	Nitrogen
76-B	T	44.6	- 2	0.17	42,140	15.5	1/4-inch sphere	Nitrogen
76-B	Max	44.6	- 2	0.17	43,150	12.7	1/4-inch sphere	Nitrogen
76-B	N	44.6	- 2	0.17	23,410	10.0	1/4-inch sphere	Nitrogen
76-B	N	44.6	- 2	0.17	4,390	6.5	1/4-inch sphere	Nitrogen
76-B	N	44.6	- 2	0.17	3,060	5.1	1/4-inch sphere	Nitrogen
76-C	F	73.9	- 2	1	5,080	65	1/4-inch sphere	Nitrogen
76-C	F	73.9	- 2	1	4,610	50	1/4-inch sphere	Nitrogen
76-C	Min	73.9	- 2	1	4,460	40	1/4-inch sphere	Nitrogen
76-C	T	73.9	- 2	1	15,940	30	1/4-inch sphere	Nitrogen
76-C	T	73.9	- 2	1	41,830	20	1/4-inch sphere	Nitrogen
76-C	Max	73.9	- 2	1	99,730	15.7	1/4-inch sphere	Nitrogen
76-C	N	73.9	- 2	1	43,980	11.7	1/4-inch sphere	Nitrogen
76-C	N	73.9	- 2	1	10,680	5.9	1/4-inch sphere	Nitrogen
76-D	F	76.1	- 1	1	5,090	64	1/4-inch sphere	Nitrogen
76-D	Min	76.1	- 1	1	4,910	49	1/4-inch sphere	Nitrogen
76-D	T	76.1	- 1	1	6,010	36	1/4-inch sphere	Nitrogen
76-D	T	76.1	- 1	0	10,150	31	1/4-inch sphere	Nitrogen
76-D	T	76.1	- 1	0	24,910	26	1/4-inch sphere	Nitrogen
76-D	Max	76.1	- 1	0	46,420	16.3	1/4-inch sphere	Nitrogen
76-D	N	76.1	- 1	0	32,140	12.3	1/4-inch sphere	Nitrogen
76-D	N	76.1	- 1	0	12,550	8.5	1/4-inch sphere	Nitrogen
76-E	F	46.3	- 1	1	4,300	71	1/4-inch sphere	Nitrogen
76-E	Min	46.3	- 1	1	4,090	51	1/4-inch sphere	Nitrogen
76-E	T	46.3	- 1	1	7,140	37	1/4-inch sphere	Nitrogen
76-E	T	46.3	- 1	0	3,180	34	1/4-inch sphere	Nitrogen
76-E	T	46.3	- 1	0	10,320	31	1/4-inch sphere	Nitrogen
76-E	T	46.3	- 1	0	19,340	22	1/4-inch sphere	Nitrogen
76-E	Max	46.3	- 1	0	20,550	11.3	1/4-inch sphere	Nitrogen
				Run 77				
77-A	F	72.3	0	1	3,540	65	1-inch sphere	Nitrogen
77-A	F	72.3	0	1	3,180	50	1-inch sphere	Nitrogen
77-A	T	72.3	0	0	8,520	28	1-inch sphere	Nitrogen
77-B	F	77.1	0	1	2,960	47	1-inch sphere	Nitrogen
77-B	Min	77.1	0	1	2,840	43	1-inch sphere	Nitrogen
77-B	T	77.1	0	0	12,500	30	1-inch sphere	Nitrogen
77-C	Min	77.8	0	1	3,190	47	1-inch sphere	Nitrogen
77-C	T	77.8	0	1	3,370	42	1-inch sphere	Nitrogen
77-C	T	77.8	0	1	15,740	38	1-inch sphere	Nitrogen
77-C	T	77.8	0	1	42,980	27	1-inch sphere	Nitrogen
77-C	Max	77.8	0	1	76,560	21	1-inch sphere	Nitrogen
77-C	N	77.8	0	1	49,070	14.7	1-inch sphere	Nitrogen
77-C	N	77.8	0	1	24,990	11.7	1-inch sphere	Nitrogen
77-D	Min	73.7	0	1	3,060	48	1-inch sphere	Nitrogen
77-D	T	73.7	0	1	3,380	40	1-inch sphere	Nitrogen
77-D	T	73.7	0	1	12,400	36	1-inch sphere	Nitrogen
77-D	T	73.7	0	0	14,450	30	1-inch sphere	Nitrogen
77-D	T	73.7	0	0	8,990	28	1-inch sphere	Nitrogen
77-D	T	73.7	0	0	6,340	27	1-inch sphere	Nitrogen
77-D	T	73.7	0	0	4,770	26	1-inch sphere	Nitrogen
77-E	Min	74.2	0	1	3,000	44	1-inch sphere	Nitrogen
77-E	T	74.2	0	1	9,820	35	1-inch sphere	Nitrogen
77-E	T	74.2	0	1	47,520	27	1-inch sphere	Nitrogen
77-E	T	74.2	0	0	49,980	26	1-inch sphere	Nitrogen
77-E	T	74.2	0	0	30,760	23.4	1-inch sphere	Nitrogen
77-E	T	74.2	0	0	15,920	21.4	1-inch sphere	Nitrogen

Run Number	Boiling Region	Pressure	Subcooling	a/g	q/A	$T-T_{sat}$	Configuration	Pressurizing Medium
77-E	T	74.2	0	0	22,430	19.4	1-inch sphere	Nitrogen
77-E	Max	74.2	0	0	25,550	17.9	1-inch sphere	Nitrogen
77-E	N	74.2	0	0	22,480	13.4	1-inch sphere	Nitrogen
77-E	N	74.2	0	0	17,030	9.9	1-inch sphere	Nitrogen
77-F	Min	44.1	0	1	2,580	49	1-inch sphere	Nitrogen
77-F	T	44.1	0	1	5,270	39	1-inch sphere	Nitrogen
77-F	T	44.1	0	1	12,830	36	1-inch sphere	Nitrogen
77-F	T	44.1	0	1	19,090	32	1-inch sphere	Nitrogen
77-F	T	44.1	0	0	29,140	29	1-inch sphere	Nitrogen
77-F	T	44.1	0	0	23,200	27.4	1-inch sphere	Nitrogen
77-F	T	44.1	0	0	17,500	26.2	1-inch sphere	Nitrogen
77-F	T	44.1	0	0	5,930	24.6	1-inch sphere	Nitrogen
77-G	T	43.4	0	1	3,680	43	1-inch sphere	Nitrogen
77-G	T	43.4	0	1	9,610	39	1-inch sphere	Nitrogen
77-G	T	43.4	0	1	21,820	34.5	1-inch sphere	Nitrogen
77-G	T	43.4	0	1	58,000	25.4	1-inch sphere	Nitrogen
77-G	T	43.4	0	0	45,570	21.1	1-inch sphere	Nitrogen
77-G	T	43.4	0	0	10,170	19.7	1-inch sphere	Nitrogen
77-G	T	43.4	0	0	1,230	19.2	1-inch sphere	Nitrogen
77-G	T	43.4	0	0	17,980	18.4	1-inch sphere	Nitrogen
77-G	Max	43.4	0	0	18,990	15.5	1-inch sphere	Nitrogen
77-G	N	43.4	0	0	18,710	12.1	1-inch sphere	Nitrogen
77-G	N	43.4	0	0	13,450	10.5	1-inch sphere	Nitrogen
77-G	N	43.4	0	0	9,440	9.9	1-inch sphere	Nitrogen
77-H	F	74.2	0	1	3,150	48	1-inch sphere	Nitrogen
77-H	Min	74.2	0	1	2,580	40	1-inch sphere	Nitrogen
77-H	T	74.2	0	1	22,790	31.4	1-inch sphere	Nitrogen
77-H	T	74.2	0	0.17	13,570	29.6	1-inch sphere	Nitrogen
77-H	T	74.2	0	0.17	6,910	29	1-inch sphere	Nitrogen
77-H	T	74.2	0	0.17	17,460	27	1-inch sphere	Nitrogen
77-H	T	74.2	0	0.17	39,160	21.4	1-inch sphere	Nitrogen
77-H	Max	74.2	0	0.17	53,380	18	1-inch sphere	Nitrogen
77-H	N	74.2	0	0.17	38,060	13.9	1-inch sphere	Nitrogen
77-I	T	44.0	0	1	2,660	46.5	1-inch sphere	Nitrogen
77-I	T	44.0	0	1	7,850	37.8	1-inch sphere	Nitrogen
77-I	T	44.0	0	1	15,790	34.2	1-inch sphere	Nitrogen
77-I	T	44.0	0	1	26,540	31.1	1-inch sphere	Nitrogen
77-I	T	44.0	0	0.17	45,440	25.6	1-inch sphere	Nitrogen
77-I	T	44.0	0	0.17	40,350	23.7	1-inch sphere	Nitrogen
77-I	T	44.0	0	0.17	19,970	22.7	1-inch sphere	Nitrogen
77-I	T	44.0	0	0.17	33,700	21.15	1-inch sphere	Nitrogen
77-I	T	44.0	0	0.17	56,160	21.05	1-inch sphere	Nitrogen
77-I	Max	44.0	0	0.17	76,390	19.2	1-inch sphere	Nitrogen
77-I	N	44.0	0	0.17	50,730	17.1	1-inch sphere	Nitrogen
77-I	N	44.0	0	0.17	30,880	14.2	1-inch sphere	Nitrogen
77-I	N	44.0	0	0.17	13,290	11.5	1-inch sphere	Nitrogen
77-I	N	44.0	0	0.17	8,190	10.6	1-inch sphere	Nitrogen
77-I	N	44.0	0	0.17	3,901	9.2	1-inch sphere	Nitrogen

2. SAMPLE PHOTOGRAPHS

One representative frame print is presented for each test surface and level of ΔT_{sat} for which photographs were obtained. Irregularly shaped dark object at right center of photographs in Figs. A-1 through A-4 is spacer between inner and outer walls of transparent dewar. Wire frameworks beside test surfaces provided absolute measurement reference.

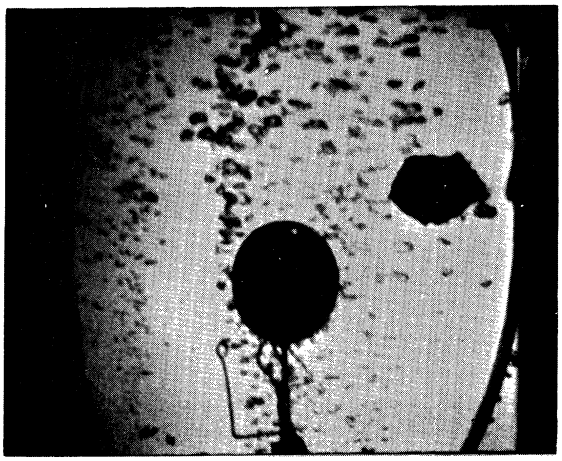

Measurement Reference
ΔT_{sat} = 0°F

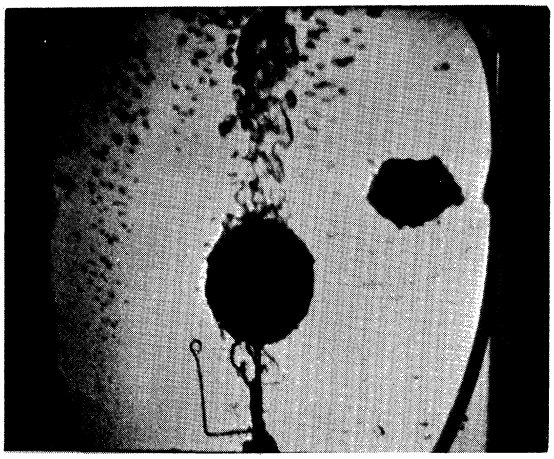

ΔT_{sat} = 100°F

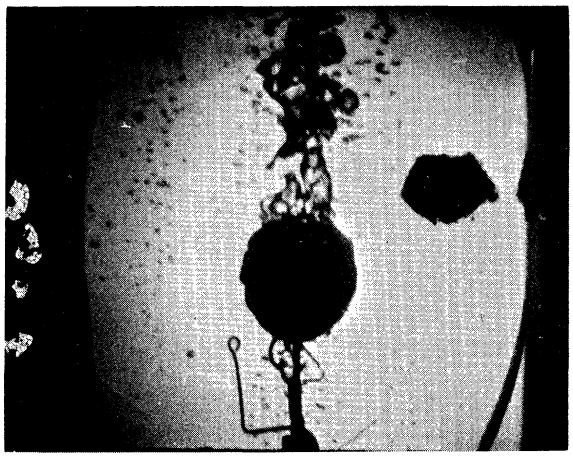

ΔT_{sat} = 200°F

ΔT_{sat} = 300°F

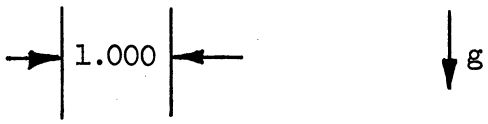

1-inch diameter sphere
Saturated liquid
P = 1 atm
(a/g) = 1

Fig. A-1. Photographs of film boiling on a sphere.

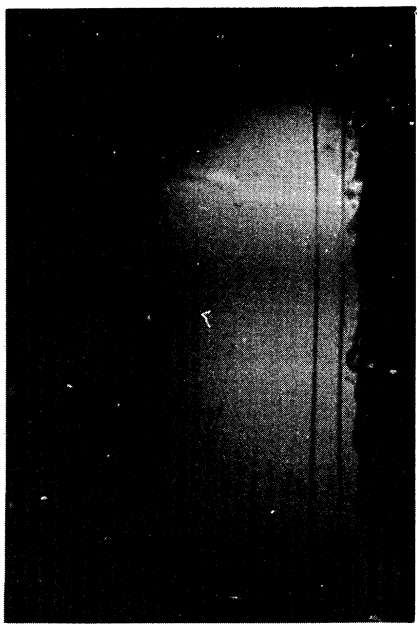

ΔT_{sat} = 100°F

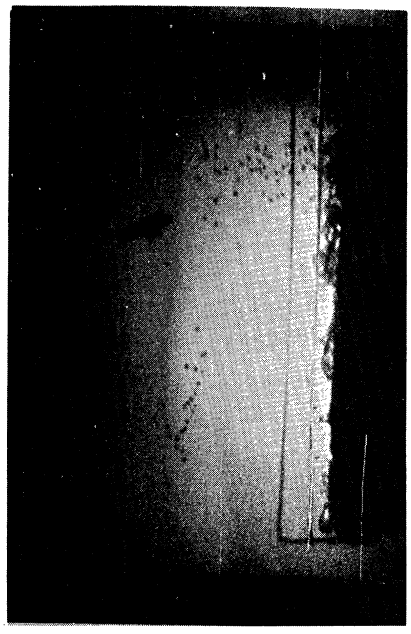

ΔT_{sat} = 200°F

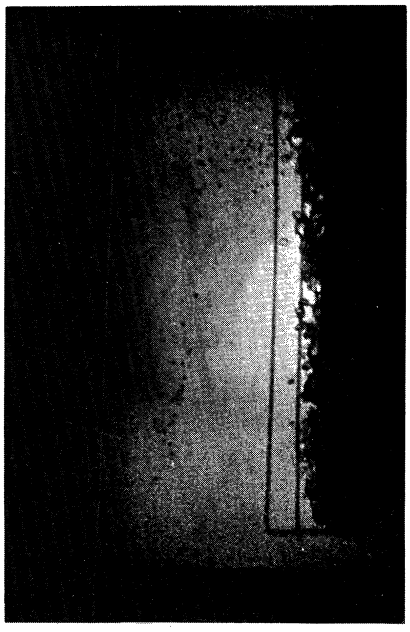

ΔT_{sat} = 300°F

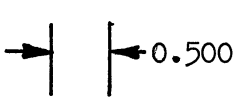

3-inch Diameter Vertical Disk
Saturated Liquid
P = 1 atm
(a/g) = 1

Fig. A-2. Photographs of film boiling on a vertical disk.

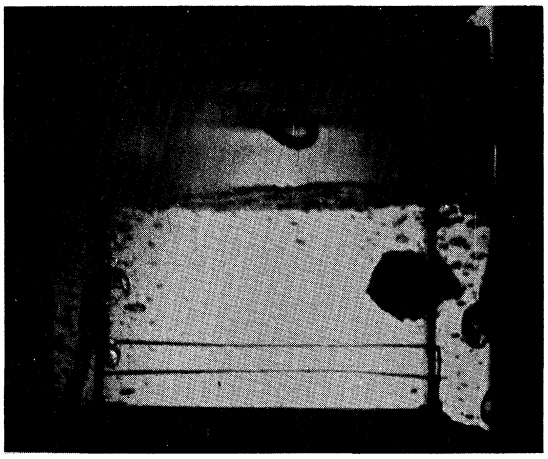

Measurement Reference
ΔT_{sat} = 0°F

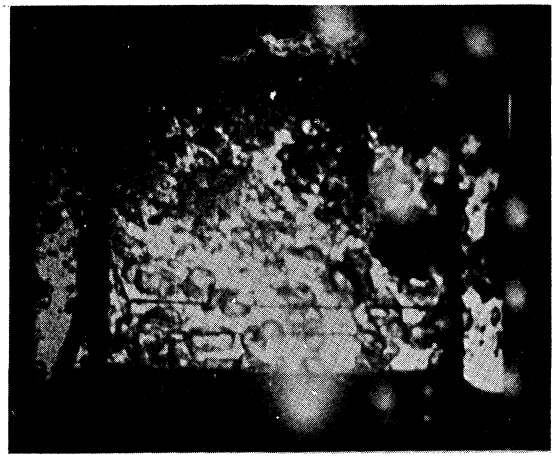

ΔT_{sat} = 100°F

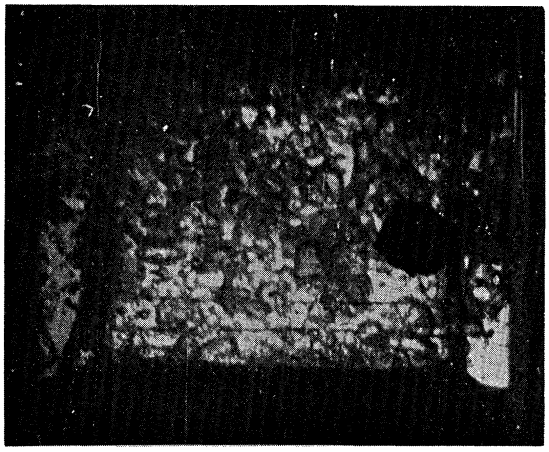

ΔT_{sat} = 200°F

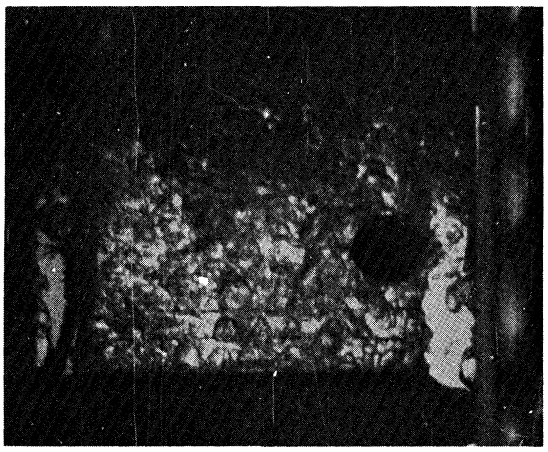

ΔT_{sat} = 300°F

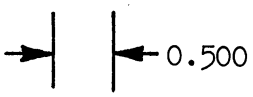

3-inch diameter horizontal disk
Heating up
Saturated liquid
P = 1 atm
(a/g) = 1

Fig. A-3. Photographs of film boiling on a horizontal disk heating up.

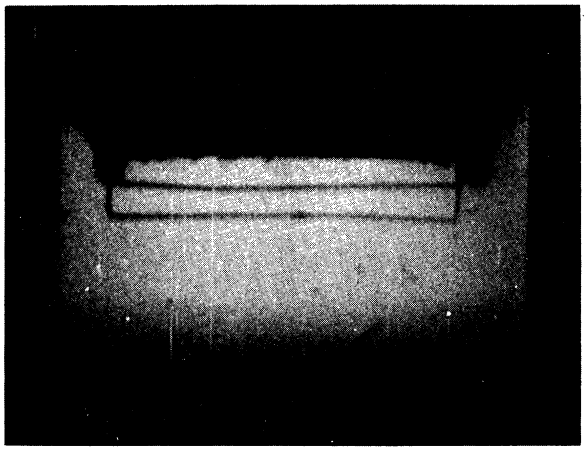

ΔT_{sat} = 100°F

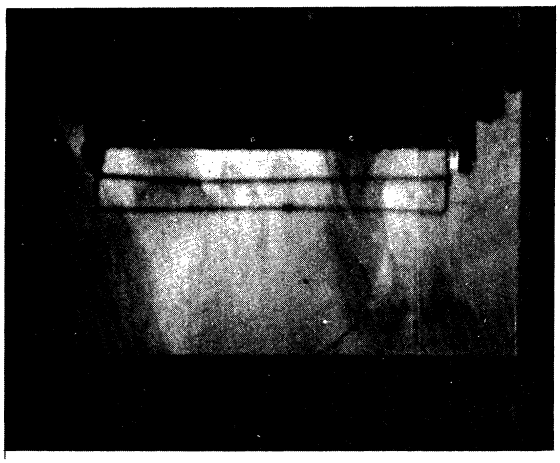

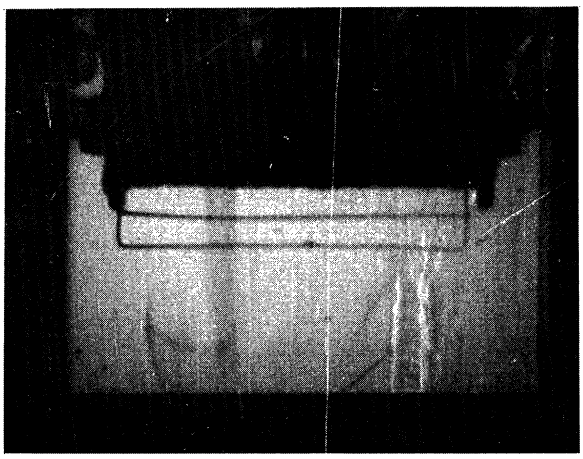

ΔT_{sat} = 200°F

ΔT_{sat} = 300°F

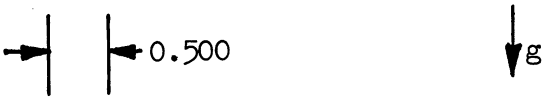

3-inch diameter horizontal disk
Heating down
Saturated liquid
P = 1 atm
(a/g) = 1

Fig. A-4. Photographs of film boiling on a horizontal disk heating down.

3. REDUCED PHOTOGRAPHIC DATA

Column Headings:

ΔT_{sat}: in °F

Frame Number: for identification purposes

Separation Point—R: angular location above which vapor no longer flows along the sphere surface, right side

Separation Point—L: angular location above which vapor no longer flows along the sphere surface, left side

Film Thickness at Angular Location: film thickness in inches, angular location in degrees clockwise from top of sphere

Position: distance in inches from bottom of vertical plate or left side of horizontal plate

Film Thickness: in inches

1-INCH DIAMETER SPHERE

ΔT_{sat}	Frame No.	Separation Point-R	Separation Point-L	Film Thickness at Angular Location									
				30°	60°	90°	130°	160°	200°	230°	270°	300°	330°
100°	1	21°	338°	.040	.018	.019	.013	.017	.026	.018	.028	.022	.025
100°	2	30°	325°	.027	.028	.023	.013	.008	.017	.018	.019	.022	.025
100°	3	45°	305°	.115	.018	.023	.009	.008	.009	.018	.014	.018	.127
200°	1	20°	300°		.027	.019	0	.008	.013	018	.019	.026	
200°	2	29°	335°		.028	.037	.017	.013	.017	.018	.014	.035	
200°	3	42°	305°		.028	.023	0	.008	.009	.009	.019	.026	
200°	4	19°	355°		.009	.009	0	.017	.013	.022	.014	.035	
200°	5	8°	340°		.028	.014	.009	.013	.009	.018	.028	.026	
300°	1	5°	332°	.035	.035	.014	.013	.017	.017	.018	.027	.044	.101
300°	2	11°	331°	.052	.017	.055	.013	.025	.017	.027	.036	.088	.034
300°	3	30°	308°	.017	.017	.055	.026	.034	.017	.036	.036	.027	
300°	4	21°	316°	.078	.026	.045	.017	.025	034	.018	.027	.044	.437
300°	5	38°	320°	.322	.009	.045	.017	.034	.034	.027	.036	.035	.352

VERTICAL DISK

ΔT_{sat}	Frame No.		Experimental Measurements					
			1	2	3	4	5	6
100°	1	Position	.12	.63	1.12	1.85	2.37	
100°		Film Thickness	.029	.048	.058	.096	.077	
100°	2	Position	.96	1.05	1.31	2.46	2.78	
100°		Film Thickness	.058	.067	.087	.096	.087	
100°	3	Position	.30	1.47	1.58	2.31		
100°		Film Thickness	.058	.067	.077	.087		
100°	4	Position	.50	.77	2.21	2.56		
100°		Film Thickness	.058	.058	.087	.106		
200°	1	Position	.15	.76	1.42	2.13	2.54	
200°		Film Thickness	.035	.069	.086	.173	.155	
200°	2	Position	.22	.62	.93	1.55	2.70	
200°		Film Thickness	.052	.052	.069	.086	.147	
200°	3	Position	.43	1.22	1.75	1.89	2.46	
200°		Film Thickness	.043	1078	.095	.121	.112	
200°	4	Position	.51	.84	2.05	2.47	2.84	
200°		Film Thickness	.061	.086	.130	.138	.156	
200°	5	Position	.24	1.10	1.28	1.36	2.63	
200°		Film Thickness	.043	.078	.078	.112	.155	
300°	1	Position	.14	.52	1.08	1.38	2.35	
300°		Film Thickness	.102	.092	.092	.133	.153	
300°	2	Position	.89	1.27	1.55	1.97	2.29	
300°		Film Thickness	.072	.082	.102	.112	.112	
300°	3	Position	.37	.49	.73	1.16	1.69	2.16
300°		Film Thickness	.051	.061	.051	.082	.072	.143
300°	4	Position	1.46	1.83	2.42	2.68	2.83	
300°		Film Thickness	.061	.133	.173	.173	.163	
300°		Position	.81	1.01	1.76	2.10	2.71	
300°		Film Thickness	.061	.061	.061	.092	.102	

HORIZONTAL DISK HEATING UP

ΔT_{sat}	Frame No.		Experimental Measurements					
			1	2	3	4	5	6
100°	1	Position	.11	1.08	2.11	2.66		
100°		Film Thickness	.033	.022	.028	.028		
100°	2	Position	.71	1.68	1.94	2.59	2.83	
100°		Film Thickness	.044	.039	.039	.033	.039	
100°	3	Position	.19	1.28	1.58	1.99		
100°		Film Thickness	.033	.028	.044	.028		
100°	4	Position	.42	.98	1.79	2.15		
100°		Film Thickness	.022	.033	.044	.033		
100°	5	Position	.86	1.15	1.72	2.06	2.40	
100°		Film Thickness	.044	.022	.033	.033	.056	
200°	1	Position	.14	.96	1.29	1.88	2.78	
200°		Film Thickness	.122	.089	.111	.133	.167	
200°	2	Position	.45	.88	1.54	2.20	2.69	
200°		Film Thickness	.144	.167	.167	.189	.178	
200°	3	Position	.53	1.03	1.85	2.73	2.97	
200°		Film Thickness	.111	.156	.178	.144	.122	
200°	4	Position	.45	.91	1.16	1.74	2.12	2.86
200°		Film Thickness	.100	.100	.089	.122	.122	.100
200°	5	Position	.35	.84	1.18	2.03	2.90	
200°		Film Thickness	.056	.122	.089	.056	.078	
300°	1	Position	.95	1.25	1.62	2.24	2.93	
300°		Film Thickness	.066	.082	.082	.106	.066	
300°	2	Position	.32	1.01	1.40	1.54	2.49	
300°		Film Thickness	.090	.074	.098	.066	.082	
300°	3	Position	.89	1.05	1.69	2.35	2.65	
300°		Film Thickness	.098	.041	.066	.057	.098	
300°	4	Position	.20	.85	1.46	2.41	2.70	
300°		Film Thickness	.057	.057	.098	.082	.049	
300°	5	Position	.45	.80	1.44	2.15	2.56	
300°		Film Thickness	.090	.090	.082	.106	.115	

HORIZONTAL DISK HEATING DOWN

ΔT_{sat}	Frame No.		Experimental Measurements				
			1	2	3	4	5
100°	1	Position	.67	1.26	1.79	2.33	2.89
100°		Film Thickness	.041	.041	.049	.049	.057
100°	2	Position	.52	1.11	1.67	2.18	2.74
100°		Film Thickness	.041	.033	.041	.041	.041
100°	3	Position	.38	.99	1.56	2.08	2.65
100°		Film Thickness	.041	.041	.041	.041	.041
100°	4	Position	.25	.88	1.47	1.99	2.54
100°		Film Thickness	.062	.029	.041	.041	.L45
100°	5	Position	.07	.77	1.36	2.44	2.82
100°		Film Thickness	.066	.041	.037	.045	.049
200°	1	Position	.29	1.02	1.65	2.29	2.88
200°		Film Thickness	.029	.041	.049	.041	.033
200°	2	Position	.15	.92	1.52	1.97	2.76
200°		Film Thickness	.029	.037	.041	.037	.029
200°	3	Position	.40	1.11	1.75	2.35	2.95
200°		Film Thickness	.041	.053	.053	.049	.041
200°	4	Position	.48	1.20	1.84	2.40	2.68
200°		Film Thickness	.037	.057	.057	.041	.041
200°	5	Position	.61	.77	1.33	1.96	2.52
200°		Film Thickness	.033	.041	.053	.049	.041
300°	1	Position	.61	1.17	1.92	2.40	2.91
300°		Film Thickness	.058	.053	.058	.053	.053
300°	2	Position	.47	1.07	1.76	2.28	2.80
300°		Film Thickness	.053	.058	.069	.062	.077
300°	3	Position	.39	.96	1.64	2.18	2.70
300°		Film Thickness	.062	.062	.069	.062	.053
300°	4	Position	.28	.83	1.51	2.10	2.61
300°		Film Thickness	.062	.058	.053	058	.053
300°	5	Position	.10	.74	1.39	2.02	2.54
300°		Film Thickness	.053	.058	.053	.065	062
300°	6	Position	.21	.68	1.28	1.84	2.47
300°		Film Thickness	.058	.062	.062	.065	.062

APPENDIX B

ANALYSIS OF THE FILM THICKNESS ON A FLAT PLATE HEATING DOWN

The physical model used to analyze film thickness on a flat plate heating down assumes a finite dimension for the flat plate. Infinite horizontal dimensions for the flat plate reduce the problem to that presented in Section VII.A.3.a, i.e., film formation at zero gravity. Finite dimensions result in flow of the vapor parallel as well as normal to the plate. If the plate is finite in one direction only, the flow is two-dimensional; if it is finite in two directions, the flow is three-dimensional. The general analysis of the problem requires the simultaneous solution of both the energy and the momentum equations. This would give the temperature and velocity distributions, along with the vapor film thickness. An estimation of the deviation of the liquid-vapor interface from a true horizontal is possible by considering the momentum equation alone, using an assumed velocity profile in the vapor film. Several different models are possible.

The simplest model, Model I, utilizes a plate which is finite in one direction and has a uniform velocity profile in the film. This model is shown in Fig. B-1. A parabolic velocity profile in the film is probably a better approximation to the actual profile. This provides a second model, Model II. The physical surface used for obtaining the experimental data was a disk, so a disk is used for a flat plate in Models III and IV. Flow around the disk would be axisymmetrical. Models III and IV utilize a disk with uniform and parabolic velocity profiles in the film, respectively.

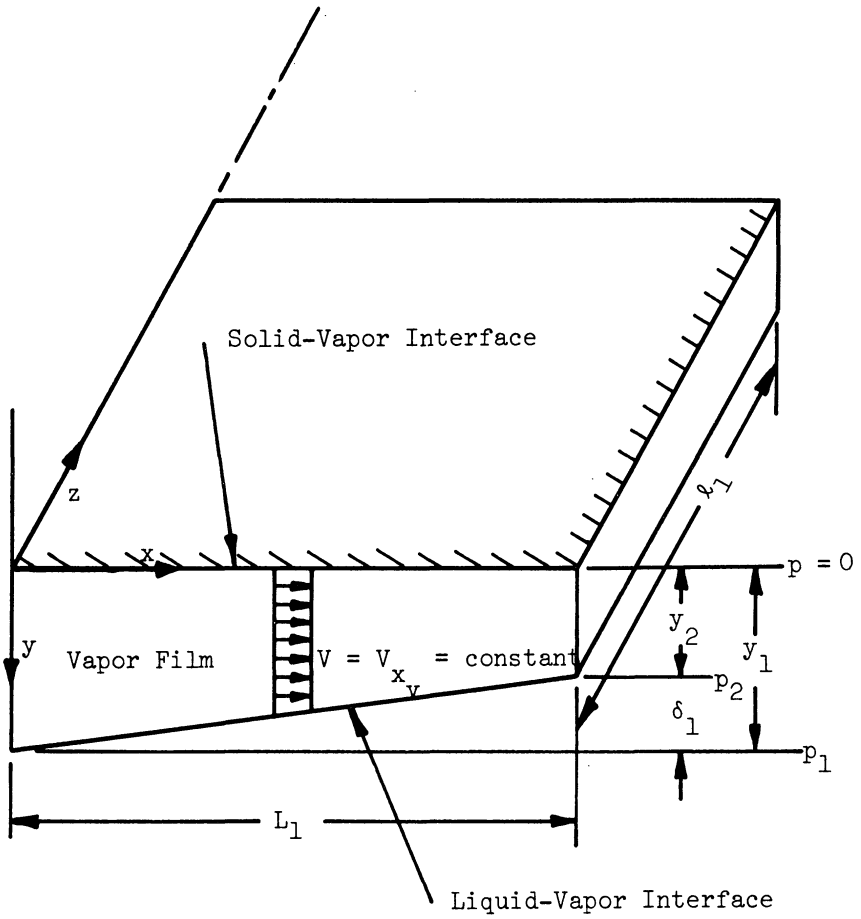

Flat Plate - Model I

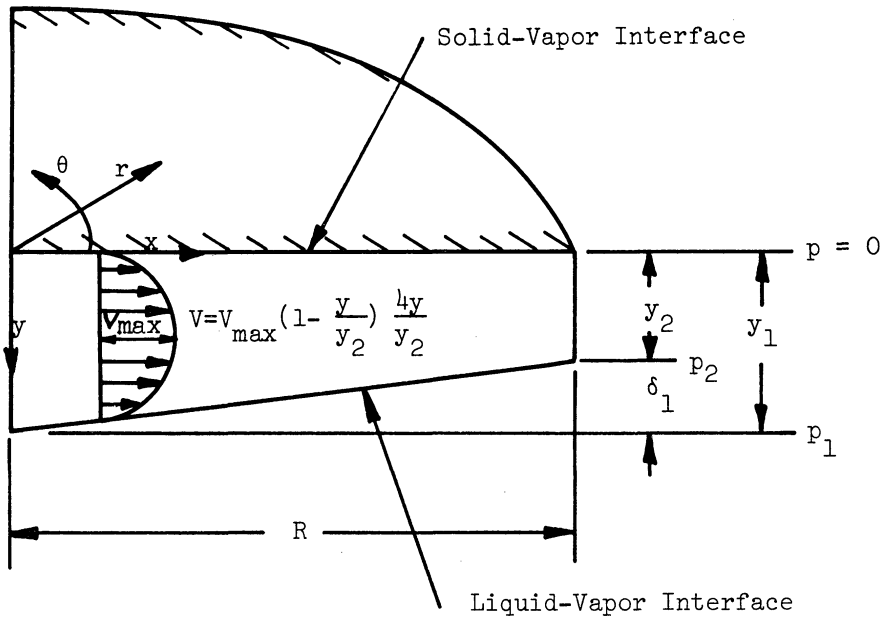

Disk - Model IV

Fig. B-1. Plate and disk configurations.

The disk with the parabolic velocity profile in the film, Model IV, should most nearly approach the actual situation. This model is shown in Fig. B-1.

It was assumed that the process was one which could be treated as a steady-state phenomenon. The vapor was considered to be an inviscid fluid. It was assumed there was no flow in the z-direction (plate) or θ-direction (disk), that $dp/dy = 0$ in the vapor, that dp/dx = constant, and that $y_1 \gg \delta_1$.

The assumption of no flow in one direction limits the number of dimensions which must be treated in the problem. The assumption $dp/dy = 0$ in the vapor eliminates consideration of flow in the vapor normal to the plate. The assumption dp/dx = constant amounts to assuming that the vapor film thickness varies linearly with x. The assumption $y_1 \gg \delta_1$ permits the film to be approximated by a film of uniform thickness in certain aspects of the calculations. With these assumptions, the momentum equation is

$$\sum \vec{F} = \oint_A \rho \vec{V}(\vec{V}\cdot\hat{n})dA \qquad \text{(B-1)}$$

where

$$\sum \vec{F} = -\oint_A p\hat{n}dA \qquad \text{(B-2)}$$

For the plate, the significant direction of the motion is along the x-axis. Writing the momentum equation for this component

$$\sum F_x = \oint_A \rho V_x(\vec{V}\cdot\hat{n})dA \qquad \text{(B-3)}$$

and noting that p_1 and p_2 may be expressed in the form $\rho_\ell y \frac{g}{g_o}$, it may be

shown that

$$\Sigma F_x = \frac{\rho_\ell}{2} \frac{g}{g_o} \ell_1 (y_1^2 - y_2^2) \qquad \text{(B-4)}$$

$$\oint_A \rho V_x (\vec{V} \cdot \hat{n}) dA = \rho_v y_2 V_{x_v}^2 \ell_1 \frac{1}{g_o} \qquad \text{(B-5)}$$

For a steady-state system, conservation of mass requires that the mass flowing into the system be equal to the mass flowing out. For this system, where the mass flow of vapor in is the result of evaporation of the liquid, the mass flow in is a function of the heat transfer rate, the average enthalpy difference between liquid and vapor, and the heat transfer area. Equating the mass flow in and the mass flow out we may write

$$\dot{m} = \left[\frac{(q/A) \cdot L \cdot \ell_1}{h_{fg}'}\right] = \rho_v y_2 \ell_1 V_{x_v} \qquad \text{(B-6)}$$

from which it may be seen that

$$V_{x_v} = \frac{(q/A) \cdot L}{h_{fg}' \rho_v y_2} \qquad \text{(B-7)}$$

Expressing the term $(y_1^2 - y_2^2)$ as $(y_1 - y_2)(y_1 + y_2)$ and noting that $(y_1 - y_2) = \delta_1$ and, since $y_1 >> \delta_1$, $y_1 \cong y_2$, and $(y_1 + y_2) \cong 2y_1$, we may rewrite $(y_1^2 - y_2^2)$ as $2y_1\delta_1$. Substituting into Eqs. (B-3) through (B-7), the expression

$$\delta y_1^2 = \left[\frac{(q/A) \cdot L}{h_{fg}'}\right]^2 \cdot \frac{1}{\rho_\ell \rho_v g} \qquad \text{(B-8)}$$

is obtained which expresses the film thickness and thickness variation in terms of measurable parameters for Model I.

If a parabolic velocity profile is assumed, Model II, in the form

$$V_{x_v} = V_{max} \frac{4y}{y_2^2} (y_2 - y) \tag{B-9}$$

Eqs. (B-5) through (B-8) become, respectively

$$\oint_A \rho V_x (\vec{V} \cdot \hat{n}) dA = \frac{8}{15} \rho_v y_2 V_{max}^2 \ell_1 \frac{1}{g_o} \tag{B-10}$$

$$\dot{m} = \left[\frac{(q/A) \cdot L \cdot \ell_1}{h'_{fg}} \right] = \frac{2}{3} \rho_v y_2 \ell_1 V_{max} \tag{B-11}$$

$$V_{max} = \frac{\frac{3}{2} (q/A) L}{h'_{fg} \rho_v y_2} \tag{B-12}$$

$$\delta_1 y_1^2 = \frac{6}{5} \left[\frac{(q/A) \cdot L}{h'_{fg}} \right]^2 \frac{1}{\rho_v \rho_\ell g} \tag{B-13}$$

For the axisymmetric case with a uniform velocity profile, Model III, Eqs. (B-4) through (B-8) become, respectively

$$\Sigma F_x = \rho_\ell \frac{g}{g_o} R \left[y_1^2 - y_2^2 - \frac{2}{3} (y_1 - y_2)^2 - \frac{1}{3} \frac{R(y_1 - y_2)(y_1 + 2y_2)}{\sqrt{R^2 + (y_1 - y_2)^2}} \right] \tag{B-14}$$

$$\oint_A \rho V_x (\vec{V} \cdot \hat{n}) dA = \rho_v y_2 V_{x_v}^2 R \frac{1}{g_o} \tag{B-15}$$

$$\dot{m} = \left[\frac{(q/A) \cdot \frac{\pi}{4} \cdot R^2}{h'_{fg}} \right] = \rho_v \cdot V_{r_v} \cdot \frac{\pi}{2} R y_2 \tag{B-16}$$

$$V_{r_v} = \frac{(q/A) \cdot R}{h'_{fg} \rho_v y_2} \tag{B-17}$$

$$V_{x_v} = V_{r_v} \cos \theta \tag{B-18}$$

$$\delta_1 y_1^2 - \frac{2}{3}\delta_1^2 y_1 = \left[\frac{(q/A)\cdot R}{h_{fg}'}\right]^2 \cdot \frac{1}{\rho_\ell \rho_v g} \qquad \text{(B-19)}$$

When Eq. (B-9) is used for the velocity profile, Model IV, the axisymmetric Eqs. (B-15), (B-16), (B-17), and (B-19) become

$$\oint_A \rho V_x(\vec{V}\cdot\hat{n})dA = \frac{8}{15}\rho_v V_{max}^2 R y_2 \cdot \frac{1}{g_o} \qquad \text{(B-20)}$$

$$\dot{m} = \left[\frac{(q/A)\cdot\frac{\pi}{4}\cdot R^2}{h_{fg}'}\right] = \rho_v V_{max}\frac{\pi}{3} R y_2 \qquad \text{(B-21)}$$

$$V_{max} = \frac{\frac{3}{4}(q/A)R}{h_{fg}'\rho_v y_2} \qquad \text{(B-22)}$$

$$\delta_1 y_1^2 - \frac{2}{3}\delta_1^2 y_1 = \frac{3}{10}\left[\frac{(q/A)\cdot R}{h_{fg}'}\right]^2 \frac{1}{\rho_\ell \rho_v g} \qquad \text{(B-23)}$$

Solutions of Eqs. (B-8), (B-13), (B-19), and (B-23) using measured or estimated physical parameters permits a determination of the relationship between y_1 and δ_1. If y_1 is measured, an estimate for δ_1 may be made. The explicit determination of y_1, and hence δ_1, would result from the simultaneous solution with the energy equation.

APPENDIX C

THE EFFECT OF AIR DRAG ON MEASURED (a/g) DURING FREE FALL

The drag force acting on a body moving through the air is given as[57]

$$F_D = \frac{1}{2} \rho V^2 C_D A \qquad \text{(C-1)}$$

where

ρ = density of air

V = velocity of body relative to the air

C_D = drag coefficient

A = area of body normal to air flow

The velocity of the test packages at the instant of impact is 45 feet per second. Using a reference length of 1 foot, the Reynold's Number varies from about 10^4 soon after the package is released to 3×10^5 at impact. In this range, the C_D of the first test package should be approximately that of a flat plate in three-dimensional flow, i.e., 1.17.[58] The C_D of the second test package should be approximately that of a rounded head cylinder in three-dimensional flow, i.e., 0.2.[58]

The free fall (q/A) vs. ΔT_{sat} data are evaluated during the period from 0.7 to 1.4 seconds after release. The transitory effects caused by the release have diappeared by 0.7 second, and impact occurs at 1.4 seconds. Using the measured frontal areas of the packages (1.55 feet^2 for the first package and 1.07 feet^2 for the second package) and the velocities cor-

responding to the above times (22.5 feet per second at 0.7 second, 45.0 feet per second at 1.4 seconds) the forces acting on the packages may be calculated using Eq. (C-1). They are

F_D(first package, 0.7 second) = 1.07 lbf

F_D(first package, 1.4 seconds) = 4.28 lbf

F_D(second package, 0.7 second) = 0.124 lbf

F_D(second package, 1.14 seconds) = 0.465 lbf

The force due to air drag on the second test package is approximately 10% of the force due to air drag on the first test package.

Using the relationship

$$\left(\frac{a}{g}\right)_{\text{free fall}} = \frac{F_{D\text{free fall}}}{F_{(a/g)=1}} \qquad \text{(C-2)}$$

and the above values of F_D, noting that the weight of the first package is 120 pounds and the weight of the second package is 135 pounds,

(a/g) (free fall, first package, 0.7 second) = 0.0090

(a/g) (free fall, first package, 1.4 seconds) = 0.0357

(a/g) (free fall, second package, 0.7 second) = 0.00093

(a/g) (free fall, second package, 1.4 seconds) = 0.00374

For the first test package, the effective (a/g) during free fall will range from 0.01 to 0.035 because of variation in air drag. Any effects due to guide wire drag would further increase the value of (a/g). Because (q/A) and ΔT_{sat} are evaluated prior to package impact, (a/g) increases due to air drag should be in the range $0.01 < (a/g) < 0.03$.

For the second test package, the effective (a/g) during free fall for the outer package will range from 0.001 to 0.0037. The inner package should not feel any effect of the air drag on the outer package, and so should experience a lower (a/g) than the outer package.

APPENDIX D

EVALUATION OF THE LUMPED ANALYSIS APPROXIMATION

When a spherical solid at a high temperature is immersed in a liquid at a lower temperature, unsteady conduction takes place in the sphere. The reference parameter describing the internal differences in temperature for this problem is the Biot Number,

$$Bi = \frac{\bar{h}R}{k_s} = \frac{R/k}{1/\bar{h}} \qquad (D\text{-}1)$$

which can be interpreted as the ratio of internal to external thermal resistances. When the Biot Number is less than approximately 0.1, the solid may be treated as a lumped system with a fair degree of precision. When the Biot Number is greater than 0.1, the solid must be treated as a distributed system, and analytical solutions are generally available only for limited types of boundary conditions. The use of numerical solutions is required for general cases.

A calculation of the Biot Number for the 1-inch diameter sphere in the film-boiling region, using values of $\bar{h}$ from measurements assuming lumped conditions, gives values of less than 0.02 for all combinations of pressure and subcooling investigated. Carslaw and Jaeger[59] have presented a solution to evaluate the temperature at any point in a sphere as a function of time after a heat flux, (q/A), has suddenly been imposed. They give

$$T(t,r) - T_o = \frac{3(q/A)t}{\rho_{sd}C_{p_{sd}}R} + \frac{(q/A)(5r^2-3R^2)}{10k_{sd}R}$$

$$- \frac{2(q/A)R^2}{k_{sd}r} \sum_{n=1}^{\infty} \frac{\sin(r\lambda_n/R)}{\lambda_n^2 \sin\lambda_n} e^{-\alpha_{sd}\lambda_n^2 t/R^2} \qquad \text{(D-2)}$$

where

$T(t,r)$ = temperature at time t and radius r

T_o = temperature at time zero

R = radius of sphere

$0 \leq r \leq R$

α = thermal diffusivity

$\lambda_n, n = 1,2,\ldots,$ are the positive roots of $\tan\lambda = \lambda$

Equation (D-2) was evaluated for r=0 and r = R = 1/2 inch with (q/A) = 10^4 Btu/hr-ft^2, $C_{p_{sd}}$ = 0.08 Btu/lbm-°F, ρ_{sd} = 558 lbm/ft^3, k_{sd} = 224 Btu/hr-ft-°F, and t = 1 second. The heat flux used might be considered an upper limit for film boiling under the conditions present. A difference of 0.93°F was predicted between the temperature at the center and the temperature at the surface of the sphere. In view of the small Biot Number with film boiling, it appears reasonable to expect that the rates of change of center and surface temperature will not differ significantly. The error in calculating (q/A) due to assuming a uniform temperature in the sphere would be due to this difference, and to variations in C_p with T within the sphere. This is less than 0.05%, which may be neglected.

In the nucleate and transition boiling regions, values of the Biot Number are of the order of magnitude of one, indicating that computation of

the surface heat flux will require evaluation of the distributed nature of temperatures in the sphere. This is accomplished using finite difference procedures, with the measured surface temperatures as inputs.

The flow sheet for the computer program is shown in Fig. D-1, and the program listing is shown in Fig. D-2. The computer language used is MAD.

The program takes the raw time vs. surface temperature data and fits a fifth order polynomial to the first five points using the method of least mean squares. It divides the sphere into ten concentric shells about a spherical core and calculates the heat flux into the sphere in terms of the enthalpy change of each shell evaluated at intervals of 0.00010 second between the second and fourth points (see Fig. D-3). The heat flux, surface shell temperature, next shell temperature, and spherical core temperature, as well as ΔT_{sat} and some other computational information, are printed out for the third point. The first data point is then dropped, the sixth data point is added to become the new fifth point, a new polynomial is fit to the data points, and the process is repeated. After all of the data points have been handled in this way the results are printed and plotted as shown in Chapter V.

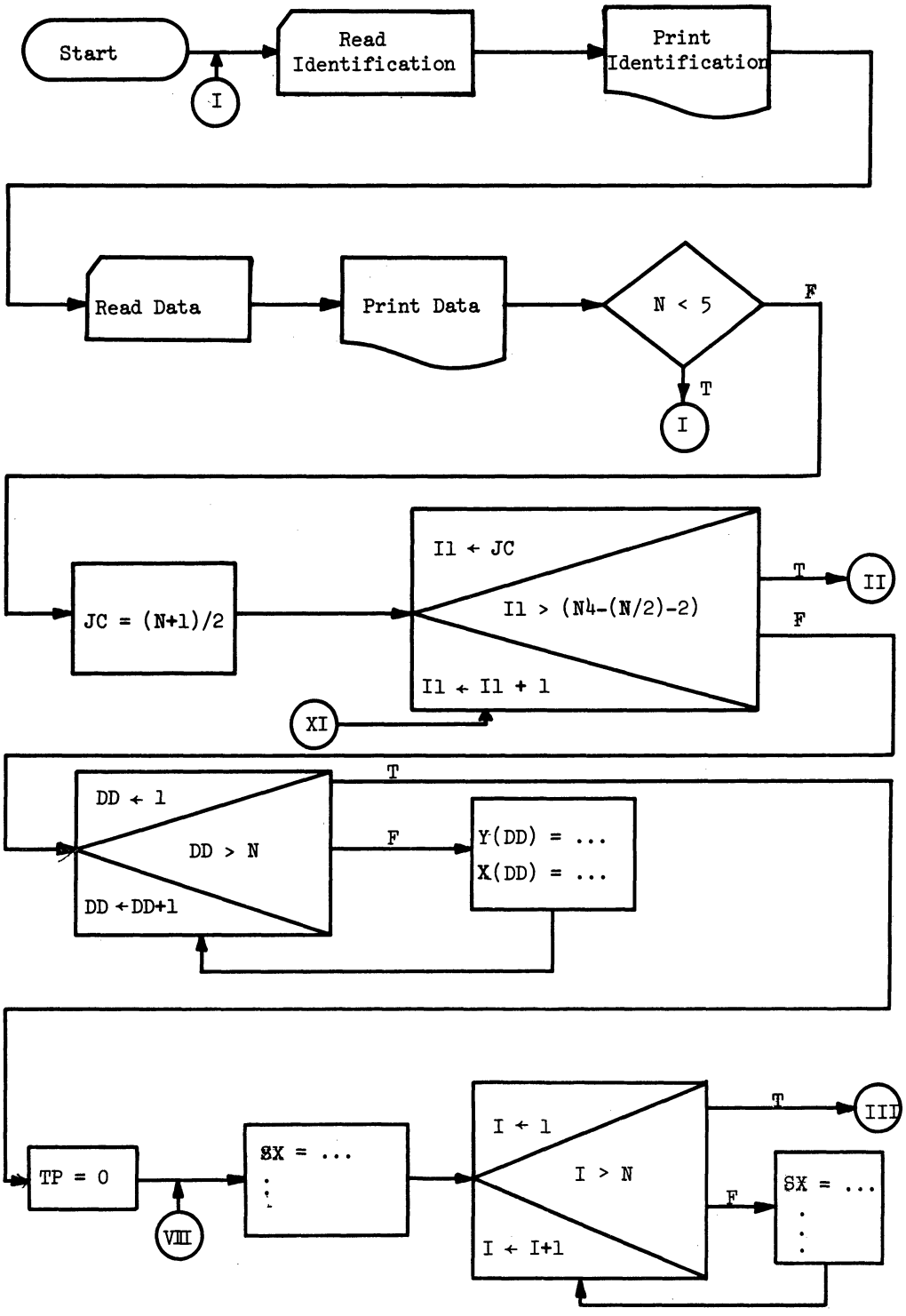

Fig. D-1. Flow sheet for digital computer program.

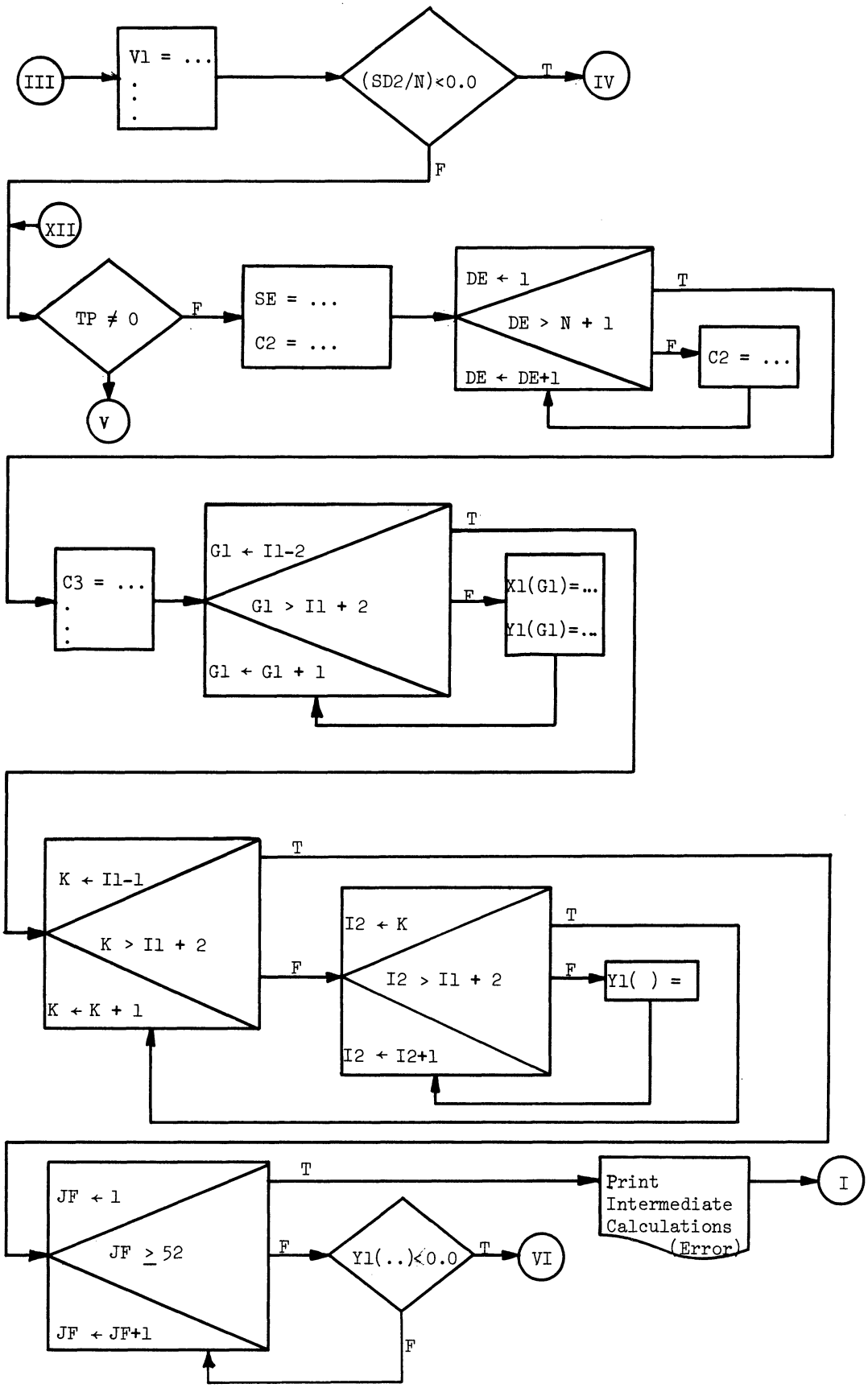

Fig. D-1 (Continued)

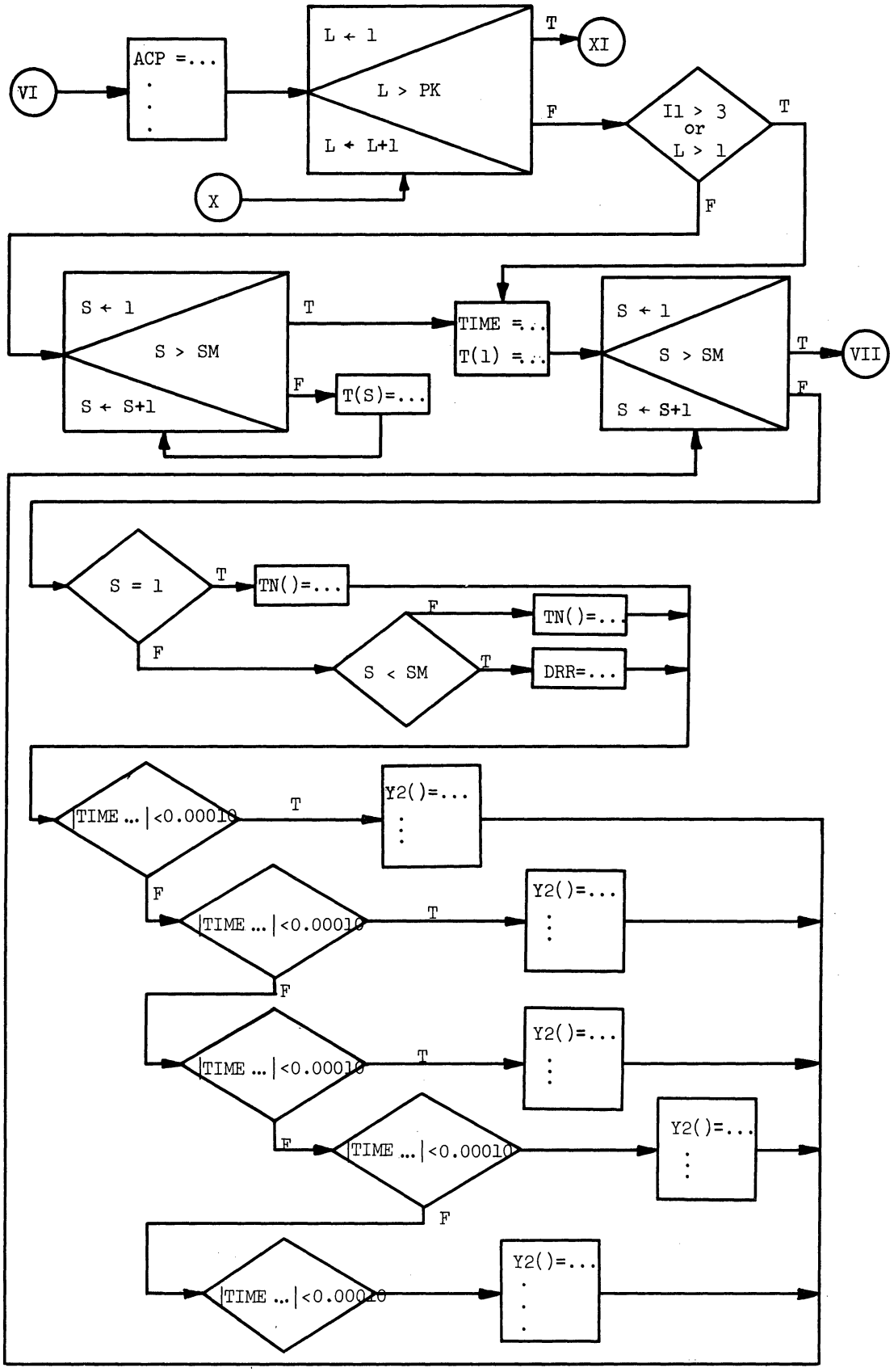

Fig. D-1 (Continued)

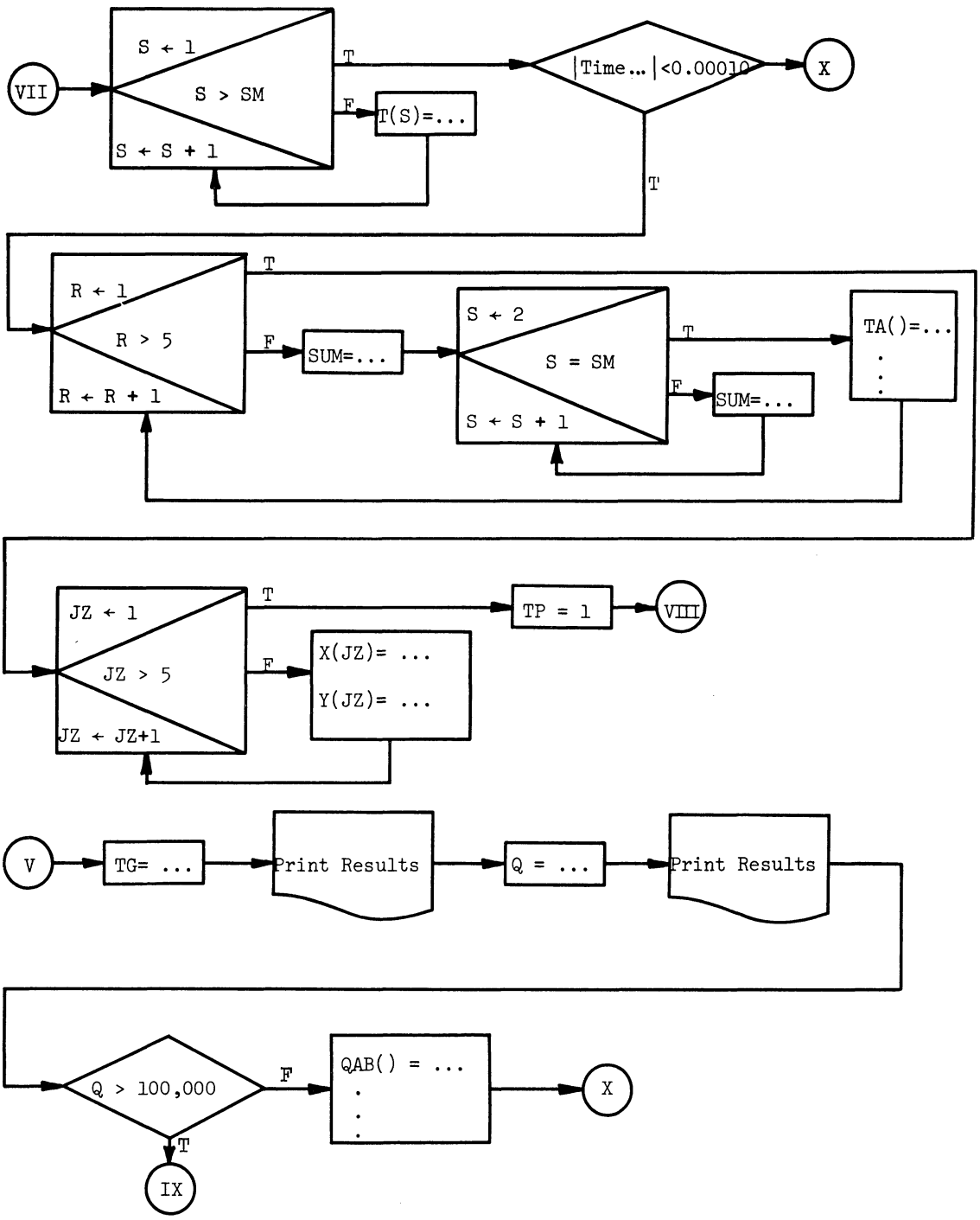

Fig. D-1 (Continued)

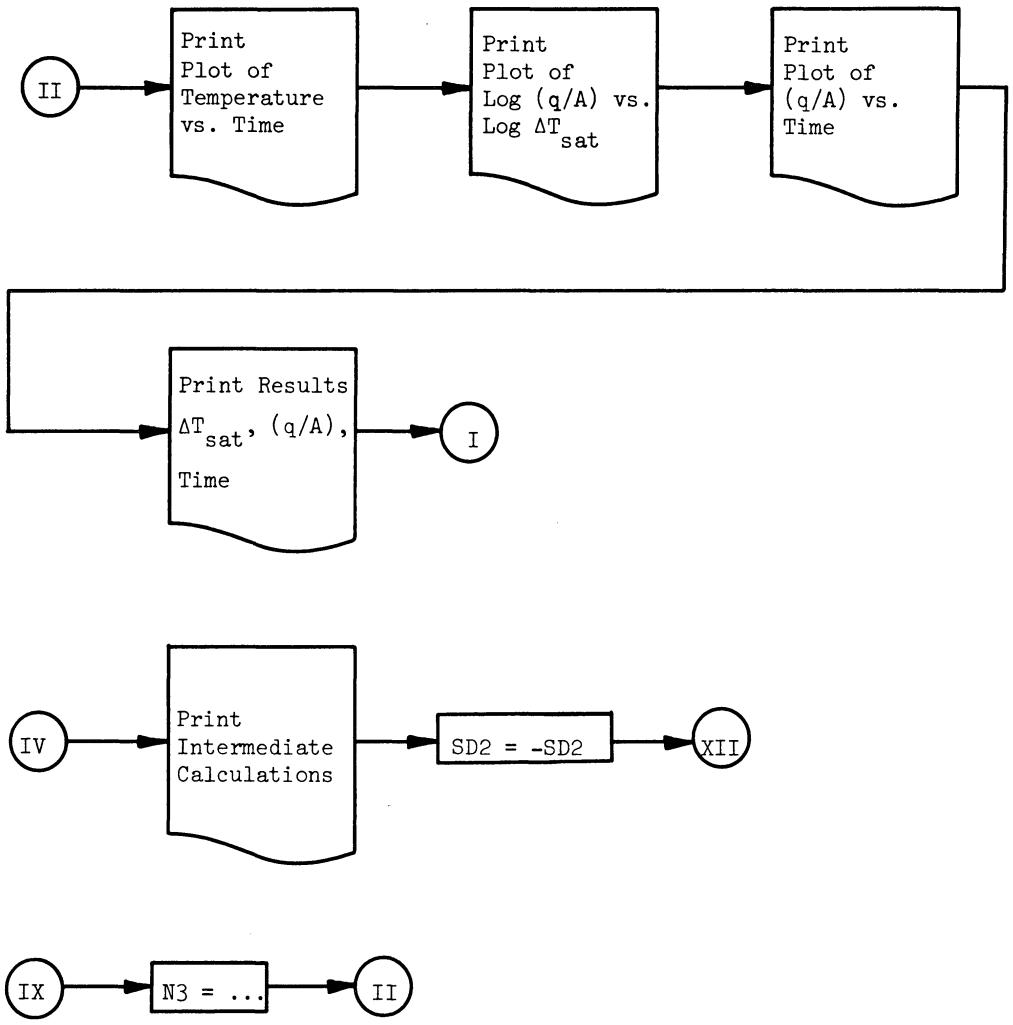

Fig. D-1 (Concluded)

```
$COMPILE MAD, EXECUTE, DUMP, PRINT OBJECT, PUNCH OBJECT                    053478   04/18/67     12:02 41.7 AM

MAD (06 JAN 1967 VERSION) PROGRAM LISTING ... ... ...


START       CONTINUE                                                                                    *001
            INTEGER RUN,I1,I2,K,L,R,S,SM,N,N1,N3,N4,J8,J9,J12,J14,J15                                   *002
            INTEGER J16,G1,JA,JC,JF                                                                     *003
            INTEGER DD,DE,I,C3,C4                                                                       *004
            INTEGER TP,JZ                                                                               *005
            DIMENSION X(25),Y(25),X1(100),Y1(2500,Y1DIM),X2(100),Y2(121,Y2DIM)                          *006
            DIMENSION X3(100),Y3(121,Y3DIM),T(100),TN(100),TA(100),RUN(12)                              *007
            DIMENSION CTEM(52),CCP(52),GRAPH(867),EX(100),WY(100),STDX(120)                             *008
            DIMENSION STDY(120),STAX(120),STAY(120),DATAX(100),DATAY(100)                               *009
            DIMENSION DATX(100),DATY(100),TIM(100),TEM(100),QAB(100),DTT(100)                           *010
            VECTOR VALUES Y1DIM = 2,1,50                                                                *011
            VECTOR VALUES Y2DIM = 2,1,11                                                                *012
            VECTOR VALUES Y3DIM = 2,1,11                                                                *013
            VECTOR VALUES OUT= $1H1, 12C6*$                                                             *014
            VECTOR VALUES OUT1=$1HO,12C6*$                                                              *015
            VECTOR VALUES IN=$12C6*$                                                                    *016
            VECTOR VALUES ABS=$1HO,S30,24HLOG (TS-TSAT), DEGREES F*$                                    *017
            VECTOR VALUES LFO=$   TEMPERATURE, DEG F                    *$                              *018
            VECTOR VALUES ABS1=$1HO,S50,22HRELATIVE TIME, SECONDS*$                                     *019
            VECTOR VALUES ORD=$     LOG Q/A, BTU/HR-FT2         *$                                      *020
            VECTOR VALUES  QA=$         Q/A, BTU/HR-FT2         *$                                      *021
            VECTOR VALUES EX(1)= 0.0,0.301,                                                             *022
           1      0.477,0.602,0.699,0.778,0.845,0.903,0.954,1.0,                                        *022
           2 1.301,1.477,                                                                               *022
           3  1.602,1.699,1.778,1.845,1.903,1.954,2.0,                                                 *022
           4 2.301,2.477,                                                                               *022
           5  2.602,2.699,2.778,2.845,2.903,2.954,3.0                                                  *022
            VECTOR VALUES WY(1)= 3.0,3.301,                                                             *023
           1  3.477,3.602,3.699,3.778,3.845,3.903,3.954,4.0,                                           *023
           2 4.301,4.477,                                                                               *023
           3  4.602,4.699,4.778,4.845,4.903,4.954,5.0                                                  *023
            VECTOR VALUES STDX(1)= 5.8,6.0,6.2,6.4,6.6,6.8,7.0,7.2,7.6,8.0,8.5,                         *024
           1 9.0,9.5,10.0,11.,12.,13.,14.,15.,16.,17.,18.,19.,20.,21.,                                  *024
           1 22.,23.,24.,25.,26.,27.,28.,29.,30.,31.,32.,33.,34.,35.,36.,                               *024
           1 37.,38.,39.,40.,42.,44.,46.,48.,50.,52.,54.,56.,58.,60.,62.,                               *024
           1 64.,66.,68.,70.,72.,76.,80.,85.,90.,95.,100.,110.,120.,                                    *024
           1     130.,140.,150.,160.,170.,180.,190.,200.,210.,220.,230.,                                *024
           1 240.,250.,260.,270.,280.,290.,300.,310.,320.,330.,340.,350.,                               *024
           1 360.                                                                                       *024
            VECTOR VALUES STDY(1)= 1350.,1500.,1700.,1900.,2100.,2300.,2550.,2800.,                     *025
           1 3400.,4000.,4900.,6000.,7200.,8500.,11900.,15700.,20900.,                                  *025
           1 26600.,33700.,39200.,43000.,44750.,46000.,46250.,46250.,                                   *025
           1 45800.,45000.,44000.,42200.,40500.,38750.,36500.,34000.,                                   *025
           1 30700.,27500.,24300.,21700.,19700.,15000.,12000.,9700.,7500.,                              *025
           1 6000.,4550.,2650.,1725.,1680.,1690.,1725.,1760.,1805.,1845.,                               *025
           1 1890.,1920.,1960.,2000.,2040.,2080.,2115.,2150.,2235.,2300.,                               *025
           1 2400.,2490.,2585.,2675.,2860.,3020.,3200.,3380.,3550.,3710.,                               *025
           1 3900.,4050.,4225.,4400.,4575.,4750.,4900.,5050.,5225.,5400.,                               *025
           1 5575.,5750.,5900.,6025.,6200.,6400.,6550.,6700.,6850.,7000.                                *025
            VECTOR VALUES CTEM(1)= -360.,-350.,-340.,-330.,-320.,-310.,-300.,-290.,                     *026
           1 -280.,-270.,-260.,-250.,-240.,-230.,-220.,-210.,-200.,-190.,                               *026
           1 -180.,-170.,-160.,-150.,-140.,-130.,-120.,-110.,-100.,-90.,                                *026
           1 -80.,-70.,-60.,-50.,-40.,-30.,-20.,-10.,0.0,10.,20.,30.,40.,                               *0
```

Fig. D-2. Digital computer program listing.

```
1 50.,60.,70.,80.,90.,100.,110.,120.,130.,140.                          *026
  VECTOR VALUES CCP(1)= 0.0305,                                         *027
1              .0359,.0407,.045,.0489,.0524,.0557,.0589,                *027
1 .0618,.0642,.0662,.0681,.0699,.0716,.0732,.0747,.076,.0773,           *027
1 .0784,.0794,.0804,.0813,.0822,.0831,.0839,.0847,.0854,.086,           *027
1 .0866,.0872,.0877,.0882,.0886,.0891,.0895,.0899,.0903,.09065,         *027
1 .091,.09125,.09155,.0918,.09205,.0923,.0925,.0927,.09285,             *027
1 .093,.09315,.09325,.0934                                              *027
  MPY=2.302585                                                          *028
  N1=92                                                                 *029
  J14=28                                                                *030
  J15=19                                                                *031
  READ FORMAT IN, RUN(1)...RUN(12)                                      *032
  PRINT FORMAT OUT, RUN(1)...RUN(12)                                    *033
  READ DATA                                                             *034
  PRINT RESULTS N4,N,RO,VOA,DR,IC,DS,SM,RZ,TSAT,TIM(1)...TIM(N4),       *035
1 TEM(1)...TEM(N4)                                                      *035
  WHENEVER N .L. 5, TRANSFER TO START                                   *036
  JC=(N+1)/2                                                            *037
  THROUGH LOOPB,FOR I1=JC,1,I1.G.(N4-(N/2)-2)                           *038
  THROUGH LU1, FOR DD=1,1,DD.G.N                                        *039  01
  Y(DD)=(TEM(DD+I1-JC+2)-TEM(DD+I1-JC))/(TIM(DD+I1-JC+2)                *040  02
1 -TIM(DD+I1-JC))                                                       *040
LU1       X(DD)=TIM(DD+I1-JC+1)                                         *041  02
  TP=0                                                                  *042  01
HRZ       SX=0.0                                                        *043  01
  SX2 = 0.0                                                             *044  01
  SX3 = 0.0                                                             *045  01
  SX4 = 0.0                                                             *046  01
  SX5 = 0.0                                                             *047  01
  SX6 = 0.0                                                             *048  01
  SY  = 0.0                                                             *049  01
  SXY = 0.0                                                             *050  01
  SX2Y= 0.0                                                             *051  01
  SX3Y= 0.0                                                             *052  01
  SY2 = 0.0                                                             *053  01
  THROUGH LPA, FOR I = 1, 1, I .G. N                                    *054  01
  SX  = SX  + X(I)                                                      *055  02
  SX2 = SX2 + X(I) .P. 2                                                *056  02
  SX3 = SX3 + X(I) .P. 3                                                *057  02
  SX4 = SX4 + X(I) .P. 4                                                *058  02
  SX5 = SX5 + X(I) .P. 5                                                *059  02
  SX6 = SX6 + X(I) .P. 6                                                *060  02
  SY = SY + Y(I)                                                        *061  02
  SXY = SXY + Y(I)*X(I)                                                 *062  02
  SX2Y = SX2Y + Y(I)*X(I)*X(I)                                          *063  02
  SX3Y = SX3Y + Y(I)*X(I) .P. 3                                         *064  02
LPA       SY2 = SY2 + Y(I)*Y(I)                                         *065  02
  V1= N/(N*SX2 -SX*SX)                                                  *066  01
  V2=(SX*SX3/N)-SX4                                                     *067  01
  V5=SX2/N                                                              *068  01
  V6=SX*SX2-N*SX3                                                       *069  01
  V7=SX2*SX3/N-SX5                                                      *070  01
  V9=SXY-SX*SY/N                                                        *071  01
  V11=1/(SX4-(SX2*SX2/N)-((V6/N)*(V6/N)*V1))                            *072  01
  V13=SX2Y-V5*SY+V1*V9*V6/N                                             *073  01
  V15=V1*(V6/N)*V2+V7                                                   *074  01
  V16=SX3Y-(SX3*SY/N)-SX4*V1*V9-SX5*V11*V13                             *075  01
  V17=SX2*SX3/N-SX4*V1*V6/N                                             *076  01
  V18=SX3*SX3/N-SX4*V1*V2-SX5*V11*V15                                   *077  01
```

Fig. D-2 (Continued)

```
      V19=SX*SX3/N                                                          *078          01
      A3=(V16+V1*V9*V19+(V17+V1*V6*V19/N)*V11*V13)/(SX6-V18-V1*V2*           *079          01
     1 V19-V11*V15*(V17+V1*V6*V19/N))                                       *079
      A2=V11*(V13+V15*A3)                                                   *080          01
      A1=V1*(V9+(V6/N)*A2+V2*A3)                                            *081          01
      A0=(1./N)*(SY-A1*SX-A2*SX2-A3*SX3)                                    *082          01
      SD2=SY2-(A0*SY+A1*SXY+A2*SX2Y+A3*SX3Y)                                *083          01
      WHENEVER (SD2/N).L.0.0, TRANSFER TO ERRRT                             *084          01
HRA   WHENEVER TP.NE.0, TRANSFER TO HRX                                     *085          01
      SE=SQRT.(SD2/N)                                                       *086          01
      C2=0.0                                                                *087          01
      THROUGH LU2, FOR DE=1,1,DE.G.(N+1)                                    *088          01
LU2   C2=C2+(TEM(DE+I1-JC+1)+TEM(DE+I1-JC))*(TIM(DE+I1-JC+1)                *089          02
     1 -TIM(DE+I1-JC))/2.                                                   *089
      C3=I1-JC+N+2                                                          *090          01
      C4=I1-JC+1                                                            *091          01
      C1=(C2-(A0/2.)*((TIM(C3).P.2)-(TIM(C4).P.2))                          *092          01
     1       -(A1/ 6.)*((TIM(C3).P.3)-(TIM(C4).P.3))                        *092
     1       -(A2/12.)*((TIM(C3).P.4)-(TIM(C4).P.4))                        *092
     1       -(A3/20.)*((TIM(C3).P.5)-(TIM(C4).P.5)))/                      *092
     1 (TIM(C3)-TIM(C4))                                                    *092
      B0=A0                                                                 *093          01
      B1=A1                                                                 *094          01
      B2=A2                                                                 *095          01
      B3=A3                                                                 *096          01
      THROUGH LOOPC, FOR G1=(I1-2),1,G1.G.(I1+2)                            *097          01
      X1(G1)=X(G1-I1+3)                                                     *098          02
LOOPC Y1(G1,(I1-2))=A0*X1(G1)+A1*X1(G1)*X1(G1)/2.                           *099          02
     1 +A2*X1(G1).P.3/3.+A3*X1(G1).P.4/4.+C1                                *099
      THROUGH LOOPD, FOR K=I1-1,1,K.G.(I1+2)                                *100          01
      THROUGH LOOPD,FOR I2=K,1,I2.G.(I1+2)                                  *101          02
LOOPD Y1(I2,K)=(Y1(I2,K-1)-Y1(I2-1,K-1))/(X1(I2)-X1(I2-K+I1-2))             *102          03
      THROUGH LPR, FOR JF=1,1,JF.GE.52                                      *103          01
LPR   WHENEVER (Y1(I1,(I1-2))-CTEM(JF)).L.0.0,TRANSFER TO HR3               *104          02
      PRINT RESULTS JF,CTEM(JF),A0,A1,A2,A3,X1(I1-2)...X1(I1+2),            *105          01
     1 Y1((I1-2),(I1-2))...Y1((I1+2),(I1-2))                                *105
      TRANSFER TO START                                                     *106          01
HR3   ACP=CCP(JF-1)+((CCP(JF)-CCP(JF-1))*(Y1(I1,(I1-2))-CTEM(JF-1))         *107          01
     1 /10.0)                                                               *107
      CQ=RO*DR*DR*3600./(TC*DS)                                             *108          01
      MM=ACP*CQ                                                             *109          01
      PK=(X1(I1+1)-X1(I1-1))/DS                                             *110          01
      THROUGH LOOPB, FOR L=1,1,L.G.PK                                       *111          01
      WHENEVER I1.G.3 .OR.L.G.1,TRANSFER TO PSI                             *112          02
      THROUGH LOOPE, FOR S=1,1,S.G.SM                                       *113          02
LOOPE T(S)=Y1(2,1)                                                          *114          03
PSI   TIME=X1(I1-1)+L*DS                                                    *115          02
      T(1)=B0*TIME+B1*TIME.P.2/2.+B2*TIME.P.3/3.+B3*TIME.P.4/4.+C1          *116          02
      THROUGH LOOPG, FOR S=1,1,S.G.SM                                       *117          02
      WHENEVER S.E.1                                                        *118          03
      TN(1)=T(1)                                                            *119       01 03
      OR WHENEVER S.L. SM                                                   *120       01 03
      DRR=DR/(RZ-(S-1)*DR)                                                  *121       01 03
      TN(S)=(T(S+1)*(1.-DRR)+T(S-1)*(1.+DRR)+(MM-2.)*T(S))/MM               *122       01 03
      OTHERWISE                                                             *123       01 03
      TN(S)=(6.*T(S-1)+(MM-6.)*T(S))/MM                                     *124       01 03
      END OF CONDITIONAL                                                    *125       01 03
      WHENEVER .ABS.(TIME-(X1(I1)-2.*DS)).L.0.00010                         *126          03
      Y2(S,1)=TN(S)                                                         *127       01 03
      X2(1)=TIME                                                            *128       01 03
```

Fig. D-2 (Continued)

```
                R=1                                                                  *129          01    03
                OR WHENEVER .ABS.(TIME-(X1(I1)-DS)).L.0.00010                        *130          01    03
                Y2(S,2)=TN(S)                                                        *131          01    03
                X2(2)=TIME                                                           *132          01    03
                R=2                                                                  *133          01    03
                OR WHENEVER .ABS.(TIME-X1(I1)).L.0.00010                             *134          01    03
                Y2(S,3)=TN(S)                                                        *135          01    03
                X2(3)=TIME                                                           *136          01    03
                R=3                                                                  *137          01    03
                OR WHENEVER .ABS.(TIME-(X1(I1)+DS)).L.0.00010                        *138          01    03
                Y2(S,4)=TN(S)                                                        *139          01    03
                X2(4)=TIME                                                           *140          01    03
                R=4                                                                  *141          01    03
                OR WHENEVER .ABS.(TIME-(X1(I1)+2.*DS)).L.0.00010                     *142          01    03
                Y2(S,5)=TN(S)                                                        *143          01    03
                X2(5)=TIME                                                           *144          01    03
                R=5                                                                  *145          01    03
                TD=Y2(1,3)-TSAT                                                      *146          01    03
LOOPG           END OF CONDITIONAL                                                   *147          01    03
                THROUGH LOOPH,FOR S=1,1,S.G.SM                                       *148                02
LOOPH           T(S)=TN(S)                                                           *149                03
                WHENEVER .ABS.(TIME-(X1(I1)+2.*DS)).L.0.00010                        *150                02
                THROUGH LOOPL,FOR R=1,1,R.G.5                                        *151          01    02
                SUM=((SM-1.).P.2*Y2(1,R))/2.                                         *152          01    03
                THROUGH LOOPJ, FOR S=2,1,S.E.SM                                      *153          01    03
LOOPJ           SUM=SUM+((SM-S).P.2)*Y2(S,R)                                         *154          01    04
                TA(R)=3.*SUM/((SM-1.).P.3)                                           *155          01    03
                X3(R)=X2(R)                                                          *156          01    03
LOOPL           Y3(R,1)=TA(R)                                                        *157          01    03
                THROUGH LPZ, FOR JZ=1,1, JZ.G.5                                      *158          01    02
                X(JZ)=X3(JZ)-TIME+2.*DS                                              *159          01    03
LPZ             Y(JZ)=TA(JZ)                                                         *160          01    03
                TP=1                                                                 *161          01    02
                TRANSFER TO HRZ                                                      *162          01    02
HRX             TG=A1+2.*A2*X(3)+3.*A3*X(3)*X(3)                                     *163          01    02
                PRINT RESULTS  X2(1),X2(2),X2(3),X2(4),X2(5),TIME,TG,X(3)            *164          01    02
                Q=RO*ACP*TG*VUA*3600.                                                *165          01    02
                PRINT RESULTS X2(3),Y2(1,3),Y2(2,3),Y2(11,3),ACP,Q,TD,SE             *166          01    02
                WHENEVER Q .G. 100000.0, TRANSFER TO LP2                             *167          01    02
                QAB  (I1-JC+1)=.ABS.(Q)                                              *168          01    02
                DTT  (I1-JC+1)=TD                                                    *169          01    02
                DATAX(I1-JC+1)=.ABS.(TD)                                             *170          01    02
                DATAY(I1-JC+1)=QAB(I1-JC+1)                                          *171          01    02
                END OF CONDITIONAL                                                   *172          01    02
LOOPB           CONTINUE                                                             *173                02
LP3             N3=I1-JC                                                             *174
                PRINT COMMENT $1$                                                    *175
                EXECUTE SETPLT.(1,TIM(1),TEM(1),N4,$*$,38,LFO)                       *176
                PRINT FORMAT ABS1                                                    *177
                PRINT FORMAT OUT1, RUN(1)...RUN(12)                                  *178
                THROUGH LPK,FOR J9=1,1,J9.G.N1                                       *179
                STAX(J9)=     ELOG.(STDX(J9))/MPY                                    *180                01
LPK             STAY(J9)=     ELOG.(STDY(J9))/MPY                                    *181                01
                THROUGH LPO, FOR J16=1,1,J16.G.N3                                    *182
                DATX(J16) =ELOG.(DATAX(J16))/MPY                                     *183                01
LPO             DATY(J16) =ELOG.(DATAY(J16))/MPY                                     *184                01
                EXECUTE PLOT1.(0,2,25,3,33)                                          *185
                EXECUTE PLOT2.(GRAPH,3.,0.,5.,3.)                                    *186
                THROUGH LPJ,FOR J12=1,1,J12.G.J14                                    *187
                EXECUTE PLOT3.($+$,EX(J12),3.0,1)                                    *188                01
```

Fig. D-2 (Continued)

```
      EXECUTE PLOT3.($+$,EX(J12),4.0,1)                                  *189   01
LPJ   EXECUTE PLOT3.($+$,EX(J12),5.0,1)                                  *190   01
      THROUGH LPN,FOR J8=1,1,J8.G.J15                                    *191
      EXECUTE PLOT3.($+$,0.0,WY(J8),1)                                   *192   01
      EXECUTE PLOT3.($+$,1.0,WY(J8),1)                                   *193   01
      EXECUTE PLOT3.($+$,2.0,WY(J8),1)                                   *194   01
LPN   EXECUTE PLOT3.($+$,3.0,WY(J8),1)                                   *195   01
      EXECUTE PLOT3.($.$,STAX(1),STAY(1),N1)                             *196
      EXECUTE PLOT3.($*$,DATX(1),DATY(1),N3)                             *197
      PRINT COMMENT $1$                                                  *198
      EXECUTE PLOT4.(32,ORD)                                             *199
      PRINT FORMAT ABS                                                   *200
      PRINT FORMAT OUT1, RUN(1)...RUN(12)                                *201
      PRINT COMMENT $1$                                                  *202
      EXECUTE SETPLT.(1,TIM(4),QAB(1),(N4-6),$*$,32,QA)                  *203
      PRINT FORMAT ABS1                                                  *204
      PRINT FORMAT OUT1, RUN(1)...RUN(12)                                *205
      PRINT FORMAT OUT, RUN(1)...RUN(12)                                 *206
      PRINT RESULTS DTT(1)...DTT(N3),QAB(1)...QAB(N3),                   *207
      DATAX(1)...DATAX(N3), TIM(1)...TIM(N4)                             *207
      TRANSFER TO START                                                  *208
ERRRT PRINT COMMENT $- NEGATIVE SQUARE ROOT - ERROR IN STD DEV $         *209
      PRINT RESULTS N,A0,A1,A2,A3,SD2,(SD2/N)                            *210
      SD2=-SD2                                                           *211
      TRANSFER TO HRA                                                    *212
LP2   N3=I1-JC+1                                                         *213
      TRANSFER TO LP3                                                    *214
      END OF PROGRAM                                                     *215
```

Fig. D-2 (Concluded)

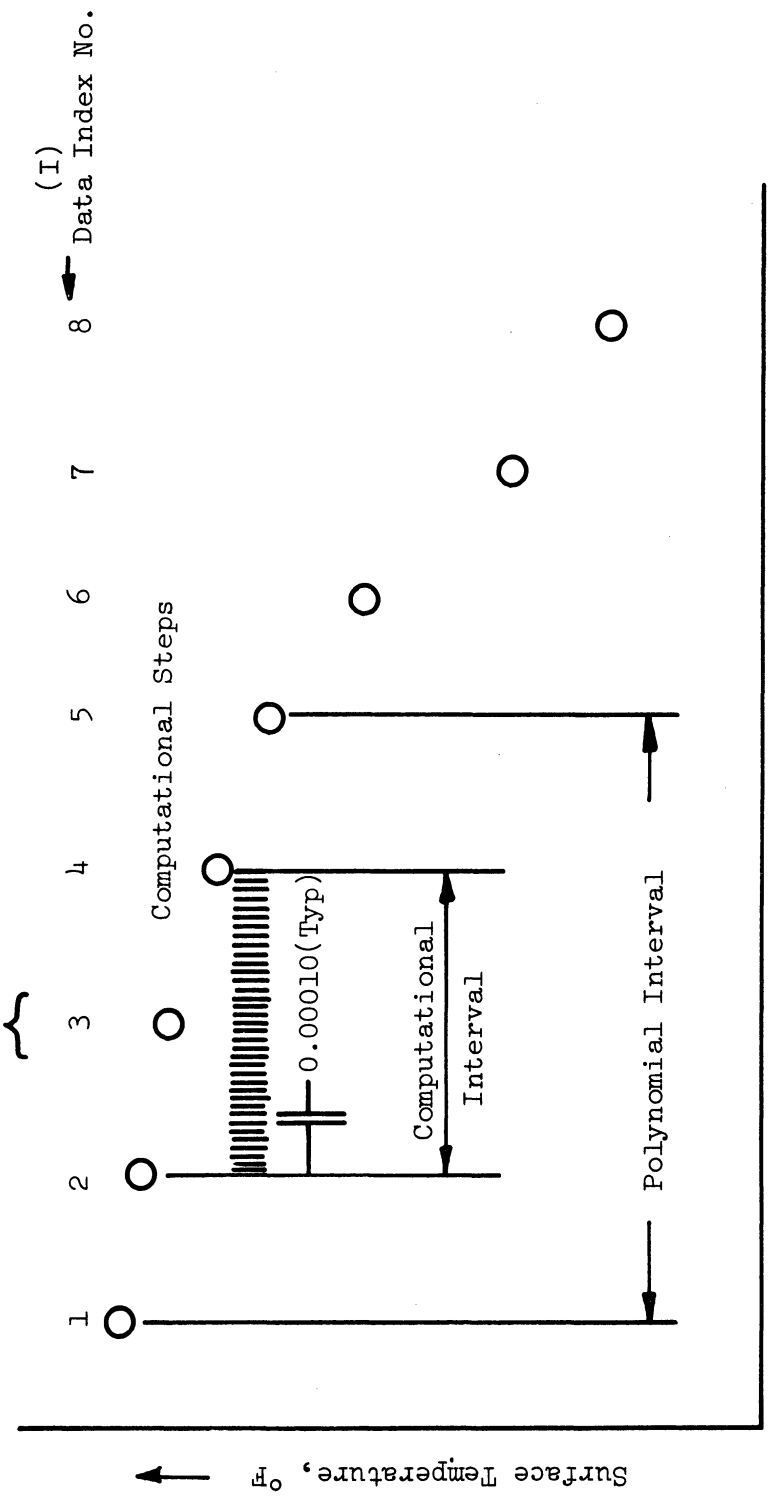

Fig. D-3. Computational procedure for digital computer program.

APPENDIX E

ANALYSIS OF THE TEST PACKAGE—STEEL CABLE—COUNTERWEIGHT SYSTEM

A sketch of the test package—steel cable—counterweight (p-c-c) system is shown in Fig. E-1. The cable is assumed to pass over two frictionless pulleys and to be weightless and inextensible. Writing the equations of motion for the test package and the counterweight.

$$\Sigma F_y = ma_y \tag{E-1}$$

or

$$F_c - m_c g = m_c a_s \tag{E-2}$$

$$m_p g - F_c = m_p a_s \tag{E-3}$$

for which the solution is

$$\frac{a_s}{g} = \frac{m_p - m_c}{m_p + m_c} \tag{E-4}$$

$$F_c = m_c g \left(1 + \frac{a_s}{g}\right) \tag{E-5}$$

where

ΣF_y = sum of the forces in the y-direction

m = mass

m_c = mass of counterweight

m_p = mass of test package

a_y = acceleration in y-direction

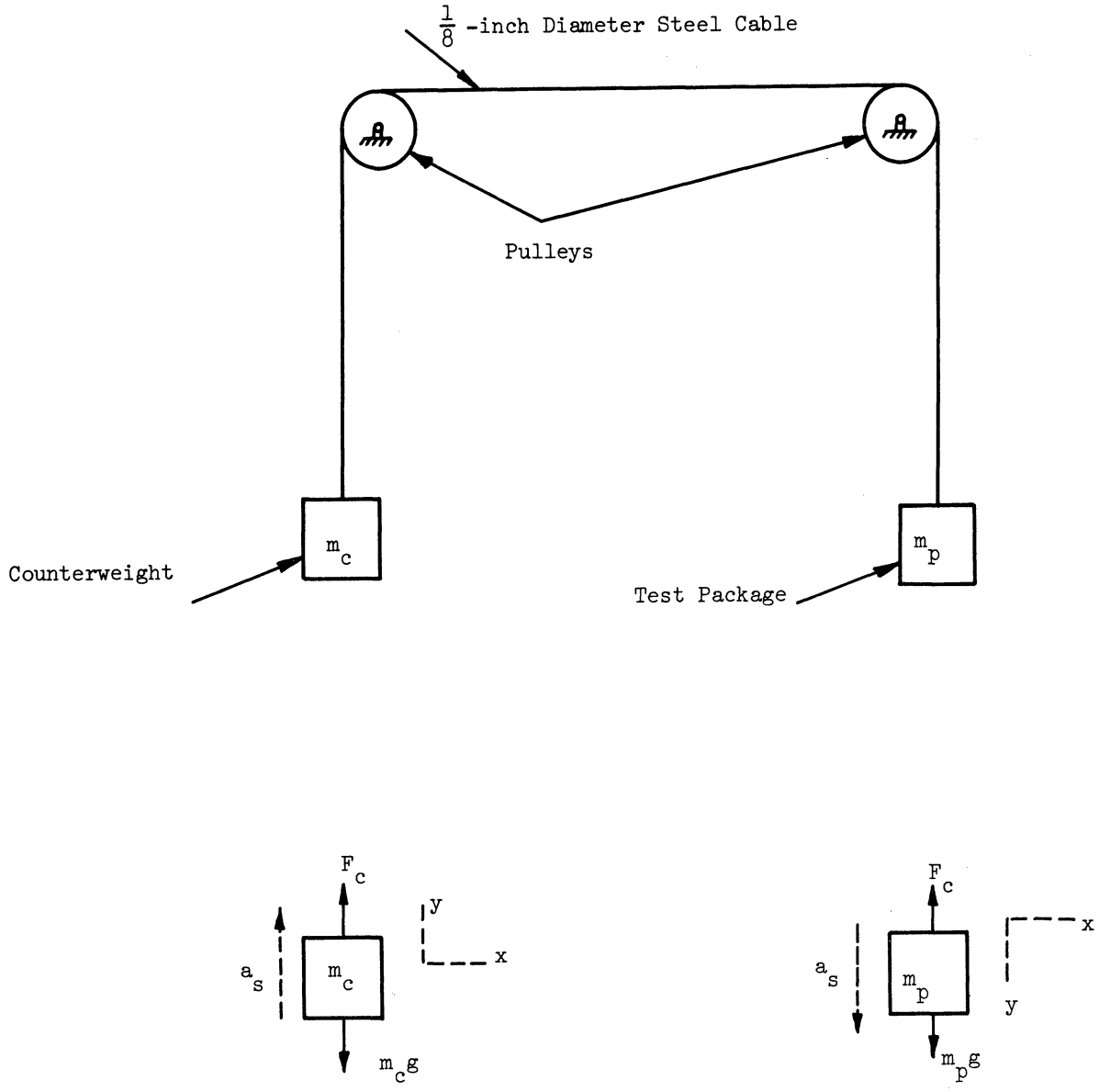

Fig. E-1. Sketch and free-body diagram of test package—steel cable—counterweight system.

a_s = acceleration of p-c-c system

g = acceleration due to gravity

F_c = tension in cable

The effective body force acting on a body which is moving with the test package is

$$F_B = m_B a_B \tag{E-6}$$

where

F_B = effective body force acting on body moving with test package

m_B = mass of body moving with test package

a_B = net acceleration of body moving with test package

The net acceleration

$$a_B = g - a_s$$

or

$$\frac{a_B}{g} = 1 - \frac{a_s}{g} \tag{E-7}$$

When $m_c = 0$, i.e., the test package is in free fall, $(a_s/g) = 1$, $F_c = 0$, and $(a_B/g) = 0$. This indicates that a body moving with the test package in free fall is subjected to the same forces which it would be subjected to in a zero-gravity environment.

When $m_c g = 11$ pounds and $m_p g = 120$ pounds, $(a_s/g) = 0.83$, $F_c = 20.2$ lbf, and $(a_B/g) = 0.17$. This indicates that a body moving with the test package in counterweighted drop, assuming the weights given above, is subjected to the same forces which it would be subjected to in an environment possessing

a gravitational field 17% as strong as that on the earth.

The actual p-c-c system differs from the idealized system described above. The values of (a_B/g) were measured using an accelerometer mounted on the test package. The measured values of (a_B/g) were approximately 15% higher than those calculated using Eq. (E-7) for counterweighted drop. This difference is attributed primarily to friction losses in the pulleys and bending losses in the cable, with a small effect due to guide wire drag, which increase the effective mass of the counterweight, and thus (a_B/g).

The assumption that the steel cable is inextensible is not a good assumption for this system. The measured spring constant was 308 lbf/in. The dynamic system may be represented as shown in Fig. E-2, with m_c and m_p each resting on a frictionless surface and connected by a spring with spring constant k_c and F_{Bp} and F_{Bc} representing the gravity forces acting on the test package and counterweight, respectively. An initial deflection of the spring is considered, depending on whether the system is initially restrained at the counterweight or test package, A or B in Fig. E-2. The equations of motion may be written as

$$m_c \frac{d^2x_c}{dt^2} - k_c(x_p-x_c) + F_{Bc} = 0 \qquad \text{(E-8)}$$

$$m_p \frac{d^2x_p}{dt^2} + k_c(x_p-x_c) - F_{Bp} = 0 \qquad \text{(E-9)}$$

When the system is initially restrained at the counterweight, A in Fig. E-2, the test package acceleration is

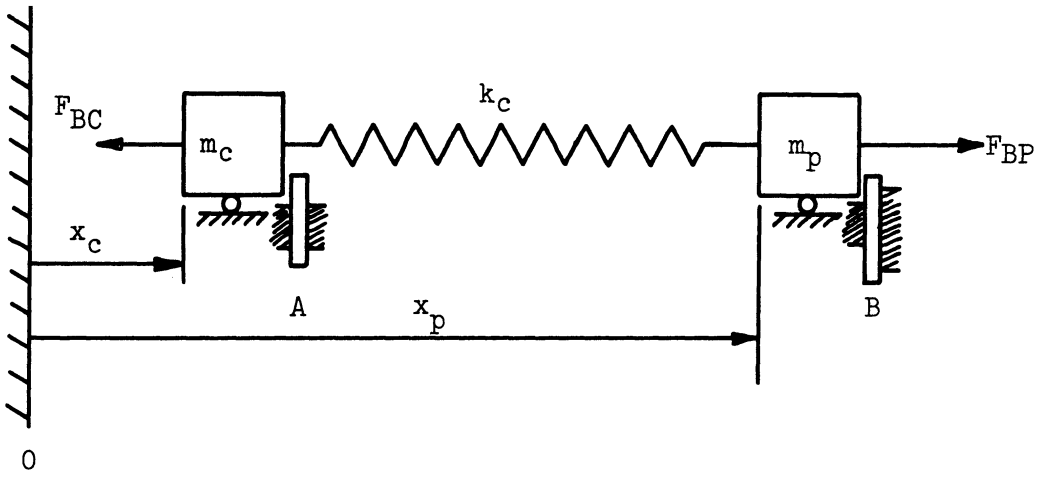

Fig. E-2. The test package—steel—cable counterweight system as an idealized mass-spring-mass system.

$$\frac{d^2x_p}{dt^2} = \frac{m_p-m_c}{m_p+m_c}(1-\cos \omega t)g \qquad \text{(E-10)}$$

where ω is the natural frequency of the system. The solutions for ω are

$$\omega = \sqrt{\frac{k_c(m_p+m_c)}{m_p m_c}} \quad , \quad 0 \qquad \text{(E-11)}$$

Using values of k_c = 308 lbf/inch, $m_c g$ = 11 lbf, and $m_p g$ = 120 lbf in Eq. (E-11), ω = 108.8 radians/sec, and the predicted oscillation frequency, f, for the system is 17.3 Hertz. This solution assumes no damping in the system, and therefore gives an upper limit for f. The general solution of Eqs. (E-8) and (E-9) with the appropriate initial conditions, given as Eq. (E-10), shows that the effective body force present on the test package will oscillate about the steady value. Evaluating Eq. (E-10) using the values given above, the test package acceleration is given as

$$\frac{d^2x_p}{dt^2} = 0.83(1-\cos 108.8t)g \qquad \text{(E-12)}$$

which predicts that an accelerometer mounted on the test package would show an average value of (1-0.83)g = 0.17g, but with a superimposed oscillation of amplitude 0.83g.

When the system is initially restrained at the package, B in Fig. E-2, the test package acceleration is

$$\frac{d^2x_p}{dt^2} = \frac{m_p-m_c}{m_p+m_c}\left(1 + \frac{m_c}{m_p}\cos \omega t\right)g \qquad \text{(E-13)}$$

Using the values given previously, the test package acceleration is given as

$$\frac{d^2x_p}{dt^2} = 0.83(1+0.09 \cos 108.8t)g \qquad \text{(E-14)}$$

which predicts that an accelerometer mounted on the test package would show an average value of (1-0.83)g = 0.17g, but with a superimposed oscillation of amplitude 0.076g.

Measurements of (a_B/g) as a function of time using the values of k_c, $m_c g$, and $m_p g$ given previously were obtained and are shown in Fig. E-3. The chart labeled "counterweight released in basement" was obtained using the cable to support the test package (A in Fig. E-2). The chart labeled "package released by burning wire" was obtained using the cable to support the counterweight (B in Fig. E-2). The initial amplitude of the oscillations in (a_B/g) are much larger for the case where the largest mass (the test package) was being supported. This amplitude decreases over the first several cycles, indicating that damping is taking place. The oscillation frequency is the same for both measurements, approximately 13 Hertz. If viscous damping is assumed, a value of the damping factor of 0.66 is indicated. The damping is probably not viscous, because a damping factor of 0.66 indicates large damping, but relatively little damping is indicated on the traces.

The appearance of the traces on Fig. E-3 indicates that several factors probably influence the oscillation behavior of the p-c-c system. The pulleys over which the cable passes, internal damping in the cable, the fact that the cable cannot sustain compressive forces and the possibility of some internal oscillation within the test package itself, are probably among the most significant.

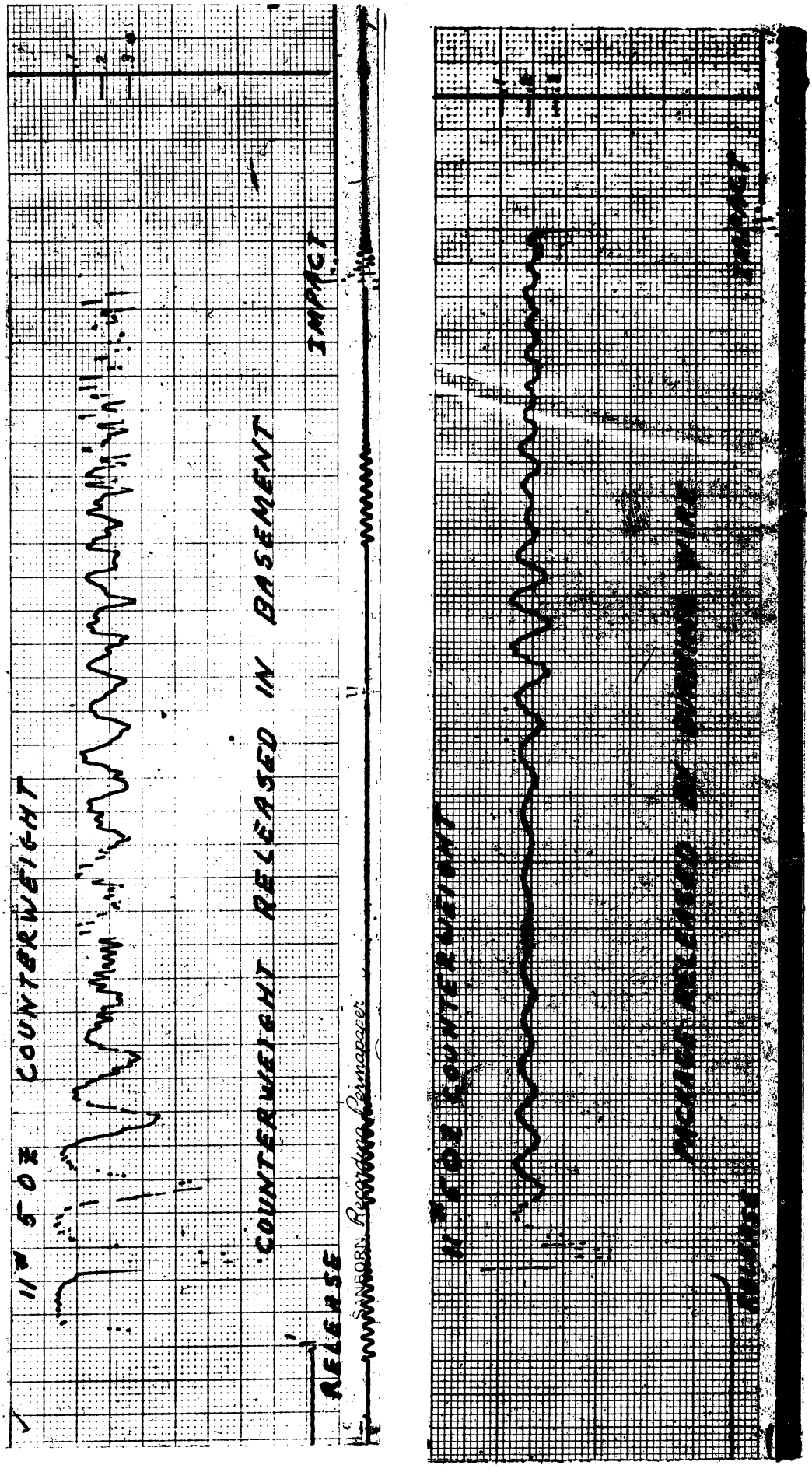

Fig. E-3. Accelerometer records of (a_B/g).

With these limitations in mind, it is interesting to compare the traces of Fig. E-3 with the predictions of Eqs. (E-12) and (E-14). When the counterweight is released, the initial large irregular oscillations are probably caused by the counterweight trying to compress the cable (with resultant cable buckling) then dropping back down to again put the cable in tension. The ±0.83g oscillation predicted is not sustained, although it may be present in the first cycle.

When the package is released, a more regular trace is obtained. Cable buckling is probably not a problem for this case. The maximum amplitude of the acceleration variation is less than ±0.1g, which is approximately as predicted by Eq. (E-14). A beat in the oscillation amplitude may be seen, but there is no obvious cause for this.

BIBLIOGRAPHY

1. McAdams, W. H. Heat Transmission, 3rd edition, McGraw-Hill Book Co., New York, 1954.

2. Kreith, F. Principles of Heat Transfer, 2nd edition, International Textbook Co., Scranton, Pa., 1965.

3. Berenson, P. J. "Film Boiling Heat Transfer from a Horizontal Surface," Trans. ASME Journal of Heat Transfer, Series C, 83, 351-358 (1961).

4. Zuber, N. "Hydrodynamic Aspects of Boiling Heat Transfer," Atomic Energy Commission Report No. AECU-4439, Physics and Mathematics, June 1959.

5. Zuber, N. "On the Stability of Boiling Heat Transfer," ASME 57-HT-4.

6. Adelberg, M. "Boiling, Condensation and Convection in a Gravitational Field," Paper presented at the 55th National Meeting of the A.I.Ch.E., Houston, Texas, Feb. 1965.

7. Clark, J. A. and Merte, H. "Boiling Heat Transfer to a Cryogenic Fluid in Both Low and High Gravity Fields," Paper presented at the XIth International Congress of Refrigeration, Munich, Germany, Aug.-Sept. 1963.

8. Keshock, E. G. and Siegel, R. "Forces Acting on Bubbles in Nucleate Boiling Under Normal and Reduced Gravity Conditions," NASA TN-D-2299, Aug. 1964.

9. Cochran, T. H. and Aydelott, J. C. "Effects of Subcooling and Gravity Level on Boiling in the Discrete Bubble Region," NASA Technical Note TN D-3449, Sept. 1966.

10. Beckman, W. A. and Merte, H. "A Photographic Study of Boiling in an Accelerating System," Trans. ASME Journal of Heat Transfer, Series C, 87, 374-380 (1965).

11. Rohsenow, W. M. "A Method of Correlating Heat Transfer Data for Surface Boiling of Liquids," Trans. ASME, 74, 969-976 (1952).

12. Michenko, N. "On the Problem of Heat Transfer in Nucleate Boiling," Energomashinostroenie, No. 6, 17-21 (1960).

BIBLIOGRAPHY (Continued)

13. Forster, H. K. and Zuber, N. "Growth of a Vapor Bubble in a Superheated Liquid," Journal of Applied Physics, 24, 474-478 (1954).

14. Engelberg-Forster, K. and Greif, R. "Heat Transfer to a Boiling Liquid—Mechanisms and Correlations," Trans. ASME Journal of Heat Transfer, Series C, 81, 43-53 (1959).

15. Frederking, T.H.K. "Gravity Effects on Interfacial Kinematics in Ordinary Boiling Systems," Paper presented at the Symposium on Two-Phase Flow, University of Exeter, Exeter, June 1965.

16. Merte, H., Jr. and Clark, J. A. "Pool Boiling in an Accelerating System," Trans. ASME Journal of Heat Transfer, Series C, 83, 233-242 (1961).

17. Costello, C. P. and Tuthill, W. E. "Effects of Acceleration on Nucleate Pool Boiling," Paper presented at the A.I.Ch.E.-I.M.I.Q. Joint Meeting, Mexico City, Mexico, June 1960.

18. Sherley, J. E. "Nucleate Boiling Heat Transfer Data for Liquid Hydrogen at Standard and Zero Gravity," Advances in Cryogenic Engineering, 8, Ed., K. D. Timmerhaus, Plenum Press, 495-500 (1963).

19. Merte, H. and Clark, J. A. "Boiling Heat Transfer With Cryogenic Fluids at Standard, Fractional, and Near-Zero Gravity," Trans. ASME Journal of Heat Transfer, Series C, 86, 351-359 (1964).

20. Noyes, R. C. "An Experimental Study of Sodium Pool Boiling Heat Transfer," Trans. ASME Journal of Heat Transfer, Series C, 85, 125-131 (1963).

21. Chang, Y. P. and Snyder, N. W. "Heat Transfer in Saturated Boiling," Chemical Engineering Progress Symposium Series, 56, No. 30, 1960.

22. Kutateladze, S. S. "A Hydrodynamic Theory of Changes in the Boiling Process Under Free Convection Conditions," Izv. Akad. Nauk. SSSR, Otd. Tekh. Nauk. No. 4, 529-536 (1951).

23. Moissis, R. and Berenson, P. J. "On the Hydrodynamic Transitions in Nucleate Boiling," Trans. ASME Journal of Heat Transfer, Series C, 85, 221-229 (1963).

24. Siegel, R. "Effects of Reduced Gravity on Heat Transfer," Proposed NASA Survey Article for Advances in Heat Transfer, March 1966.

BIBLIOGRAPHY (Continued)

25. Usiskin, C. M. and Siegel, R. "An Experimental Study of Boiling in Reduced and Zero Gravity Fields," Trans. ASME Journal of Heat Transfer, Series C, 83, 243-253 (1961).

26. Steinle, H. F. "An Experimental Study of the Transition from Nucleate to Film Boiling Under Zero-Gravity Conditions," Proceedings of the 1960 Heat Transfer and Fluid Mechanics Institute, Stanford University, 208-219, June 1960.

27. Bromley, L. A. "Heat Transfer in Stable Film Boiling," Chemical Engineering Progress, 46, 221-227 (1950).

28. Hamill, T. D. and Baumeister, K. J. "Film Boiling Heat Transfer from a Horizontal Surface as an Optimal Boundary Value Process," Proceedings of the Third International Heat Transfer Conference, Chicago, Ill., Aug. 1966.

29. Baumeister, K. J., Hamill, T. D., Schwartz, F. L., and Schoessow, G. J. "Film Boiling Heat Transfer to Water Drops on a Flat Plate," Paper presented at the 8th National Heat Transfer Conference, Los Angeles, Calif., Aug. 1965.

30. Hsu, Y. Y. and Westwater, J. W. "Approximate Theory for Film Boiling on a Vertical Surface," Chemical Engineering Progress Symposium Series, 56, No. 30, 15-24 (1960).

31. Frederking, T.H.K. and Clark, J. A. "Natural Convection Film Boiling on a Sphere," Advances in Cryogenic Engineering, 8, 501-506 (1963).

32. Clark, J. A. and Merte, H. "Nucleate, Transition, and Film Boiling Heat Transfer at Zero Gravity," Paper presented at the 2nd Symposium on Physical and Biological Phenomena under Zero-G Conditions, Jan. 1963.

33. Merte, H. and Clark, J. A. "Boiling Heat Transfer with Cryogenic Fluids at Standard, Fractional, and Near-Zero Gravity," Report IP-616, The University of Michigan, Industry Program of the College of Engineering, April 1963.

34. Pomerantz, M. L. "Film Boiling on a Horizontal Tube in Increased Gravity Fields," Trans. ASME Journal of Heat Transfer, Series C, 86, 213-219 (1964).

BIBLIOGRAPHY (Continued)

35. Heath, C. A. and Costello, C. P. "Some Effects of Geometry, Orientation and Acceleration on Pool Film Boiling of Organic Fluids," Trans. ASME Journal of Engineering for Industry, Series B, 88, 17-23 (1966).

36. Class, C. R., DeHaan, J. R., Piccone, M., and Cost, R. B. "Boiling Heat Transfer to Liquid Hydrogen from Flat Surfaces," Advances in Cryogenic Engineering, 5, 254-261 (1960).

37. Strobridge, T. R. "The Thermodynamic Properties of Nitrogen from 64 to 300°K Between 0.1 and 200 Atmospheres," National Bureau of Standards Technical Note 129, Jan. 1962.

38. Goldsmith, A., Waterman, T. E., and Hirschhorn, H. J. Handbook of Thermophysical Properties of Solid Materials Volume I: Elements, The Macmillan Co., New York, 1961.

39. Scott, R. B. Cryogenic Engineering, D. Van Nostrand, Princeton, New Jersey, 1959.

40. Johnson, H. A., Editor, Boiling and Two-Phase Flow for Heat Transfer Engineers, A University of California Engineering Extension Division lecture series held at Berkely and Los Angeles, May 27-28, 1965.

41. Johnson, V. J., Editor, "A Compendium of the Properties of Materials at Low Temperature (Phase I) Part I. Properties of Fluids," WADD Technical Report 60-56, Oct. 1960.

42. Frederking, T.H.K. Personal communication.

43. Hosler, E. R. and Westwater, J. W. "Film Boiling on a Horizontal Plate," ARS Journal, 32, 553-558 (1962).

44. Seader, J. D., Miller, W. S., and Kalvinskas, L. A. "Boiling Heat Transfer for Cryogenics--Final Report," Rocketdyne Report R-5598, May 1964.

45. Manson, L. and Seader, J. D. "Study of Boiling Heat Transfer with Lox, LH_2 and LN_2--Final Report," Rocketdyne Report R-6259, July 1965.

46. Chang, Y. P. "Wave Theory of Heat Transfer in Film Boiling," Trans. ASME Journal of Heat Transfer, Series C, 81, 1-12 (1959).

47. Lienhard, J. H. and Wong, P.T.Y. "The Dominant Unstable Wavelength and Minimum Heat Flux During Film Boiling on a Horizontal Cylinder," Trans. ASME Journal of Heat Transfer, Series C, 86, 220-226 (1964).

BIBLIOGRAPHY (Concluded)

48. Bellman, R. and Pennington, R. H. "Effects of Surface Tension and Viscosity on Taylor Instability," Quarterly of Applied Mathematics, 12, 151 (1954).

49. Breen, B. P. and Westwater, J. W. "Effect of Diameter of Horizontal Tubes on Film Boiling Heat Transfer," Chemical Engineering Progress, 58, 67-72 (1962).

50. Ellion, M. E. "A Study of the Mechanism of Boiling Heat Transfer," Jet Propulsion Laboratory Memorandum No. 20-88, Pasadena, Calif., March 1954.

51. Cess, R. D. and Sparrow, E. M. "Subcooled Forced-Convection Film Boiling on a Flat Plate," Trans. ASME Journal of Heat Transfer, Series C, 83, 377-378 (1961).

52. Sparrow, E. M. and Cess, R. D. "The Effect of Subcooled Liquid on Laminar Film Boiling," Trans. ASME Journal of Heat Transfer, Series C, 84, 149-156 (1962).

53. Yang, W. J. "Phase Change of One Component Systems in a Container," A.I.Ch.E. 63-A-48.

54. Chang, Y. P. "A Theoretical Analysis of Heat Transfer in Natural Convection and in Film Boiling," Trans. ASME, 79, 1501-1513 (1957).

55. Zuber, N., Tribus, M. and Westwater, J. W. "The Hydrodynamic Crisis in Pool Boiling of Saturated and Subcooled Liquids," Proceedings of the International Conference on Developments in Heat Transfer, ASME, New York, 230-236 (1962).

56. Clark, J. A. "Appendix, Heat Transfer," To be published in Cryogenic Technology, John Wiley and Sons, 1962.

57. Shapiro, A. H. The Dynamics and Thermodynamics of Compressible Fluid Flow, Ronald Press, New York, N.Y., 1953.

58. Hoerner, S. Fluid Dynamic Drag, S. Hoerner, Midland Park, N.J., 1959.

59. Carslaw, H. S., and Jaeger, J. C. Conduction of Heat in Solids, 2nd edition, Oxford University Press, London, 1959.